APL Materials ROADMAP scitation.org/journal/apm

Roadmap on organic–inorganic hybrid perovskite semiconductors and devices

Cite as: APL Mater. 9, 109202 (2021); doi: 10.1063/5.0047616
Submitted: 15 February 2021 • Accepted: 14 July 2021 •
Published Online: 26 October 2021

View Online Export Citation CrossMark

Lukas Schmidt-Mende,[1,a] Vladimir Dyakonov,[2] Selina Olthof,[3] Feray Ünlü,[3] Khan Moritz Trong Lê,[3] Sanjay Mathur,[3] Andrei D. Karabanov,[4] Doru C. Lupascu,[4] Laura M. Herz,[5,6] Alexander Hinderhofer,[7] Frank Schreiber,[7] Alexey Chernikov,[8,9] David A. Egger,[10] Oleksandra Shargaieva,[11] Caterina Cocchi,[11] Eva Unger,[11] Michael Saliba,[12] Mahdi Malekshahi Byranvand,[13] Martin Kroll,[14] Frederik Nehm,[15] Karl Leo,[14] Alex Redinger,[15] Julian Höcker,[2] Thomas Kirchartz,[16] Jonathan Warby,[17] Emilio Gutierrez-Partida,[17] Dieter Neher,[17] Martin Stolterfoht,[17] Uli Würfel,[18,19] Moritz Unmüssig,[18,19] Jan Herterich,[18,19] Clemens Baretzky,[18,19] John Mohanraj,[20] Mukundan Thelakkat,[20,21] Clément Maheu,[22] Wolfram Jaegermann,[22] Thomas Mayer,[22] Janek Rieger,[23] Thomas Fauster,[23] Daniel Niesner,[23] Fengjiu Yang,[24] Steve Albrecht,[24,25] Thomas Riedl,[26,27] Azhar Fakharuddin,[1] Maria Vasilopoulou,[28] Yana Vaynzof,[29] Davide Moia,[30] Joachim Maier,[30] Marius Franckevičius,[31] Vidmantas Gulbinas,[31] Ross A. Kerner,[32] Lianfeng Zhao,[32] Barry P. Rand,[32,33] Nadja Glück,[34] Thomas Bein,[34] Fabio Matteocci,[35] Luigi Angelo Castriotta,[35] Aldo Di Carlo,[35,36] Matthias Scheffler[37,38] and Claudia Draxl[37,38]

For affiliations, please see the end of the Reference section

ABSTRACT

Metal halide perovskites are the first solution processed semiconductors that can compete in their functionality with conventional semiconductors, such as silicon. Over the past several years, perovskite semiconductors have reported breakthroughs in various optoelectronic devices, such as solar cells, photodetectors, light emitting and memory devices, and so on. Until now, perovskite semiconductors face challenges regarding their stability, reproducibility, and toxicity. In this Roadmap, we combine the expertise of chemistry, physics, and device engineering from leading experts in the perovskite research community to focus on the fundamental material properties, the fabrication methods, characterization and photophysical properties, perovskite devices, and current challenges in this field. We develop a comprehensive overview of the current state-of-the-art and offer readers an informed perspective of where this field is heading and what challenges we have to overcome to get to successful commercialization.

© 2021 Author(s). All article content, except where otherwise noted, is licensed under a Creative Commons Attribution (CC BY) license (http://creativecommons.org/licenses/by/4.0/). https://doi.org/10.1063/5.0047616

TABLE OF CONTENTS

I. INTRODUCTION 3
II. FUNDAMENTAL MATERIAL PROPERTIES 3
A. Compositional engineering 3
1. Perovskite structure and compositional engineering 3
2. Current and future challenges 5
3. Advances in science and engineering to meet these challenges 6
4. Concluding remarks 7
B. Bandgap engineering in halide perovskites 8
1. Status of area 8
2. Current and future challenges 9
3. Current status 9
4. Concluding remarks 10
C. Dielectric effects 10
1. Status of the area 10
2. Current and future challenges 12
3. Advances in science and engineering to meet these challenges 13
4. Concluding remarks 14

© Author(s) 2021

D. Charge carrier mobility . . . 15
1. Status of the area . . . 15
2. Current and future challenges . . . 15
3. Advances in science and engineering to meet these challenges . . . 15
4. Concluding remarks . . . 16
E. Structural investigations . . . 16
1. Status of the area . . . 16
2. Current and future challenges . . . 17
3. Advances in science and engineering to meet these challenges . . . 17
4. Concluding remarks . . . 18
F. 2D materials: Fundamental properties . . . 18
1. Status of the area . . . 18
2. Progress . . . 19
3. Current and future challenges . . . 20
4. Concluding remarks . . . 20
III. FABRICATION . . . 20
A. Solution-chemistry of hybrid perovskite semiconductors . . . 20
1. Status of the area . . . 20
2. Current and future challenges . . . 21
3. Advances in science and engineering to meet these challenges . . . 21
4. Concluding remarks . . . 22
B. Perovskite processing . . . 22
1. Status of the area . . . 22
2. Concluding remarks . . . 25
C. Thermal sublimation of perovskite films . . . 25
1. Status of the area . . . 25
2. Current and future challenges . . . 25
3. Advances in science and engineering to meet these challenges . . . 26
4. Concluding remarks . . . 26
D. CVD growth of perovskites . . . 26
1. Status of the area . . . 26
2. Current and future challenges . . . 27
3. Advances in science and engineering to meet these challenges . . . 28
4. Concluding remarks . . . 28
E. Hybrid perovskite crystals: Growth, characterization, and application . . . 28
1. Status of the area . . . 28
2. Current and future challenges . . . 29
3. Advances in science and engineering to meet these challenges . . . 30
4. Concluding remarks . . . 30
IV. CHARACTERIZATION AND PROPERTIES . . . 30
A. High open circuit voltage . . . 30
1. Status of the area . . . 30
2. Current and future challenges . . . 31
3. Advances in science . . . 32
4. Concluding remarks . . . 32
B. Charge recombination in the bulk and at the interfaces . . . 32
1. Status of the area . . . 32
2. Current and future challenges . . . 33
3. Progress . . . 34
4. Concluding remarks . . . 34
C. Interfaces . . . 34
1. Status of the area . . . 34
2. Current and future challenges . . . 35
3. Progress . . . 35
4. Concluding remarks . . . 36
D. Electron and hole transport layers . . . 36
1. Status of the area . . . 36
2. Evolution of ETL and HTL in PSCs . . . 37
3. Current and future challenges . . . 37
4. Advances in science and technology to meet challenges . . . 37
5. Concluding remarks . . . 38
E. Chemical composition and electronic structure of buried interfaces in perovskite solar cells using photoelectron spectroscopy . . . 38
1. Status of the area . . . 38
2. Current and future challenges . . . 39
3. Advances in science . . . 39
4. Concluding remarks . . . 40
F. Crystalline surfaces for momentum-resolved experiments . . . 40
1. Status of the area . . . 40
2. Current and future challenges . . . 40
3. Progress . . . 41
4. Epitaxial growth of CsPbBr3 on Au(100) . . . 41
5. Electronic structure of epitaxial CsPbBr3 on Au(100) . . . 41
6. Concluding remarks . . . 41
V. PEROVSKITE DEVICES . . . 42
A. Perovskite-based tandem solar cells . . . 42
1. Status of the area . . . 42
2. Current and future challenges . . . 43
3. Advances in science . . . 44
4. Concluding remarks . . . 45
B. Applications beyond solar cells . . . 46
1. Status of the area . . . 46
2. Current and future challenges . . . 47
3. Concluding remarks . . . 49
C. Perovskite materials for light emission . . . 49
1. Status of the area . . . 49
2. Current and future challenges . . . 51
3. Concluding remarks . . . 51
VI. CURRENT CHALLENGES . . . 51
A. Measurement protocol . . . 51
1. Status of the area . . . 51
2. Current and future challenges . . . 52
3. Proposed measurement procedures . . . 53
4. Concluding remarks . . . 53
B. Reproducibility . . . 53
1. Status of the area . . . 53
2. Current and future challenges . . . 54
3. Advances in science and engineering to meet these challenges . . . 55
4. Concluding remarks . . . 56
C. Ion migration . . . 56

© Author(s) 2021

1. Status of the area . . . 56
2. Current and future challenges . . . 57
3. Advances in science . . . 57
4. Concluding remarks . . . 57
D. Stability . . . 58
1. Status of the area . . . 58
2. Current and future challenges in this area . . . 59
3. Concluding remarks . . . 61
E. Corrosion of contacts . . . 61
1. Status of the area . . . 61
2. Current and future challenges . . . 61
3. Advances in science and engineering to meet these challenges . . . 63
4. Concluding remarks . . . 63
F. Replacement of toxic lead . . . 63
1. Status of the area . . . 63
2. Current and future challenges . . . 64
3. Advances in science and engineering to meet these challenges . . . 64
4. Concluding remarks . . . 65
G. Perovskite solar modules: Progress, challenges, and future applications . . . 65
1. State of the art . . . 65
2. Current and future challenges . . . 66
3. Concluding remarks . . . 67
H. Data-driven prediction of novel hybrid perovskites . 67
1. Status of the area . . . 67
2. Current and future challenges . . . 67
3. Progress . . . 68
4. Concluding remarks . . . 68

I. INTRODUCTION

Lukas Schmidt-Mende, Vladimir Dyakonov, Selina Olthof

In the last decade, research on metal halide perovskites has made tremendous progress. The certified efficiency of perovskite solar cells (PSCs) has increased drastically to over 25% (see Fig. 1) and can now compete in this respect with Si-technology. The simple fabrication, including even processing from solution, opens the possibility to integrate perovskite processing into an industrial roll-to-roll fabrication, which allows mass production at low cost. Applications are not limited to single junction solar cells anymore. The chemical tuning of the bandgap of the material makes it especially interesting for application in tandem solar cells. Additionally, also other applications, such as light emitting devices, photodetectors, and memory devices, have already been successfully demonstrated.

Researchers have significantly increased their understanding of the material class, concerning, for example, the requirements to form stable 3D perovskites or employing larger cations for 2D structure formation. Intriguingly, the success of this novel high performance semiconductor revived the search by theoreticians and material scientists to look beyond and explore further promising complex perovskite compositions.

In this Roadmap, we cover important research aspects concerning metal halide perovskite semiconductors. We address in Sec. II some fundamental properties and the specific features of this material class. In Sec. III, we cover aspects of fabrication. The processing of efficient perovskite semiconductor films has been improved drastically over the last few years. Nevertheless, the solution chemistry is still an important research field, and processing of efficient perovskites films from solution, sublimation, and chemical vapor deposition (CVD) needs further investigation. Next to thin films, the growth of single crystals has been demonstrated.

The characterization and understanding of devices (see Sec. IV) has been drastically improved since the first report of a solar cell application. However, many details of the underlying physical mechanisms are still hardly understood. Next to the perovskite film itself, the interface formation and the adjacent transport layers (TLs) play a decisive role for the device efficiency and stability.

While perovskite solar cells are the main focus of this Roadmap, we also address tandem solar cell stacks in combination with non-perovskite absorbers as well as applications beyond solar cells, such as lasing and light emitting diodes (LEDs) in Sec. V. There are still major challenges, which we address in Sec. VI. In particular, if it comes to commercialization, many additional aspects need to be taken into account. Currently, the correct and precise measurement of perovskite-based devices is still an issue as well as the reproducibility. The role of ion migration and charge carrier mobility in the device and at the interface is still only partly documented. The attempts to replace the toxic lead in these thin films with less toxic materials have only been partly successful. One major challenge remains to be solved is the stability of the devices. Even though there has been tremendous progress, the device stability is still not comparable to silicon devices. This makes data-driven prediction of novel hybrid perovskites an exciting option to find materials overcoming the current limitations. When it comes to commercialization, one also needs to consider fabrication issues related to upscaling laboratory-scale devices to larger areas.

Despite these challenges concerning understanding device physics and functionality, there has been no material class in the recent past that attracted such high interest and introduced a paradigm change concerning the efficiency of solution processed semiconductors for solar cells. In this Roadmap, we summarize various important aspects to provide an overview of the current status of perovskite semiconductor research and indicate promising directions for future research efforts.

II. FUNDAMENTAL MATERIAL PROPERTIES

Feray Ünlü, Khan Moritz Trong Lê, Sanjay Mathur, Selina Olthof, Andrei D. Karabanov, Doru C. Lupascu, Laura Herz, Alexander Hinderhofer, Frank Schreiber, Alexey Chernikov, David A. Egger

A. Compositional engineering

Feray Ünlü, Khan Moritz Trong Lê, Sanjay Mathur

1. Perovskite structure and compositional engineering

Single perovskites generally adopt the crystal structure similar to $CaTiO_3$, which is described with the ABX_3 formula, where the

© Author(s) 2021

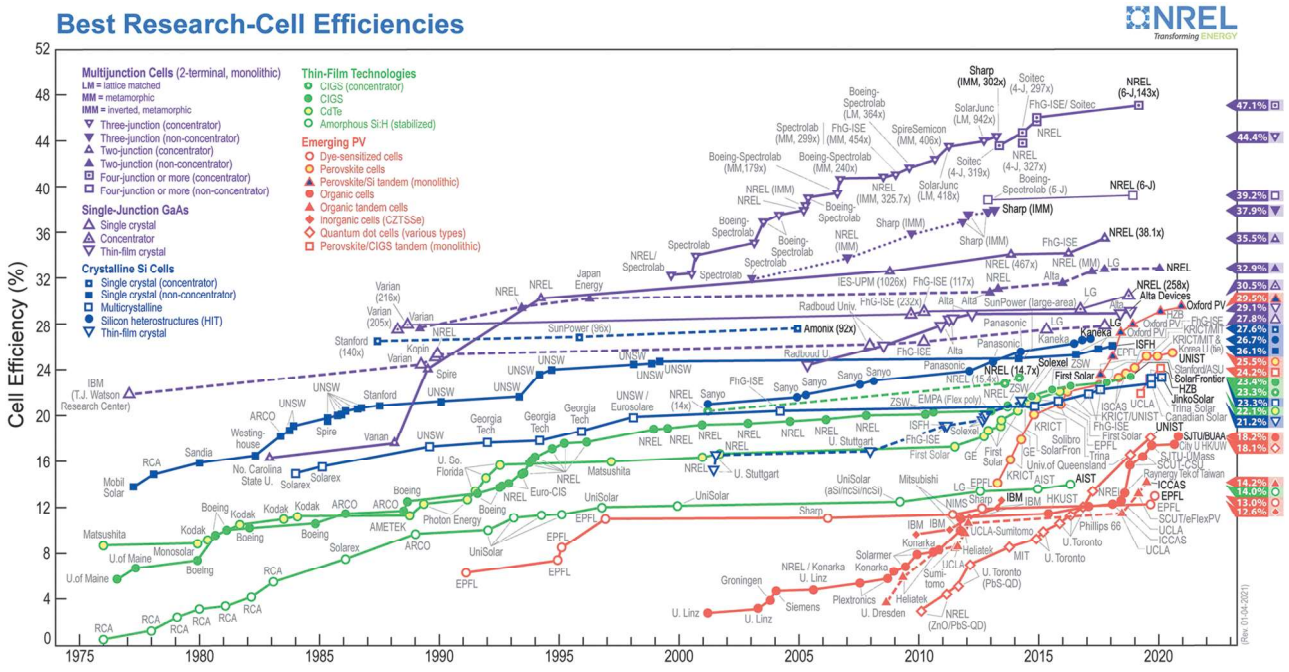


FIG. 1. Development of solar cell efficiencies over the years.[1]

B-cation is coordinated octahedrally by X-anions and the A-cation fills the cuboctahedral voids and compensates the negative charge. Single metal halide perovskites (MHPs) adopt the ABX_3 structure consisting of a three-dimensional network of corner-sharing BX_6 octahedra, where the B atom is a group 14 metal cation (typically Sn^{2+} or Pb^{2+}) and X is typically Cl, Br, or I. On the A-site, Cs^+ or organic cations, such as $CH_3NH_3^+$ (MA) and $NH_2CH{=}NH_2^+$ (FA), can be used that are chosen to balance the total charge and to stabilize the lattice. For achieving structural stability in a 3D perovskite, the ionic radii of the cation and anions should follow the empirically derived Goldschmidt tolerance factor t given by the radii of A (r_A), B (r_B), and X (r_X),[2]

$$t = \left(\frac{r_A + r_X}{\sqrt{2} r_B + r_X} \right). \tag{1}$$

Tolerance factors between 0.71 and 0.9 result in tetragonal or orthorhombic structures. For halide perovskites (X = F, Cl, Br, and I), the tolerance factor follows $0.81 < t < 1.11$. If t lies in the range 0.89–1.0, a cubic structure is likely to be stabilized, whereas higher t values (>1.0) result in a hexagonal structure.[3,4] Recent analysis of structural data has shown that the tolerance factor t can differentiate between perovskite and non-perovskite materials in only 74% cases and a new tolerance factor (τ) was recently introduced that derives the structural predictions from the same parameters (composition, oxidation state, and ionic radii) and higher accuracy (>90%),[5]

$$\tau = \frac{r_X}{r_B} - n_A - \frac{\frac{r_A}{r_B}}{\ln\left(\frac{r_A}{r_B}\right)}. \tag{2}$$

Despite these parametric guidelines, structural transformation is common for any given perovskite composition, with higher symmetry structures being prevalent at high temperatures. Based on these considerations, the large ionic radii of Pb^{2+} (188 pm) and of halides (e.g., I^-, 220 pm) limit the ionic radius of the A site cation. As a result, only organic cations with two or three C–C/C–N bonds or inorganic cations, such as Cs^+ (188 pm), can form stable 3D perovskites.[6] The crystal lattice of the perovskite is associated with a certain flexibility and defect-tolerance such that constituting ions can move and migrate within the lattice.[7] The migration of ions and their mobility in the lattice causes the drift in ionic defects already at room temperature, which is responsible for the hysteresis of energy devices.[8,9] On the other hand, the geometrical stability and allowed range of tolerance offer a broad compositional space for chemical engineering of new perovskites by systematic substitution of cationic and anionic constituents and to obtain mixed-cation or mixed-anion perovskites through isovalent substitution in the parent (AMX_3) compound. In this context, the compositional engineering is shown to be a viable strategy for tuning the optoelectronic properties and to control the phase stability and check detrimental phase transformations.[10,11] Low formation energies allow facile exchange of ions within the A- and X-sites, whereas the formation energy of B-site doping is higher.[12,13]

a. Anion mixing and exchange in halide perovskites. Given the fast anion exchange kinetics in hybrid perovskites, a broad range of compositions have been synthesized by *in situ* processing or post-synthesis chemical transformations. Intermixing of bromides or chlorides in the iodide perovskites has shown to be effective in changing the transport behavior of charge carriers and the bandgap energies.[14,15] For instance, the lattice parameters and bandgap energy of $MAPb(I_{1-x}Br_x)_3$ were observed to linearly scale-up in relation to the Br^- content.[16] Furthermore, the inclusion of chloride into $MAPbI_3$ was found to significantly enhance electron and hole diffusion lengths over 1 μm in the mixed halide $MAPb(I_{1-x}Cl_x)_3$,

© Author(s) 2021

which is ten times higher compared to diffusion lengths in $MAPbI_3$.[17,18] The influence of halide anions on the perovskite's bandgap is further described in Sec. II B.

b. A-site cation mixing and exchange in halide perovskites. A-site cation engineering includes the partial substitution of the parent organic or inorganic (e.g., MA or Cs^+) cation by one or more co-cations, such as formamidinium (FA^+) and/or other alkali metal cations (K^+, Rb^+), considering the appropriate sizes to maintain the tolerance factor. This approach was particularly successful in optimizing the stability of perovskites against undesired phase transitions, nonradiative defect sites, and was shown to be effective in enhancing carrier lifetimes and bestowing chemical stability under ambient conditions. The perspective of A-site cation engineering in tuning the functional properties and structural stability of halide perovskites were recently elaborated by Mathur and co-workers that can be found elsewhere.[19] When considering the connectivity of the metal halide octahedra as the classification element, the perovskites also exist, besides the 3D configurations, in 2D layered structures, 1D chains, and 0D isolated structures.[20] Since there are no size rules for low dimensional networked perovskites, A-site cations of different lengths can be introduced, and therefore, low-dimensional perovskites offer tunable bandgaps and absorption/emission properties. Mitzi reported on 2D layered perovskites analogous to Ruddlesden–Popper phases with organic ammonium cations ($R–NH_3^+$); here, the MX_4^{2-} anions are surrounded on both sides by organic cations stabilized by hydrogen-bonding.[21] For 2D perovskites, the interlayer spacing between the inorganic layers is the determining factor for bandgap tuning, the longer the interlayer spacing, the wider is the bandgap. Hence, a combination of 2D and 3D perovskites is promising in terms of developing high efficiency solar cells with long-term stability. In 2D/3D systems, small organic cations are partially replaced by bulkier organic spacer cations; for instance, Grancini *et al.* reported one-year stable and hole transport layer (HTL)-free 2D/3D $(AVA)_{0.3}(MA)_{0.7}PbI_3$ [(AVA) aminovaleric acid, $HOOC(CH_2)_4NH_3$] PSC, without any obvious loss in power conversion efficiency (PCE 12.9%) in power conversion efficiency (PCE 12.9%) under ambient air.[22] In addition, LEDs based on mixed layered perovskite materials were shown to display impressive performance and stability due to the mixed compounds acting as a photocarrier concentrator, funneling the charge carriers from high-bandgap materials to the lowest-bandgap ones to ultimately boost the external quantum efficiency (EQE).[23] More details on 2D perovskites and their properties will be discussed in Sec. II F.

c. B-site cation mixing and exchange in halide perovskites. B-site doping was shown to be very effective in tuning the bandgap and to influence the charge carrier dynamics of the perovskites. For example, substitution of the Pb^{2+} site in lead-based perovskite thin films or single crystals by isovalent Sn^{2+} was found to reduce the bandgap,[12,13] leading to broadening of the absorption range[24] and longer charge carrier lifetimes.[24] The Sn^{2+}-doping also offers a plausible alternative to reduce the amount of Pb^{2+} content in perovskite compositions. In analogy, Ge^{2+} was recently incorporated into the double cation $FA_{0.83}MA_{0.17}Ge_xPb_{1-x}(I_{0.9}Br_{0.1})_3$ where the solubility of GeI_2 was ameliorated by MACl additive achieving PCE over 22% and enhanced stability and photoluminescence (PL) lifetimes.[25] Moreover, Ge^{2+}-doping in Sn based perovskites evolved to a strategic pathway to suppress the self-oxidation of Sn^{2+} to Sn^{4+}, which in combination with A-site cation engineering and surface passivation has achieved a PCE of up to 13% so far.[26] Other bivalent dopants, such as earth alkali metals (Ca^{2+}, Sr^{2+}, or Ba^{2+}), are reported to affect the bandgap and crystalline phase.[27,28] Looking at other main group elements, it was reported that Bi^{3+}- or In^{3+}-doping stabilizes the photoactive black perovskite phase at lower temperatures.[29,30] Transition metals, such as Mn^{2+}, were investigated thoroughly in $CsPbX_3$ nanocrystals, leading to enhancement of long-lifetime luminescence by generating an additional exciton state associated with the Mn d–d emission.[31] Rare-earth elements, such as lanthanoids, were used in perovskite nanocrystals achieving down- and up-conversion and quantum cutting.[31]

2. Current and future challenges

a. The ion mobility and phase segregation challenge. The emergence of perovskite solar cell (PSC) technology manifests the potential of chemical transformation in developing and designing new materials. In this context, the organic–inorganic hybrid perovskites have moved from phenomenological studies on compositional engineering and structure–property relations to establish themselves as drivers of an alternative photovoltaic (PV) technology as evident in their superior optoelectronic properties, summarized for a few representative compositions in Table I. While A-site cation engineering shows enhanced phase stability and durability under ambient conditions along with tunable bandgap properties through halide mixing, there are still stability issues under illumination, solar cell operation, or reverse bias conditions due to ionic migration and phase segregations in photoabsorber materials (Fig. 2). The ionic conductivity in perovskite halides was described as early as 1983[32] where in $MAPbI_3$, the I^- anion was determined to be the major migrating species with four orders of magnitude higher mobility than the MA^+ cation.[33] In particular, in mixed halide or multiple cation perovskites, the ion migration can lead to phase segregation. The phenomenon of J/V hysteresis (different voltage scanning direction with differing output current) is connected to the ion-migration (see Sec. VI C) induced poling of the perovskite,[34] causing reactions with adjacent (charge transport) layers and electrodes leading to overall device degradation.[35] Although belonging to the most efficient hybrid perovskite absorbers, mixed I/Br compositions tend to phase segregate under illumination leading to, e.g., I^--rich and Br^--rich phases.[36] Furthermore, organic–inorganic hybrid perovskites can suffer under thermal fluctuations, e.g., under reverse bias, which can lead to local heating and damage of the solar cell due to volatile organic components.[37] A possible solution against volatile components is to switch to the all-inorganic perovskites $CsPbX_3$; however, the wider bandgap due to mismatch of orbital energies and polymorphism are currently persisting challenges. One of the advantages of halide perovskite photovoltaics is their solution processability at low temperatures; however, the resulting polycrystalline thin films possess high defect density and pinholes that are detrimental for the functional performance. In particular, at the surface of perovskite films and grain boundaries, a large number of defects are present as the outermost ions are not saturated. The vacancies lead to trap states (energy levels in the perovskites bandgap) that reduce the overall charge transport and thereby the solar cell efficiencies, although these are shallow traps (near the band edges).[38] These limitations have been overcome by passivating the surface through chelation of molecular reagents.[39,40]

© Author(s) 2021

TABLE I. The highly efficient perovskite compositions leading to solar cells with PCEs beyond 20%.

Perovskite	E_g (eV)	V_{oc} (V)	Jsc (mA/cm^2)	FF (%)	PCE (%)	References
$MAPbI_3$	1.55	1.16	22.4	83	21.6	Kogo *et al.*[41]
$FAPbI_3$	1.47	1.22	25.18	74.6	21.07	Zhang *et al.*[42]
$FA_{0.1}MA_{0.9}PbI_3$	1.54	1.08	23.61	79.6	20.26	Zhang *et al.*[43]
$(FAPbI_3)_{0.92}(MAPbBr_3)_{0.08}$	1.53	1.16	24.5	82.3	23.4	Yoo *et al.*[44]
$(FAPb_3)_{0.95}(MAPbBr_3)_{0.05}$	1.51	1.14	24.92	79.6	22.7	Jung *et al.*[45]
$Cs_{0.05}(MA_{0.17}FA_{0.83})_{0.95}Pb(I_{0.83}Br_{0.17})_3$	1.62	1.15	23.5	78.5	21.1	Saliba *et al.*[46]
$Rb_{0.05}(Cs_{0.05}MA_{0.17}FA_{0.83})_{0.95}Pb(I_{0.83}Br_{0.17})_3$	1.63	1.19	24.5	77	20.6	Saliba *et al.*[47]
$K_{0.04}(Cs_{0.05}MA_{0.15}FA_{0.85})_{0.95}Pb(I_{0.85}Br_{0.15})_3$	1.65	1.13	22.95	79	20.56	Bu *et al.*[48]
$GA_{0.02}Cs_{0.05}MA_{0.15}FA_{0.79}Pb(I_{0.82}Br_{0.19})_3$	1.62	1.18	23.64	75	20.96	Jung *et al.*[49]
$K_{0.03}Cs_{0.05}(FA_{0.87}MA_{0.13})_{0.92}(Ge_{0.03}Pb_{0.97})\ (I_{0.9}Br_{0.1})_3$	⋯	1.18	24.67	78	22.7	Kim *et al.*[25]

b. Open questions regarding perovskite precursor inks and the final perovskite thin films. The straightforward chemical synthesis was one of the triggers in witnessing the combinatorial explosion of compositionally engineered hybrid perovskites; however, the fundamental mechanism and insights into the formation of precursors, nature of chemical species in precursor solutions, existence of dynamic equilibria, and controlling effects of solvents (polar/non-polar) remain elusive. A better understanding of nucleation of perovskite crystals and their transformation on the substrate in a single phase perovskite composition is crucial for their application in devices and scale-up of the technology readiness level from prototypes to industrial production. Controlled synthesis of perovskite precursor ink, including precursor-intermediates that can be influenced both *in situ* (inks) and *ex-situ* (on-substrate) by coordinating ligands, is one of the deterministic factors for achieving a reproducible figure of merit for perovskite materials and devices produced in different laboratories. In particular, a better understanding of both homogeneous and heterogeneous nucleation of perovskite crystallites is inevitable to decipher the role of surface chemistry, purity of starting materials and employed solvents as well as additives in solution concentration, and precursor ratios and quality of chemicals to comprehend the various synthetic concepts that have been designated as novel and unique, albeit minimal differences in the underlying chemical interactions and nature of species. Since the interplay of above-mentioned factors is essential for homogeneous crystallization, the reproducibility of "ideal" inks continues to be difficult that aggravates with the increasing number of components, for instance, in multi-cation and anion systems. The high variability of compositions and properties makes it difficult to predict solar cell parameters, i.e., J_{sc} or V_{oc}, and associated energy losses when compared with the technological maturity of silicon photovoltaics. Current challenges of perovskite inks include a comprehensive understanding of nucleation and growth of perovskite crystals in solution and stabilization of perovskite inks to prevent uncontrolled growth and precipitation of thermodynamically preferred species from a mixture of components that is an intrinsic barrier in the scalability and shelf-life of perovskite inks that are crucial for deposition techniques, such as spin-coating, ink-jet printing, or slot die coating. In addition, relatively less attention has been devoted to fundamental studies on the chemical structure of perovskites based on mixed-cation compositions, for instance, there are no conclusive single crystal data for multi-component perovskites, which would elaborate the structural and positive influence of small amounts of dopants on the photoconversion efficiency. In addition, the homogeneity of distribution in such multiple-cation and mixed anion perovskites and its impact on the device are still an open question.

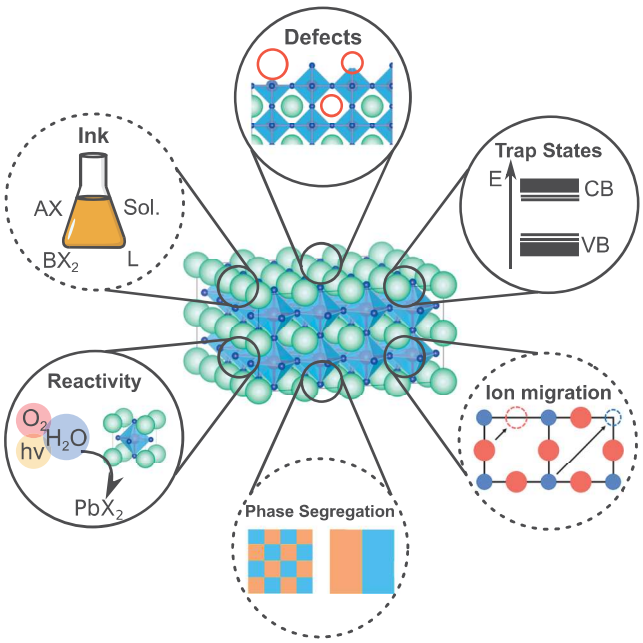


FIG. 2. Current challenges for hybrid perovskite research.

3. Advances in science and engineering to meet these challenges

a. Compositional engineering in bulk and surface. Long-term stability of perovskite materials and devices represents one of the crucial requirements besides the high efficiency to achieve large-scale production and commercialization of halide perovskite PV technology. To reach structural stability the A-site cation alloying has proved to be a viable concept to achieve a tolerance fit.[50] For example, Knight and Herz reported that the triple A-site cation

© Author(s) 2021

(Cs, FA, and MA) and quadruple cation (Cs, FA, MA, and Rb) seem to be particularly stable. Similarly, the mixing of the 25% Sn/75% Pb perovskite can lead to increased photostability; however, more research is needed to evaluate the stoichiometric balance and its interrelation to structural and electronic stability [auto-oxidation of Sn(II)].[51] Additionally, suppression of ion migration leading to phase segregation is mandatory to retain long-term stability under device operation and illumination. Among the common approaches to reduce ionic drift includes the implementation of polymers or organic molecules as barriers and surface passivating agents.[52,53] Implementation of 2D perovskites is another effective strategy to suppress ion migration, although this method is not applicable to all perovskite compositions as specific ligands are necessary. Furthermore, addition of chloride is shown to be effective in reducing the halide phase segregation, which is related to improvement of grain growth, crystallinity, grain boundary passivation, reduction in halide defect densities, and increased energetic barrier for halide migration.[36] Hence, compositional engineering is essential for designing stable and efficient perovskite absorbers; however, in order to progress faster and facilitate the screening of suitable chemical compositions, machine learning (ML) approaches are emerging as effective and effort-saving strategies.

b. Machine learning: A modern tool in designing efficient and stable lead halide perovskites. With more powerful computing and advances in artificial intelligence, machine learning (ML) based approaches hold the promise for faster and more efficient investigation of new materials. Instead of empirical strategies, the optimal parameters are developed by training the machine with reliable data and a working algorithm. First-principle calculations (structure–property relation by quantum mechanical methods) are computationally demanding; however, an algorithm based ML can reduce the resources and make predictions by learning from existing data.[54] For example, 333 data points collected from 2000 publications were fed into a system to predict high performance perovskite compositions for solar cells based on the prediction of underlying physical phenomena to some extent.[55] Li *et al.* used similar approaches with data derived from high throughput density-functional theory (DFT) calculations to demonstrate alternative and economic pathways than iterative experimental attempts. They evaluated the compositional engineering with respect to perovskite stability to suggest more effective predictions that go beyond the conclusions drawn from the empirical tolerance factor.[56] Castelli *et al.* demonstrated the computational screening of oxide containing perovskites using the computational materials repository. Their work showed that out of a huge number of possible perovskites (around 19 000), only 47 were interesting for water splitting applications,[57,58] manifesting the power of computational methods in order to save experimental resources and time. However, also DFT calculations need a lot of computational energy and time; therefore, machine learning models can reduce these cost factors. For instance, Li and co-workers demonstrated the application of machine learning models to predict the thermodynamic stability of oxide perovskites using a DFT database of 1900 oxide perovskite energies, ending up with four stable compositions.[59] Similar studies for the discovery of new and stable perovskite structures were made by using machine learning approaches and the field is still under development.[60–62] Furthermore, Kirman *et al.* used machine learning to create a high-throughput system for perovskite single crystal synthesis.[63] Hartono *et al.* investigated organic halide capping layers for $MAPbI_3$ surface passivation by a machine learning framework, in which 21 different organo-halide capping layers were screened in order maintain perovskite stability under ambient conditions.[64] The further development of ML processing is beneficial for investigating mechanisms, predicting device performances, and facilitating the experimental challenges to synthesize perovskite materials with adequate compositions and even proposing non-hazardous alternatives.

4. Concluding remarks

a. Perovskite solar cell technology and commercialization—The marketability gap. The high photoconversion efficiencies and possible low production and material cost (attributed to solution processability, cheap perovskite materials, alternative low-cost electrodes, and charge selective layers) have established hybrid perovskites as a potential contender to challenge silicon or other semiconductor photovoltaics. The application of perovskite materials and fabrication of devices in industrial environment has been successfully demonstrated;[65] however, what is holding back the large-scale deployment of perovskite-based solar cells is the instability and shorter lifespan of perovskite absorbers. The challenge of environmental deterioration of perovskites has been tackled by encapsulation technologies,[66] although the intrinsic instabilities of the material under applied voltage, light-soaking, thermal stress reflected in hysteresis, and performance drift continue to compromise the long-term stability. Furthermore, the use of expensive charge selective materials, e.g., spiro-OMeTAD, and gold electrode in the highly efficient PSCs increases the levelized cost of electricity (LCOE) by up to 500%–800% compared to the FTO/SnO_2/perovskite/NiO/Cu module, which was calculated to be 4.43 US cents kW h^{-1} (in comparison, the single junction Si-module has 5.50 US cent kW h^{-1}).[67] Therefore, a lot more research and concerted efforts are necessary to address the shortcomings of charge carrier transport, ionic mobilities, and main sources of losses in bulk and at the interfaces, which is a materials challenge.

Therefore, using the big dataset from the perovskite research community as a basis, compositional engineering coupled with modern machine learning systems can enable faster transition of perovskite science and technology toward commercialization. Beside this, investigations based on solution chemistry, crystal structure, nucleation, defect engineering, and device physics are essential to ensure a steady growth in understanding of the perovskite material as the class of perovskite material offers relatively unexplored versatility in applications.

b. The multi-purpose perovskite materials: Beyond solar cell applications. Other potential applications of perovskites include near-infrared (NIR) solid-state and wavelength tunable 390–790 nm whispering-gallery nanolasers based on $CH_3NH_3PbI_{3-a}X_a$ (X = I, Br, and Cl).[68,69] Compositional engineering of perovskites is also beneficial for increasing the stability of FET devices, as shown by Cs incorporation into the $MAPbI_3$ lattice and employing Rb as the passivating agent.[70] Hybrid perovskites were also found to be useful for photodetection[71] and as sensors for a variety of gases, such as NH_3, O_2, and NO_2, and even some volatile organic compounds.[72–74] Within the last decade, interest in the lead halide perovskite based

© Author(s) 2021

LED has rapidly increased, as the fabrication cost is comparable to organic LEDs (see Sec. V C). The operational stability, however, is far behind, and the half-lifetime of a few hours under continuous bias is significantly short when compared to the >10 000 h of lifetime needed to compete with organic light emitting diodes (OLEDs). Nevertheless, the beneficial effects of compositional engineering efforts as demonstrated in the improvement of the PV performance also underscore the potential for further development, especially in the exploration of new application fields (see Sec. V B) for this interesting class of functional materials.

B. Bandgap engineering in halide perovskites

Selina Olthof

1. Status of area

Halide perovskites, with the structure ABX_3, can be composed of a variety of different cation and anion species, as introduced in Sec. II A. Depending on this composition, the bandgap E_g can vary from ~1.2 to 3.6 eV, as summarized in Fig. 3(a), for all primary lead and tin compounds (discussion on Ge will be omitted in this section).[75]

This variability in E_g is highly intriguing for the field of optoelectronics as the bandgap can be tailored to meet the individual need. For example, for single absorber solar cells, a bandgap around 1.3 eV is ideal, while as a wide gap cell in tandem applications, much larger bandgaps are desired (for example, ~1.7 eV in combination with a silicon sub-cell; see Sec. V A for further examples). In the case of light emission (see Secs. V B and V C), appropriate bandgaps for display applications range from ~2 eV for red emission to ~2.8 eV for blue emission.

The changes in bandgap come about due to differences in the valence band (VB) and conduction band (CB) position that are influenced by the atomistic level positions, the lattice size, and lattice distortion. Band structure calculations show[76] that the top of the VB consists of hybridized metal s (M_s) and halide p (X_p) states, as sketched in Fig. 3(b). The VB is therefore directly influenced by the energetic position of the atomic M_s and X_p orbitals that are related to the element's electronegativity χ [with $\chi(Pb) < \chi(Sn)$ and $\chi(I) < \chi(Br) < \chi(Cl)$]. Hence, a change in metal or halide component will lead to a shift in the VB, as depicted in Figs. 3(b-ii) and Figs. 3(b-iii). The bottom of the CB consists of metal p (M_p) and halide s (X_s) orbitals. The orbital overlap is smaller for the conduction band, and therefore, hybridization is not as pronounced, leading to a more ionic bond in which the CB is dominated by the metal state; it was found that the atomic p states of Sn (i.e., 4p) and Pb (5p) are rather similar in energy [Fig. 3(b-ii)].[75]

The onsets of CB and VB are furthermore affected by the lattice size, which is determined by the ionic radii of the different anions and cations. As depicted in Fig. 3(b-iv), a smaller lattice will result in confinement effects, shifting the atomic levels slightly upward affecting both VB and CB. In addition, the hybridization will increase, which mainly affects the VB and shifts it upward.

Finally, also the bond angles will affect the degree of hybridization. The highest orbital overlap is achieved in a cubic perovskite structure, resulting in a small bandgap. In a phase transition, e.g., to a tetragonal or orthorhombic structure due to a lowering of the temperature or introduction of an ion with large mismatch in radius, the lattice becomes distorted and the degree of hybridization will reduce.

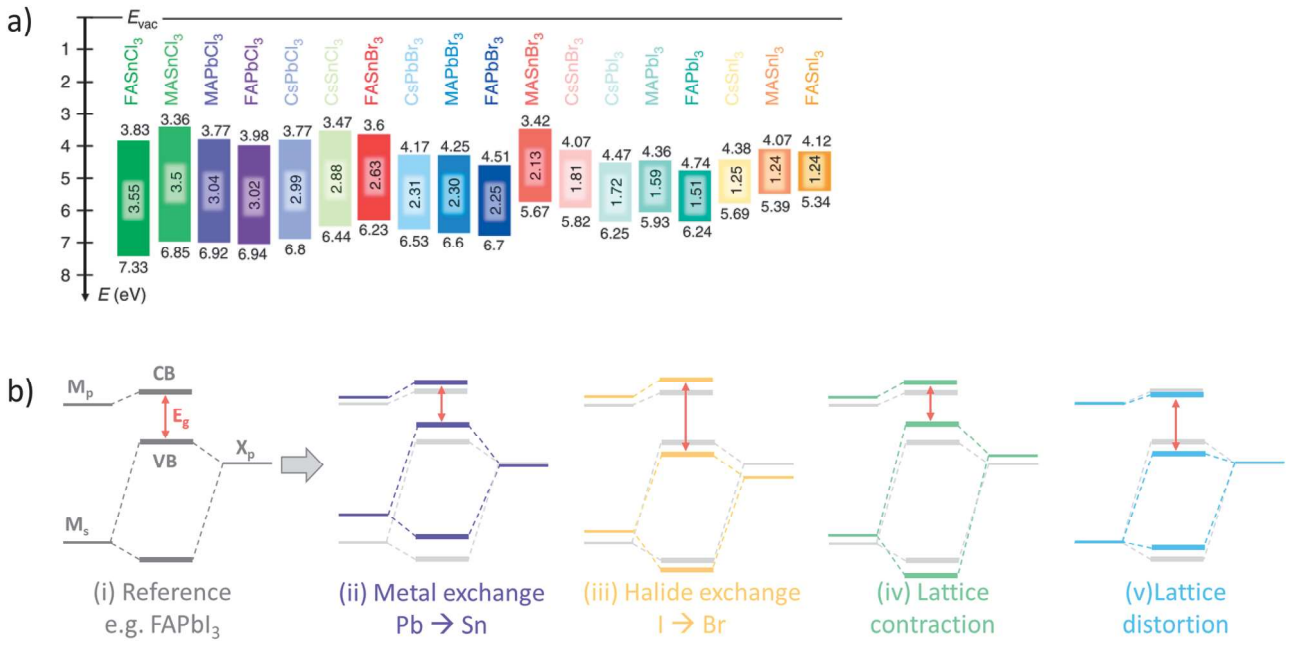


FIG. 3. Bandgap changes in the halide perovskite: (a) Experimentally determined changes in bandgap due to variations in perovskite composition. Reproduced with permission from Tao *et al.*, Nat. Commun. **10**, 2560 (2019). Copyright 2019 Nature Publishing Group. (b) Schematic energy level diagrams, showing how the perovskite VB and CB are formed from the atomic metal and halide states and how changes in composition, lattice size, or lattice distortion influence these levels. The image is adapted from Refs. 75 and 79.

© Author(s) 2021

This will lead to a lowering of the VB, as sketched in Fig. 3(b-v), thereby increasing the bandgap; again, the CB is likely not affected as much due to its stronger ionic character.

Obviously, not only pure ABX_3 perovskite structures can be prepared but also different ions can be mixed on the A, B, or X site. This way, the bandgap can be gradually tuned as was already shown in the 1970s by cooling melts containing appropriate proportions of precursors, e.g., by Barrett *et al.* for $CsSnBr_xCl_{1-x}$[77] or by Weber for $MAPbBr_xI_{1-x}$.[78] Reports regarding recent thin film measurements will be discussed below.

2. Current and future challenges

A critical issue when it comes to the comparability and validity of reported perovskite bandgaps is the inconsistency with which these values are determined. Often, the transmission T through a layer of material is analyzed, and from this, the absorbance A (with $A = -\log T$) or decadic absorption coefficient α (with $\alpha = A$/layer thickness) is reported. Less often, also the reflection is included in the analysis, which nevertheless is necessary to correctly determine A and α. Strictly speaking, from such a transmission and/or reflection measurement, the absorption/reflection *onset* can be extracted, which is not identical to the bandgap.

For a direct bandgap, where VB and CB exhibit a square root dependency on energy, the following relationship can be derived:

$$(\alpha h\nu)^2 \propto (h\nu - E_g).$$

Therefore, plotting $(\alpha h\nu)^2$ vs the photon energy in a so-called Tauc plot results in a straight line from which the optical gap can be extracted. In the case of an indirect semiconductor, the exponent of the left-hand side term changes to 1/2; for 3D halide perovskites, theoretical calculations consistently show direct transitions at the R point, so the equation shown above should be valid. Performing this Tauc plot analysis is commonly considered to be the more accurate approach for bandgap determination; however, there are limitations: (i) Issues can arise from the presence of trap or impurity states where the distributions of CB and VB electronic states do not terminate abruptly at the band edges. Using, e.g., photothermal deflection spectroscopy, which can measure down to very low values of α, transitions between localized and tail states can be seen as widening of the so-called Urbach tails or even as distinct sub-bandgap features; only above the Urbach tail region a Tauc plot analysis is meaningful. Even though gap state formation is not very pronounced in the defect tolerant halide perovskites, they have been observed, for example, in mixed halide systems.[80] Telling apart bandgap changes and defect state formation is not trivial. In the past, bandgap narrowing of a perovskite crystal by impurity Bi-doping has been reported.[81] However, follow up experiments suggest that this change was caused by a change in defect concentration.[82] (ii) Furthermore, if an exciton feature is present, then fitting the onset using a Tauc plot is inaccurate;[83] rather the theory described by the Elliott formula should be applied.[84] Here, the absorption of parabolic continuum states (band-to-band transition) is combined with an additional discrete absorption by an excitonic state. From such fits, values of the excitonic binding energy and bandgap can be deduced. However, due to the large number of fitting parameters, values extracted, e.g., for $MAPbI_3$ at room temperature using this approach vary between 5 and 29 meV. For a review over recent results, we refer to Ref. 85. In particular, lead-based halide perovskites show a rather distinct exciton feature at the band edge (see, e.g., the supplementary material of Ref. 75), which can lead to inconsistencies in reported values.

As a final remark, it should be checked whether the intended perovskite composition is indeed given in the prepared thin film. It is well-known that when processing a $MAPb(I_xCl_y)_3$ precursor solution, the incorporation of Cl ions into the perovskite crystal lattice is viable only in small quantities.[86] Furthermore, solubility issues can lead to deviations from the intended film composition, especially for Cs-containing precursors. Similarly, in the case of thermal evaporation, the severe issues related to monitoring the actual evaporate rates of the small organic cations[87] can lead to deviations in the final film composition.

3. Current status

Even though these issues regarding consistency in data evaluation prevail, we want to give an overview over the changes that can be introduced in the bandgap when the perovskite composition is tuned. For brevity, we focus on thin film measurements, therefore leaving out research on single crystals or nanoparticles.

The first work looking at mixed halide perovskite compositions was published by Noh *et al.* in 2013, investigating $MAPb(I_{1-x}Br_x)_3$.[16] They found a gradual reduction in lattice size with the increasing Br content accompanied by an apparent change in color from black to red and yellow. The change in bandgap from 1.58 to 2.28 eV is not linear and can be described by a bowing equation,

$$E_g = x \cdot E_1 + (1-x) \cdot E_2 - bx(1-x).$$

Here, the first two terms describe a linear change in bandgap between E_1 and E_2, and the last term introduces non-linearity with a bowing parameter b. The reasons for the non-linear behavior is still a subject of debate and could be related to changes in bond angles and the mixing of atomic states; for further reading, we refer, e.g., to Refs. 88 and 89. A similar bowing behavior was observed for $MAPb(Br_{1-x}Cl_x)_3$ (E_g varying between 2.42 and 3.16 eV)[90] and $CsPb(I_{1-x}Br_x)_3$ (E_g between 1.77 and 2.38 eV).[91] For $FAPbI_yBr_{3-y}$, the gap can be tuned from 1.48 to 2.23 eV, but no 3D perovskite can be formed for the intermediate compositions of $y = 0.5$–0.7 due to lattice instabilities.[92,93] This can be circumvented by introducing a fraction of the smaller cations MA or Cs.[93–95] Less studies on halide mixing have been published for tin based perovskites so far; here, the changes seem to be rather linear, for example, in $MASn(I_{1-x}Br_x)_3$ (E_g 1.3–2.15 eV)[96,97] and $CsSn(I_{1-x}Br_x)_3$ (E_g 1.31–1.75 eV).[98]

The bowing effect is more pronounced in the case of mixed-metal perovskites where it can even lead to a bandgap narrowing with respect to the values of the pure materials. This can extend the absorption into the infrared region, as first reported by Stoumpos *et al.* for $MASn_xPb_{1-x}I_3$.[99] Absolute values reported in the literature differ somewhat due to the issues discussed above, but it seems that a reduction by 50–130 meV can be achieved in this mixed system compared to pure $MASnI_3$;[89,99,100] in the case of $FASn_xPb_{1-x}I_3$, the reduction is 100–200 meV.[79,88,89] For Br compounds, the reported results are less consistent, but bandgap narrowing in thin films has also been observed.[89,101,102] In an extensive study, Rajagopal *et al.* showed[89] that the amount of bowing in the mixed-metal perovskite scales with the macrostrain present in the pure films, which affects octahedral tilting and lattice distortion.

© Author(s) 2021

Mixing A-site cations has only little effect on the bandgap, introduced by minor modifications in crystal size or variations in bond angles. Such a variation of the A site cations is rather of interest for changing the phase or temperature stability of a perovskite system (see Sec. II A). Changes in E_g are mostly less than 100 meV, as, e.g., reported for $FA_xMA_{1-x}PbI_3$[103,104] and $FA_xMA_{1-x}PbBr_3$.[94] However, in mixed perovskites with significant changes in lattice distortion, the effect can be larger than 200 meV.[79,105]

4. Concluding remarks

Overall, there is a complex interplay between variations in atomistic energy levels, lattice size, and octahedral tilting/strain that leads, in most cases, to some degree of non-linearity in the bandgap change when the composition of a perovskite film is gradually tuned, as depicted in Fig. 4. With these different effects at play, it is not trivial to predict E_g values of mixed perovskite systems, and carefully evaluated and consistent measurements are needed to provide this information.

As a further remark, the bandgap can be influenced by other parameters, such as temperature, pressure, or confinement effects in nanoparticles. For brevity, these topics have not been discussed here but present further avenues that widen the utilization of this material class and can help to understand their fundamental properties.

C. Dielectric effects

Andrei D. Karabanov, Doru C. Lupascu

1. Status of the area

The high efficiency of perovskite solar cells relies on high carrier mobilities, effectiveness of exciton break-up, and a long lifetime of the generated charge carriers. In this section, we show that all three are directly related to dielectric effects.

In order to understand dielectric effects, one has to realize that these can be very scale dependent. Before entering into the details of halide perovskites, we will outline a few general aspects.[106]

Dielectric effects reflect the response of matter to an electric field WITHOUT DC conductivity. So essentially, one has to consider the response of a capacitor to an electric field keeping in mind that this capacitive effect can occur on very different length scales. Under AC-electric fields, conductive components will arise also in the dielectric response, which is the reason why complex impedance is introduced.

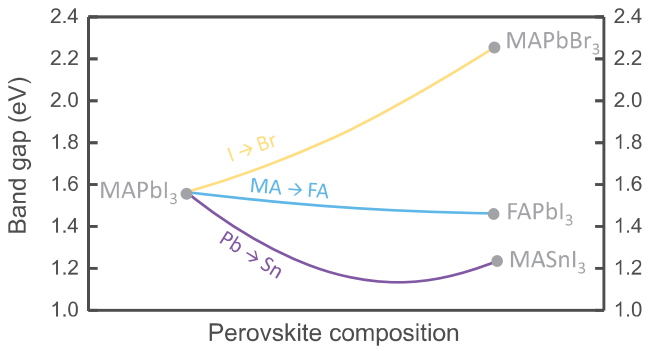


FIG. 4. Schematic change in bandgap upon the replacement of various A, B, or X site ions starting from $MAPbI_3$. Non-linear changes (i.e., bandgap bowing) are present to some degree in most cases, while bandgap narrowing is only observed for Pb–Sn mixtures.

The simplest dielectric effect is realized in the deformation of the electronic shell of an atom with respect to the position of the nucleus. Under an external field, the atom itself thus forms an electric dipole. After field removal, such an atomic dipole disappears. A similar effect can occur one scale up. In particular, in an ionic crystal, the positions of the ions are shifted under the action of an external field. Dipole formation now arises due to the shifting of the relative positions of the positive and negative ions of the lattice. After field removal, everything returns to its initial state: this is termed paraelectric behavior.

If a relative shift of ionic positions arises in a crystal lattice without the application of an external electric field, one is concerned with pyroelectric behavior because this shift is typically temperature dependent. Most systems display vanishing shifts at high temperatures and ordering when temperature is lowered. If such ordering generates permanent ordered dipoles, pyroelectric order arises. This is intrinsically related to a reduction in crystal symmetry. The most common mechanism driving the phase transition into an ordered electric state is the soft phonon effect, namely, a loss of stiffness of the crystal for one or more of its ions in the unit cell.[107] Crystals showing pyroelectric effects cannot have a center of symmetry in the point group of their crystal structure. This type of ordering is classified as long range because the ordered state extends over large parts of the prototype crystal, namely, a "domain" of electrical ordering.

If such an ordered state can be electrically reversed in between different stable orientations in the crystal, it is called the ferroelectric effect. Thus, a prerequisite for ferroelectricity is a non-centrosymmetric crystal symmetry and multiple stable orientations of mutually ordered dipoles within the same crystal.

Another contribution to dielectric effects arises if electric dipoles exist intrinsically, namely, if we are concerned with dipole molecules. The best known example is the water molecule. In halide perovskites, the methylammonium ion, among others, is an electric dipole molecule. Also many liquid crystals contain dipole molecules and show ordering. In certain cases, the ordering of the molecules can also be of long range character, and a ferroelectric effect is known in certain smectic liquid crystals.[108]

The rotational motion of the MA ion was early on suggested to contribute to the dielectric response[109] as was later verified in experiment.[110,111] Chen *et al.*[112] showed in experiment that point defect interaction with MA ions highly influences photoconductivity and the Hall effect. Single crystals show much better photoconductivity than thin films. Solution grown films contain the highest number of defects.[112] Despite the encountered very high numbers of defects, the authors already evoked the dipolar screening by the MA ions to warrant good conduction nevertheless.[112]

In a previous work, we showed that despite many theoretical assumptions in this sense, $MAPbCl_3$, $MAPbBr_3$, or $MAPbI_3$ are not ferroelectric. They exhibit an antiferroelectric phase transition in the range 100–150 K[110] and show no long range ordering above this temperature. The ionic lattice shows paraelectric behavior with a very high dielectric constant of roughly $\varepsilon_r = 30$ up to very high

© Author(s) 2021

frequencies in the gigahertz range (~10^{10} Hz). In particular, we want to emphasize that these three solar cell materials are NOT ferroelectric at room temperature.

The fundamentally interesting effect in the methylammonium-containing materials is the dipole of the methylammonium ion itself. It is known that water molecules, due to their high dipole moment, strongly interact with ions and other matter. One of the effects is micellon formation, namely, the ordering of the molecules around a charged entity, typically in the radial direction and oriented to mitigate the field of the charge carrier at the center, a typical screening effect. This effect, e.g., dominates dissolution of ionic crystals. A micellon is a local state of ordering. It arises in suspensions, emulsions, ceramic slurries, biological systems, etc.

The interesting fact about the halide perovskites containing methylammonium or formamidinium is that these molecules can rotate in their lattice locations WITHOUT long range ordering. Thus, their response is very similar to a state in which they would be in a liquid state and can in a broader sense be compared to spin glass states in magnetic systems.

Now, the charged entities in a semiconductor are an electron or a hole. We proved experimentally[110] that two mechanisms screen the electric charge of these electronic charge carriers. The first and classical mechanism is the formation of a Fröhlich polaron, namely, the relaxation of the crystal lattice of an ionic solid toward the charge. The second one arises due to the very local reorientation of the methylammonium dipole ions toward the respective charge.

We called the entity, charge carrier plus rotated dipole ion, a *micellon*. This micellon provides roughly 50% of the screening effect, namely, an increase in the relative dielectric constant. The remainder stems from ionic shifts in the unit cell, the classical Fröhlich polaron formation. The combination of both was termed hyperpolaron by us (Fig. 5)[110] in order to illustrate the strong impact of this new type of charge carrier, which is solely due to dielectric screening on the properties of the methylammonium lead halides and potentially other crystals of this family that provide rotating molecules within the crystal structure.

The next question now concerns exciton breakup: How does a high local dielectric response alter the exciton binding energy? A useful analogous picture to understand the role of the dipole ions is to imagine this like a dissolution process of an ionic entity in water. The breakup of the ionic bond is much facilitated by the gain in energy due to the adherence of the surrounding water molecule dipoles. After screening, the two ions can separate. A similar process arises in the methylammonium lead halides: the two charge carriers formed during light absorption, forming the exciton, rapidly become screened. On the time scale of processes, likely the exciton forms first, then polaronic screening arises, and its time constant is slightly shorter than for molecular rotation. Then, the molecules rotate to add to the screening. Effectively, the Coulomb interaction of the electron and the hole is largely reduced, which is the same as saying that the exciton binding energy drops dramatically due to the dielectric effect.

One counter argument could be that effectively the binding energy of the charge to the lattice response is very large due to polaron formation. Thus, a small polaron should form that is localized (an electronic state deep in the bandgap). The ingenious detail is that there are two mechanisms providing the screening, each operating at other typical relaxation frequencies. Thus, the coupling arises to a much broader frequency spectrum than simple lattice relaxation. This avoids total localization of the deformation of the lattice because, effectively, a jump out of the energy well mechanism operating at another frequency helps to suppress full localization and small polaron formation. One could even imagine an energetic double well problem where the difference in intrinsic frequencies could drive a beat frequency, but theoreticians will have to deal with these details in future work.

Another important aspect of the dielectric screening is its effect on localized defects, such as dopants, ionic vacancies, interstitials, or anti-site defects. All these represent electrical charges in the lattice and thus form scattering sites for electron transport. On the time scale of lattice vibrations, these defects remain localized (even though defect jumps also arise due to collective excitation by phonons, but their constructive interference is a rare event). Hence,

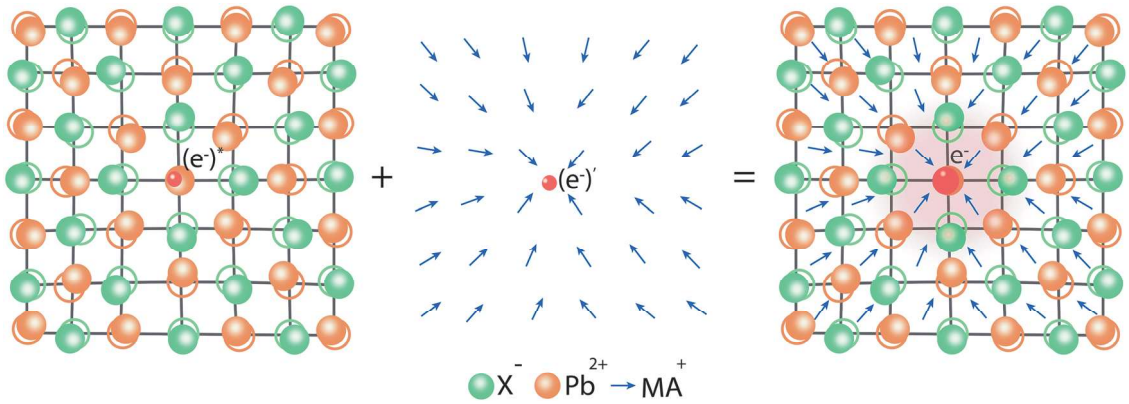


FIG. 5. Fröhlich (lattice) polaron (left), micellon (center), and the resulting hyperpolaron (right). Full screening of one electron by both mechanisms is taking place (right) up to frequencies of 10^{10} Hz; thus, the partial electronic charge is a sum of these polarization mechanisms: $(e^-)^* + (e^-)' = e^-$. Image similar to Ref. 110.

© Author(s) 2021

point defects are statically localized in the context of electron transport. Therefore, all dielectric contributions present in the crystal, even the slow components, will provide screening of the localized point defect. The charge effectively experienced by a bypassing electron or hole is smaller by a factor of 60 than in the unscreened scenario. Silicon only provides $\varepsilon_r = 11$. Dielectric defect screening in methylammonium lead halides is thus six times more effective than in silicon.

Another assumption was made that photoexcited electron and hole pairs could be separated in internal junctions between ferroelectric domains.[113] After a long debate, it was concluded that tetragonal $MAPbI_3$ is not ferroelectric for the following reasons: most importantly, the centrosymmetry of the I4/mmm space group forbids ferroelectricity and no ferroelectric P(E) hysteresis is observed.[110] Locally using scanning piezoforce microscopy, no dependence between the applied voltage and the resulting strain response and no polarity inversion with the change in the applied high voltage were seen, both being inherent to a ferroelectric.[114]

Dielectric properties of completely inorganic metal halide perovskites are also of great interest because such systems show better stability compared to hybrid halides.[115] One of the prominent examples is $CsPbX_3$. This material also has a high dielectric permittivity (Fig. 6) leading to effective screening, but the contribution from dipole rotation (e.g., the MA-ion) is not available. Thus, at low frequencies, the dielectric constant amounts to merely half of the one for $MAPbX_3$. This reduced screening, in particular, of defects can explain the lower power conversion efficiency of $CsPbX_3$ perovskite solar cells, as more charge carriers are scattered at defects and the effective charge carrier mobility is reduced.[116]

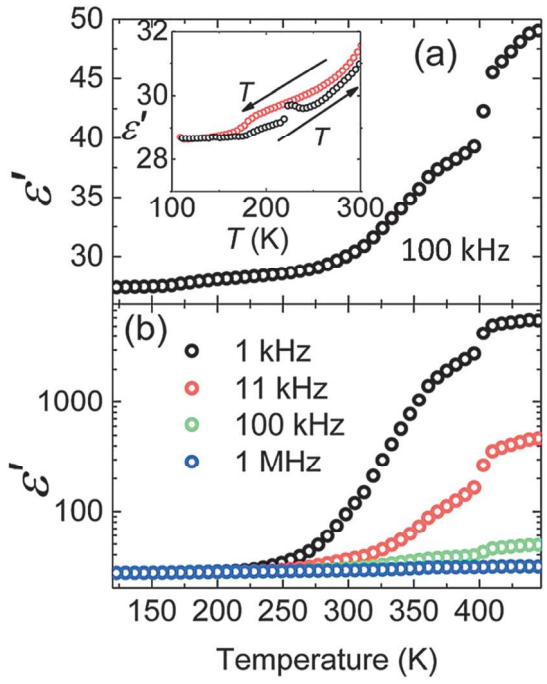


FIG. 6. (a) Real part of the dielectric permittivity vs temperature for a $CsPbBr_3$ single crystal measured at 100 kHz upon cooling; the inset shows heating and cooling. (b) Measurement of temperature dependence of the real part of the dielectric permittivity with different frequencies. Adapted from Ref. 116.

2. Current and future challenges

Polarons form in any semiconductor due to the finite dielectric response, namely, its high frequency components. The higher the dielectric constant, the stronger is the polaron formation and its associated trapping energy. Due to their very high dielectric constant, the charge carrier mobilities in the lead halide perovskites are reduced in comparison to conventional semiconductors. Miyata *et al.*[111] used broadband dielectric spectroscopy in the frequency range 10^6–10^{13} to see the response of polarons to the electric field in single crystals of all-inorganic $CsPbBr_3$ and hybrid $MAPbBr_3$.

As seen in Fig. 7, in $CsPbBr_3$, the dielectric constant is constant around $\varepsilon_r = 20$ from 1 MHz to 100 GHz and is around 60 in $(CH_3NH_3)PbBr_3$. The liquid-like rotational relaxation between 10^{10} and 10^{11} Hz of the organic polar cations (dropping from 50 down to 20) is the same mechanism as called micellon before. The lifetimes of polarons in hybrid $(CH_3NH_3)PbBr_3$ are increased because their recombination is significantly hindered by this liquid-like polarization response.[111] The change in dielectric constant from 10^6 to 10^{10} Hz by $\Delta\varepsilon_r = 10$ can be related to a dynamic stiffening of the lattice to higher frequencies, being more pronounced in a hybrid lattice than in an all-inorganic system.

The dielectric response is also partly due to the lone-pair activity of Pb^{2+}. These lone pairs can be responsible for the reduction of electron–hole recombination, leading to the increased carrier lifetimes. The polar distortions induced by lone pairs influence dielectric properties in these crystallographically centrosymmetric phases.[117]

The photoinduced change in the relative permittivity ($\Delta\varepsilon_r$) gives information about the polarization in the perovskite systems. Conventional perovskites, such as $MAPbI_3$ and $FAPbI_3$ exhibit no measurable photoinduced changes in the real component of relative permittivity ($\Delta\varepsilon_r$). Double and triple-cation perovskites show high values of $\Delta\varepsilon_r$, meaning that more complex mechanisms lead to the polarization response of double and triple-cation perovskites.[118]

$FA_{0.83}Cs_{0.17}Pb(I_{0.9}Br_{0.1})_3$ (FACs) and $(FA_{0.83}MA_{0.17})_{0.95}Cs_{0.05}Pb(I_{0.9}Br_{0.1})_3$ (FAMACs) enable high power conversion efficiencies. Hong *et al.*[118] examined the frequency-dependent time-resolved microwave conductivity (TRMC) at frequencies of 10 GHz helping to reveal molecular motions of A-site cations. $\Delta\varepsilon_r$ of the above-mentioned compounds was measured as a function of time before, during, and after illumination by a nanosecond pulsed laser.

It was found that there is a proportionality of change in relative permittivity to the photogenerated carrier density (Fig. 8).[118] ε_r decays with a shorter time constant than conductance, meaning that the photoinduced free charge carriers induce an immediate additional "dielectric" response that rapidly decreases while the lifetime of free carriers is significantly longer. The mechanisms explaining this effect locally are not yet determined. The photoinduced polarizability in FACs is larger in comparison with FAMACs.[118] The local mechanisms behind this difference remain to be determined. The local polarizability could, e.g., be related to exciton lifetimes on the different organic cations.

© Author(s) 2021

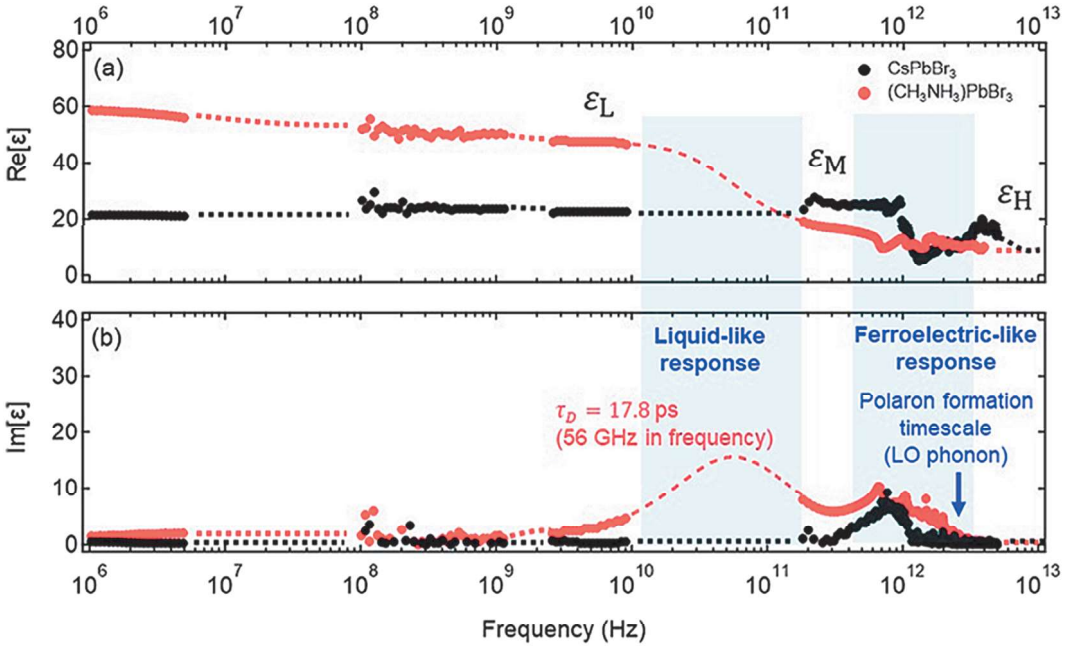


FIG. 7. (a) Real part, Re(ε), and (b) imaginary part, Im(ε), of the broadband dielectric spectra of $(CH_3NH_3)PbBr_3$ (red) and $CsPbBr_3$ (black). THz-TDS (time-domain spectroscopy) was used in the range of 0.2–5 THz, impedance spectroscopy with the micro-sized planar electrode method for 0.1–10 GHz, and impedance spectroscopy with a conventional plate capacitor method for 1–5 MHz. In the region of 1 10^{10}–2 10^{11} Hz, the Debye relaxation model was used to fit dielectric function of $(CH_3NH_3)PbBr_3$. Reprinted from Miyata *et al.*, J. Chem. Phys. **152**, 084704 (2020) with the permission of AIP Publishing.

3. Advances in science and engineering to meet these challenges

Apart from conventional 3D perovskites, 2D and 1D crystal structures are studied nowadays. Claims on ferroelectricity in these systems could be justified due to the lower symmetries of crystals, but experimental verification does not typically meet the full requirements in the "ferroelectrics"-society. As we do not want to exclude the validity of these data, a brief summary of this work follows.

Several 2D perovskite ferroelectric structures were presented recently.[119–121] The change in the dimensionality is reached by the substitution of the A-cation by organic molecules, such as benzylamine(C_7H_9N),[120] hexahydroazepine ($C_6H_{13}N$),[119] and others. Ferroelectricity can be obtained by fluorination of these structures. In this process, the substitution of one hydrogen atom (monofluorined substitution) or several hydrogen atoms (perfluorined substitution) with fluorine atoms is done. This leads to the structural change and enhancement of ferroelectric performance. One of the examples is $(PFBA)_2PbBr_4$ (PFBA = perfluorobenzylammonium)—multiaxial ferroelectric with the Aizu notation of 4/mmmFmm2(s), which shows a large piezoelectric response, a spontaneous polarization of 4.2 C cm^{-2}, a high Curie temperature of 440 K, and it is a semiconductor with a direct bandgap of 3.06 eV.[120]

Another method is the substitution of A-cations by organic molecules containing organic functional groups R or S. This leads to the possibilities of changing the photofunctionality and conductivity properties of the perovskites. Moreover, the environmental stability of these materials could help in engineering the robust and highly efficient solar cell.

Yang *et al.*[122] proposed [R-1-(4-chlorophenyl) ethylammonium]$_2PbI_4$ (R-LIPF) and [S-1-(4-chlorophenyl) ethylammonium]$_2PbI_4$ (S-LIPF) 2D lead iodide perovskites, R and S denoting the enantiomers (Fig. 9). Ferroelectricity of these materials was derived from piezoresponse force microscopy (PFM)-based hysteresis loop measurements. The spontaneous polarization was calculated using the point charge model. The bandgap from a Tauc plot is 2.34 eV, which is favorable for the application in photovoltaics.[122] At present, it cannot be said whether we are concerned about real ferroelectricity or a PFM-tip induced effect.

Polarization can be increased when additional small A-site cations are introduced in the spaces of octahedral sheets, forming a quasi-2D metal halide perovskite (MHP; formula of $R_2A_{n-1}B_nX_{3n+1}$). The higher complexity of the temperature-dependent structural phase transition in these materials in comparison to the 2D MHPs is dictated by the distortion of the octahedra due to smaller A-cations, which lead to lattice displacement, providing an additional contribution to polarization.

The multi-layered (n = 3) quasi-2D MHP $(BA)_2(MA)_2Pb_3Br_{10}$ (BA = n-butylammonium, $C_4H_9NH_3$; MA = methylammonium, CH_3NH_3) was synthesized by Li *et al.*[123] by alloying the 3D MHP $MAPbBr_3$ perovskite with n-butylammonium. The organic components, namely, MA and BA, lead to the order-disorder transition, inducing electric polarization, which can be seen in Fig. 10,

© Author(s) 2021

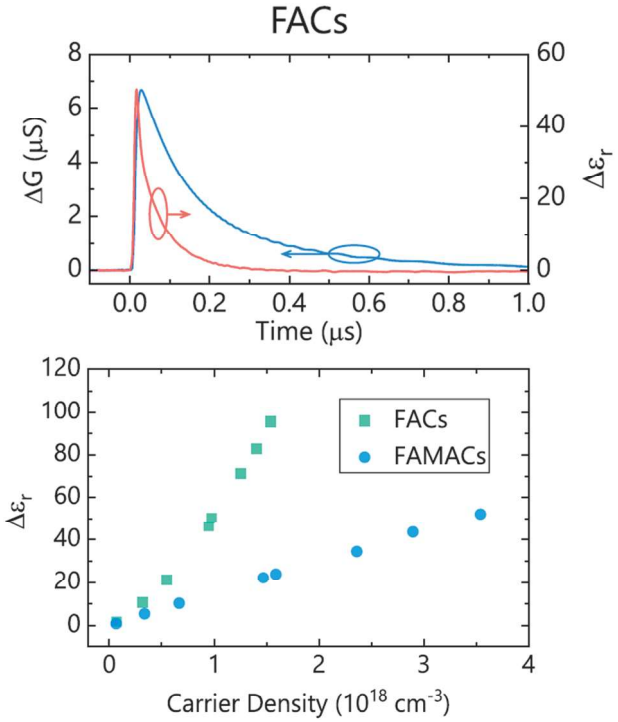


FIG. 8. Top: dependency of the real component of conductance (left axis, shown in blue) and relative permittivity (right axis, shown in red) on time. Bottom: dependency of the photoinduced change in the real part of the relative permittivity on approximate charge carrier density in $FA_{0.83}Cs_{0.17}Pb(I_{0.9}Br_{0.1})_3$ and $(FA_{0.83}MA_{0.17})_{0.95}Cs_{0.05}Pb(I_{0.9}Br_{0.1})_3$. Reprinted with permission from Hong *et al.*, J. Am. Chem. Soc. **142**, 19799 (2020). Copyright 2020 American Chemical Society.

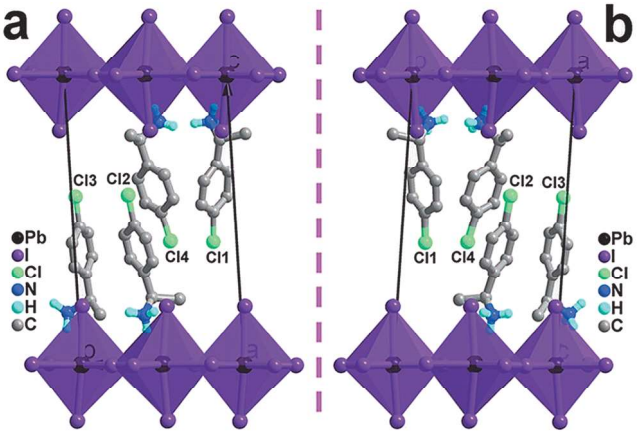


FIG. 9. Crystal structures of (a) [R-1-(4-chlorophenyl)ethylammonium]$_2$PbI$_4$ (R-LIPF) and (b) [S-1-(4-chlorophenyl)ethylammonium]$_2$PbI$_4$ (S-LIPF) 2D lead iodide perovskites, showing a mirror-image relationship. Reprinted with permission from Yang *et al.*, Adv. Mater. **31**, 1808088 (2019). Copyright 2019 John Wiley and Sons.

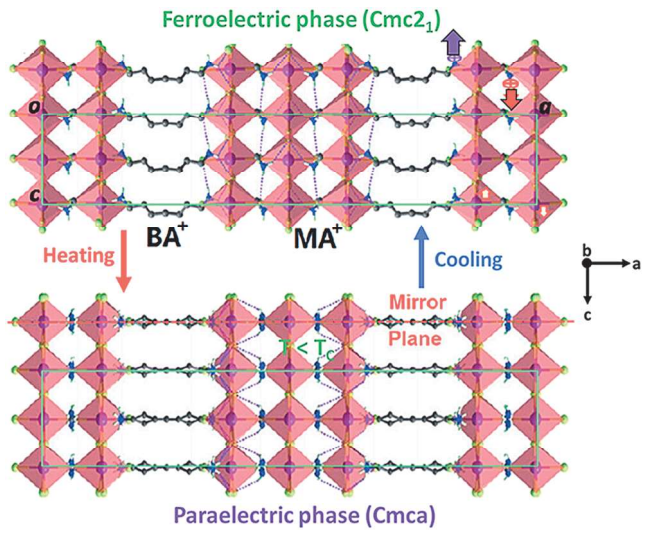


FIG. 10. Ferroelectric (Cmc21) and paraelectric (Cmca) phases of $(BA)_2(MA)_2Pb_3Br_{10}$ at 293 and 340 K, respectively. There is a deviation of negative and positive charge centers in the ferroelectric phase compared with the paraelectric phase, which is indicated by the purple and red arrows. Reprinted from Hou *et al.*, J. Appl. Phys. **128**, 060906 (2020) with the permission of AIP Publishing.

allowing for ferroelectricity. X-ray diffraction (XRD) analysis at room temperature showed that this material can be ferroelectric with a polar space group of $Cmc2_1$.[124]

A decrease in dimensionality is also possible with systems containing other organic groups as A-cations, such as (R)-(−)-1-cyclohexylethylamine (R-CYHEA, $C_8H_{15}NH_2$) or (S)-(+)-1-cyclohexylethylamine (S-CYHEA, $C_8H_{15}NH_2$), which leads to the formation of 1D R-CYHEAPbI$_3$ and S-CYHEAPbI$_3$ perovskites. These organic groups remove the inversion symmetry of the material, making it a potential ferroelectric, while the PbI_6 octahedra are responsible for the semiconducting properties. The absence of the inversion symmetry was also proven by several methods, such as density functional theory and structural and spectroscopy analysis. Ferroelectricity was confirmed with dependent synchrotron XRD, differential scanning calorimetric, temperature-dependent dielectric constant, and temperature-dependent pyroelectric current. Such materials could open new possibilities, for example, in spin-orbitronics.[125]

4. Concluding remarks

Dielectric studies play an important role in the understanding of materials for the use in the optoelectronics and photonics. The examination of different dielectric responses in a broad range of frequencies can reveal screening effects, the influence of the organic and inorganic cations on the polarizability, charge-carrier lifetime, effects stemming from the defect states, and charge carrier mobilities.

The examination of perovskite systems with different techniques, such as impedance spectroscopy, microwave or THz-time-domain spectroscopy and piezoforce microscopy, can help to reveal carrier mobilities, effectiveness of exciton breakup, and lifetime of

© Author(s) 2021

charge carriers, as well as the presence of electric polarization and ferroelectricity or the absence of these.

The challenge of revealing ferroelectricity is due to several artifacts that can arise during PFM measurements, erroneous assignment of the space group, leakage current in the ferroelectric P(E) hysteresis, and many others. Irrespective of all these techniques, a thorough understanding of the symmetry group of the crystal is the basis of assigning pyroelectric, piezoelectric, or ferroelectric effects.

D. Charge carrier mobility

Laura Herz

1. Status of the area

The performance of solar cells critically depends on efficient photocurrent extraction, which, in turn, relies on sufficient mobilities of charge carriers. As a rough guide, charge-carrier diffusion lengths, which depend on the mobility-lifetime product of charge carriers, ought to exceed the thickness of the perovskite film required to absorb a substantial fraction of the incident sunlight. Much attention has therefore been devoted toward optimizing charge-carrier mobilities in metal halide perovskites and developing a fundamental understanding of the underpinning factors.[126,127] Here, a distinction has been made between intrinsic factors, such as charge–lattice interactions that cannot fundamentally be avoided, and extrinsic issues, such as grain boundaries, defects, energetic disorder, or background doping.[126] Specifically, for the class of metal halide perovskites, the intrinsic mechanisms limiting charge-carrier mobilities are now fairly well understood.[126–130] As a first approximation, intrinsic limits are well-described within the Fröhlich model of large polarons,[131] which derives from the coupling of charge carriers to the electric polarization field generated by the collective longitudinal optical (LO) vibrational modes of the metal halide sublattice. Absolute charge-carrier mobility values derived from this model form reasonable upper limits when compared to the spread of available experimental data and seem to agree well with mobility trends with compositional variations.[126] For example, the Fröhlich model correctly predicts the experimentally observed[132] decreasing trend in charge-carrier mobility along the iodide–bromide–chloride substitution line, which derives from the increasing ionicity of the lead-halide bond and the associated changes in the dielectric response of the metal halide sub-lattice.[128–130] Similarly, increases in charge-carrier mobilities with substitution of tin for lead[126,133,134] may result from the resulting increase in LO phonon frequencies,[135] given that the Fröhlich model depends on the dimensionless ratio of LO-phonon to thermal energies. A-cation substitution (e.g., MA, FA, or Cs) has, on the other hand, been found to have insufficient influence on charge-carrier mobilities because the electric field to which charges couple arises primarily from the LO phonon mode of the lead-halide sub-lattice.[127] Such models limit the maximum charge-carrier mobilities attainable for the prototypical $MAPbI_3$ at room temperature to 100–200 $cm^2\ V^{-1}\ s^{-1}$, which is substantially lower than the equivalent value for GaAs,[127] because of $MAPbI_3$'s lower LO phonon frequency (lead is a heavy atom), higher ionicity of the polar lattice, and, in the case of conduction-band electrons, significantly higher effective mass.

2. Current and future challenges

Aside from these intrinsic limits posed by electron–phonon coupling, charge-carrier mobilities in metal halide perovskites may also be subject to extrinsic effects arising from material imperfections, which have formed a persistent challenge for a range of specific materials.[126,132–134] Charge-carrier mobilities in prototypical metal halide perovskites implemented in high-performance solar cells, e.g., $APbI_3$, where A is typically a combination of MA, FA, and Cs, are already likely to be close to what can be achieved in terms of optimized mobilities. However, lingering challenges persistently remain for specific cases, including mixed bromide–iodide lead perovskites with intermediate bromide fractions between 20% and 90%, for which poor crystallinity and charge-carrier mobility[132] combined with light-induced halide segregation[51] pose a barrier to the optimization of high-bandgap metal halide perovskites. Similarly, at the low-bandgap end, mixed lead–tin iodide perovskites have seen charge-carrier mobilities significantly suppressed by the formation of tin vacancies, which result in unintentional background hole doping that enhances the scattering of charge-carriers.[133–135] Such effects form a current hurdle to bandgap-tunability of metal halide perovskites that is particularly detrimental to the development of silicon-perovskite and all-perovskite tandem solar cells. Further challenges also remain to the development of fully accurate theoretical models of charge-carrier mobilities in metal halide perovskites that take account of the special characteristics of these materials. While the Frohlich model presents a good first approximation of electron–phonon coupling in metal halide perovskites, some difficulties arise from the inherent softness of these materials[136,137] and the presence of many atoms per unit cell, which leads to multiple LO phonon modes needing to be considered.[130] In this context, there has been much debate around the experimentally observed[138,139] $T^{-1.5}$ temperature-dependence of the charge-carrier mobility in $MAPbI_3$, which at first[140] appeared to be incompatible with a simple application of Frohlich theory. However, subsequent investigations have revealed that careful consideration of electronic couplings across the full range of low- and higher-energy LO phonon modes present in $MAPbI_3$ can replicate the experimentally observed temperature dependence suitably well.[130] In addition, anharmonicity of the lattice potential has been raised as a concern, given that metal halide perovskites tend to be fairly soft, meaning that the harmonic approximation employed by Frohlich theory could be particularly inaccurate for these materials.[51,137] Recent theoretical models[137] based on full nuclear dynamics combined with first-principles calculations avoided such implicit harmonic approximations, approximating the steep temperature-dependence of the carrier mobility in $MAPbI_3$ fairly well.[137] The extent to which such special characteristics of metal halide perovskites directly affect their optoelectronic properties will therefore form another challenge to be resolved over the coming years.

3. Advances in science and engineering to meet these challenges

With regard to bandgap-tunable metal halide perovskites comprising mixed iodide–bromide or tin–lead perovskites, further advances in charge-carrier mobilities and stable performance will no doubt be made based on the ever-improving feedback loop between material synthesis and passivation protocols and advanced

© Author(s) 2021

characterization techniques. A myriad of improvements in material morphology and reduction in defects are being made, while advanced non-contact probes of charge-carrier mobilities[126,141] have obviated the need for device fabrication to assess such parameters. However, while optimism in the field remains high with regard to raising these specific iodide–bromide and lead–tin compositions to the same optoelectronic and stability standards as their high-performing $APbI_3$ counterparts, an alternative strand has developed that focuses on the vast category of non-perovskite metal halide semiconductors.[142] Such approaches acknowledge the substantial materials space available outside the much narrower ABX_3 space,[143] including Ruddlesden–Popper two-dimensional layered perovskites, new double perovskites with mixed metals ($A_2BB'X_6$), vacancy ordered materials, networks of corner- or edge-sharing $[Metal\text{-}Halide_6]^{4-}$ octahedra, and general materials with metals in different oxidation states (e.g., 3+ and 4+). While opening a vast new materials space will offer many potential advantages not only restricted to improvements in charge-carrier mobilities but also, for example, to the pursuit of lead-free materials (see Sec. VI F), it also offers fresh challenges. Here, computational screening based on high-throughput first-principles calculations[141,143] will help to narrow down the huge parameter space, identifying promising candidates to explore for synthesis (see Sec. VI H). Continuous development of first-principles computational methods and increasing power of supercomputing infrastructures now allow for rapid materials screening, transforming the discovery of new semiconductors from the current slow, trial-and-error, "needle-in-a-haystack" search into a rapid, targeted, and systematic exploration of a vast group of potential candidate materials.[141] Further improvements in this area may also ultimately derive from the increased use of machine learning or "artificial intelligence" in such screening attempts. While such fast-screening approaches already succeed in evaluating relatively straight-forward parameters, such as chemical stability, band structure, and the resulting charge-carrier masses, more complex calculations still pose difficulties. In particular, full evaluation of charge-carrier mobilities relies on the accurate calculation of electron–phonon couplings, which still needs to be brought within reach of genuine fast-screening approaches. Such calculations may be further complicated if an enhanced presence of surfaces and increased structural flexibility potentially enhance polaronic effects in certain new metal halide semiconductors,[142] requiring a level of computational resource even higher than those currently employed for metal halide perovskites.

4. Concluding remarks

While much progress has been made over the past five years with regard to an understanding of charge-carrier mobilities in metal halide perovskites, significant work remains to be done within the wider class of metal halide semiconductors. While prototypical metal halide perovskites are now widely accepted to fall within the Frohlich picture of large polarons, some theoretical work is still required to clarify the specific couplings to existing phonon modes and the relative importance of anharmonic contributions of the lattice. Certain extrinsic material challenges also remain, in particular, for large-bandgap bromide–iodide lead perovskites and narrow-gap lead–tin perovskites. In contrast, the factors governing charge-carrier mobilities for the much wider space of non-perovskite metal halide semiconductors are still relatively unexplored. Such materials bear some resemblance to ABX_3 perovskites in that they often comprise similar octahedral building blocks. However, they may differ substantially in terms of lattice flexibility and polarizability, surfaces, and interfaces, thus opening up a vast new area of research.

E. Structural investigations

Alexander Hinderhofer, Frank Schreiber

1. Status of the area

Scattering methods (e.g., x-ray scattering and neutron scattering) are versatile tools for investigating the structure and morphology of hybrid perovskite materials. With the various scattering methods, many different characteristics of a given sample can be retrieved, including crystal structure, domain sizes, defect densities, roughness, electron densities, unit cell orientation, and phase composition.

X-ray and neutron scattering on single crystals and powder samples or thin-film samples with various degrees of texturing were used to determine the crystal structure and phase behavior of different hybrid perovskite formulations. The continuously tunable element composition of hybrid perovskites leads often to correspondingly shifting unit cell sizes and corresponding characteristics.[144]

In particular, the application of neutron scattering also allows for the determination of the position of hydrogen atoms within the unit cell and has shown that the central organic cation, often methylammonium or formamidinium, can be present in several different orientations.[145] This is related to the extremely important question of structural *dynamics* in these systems.[146]

More challenging is the structure determination for perovskite thin films, which are relevant for device applications. Such thin films are typically polycrystalline with a varying degree of texture (preferred unit cell orientation).

As a standard method for thin film characterization, often x-ray diffraction (XRD) in the classical 2θ Bragg Brentano geometry is applied or, alternatively, x-ray reflectivity (XRR) with parallel beam optics to determine the position of out-of-plane Bragg reflections. In particular, XRR from surfaces and interfaces has developed into a versatile tool, now being frequently used for the characterization of the surface/interface morphology. In the simplest version, the method measures the specular reflection, i.e., the flux of the specularly reflected radiation as a function of the angle of incidence. Specular XRR contains important information, in particular, the thicknesses and electron densities of individual layers in a layered sample as well as root-mean square roughnesses of the interfaces. For more complex structures, the interference between the layers can provide information about the overall coherence of the structure, such as the formation of superlattices.

Two additional experimental configurations are used for complete reciprocal space mapping. Using grazing-incidence small-angle x-ray scattering (GISAXS), island size distributions (small Q) can be probed and analyzed. For large values of the in-plane scattering vector $Q_{||}$, lateral structures with very small sizes (down to

© Author(s) 2021

few nm, including in-plane lattice spacings) can be probed using grazing-incidence wide angle x-ray diffraction (GIWAXS). Since, in a standard experimental configuration, the coherence width of the partially coherent primary x-ray beam is much smaller than the irradiated footprint on the sample surface, the measured signal is averaged over a statistical ensemble of all microscopic configurations of the interface.[147]

2. Current and future challenges

The demanding properties for stable highly efficient solar cell materials present several structural challenges. Even slight changes in the preparation conditions of thin perovskite thin films can lead to significant changes in the structure, texture, and morphology, which in return impact the device characteristics. This makes it essentially compulsory to include structural characterization as a matter of common practice.

Another challenge is the phase behavior of highly efficient formamidinium based perovskites. $FAPbI_3$ is unstable at room temperature and decays into a hexagonal structure. To avoid the decay, several stabilization methods can be used, for example, changing the perovskite composition or and/or solvent and temperature treatment or capping layers.[148] However, the specific phase composition of a given perovskite structure poses still a problem.

There are several challenges in the area of perovskite structure formation or conversion: for example, in high performance multiple cation perovskite materials, the cation distribution is often unknown. If a respective cation is included in the lattice, how the cations distribute (e.g., statistically vs phase-separation tendency) is sometimes unclear. This poses an interesting challenge to the structural characterization.

Another big challenge for hybrid perovskites is the fast degradation in the presence of water or oxygen. To meet this challenge, 2D-perovskites or a combination of 2D on 3D perovskite structures are applied.[150] Such structures have additional peculiarities from a structural viewpoint. The pure 2D structures include additional spacer molecules (see Sec. II F on 2D perovskites). The formation of an alternating 2D/3D structure is not possible for all kind of spacer molecules, and the domain orientation is of great importance for charge transport properties. Finally, in 2D or 3D perovskites, the 2D layer functions as a passivation against degradation. For the structural characterization, the challenge is here to obtain information on the interface between two layers. This can be achieved by applying GIWAXS and by the variation of the angle of incidence. With such a setup, depth dependent information on the crystal quality, lattice parameters, domain orientation, and the coherence length of a 2D superstructure can be obtained.[149] Some of the above issues can be addressed using scattering methods with time resolution.

3. Advances in science and engineering to meet these challenges

Real-time *in situ* scattering measurements during sample preparation or modification can be used to follow the structural evolution with a temporal resolution of down to 10 ms. The solvent layer during sample preparation can be penetrated by applying high photon energies. This allows for a detailed tracking of intermediate phases and conversion time scales, which improves the understanding of perovskite formation. Figure 11 shows, for example, the perovskite conversion of $MAPbI_3$ into $MAPbCl_3$ by the application of MACl solution on $MAPbI_3$. Figures 11(b)–11(d) shows the corresponding GIWAXS data obtained *in situ*.[151]

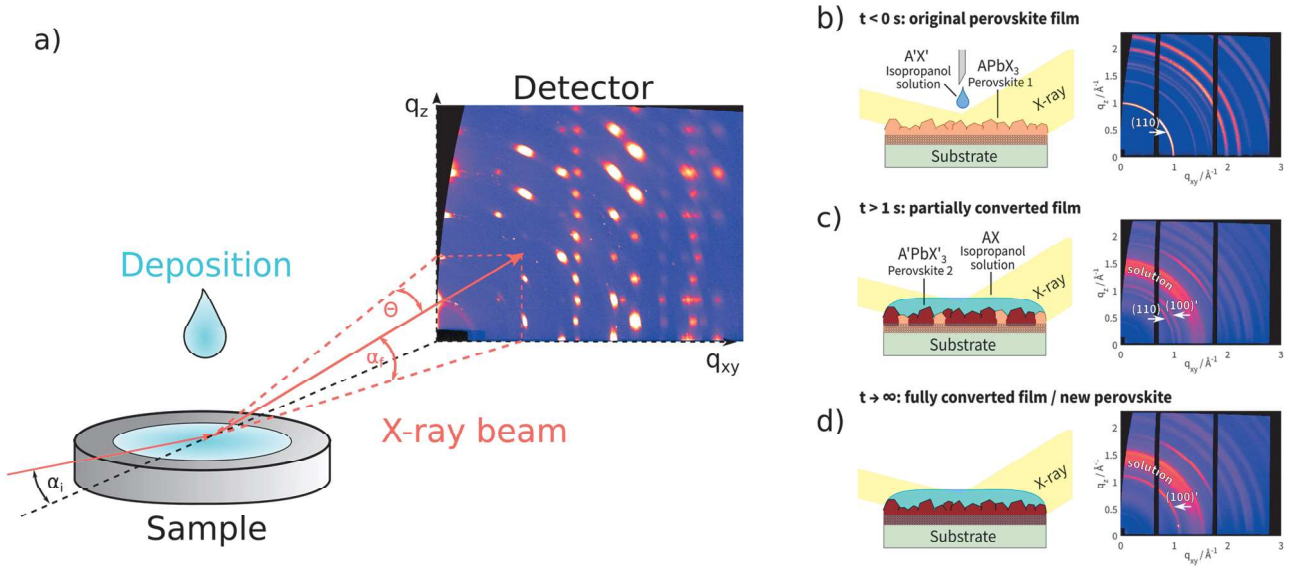


FIG. 11. (a) GIWAXS setup for *in situ* measurement during solvent deposition. (b)–(d) Illustration for the geometry of an ion exchange experiment and the progress of the conversion before (b), during (c), and after (d) the conversion of $MAPbI_3$ to $MAPbCl_3$. After drop casting of the MACl solution, the characteristic (110) peak of $MAPbI_3$ starts to disappear and the corresponding $MAPbCl_3$ (100) peak starts to appear in the GIWAXS data.[151]

© Author(s) 2021

One method to determine the element and ion distribution in mixed perovskite lattices could be anomalous x-ray scattering. Anomalous x-ray scattering (i.e., scattering employing energies near core level of specific elements) can be used to probe the distribution of the lattice site occupation of these specific elements in alloys and doped crystals. In mixed perovskites, e.g., in a mixed iodine–bromine perovskite, the correlation between iodine-occupied lattice sites and bromine-occupied lattice sites can be determined. So far, this method was mainly applied to study well-ordered inorganic perovskite structures.[152] We expect hybrid perovskite layers to be highly ordered and that anomalous dispersion x-ray scattering can be successfully applied.

4. Concluding remarks

We believe that in view of the sensitivity of the performance of perovskites to structural details, employing scattering methods is and will remain indispensable for routine characterization. Furthermore, some of the challenges to the understanding of these materials will require the application of advanced tools, such as anomalous scattering, time-resolved methods, or depth-dependent detection schemes. These require typically support from neutron or synchrotron facilities.

F. 2D materials: Fundamental properties

Alexey Chernikov, David A. Egger

1. Status of the area

In addition to three-dimensional systems, the family of metal halide perovskites hosts a rich variety of nanostructures, such as two-dimensional (2D) Ruddlesden–Popper compounds. These materials have been studied and explored for many decades[153] but have recently re-emerged with renewed interest in their potential for high-efficiency photovoltaic and light-emitting applications[154] as well as in view of their intriguing fundamental properties. This is strongly motivated by the design flexibility associated with their structural characteristics that presents opportunities from the perspectives of technology and fundamental solid state science. As schematically illustrated in Fig. 12, 2D perovskites exhibit a layered structure common for the broader family of van der Waals materials. They adopt the generic structural formula $(RNH_3)_2(A)_{n-1}BX_{3n+1}$, where RNH_3 is usually an aliphatic or aromatic cation that constitutes the spacer between perovskite layers formed by the *A*, *B*, and *X* ions with the number of sublayers denoted by the integer *n*. The release of the structural constraints that are otherwise implied for the formation of the 3D lattice offers excellent tunability of 2D metal halide perovskites, which further involve multiple types of subclasses, depending on the stacking directions in the crystal. Conceptually, these systems can be understood as natural quantum wells where the electronic excitations are confined in the inorganic layers surrounded by the organic barriers.

This structure leads to a central distinction in the optoelectronic properties of the 2D metal halide perovskites from their 3D counterparts that originates in the strongly enhanced Coulomb interaction due to both quantum confinement and, most importantly, weak dielectric screening from the organic spacer layers. It leads to the formation of highly robust exciton states with binding energies on the order of several hundreds of meV[155] that dominate the optoelectronic response of these materials. Consequently, a rather small spatial proximity of the electron and hole constituents in an exciton also results in a very strong light–matter coupling that is beneficial for efficient absorption and emission. In contrast to more traditional quantum wells or inorganic 2D semiconductors, however, the lattice of the 2D perovskites is unusually soft with characteristic features of anharmonic effects around room temperature,[156] thus promoting the coupling between excitons and lattice vibrations. Altogether, this particular combination of strong electron–electron and electron–phonon interactions

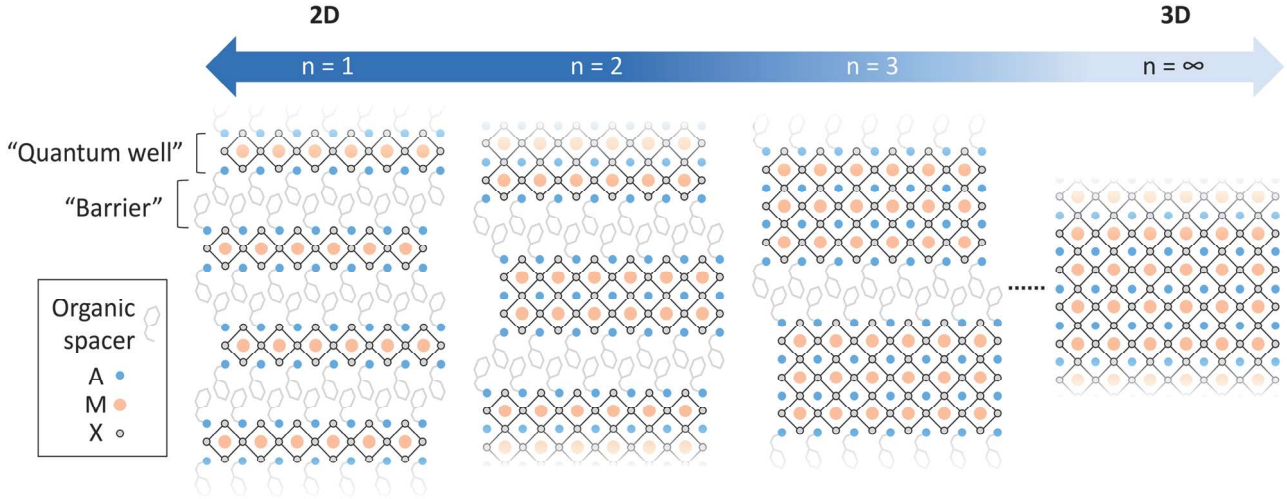


FIG. 12. Schematic illustration of the layered perovskite structure from purely 2D systems ($n = 1$) to 3D bulk ($n = \infty$).

© Author(s) 2021

renders 2D perovskites a very interesting platform for studies of fundamental many-particle phenomena in addition to their rich potential for applications.

2. Progress

In view of more recent research activities on 2D perovskites, there are several directions that are currently being explored. From the perspective of applications, these materials were found to show an improved structural stability, in particular, with respect to their exposure to moisture, including reports of photovoltaic devices with robust long-term operation.[157] 2D perovskites can also be prepared as nanoplatelets and ultra-thin layers, in close analogy to inorganic van der Waals crystals, such as graphene. Interestingly, a number of general properties of much thicker crystals, including the optical response, can be kept largely intact in these nanometer-thin structures. Among notable differences, however, is an enhancement of the exciton binding energy up to 0.5 eV and the occasional suppression of the structural phase transition characteristic for certain types of 2D metal halide perovskites.[158] More recently, fundamental properties of the excitons in these materials, such as effective masses, were also shown to strongly depend on the crystal structure and composition with distinct experimentally and theoretically demonstrated changes.[159] Furthermore, it is also interesting that 2D perovskites were found to show increased carrier lifetimes compared to their 3D analogs.[160] The key mechanisms determining their radiative and non-radiative lifetimes remain among open questions in the field. Such differences in the lifetimes, for example, could be well impacted by the changes in structure, composition, and phase-transition behavior that the pure 2D as well as the 2D–3D interfaces exhibit under various thermodynamic conditions appearing in working devices.[161]

Of particular importance remains the question regarding the spatial propagation of optical excitation in 2D metal halide perovskites. Exciton mobility is closely tied to the general nature of both exciton band structure and exciton–phonon coupling and is highly relevant for the understanding of light-harvesting and light-emitting devices based on excitonic materials. Interestingly, the diffusion of excitons in these systems has been addressed only very recently in contrast to the vast literature on this subject for their 3D counterparts. Selected results of these studies are summarized in Fig. 13. In the work by Deng *et al.*,[162] it was shown that both the exciton–exciton interactions and the effective dimensionality of the system play a crucial role for the exciton diffusivity at ambient conditions. The chemical composition of the materials and, in particular, the choice of the organic spacer turned out to be equally important, as demonstrated by Seitz *et al.*[163] and Xiao *et al.*[165] Both phenomena are found to stem from the strong variations in the strengths of the exciton–phonon coupling that depends on the stiffness of the crystal lattice. Temperature-dependent measurements of the exciton diffusivity by Ziegler *et al.*[164] then revealed a wide range of conditions from room temperature down to about 50 K, where the exciton propagation exhibits characteristic behavior of free particles in the regime of conventional diffusion. At lower temperatures, however, exciton diffusion was found to be highly anomalous, including observations of effectively negative diffusivity. The latter appeared

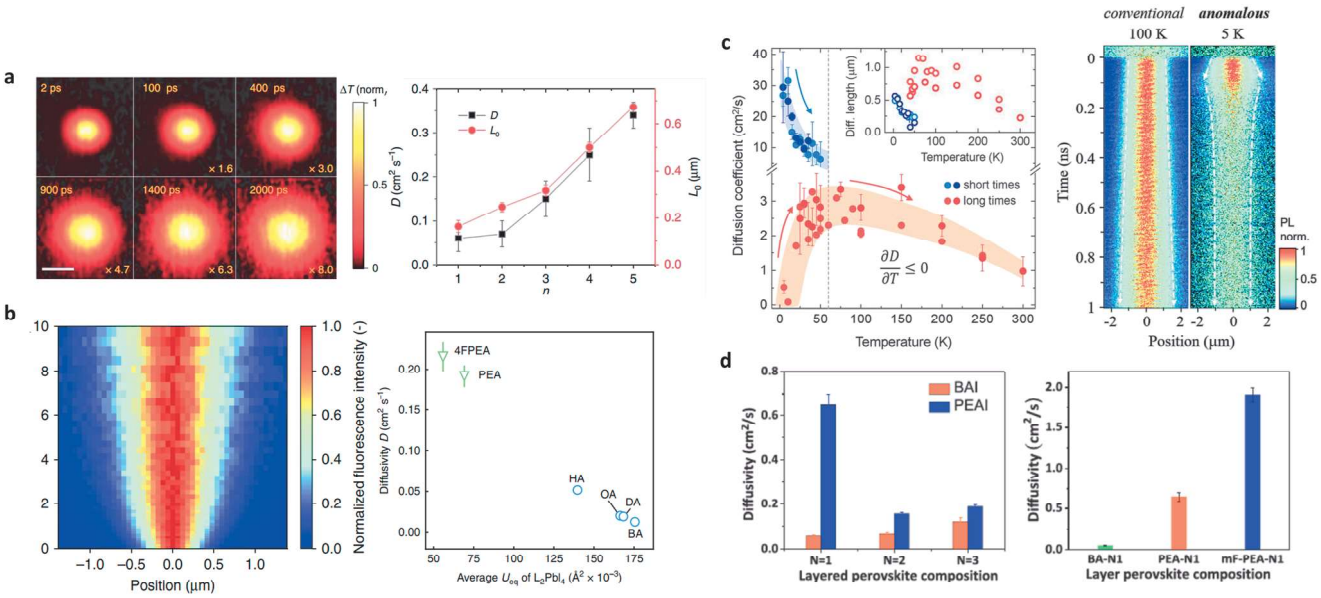


FIG. 13. Exciton diffusion in 2D perovskites: (a) influence of exciton–exciton annihilation and effective system dimensionality. Reprinted with permission from Deng *et al.*, Nat. Commun. **11**, 664 (2020). Copyright 2020 Author(s), licensed under a Creative Commons Attribution 4.0 License. (b) Impact of the organic spacer and lattice stiffness. Reprinted with permission from Seitz *et al.*, Nat. Commun. **11**, 2035 (2020). Copyright 2020 Author(s), licensed under a Creative Commons Attribution 4.0 License. (c) Temperature-dependent conventional and anomalous exciton diffusion. Reprinted with permission from Ziegler *et al.*, Nano Lett. **20**, 6674 (2020). Copyright 2020 American Chemical Society.[164] (d) Combined effects of the chemical and structural composition. Reprinted with permission from Xiao *et al.*, Adv. Mater. **32**, 2004080 (2020). Copyright 2020 John Wiley and Sons.

© Author(s) 2021

to stem from an interplay of a rapidly expanding exciton cloud, followed by a long-lived, less mobile exciton fraction with indications of localization.

3. Current and future challenges

Despite much progress in the field of 2D metal halide perovskites, a number of conceptional and technological challenges remain. For example, while there are improvements in terms of stability of 2D metal halide perovskites, it still seems necessary to continue to rely on various methods employed for material protection, especially when the samples are subjected to optical excitation. Individual approaches, such as different ways of encapsulation, turned out to be rather successful, yet it also remains unclear whether they may also affect some of the studied properties, especially for very thin layers. Further associated with that are the requirements of reproducibility and material system control that are still being explored (also see Sec. VI B). Moreover, a number of conceptual challenges to describe opto-electronic properties of 2D perovskites are intimately tied to the combination of a very strong Coulomb coupling and a highly efficient exciton–phonon interaction. Closely related is the question of how the transport of tightly bound exciton states should be fundamentally described. While there is evidence of free diffusion that resembles semi-classical quasiparticle propagation in traditional quantum wells, there are also features associated with exciton localization and thermally activated diffusion. It seems to be strongly connected to the questions of the exciton–phonon coupling, application of the polaron picture, or even effects of quantum interferences that could appear between the regimes of semi-classical diffusion and hopping for strongly localized states.[166]

These questions motivate a number of interesting challenges for future theoretical studies. It should be emphasized that 2D metal halide perovskites are challenging to be treated from first-principles considering that their crystalline unit cells involve many atoms. Furthermore, it is not clear whether their complex structures can be much simplified considering that, for example, the organic spacer cation cannot be neglected in the theory since it plays important roles in various phenomena as discussed above. Taken together, this renders theory work that would be relatively straightforward for 3D crystals, such as vibrational spectra, and quite challenging for the case of 2D perovskites. To address some of the fundamentally challenging topical questions regarding electron– and exciton–phonon effects that we emphasized above may thus very well require the development and exploration of alternative theories that are simpler numerically, such as parameterized models to complement first-principles studies.

4. Concluding remarks

In summary, 2D metal halide perovskites represent a highly interesting class of low-dimensional hybrid materials with an array of fascinating properties associated with their structural flexibility and very strong interactions of their electronic and vibronic systems. Representing a conceptual link between inorganic quantum wells and organic molecular crystals, these natural 2D structures hold much promise to explore the realm of mobile, robust quasiparticles coupled to a comparatively soft crystal lattice. Altogether, these systems offer a highly interesting material platform to study fundamental many-particle phenomena and interactions in condensed matter, motivated by both basic science and technology.

III. FABRICATION

Oleksandra Shargaieva, Caterina Cocchi, Eva Unger

A. Solution-chemistry of hybrid perovskite semiconductors

Oleksandra Shargaieva, Caterina Cocchi, Eva Unger., Michael Saliba, Mahdi Malekshahi Byranvand, Martin Kroll, Frederik Nehm, Karl Leo, Alex Redinger, Julian Höcker, Vladmir Dyakonov

1. Status of the area

A fascinating aspect of metal halide perovskites is that they are the best solution-processed materials for photovoltaic application, as illustrated in Fig. 1.[1] The success of these materials is attributed to their high defect tolerance in solution processed thin films. This opens up a myriad of processing strategies.[167] Processing procedures for metal halide perovskite thin-films as well as precursor solution compositions, here referred to as "inks," have been developed through an empirical approach based on solar cell device performance results. Most developed processing strategies are based on spin-coating as the deposition technique due to its wide availability. One of the most successful strategies involves the utilization of a mixture of solvents, and the crystallization is induced by quenching with an anti-solvent or gas-flow during the process.[168–170] Without the use of such quenching methods, the crystallization mechanism and kinetics are determined by the solvent evaporation rate.[171] For high-quality large area thin films, specially designed inks are developed in which solvents and additives fulfill the specific purpose of controlling the chemical and physical formation mechanism to result in thin-films with high optoelectronic quality and coverage.

The solvent plays a quite complex role in perovskite processing as it affects the properties of (i) the precursor inks (e.g., solubility and complexation), (ii) their processing (e.g., viscosity, evaporation rate), and (iii) the crystallization mechanism (e.g., by becoming incorporated into intermediate phases) (see Fig. 14). When preparing hybrid perovskite precursor inks, the solvent molecules interact with the precursor inducing dissociation, which is often accompanied by the coordination of solvents with the precursors and the formation of lead halide complexes of a general formula $(PbI_{2+n})^{n-} \cdot (Solvent)_m$.[172] The level of halide coordination often depends on the choice of solvent and is described in terms of coordination strength defined by solvent polarity and various solubility parameters.[173,174] Since the interaction with the solvent can be weak or strong, the choice of solvent defines the properties of the solution. The strongly binding solvents, such as dimethyl sulfoxide (DMSO), lead to the formation of complexes with a larger number of solvent molecules in the coordination sphere of Pb. The weakly

© Author(s) 2021

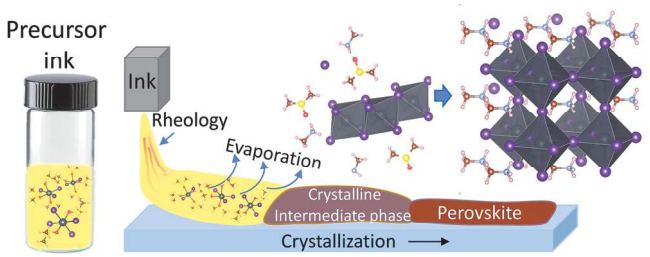


FIG. 14. Schematic representation of the role of solvent in the transformation of hybrid perovskite precursor solution into a thin film. Adapted with permission from Shargaieva *et al.*, Mater. Adv. **1**, 3314 (2020). Copyright 2020 The Royal Society of Chemistry.

interacting solvent tends to induce a stronger interaction among the precursors themselves and lead to the formation of higher coordinated polyiodide plumbates. These complexes are the key building blocks for the formation of the material from the solution. The formation of complexes and the size of colloids in the solution can also be manipulated by the addition of small molecule and polymer additives.[53,176,178]

During the deposition, the precursor concentration, solvents, and additives affect the rheological properties of precursor inks. In particular, usage of low viscosity solvents and polymeric additives is reported to improve flow properties and wetting of the solutions on the substrate aiding the nucleation and the formation of homogeneous films.[178–180] The volatility of the solvents or solvent mixtures then critically affects the crystallization kinetics.[181,182] A strong interaction between solvents and precursors can lead to the formation of crystalline intermediate phases, which then transform into perovskite phase upon full solvent removal. Weakly coordinating solvents much more readily allow for the formation of the perovskite phase upon solvent evaporation,[183] while stronger coordinating solvents often require annealing.[181] The formation of a limited amount of intermediate phases, such as $(CH_3NH_3)_2Pb_3I_8 \cdot 2DMSO$, has been found to be beneficial for the formation of high-quality perovskite layers.[184] Therefore, fine-tuning the ratio between strongly coordinating and weakly coordinating solvents is an important approach to controlling the kinetics and formation mechanism of metal halide perovskites during crystallization.

2. Current and future challenges

The quality of the thin-film depends on the chemical transformation and association of chemical building-blocks in solution into solid-state semiconductor thin-films.[174,185] Thus, the key to high-quality reproducible thin-films is understanding and, as a result, controlling the crystallization. In part, this can be achieved by designing new inks with each component of the ink fulfilling a defined function to control the chemical equilibrium between solution-complexes and thin-film formation mechanism and kinetics. It has been shown that the optimization of each parameter of the precursor solutions can lead to beneficial effects. The deliberate engineering of precursor inks requires a more in-depth understanding of the complex role of solvents and additives in precursor inks.

Establishing the key parameters for the rational engineering of precursor solutions could be achieved with the understanding of specific interactions that occur between precursors and solvents or additives. For this purpose, quantum-mechanical methods and specifically *ab initio* calculations play an essential role. Not only calculations based, for example, on (time-dependent) density-functional theory allow one to model complex systems with effective treatment of the solution environment.[186] Most importantly, they offer the flexibility to turn on or off specific coupling mechanisms. A comparison with experiments can, thus, reveal the presence and role of the underlying interaction in the examined systems and processes. The efficiency achieved by *ab initio* methods and their coupling with novel automatization tools, such as AiiDA, enable processing a large configurational space at once.[187] In this way, a rational screening for new solvents is possible. Furthermore, machine learning techniques can be applied to correlate calculated and measured data, thereby accelerating the discovery of new solvents and compounds that can be used in the role of solvent.

An additional benefit from the solvent screening is a substitution of currently used solvents for less harmful, greener, and sustainable ones. Currently, none of the commonly used solvents for the preparation of perovskite solutions (e.g., DMSO, DMF, NMP, and GBL) is satisfying both conditions of health and environmental safety.[188,189] This is especially important when moving to industrial-scale production of devices.

3. Advances in science and engineering to meet these challenges

In recent years, a number of reports have illuminated detailed mechanisms of thin-film formation during various stages of processing. In particular, the use of optical and x-ray-based techniques for monitoring structural changes during the formation of perovskite thin-films has highlighted the occurrence of crystalline intermediate phases and their phase transformation kinetics to solid-state semiconductors.[190,191] Theoretically, various models, such as the LaMer mechanism, von Weimarn crystallization rules, and Ostwald ripening, have been utilized to describe the nucleation and crystal growth processes in hybrid perovskites.[192] Combined approaches where *in situ* monitoring by means of x rays or laser reflectometry is used together with modeling of the evaporation rate demonstrate a promising direction toward understanding perovskite formation.[175,193] However, the experimental methodology to investigate the early stages of perovskite crystallization still needs to be explored. This information can potentially be obtained by employing multi-parameter monitoring where various properties (structural, optical, and electronic) are detected simultaneously. One of the promising steps toward implementation of such an approach is shown in the work of Hu *et al.*, where authors employed *in situ* grazing incidence wide-angle x-ray scattering, Fourier-transformed IR spectroscopy, and optical microscopy to monitor perovskite formation.[29] Additionally, there have been several attempts to rationalize chemical interactions in solutions and the formation of perovskite by implementing different computational methods. One of the approaches is to compare experimental data on chemical interactions in solutions and properties of precursor solutions to fundamental theoretical calculations. Recent reports indicate the presence of agglomerated iodoplumbates that are formed in high-concentration

© Author(s) 2021

solutions.[175,194] The predicted structure of these larger complexes is similar to crystalline intermediate clusters and might act as an intermediate structure between solution complexes and crystalline intermediate phases. This is particularly important as precursor solutions likely to undergo supersaturation prior to nucleation and the formation of intermediate phases.

To identify alternative "greener" solvents and solvent systems, computational methods for solvent screening have delivered promising results. A recent study by Gu *et al.* demonstrates how a combination of high-throughput screening (HTS) and a combinatorial synthesis executed with a robot can accelerate the search for suitable anti-solvents and rationalize the chemical interaction between solution complexes and anti-solvents.[195] Another interesting example is the use of machine learning combined with robot-assisted synthesis to predict the optimal conditions for the synthesis of new perovskite single crystals shown in the work of Kirman *et al.*[63]

We predict that furthering the in-depth understanding of the solvent–solvate interactions in precursor solutions and during crystallization will, in combination with high-throughput experimental methods to identify interesting solvent-mixtures and additive, catalyze the development of greener precursor solutions to process metal halide perovskites.

4. Concluding remarks

Being able to produce high-quality perovskite thin-films from solutions is a unique selling point of these materials. While a lot of developments in processing strategies and precursor solution compositions have been seemingly empirical, an increased understanding of the role of solvents and additives in the formation mechanism of metal halide perovskite thin-films from solution-complexes enables a more and more rational ink design. High-throughput synthetic methods to screen for novel precursors, solvent, and additive combinations will likely enable a swift identification of greener precursor solutions to process metal halide perovskites. We believe that a coordinated effort to illuminate the fundamental solution chemistry transformation processes through the combination of experimental and computation methods will prove highly valuable.

B. Perovskite processing

Michael Saliba, Mahdi Malekshahi Byranvand

1. Status of the area

Organic–inorganic perovskites with unique optoelectronic properties emerged as an efficient light absorber for achieving high power conversion efficiency (PCE) of perovskite solar cells (PSCs). However, the quality of the perovskite films depends on many processing parameters that require precise control during the fabrication to achieve pinhole-free (dense) films with large grains.[196]

So far, solution-processed one-step antisolvent and two-step methods utilizing spin coating techniques have been investigated for perovskite film deposition frequently (Fig. 15).[197] In the one-step, perovskite ink deposits in one step onto a substrate; however,

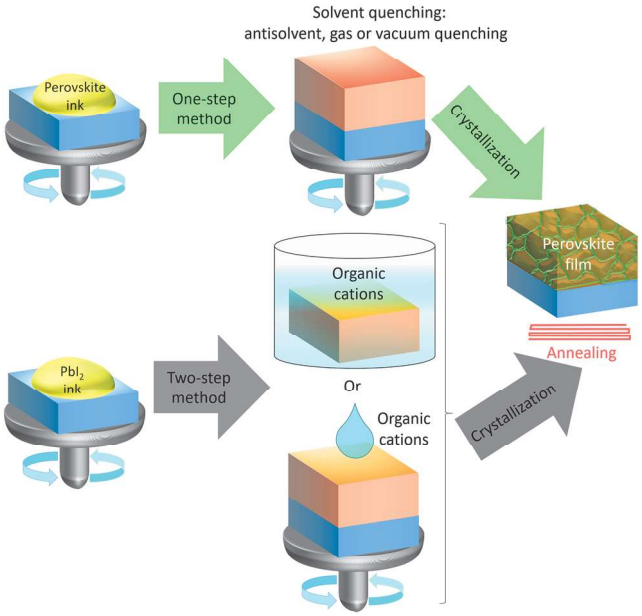


FIG. 15. Schematic illustration of one-step and two-step perovskite deposition methods.

the solvent of perovskite ink should be extracted by one of the solvent quenching approaches, such as antisolvent, gas, or vacuum quenching, to promote perovskite crystallization more efficiently.[204] In the two-step method, PbI_2 ink deposits onto a substrate at the first step, followed by the deposition of the organic cations at the second step by dipping the PbI_2 film into organic cations precursor solution[198] or by spin-coating this solution onto the PbI_2 film.[199] To date, the best PCE record of 25.2% has been achieved for small areas n-i-p mesoporous[200] and planar[201] PSCs by the one-step antisolvent method. However, considerable PCEs >24% have been reported for fabricated PSCs with a two-step method.[202,203] It should be mentioned that very promising results have been achieved by the thermal evaporation method for perovskite film deposition, presented in Sec. III C.

Figure 16 shows the typical procedure for the perovskite film crystallization. In step 1, perovskite ink must be carefully prepared based on the optimized formulation to achieve a uniform and stable perovskite film. Afterward, the perovskite ink will be deposited on the substrates (TCO-coated glass, for example) utilizing the different deposition techniques, including laboratory-scale methods (i.e., spin-coating) or large-scale methods (i.e., blade-coating, slot-die coating, inkjet printing, and spray coating) (step 2). The perovskite ink should be forced into a supersaturated state, i.e., solvent quenching, by applying antisolvent, gas quenching, vacuum solvent extraction, and air blading, on wet perovskite films (step 3), which promotes the nucleation process (step 4). Finally, crystal growth will be facilitated by annealing (step 5) with different methods, resulting in completed perovskite films. It is well known that the quality of perovskite film depends strongly on controlling the nucleation and growth rates, i.e., steps 4 and 5, which are related to the concentrations of the precursor and inducing supersaturation in the wet film. To achieve a highly uniform and dense perovskite film,

© Author(s) 2021

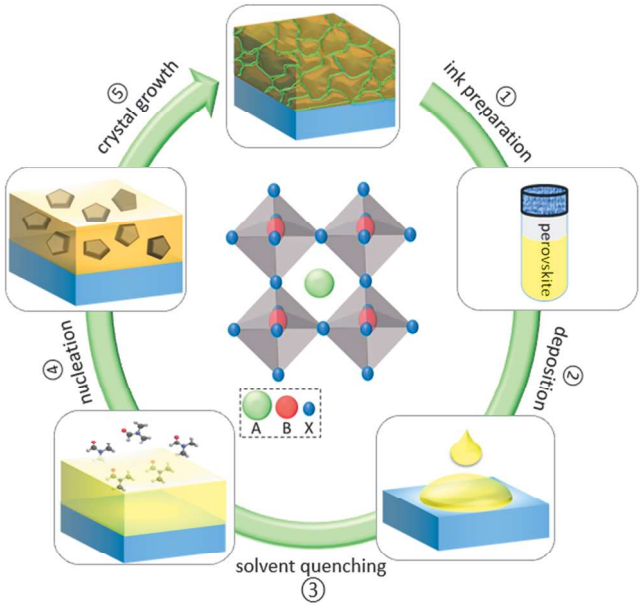


FIG. 16. Schematic illustration of the typical steps for perovskite processing.

fast nucleation and slow crystal growth have been beneficial. Altogether, given the crucial role of high-quality perovskite films for achieving high-performance PSCs, developing a reliable and repeatable crystallization process is of the essence. Here, we provide the challenges, progress, and open questions in different steps of perovskite processing.

a. Perovskite ink (step 1). A double cation perovskite, i.e., $(FAPbI_3) \times (MAPbBr_3)_{1-x}$, has been introduced as an efficient formulation for perovskite ink preparation because it helps facilitate the crystallization process and assists in stabilizing the "black phase" of $FAPbI_3$.[204] Later, Saliba *et al.*[46,47] demonstrated that adding a small amount of alkali metal cations, such as Cs^+ and Rb^+, to perovskite ink can improve the perovskite film quality further, resulting in high stabilized PCEs of 21.1% and 21.6%, respectively. Importantly, a more repeatable stabilization of the $FAPbI_3$ was achieved, which was demonstrated in various processing environments. Moreover, it has been demonstrated that adding the long-chain organic cations, such as butylammonium (BA^+) or phenylethylammonium (PEA^+), to perovskite ink converts some parts of the three-dimensional (3D) perovskite to two-dimensional (2D) phase, i.e., 2D/3D structure, resulting in a stability improvement of perovskite films.[205] Moreover, all inorganic perovskite inks also have been suggested to achieve highly stable perovskite films.[206] Solvent engineering is also critical to achieve high-quality perovskite ink. DMSO as the co-solvent of DMF in a 1:4 volume ratio is often used to obtain a stable intermediate phase of the PbI_2–DMSO–MAI adduct during the perovskite deposition, resulting in pin-hole-free and dense perovskite films.[207] However, Lee *et al.* demonstrated for the $FAPbI_3$ perovskite that the NMP co-solvent yields a more stable FAI–PbI_2–NMP intermediate phase compared to DMSO due to stronger interaction with FAI.[208] Therefore, each new perovskite component needs to consider the available co-solvents and their subsequent effect on the final film quality.

b. Perovskite ink deposition (step 2). After the solution preparation step, perovskite ink should be deposited on the surface of TCO substrates properly. The spin-coating technique has been thoroughly studied for the deposition of perovskite ink with controllable and optimized film morphology (Fig. 17). This technique has been very successful for fabricating highly efficient PSCs in the laboratory-scale, limiting to a scale of <10 cm and wasting a significant portion (>90%) of perovskite ink during the process, which is not applicable for industrializing perovskite photovoltaic (PV) technology.[209] However, the achieved science from spin-coating could be transferred to large-scale processing techniques for the deposition of perovskite ink on large substrates, enabling the industrialization of PSCs. As shown in Fig. 17, well-developed large-scale deposition techniques from other solution proceed optoelectronic technologies, i.e., organic photovoltaics (OPVs) or copper indium gallium selenides (CIGS) solar cells, such as blade coating, slot-die coating, inkjet printing, and spray coating, have been used for perovskite film deposition. These are very promising approaches as they allow roll-to-roll manufacturing processes and upscaling the perovskite photovoltaic fabrication. In the blade-coating technique, a certain amount of ink solution is poured in front of the blade and moves over the substrate at a specific speed.[210,211] This technique attracts significant attention for scale-up of this kind of solar cells, owing to its easy compatibility with a wide variety of perovskite compositions, substrates, and device structures. Slot-die coating is another promising technique for large-scale perovskite deposition, similar to the blade-coating technique (see Fig. 17).[212] Unlike blade-coating, in this technique, the perovskite ink comes out from a thin slit between

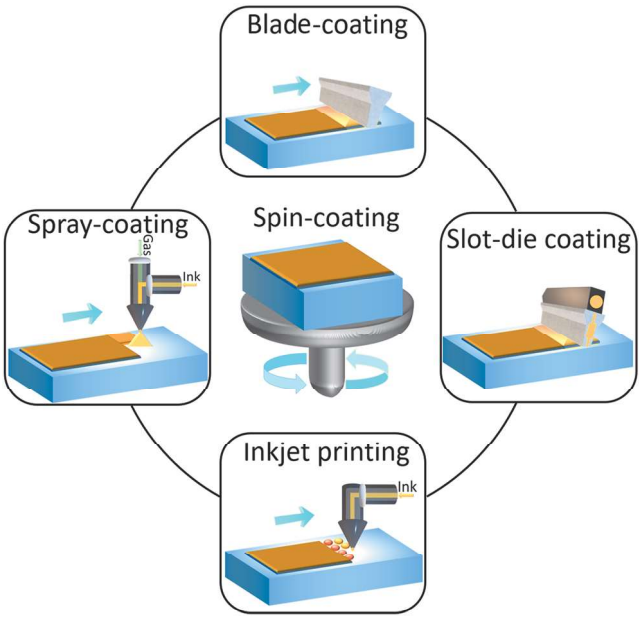


FIG. 17. Schematic illustration of spin coating, blade coating, slot-die coating, inkjet printing, and spray coating techniques for perovskite film deposition.

© Author(s) 2021

two pressed metal blocks of a coating head and consumes a bit more perovskite ink; however, the resulting perovskite film showed higher quality and reproducibility.[213] Inkjet printing emerged as a fast, facile, and economical technique to form desired patterns of large-scale perovskite film deposition.[214,215] Originally, this coating technique is a digital management technology inspired by typical office printers. Spray coating has also been used to produce thin-film photovoltaics, an appropriate method for mass production of perovskite films.[216–218] Similar to other large-scale techniques, slow solvent evaporation rate and dewetting of the substrates are the most critical challenges, leading to a low surface coverage and poor crystallinity.

Despite the impressive progress of perovskite film deposition by these techniques, the PCEs of large-scale deposited PSCs are lower than small area devices. Providing a fine and homogeneous perovskite film formation is critical in large-scale deposition techniques to reduce series resistance and increase shunt resistance, improving the PSC performance. Therefore, as detailed below, understanding the perovskite crystallization process is very important for the further development of PSCs.

c. Solvent quenching and perovskite nucleation (steps 3 and 4). Typically, perovskite inks have a moderate rate of solvent evaporation during the deposition due to the low vapor pressure of its solvents, i.e., DMF and DMSO, leading to a low density of heterogeneous nuclei and inhomogeneous perovskite films after the annealing step (step 5). Therefore, various solvent quenching techniques have been developed to increase the nucleation rate, leading to compact perovskite film with full surface coverage.

d. Antisolvent quenching. Antisolvents have been frequently used for quenching or solvent extraction of perovskite ink from the wet films, leading to rapid supersaturation of the perovskite precursor, i.e., fast nucleation, and achieving smooth and compact perovskite films [see Fig. 18(a)]. The antisolvents should be miscible with the perovskite solvents, i.e., DMF and DMSO, and should not dissolve the components of perovskite composition, i.e., PbI_2, $PbBr_2$, MAI or FAI, and so on. So far, various antisolvents, such as toluene,[204] chlorobenzene,[219] ethyl ether,[220] ethyl acetate,[221] and anisole,[222] have been established. As mentioned, the PCE record was achieved for antisolvent assisted spin-coating deposition by dripping the antisolvent onto the wet perovskite film during the spin-coating process. However, antisolvents need the spinning effect to perform maximum solvent extraction from wet films; therefore, it is challenging to use this technique for scalable deposition.

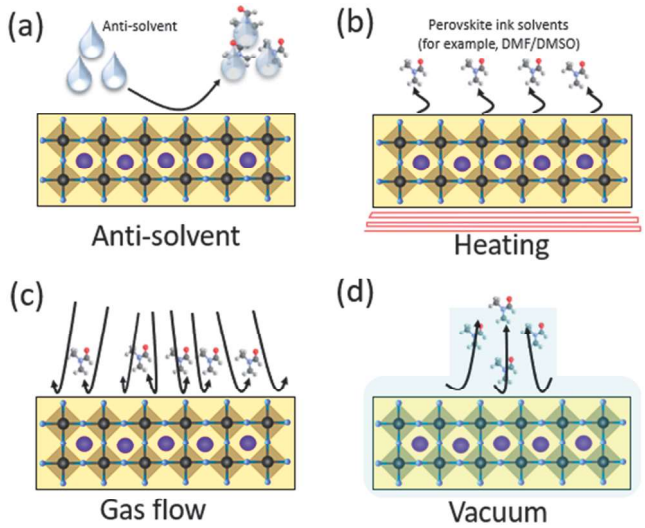


FIG. 18. Various solvent quenching techniques for perovskite film deposition: (a) antisolvent, (b) heat, (c) gas, and (d) vacuum quenching.

e. Heat quenching. Heat quenching has been determined as an efficient technique for solvent extraction from the perovskite wet films [see Fig. 18(b)].[223,224] Typically, this technique speeds up the film drying rate, accelerating the supersaturation condition and promoting the nucleation step in perovskite films. In this approach, different temperatures of 30–90 °C have been applied to wet films for the fabrication of high-quality of perovskite films.[225,226] However, heat quenching can be affected by other parameters, such as the solvent and solutes of the perovskite ink. At low temperatures (<30 °C), a discontinuous perovskite film with low surface coverage will be formed due to a slow solvent extraction rate. At high temperatures (>90 °C), substrate dewetting occurs very fast due to fast solvent extraction, leading to non-homogeneous perovskite films. Therefore, optimizing the applied temperature is critical for efficient solvent extraction, achieving high-quality perovskite films.

f. Gas quenching. Nitrogen (N_2) or dry air gas quenching technique has been introduced for solvent extraction from the as-coated wet film within a few seconds [see Fig. 18(c)], mainly used for large-scale deposition, such as blade-coating or slot-die coating of perovskite films.[227–229] In this technique, a gas knife, i.e., N_2 or air, moves with the blade simultaneously and blows the gas on the wet perovskite film to quench or extract the solvent from the ink, consequently inducing fast nucleation and achieving a full surface coverage by the perovskite film.[230] After gas blowing, a post-annealing process is needed to ensure the complete liquid-to-solid conversion. In this technique, the gas flow rate and gas temperature are the two critical parameters that need to be controlled carefully for high-quality thin films. Moreover, the solvent composition in perovskite ink should be considered as an essential factor to form a stable intermediate phase after gas quenching treatment. For example, Conings *et al.*[231] demonstrated that adding a small amount of DMSO to a DMF-based perovskite ink plays a crucial role in forming a stable intermediate precursor–DMSO complex, achieving dense and smooth perovskite films.

g. Vacuum quenching. Vacuum quenching has been introduced as another innovative technique to reach the supersaturation level of perovskite wet film quickly by extracting the solvent from the perovskite ink effectively [see Fig. 18(d)].[232,233] This technique introduced by Li and co-workers[234,235] for solvent extraction from the spin-coated wet film is producing uniform and highly crystalline perovskite films. The vacuum degree and vacuum duration are the two critical parameters in this quenching technique that should be considered to find the optimum deposition condition. Afterward, vacuum quenching has been frequently used for large-scale deposition methods. Similar to other quenching techniques, the solvent composition of perovskite ink is also an important parameter to achieve a stable intermediate phase, leading to fully covered and

© Author(s) 2021

compact perovskite film. This technique was used for both the one-step and two-step perovskite deposition methods. For example, Guo *et al.*[236] used vacuum quenching as an efficient technique to extract the superfluous solvent of the freshly deposited inorganic component PbI_2 in a two-step sequential deposition approach, achieving high-quality perovskite films.

h. Crystal growth: annealing (step 5). After the nucleation step, i.e., supersaturation point, by extracting the solvent from the perovskite ink with antisolvent, heating, gas quenching, and/or vacuum quenching processes, crystal growth should be controlled carefully by annealing the films. Typically, perovskite films are annealed (at 60–150 °C on a hot-plate for 30–60 min) to expel residual solvents from the intermediate adduct, i.e., DMSO, thereby aiding the crystallization process. However, it has been confirmed that the quality of perovskite films can also be improved by performing an annealing step in the presence of vapor of perovskite solvents, such as DMSO, DMF, or GBL.[209] New, fast, and contact-less annealing approaches, including rapid thermal annealing (RTA),[237,238] near-infrared (NIR),[239,240] flash infrared annealing (FIRA),[241–243] photonic curing or intense pulse light (IPL),[244,245] radiative thermal annealing,[246,247] laser annealing,[248,249] microwave annealing,[250] and ultraviolet annealing,[251] have been introduced to improve or simplify the perovskite crystallization. The perovskite grain sizes and film quality can be significantly affected by annealing temperature and duration.[252,602] On the one hand, increasing the annealing temperature or the annealing time can increase the grain sizes.[253,254]

On the other hand, it can increase the risk of perovskite decomposition by evaporating volatile organic components.[252,603] Therefore, finding an optimum annealing temperature and annealing time is very important to achieve efficient perovskite crystallization. It has been found that applying high temperatures in a few seconds on freshly spincoated perovskite films utilizing mentioned methods could be considered as an efficient annealing approach, improving perovskite crystallinity and cell efficiencies.

2. Concluding remarks

In conclusion, we describe the typical steps in perovskite processing applicable for different types of PSCs. We point out the critical steps during the perovskite process to achieve high-quality perovskite films and highly performing PSCs. Various laboratory- and large-scale deposition techniques are discussed. Moreover, we explore different solvent quenching and annealing methods for attaining high-quality perovskite films.

C. Thermal sublimation of perovskite films

Martin Kroll, Frederik Nehm, Karl Leo

1. Status of the area

After solution processing, sublimation in vacuum is the most used alternative for perovskite thin film preparation. Most commonly, multi-source thermal evaporation is used. Here, precursor materials are loaded into separate crucibles and heated in ultra-high vacuum (10^{-6} mbar), with the deposition rates monitored by separate quartz microbalances (QMBs). The substrate (ideally rotating for better uniformity) is mounted above the crucibles where the evaporation cones overlap. Depending on the process, the crystalline perovskite can form directly on the substrate without annealing. However, most studies include an annealing step afterward to improve film properties.

Similar to solution processing, methylammonium (MA) lead triiodide has dominated the field for a long time and is still used in the most efficient evaporated perovskite solar cells (PSCs). Since the first report of an evaporated perovskite solar cell by Liu *et al.*[257] in 2013 with an efficiency of 15.4%, several studies have improved the efficiency to over 20%.[258]

In the large-area mass production of similar technologies, such as OLED displays, thermal evaporation has been realized with very good upscaling properties, such as precise thickness control and homogeneity. Furthermore, thermal evaporation allows for highly customized multilayer stacks without the risk of damaging already deposited layers (i.e., with solvents) as well as homogeneous coating of textured substrates, such as silicon solar cells for tandem use.

In 2020, Li *et al.*[259] showed that evaporation processes show promising results for larger area solar cells. Here, an efficiency of 18.2% for 21 cm large minimodules was reported. The modules are based on an n-i-p structure with $MAPbI_3$ as the absorber. To achieve these high efficiencies, the perovskite was treated with a solution containing potassium acetate and MAI. By the post processing treatment, a defect passivation and reduction of non-radiative recombination is observed.

In recent years, thermal evaporation was successfully realized on most perovskite compositions, such as mixed halide triple cation [$CsFAMAPb(IBr)_3$],[260] MA free,[261] tin, and tin–lead based perovskites[262] and all inorganic $CsPbI_3$[690]. The cell efficiencies in those studies do not exceed 19%.

2. Current and future challenges

The challenges of thermally evaporated perovskites differ strongly from their solution-processed counterparts. In order to fabricate high quality films, the control of stoichiometry and microstructure of the deposited films is a key factor. For an accurate stoichiometry, rate control for the organic cation is crucial. The most commonly used methylammonium iodide is a small molecule with high vapor pressure, known to resublimate from the vacuum chamber walls. As a result, a gas-like behavior is observed upon evaporation, leading to a difference between QMB readings and the actual amount condensing on the substrate. Moreover, adhesion on the QMB surface and the substrate is dependent on the temperature and material purity, further increasing uncertainties in rate control and ultimately stoichiometry. These problems have led several groups to control the MAI evaporation by either vapor pressure or crucible temperature rather than the rate.

Beyond stoichiometry, film quality and device performance are strongly governed by the perovskite microstructure. For $MAPbI_3$, the crystal grain sizes are found to be significantly smaller in thermally evaporated perovskite than in solution processed films. Although the exact role of crystal grain boundaries is still under investigation, it is assumed that larger crystal grains are beneficial for the photovoltaic device performance. This also limits the development of evaporated PSCs.

© Author(s) 2021

Another limiting factor is the more complex process control during the deposition of the now commonly used the triple cation mixed halide perovskite. For these perovskites, the different evaporation behaviors and deposition characteristics of the organic and inorganic precursors have a strong influence on the stoichiometry and the crystallization of the perovskite film. Although triple cation perovskites were successfully deposited by,[260] no increase in performance was reached.

For solution based processing, additives such as acids as well as solvent engineering methods have led to an improvement in device stability, performance, and reproducibility. Besides these key properties for good perovskite solar cells, the room temperature stabilization of the low bandgap cubic phase of $FAPbI_3$ was achieved. For vacuum processes, similar techniques are more complicated and different approaches need to be developed. Post-processing surface treatments have shown improvements in the film, but this negates the advantages of the solvent-free nature of vacuum deposition.

Due to the high initial cost of vacuum systems and comparably slow deposition process in the laboratory, progress on vacuum-evaporated perovskites is significantly slower than for their solution-processed counterparts. This has also resulted in much fewer publications on evaporated perovskites over the past few years. However, similar trends were initially seen during the early stages of OLED development, which are almost exclusively produced in vacuum nowadays.

3. Advances in science and engineering to meet these challenges

As widely known but rarely mentioned in the community, results vary when using precursor materials from different commercial suppliers. In 2019, Borchert *et al.*[87] investigated methylammonium iodide from several different companies. They observed different evaporation properties in dependence of compound purity using MAI synthesized in-house as well as commercial products. By using mass spectroscopy during the evaporation process, it was possible to correlate the accuracy of QMB signals to material impurities. Interestingly, a higher amount of impurities led to a more reliable rate control, and after optimization, similar photovoltaic performances were reached. Consequently, knowledge about the precursor material is essential for an accurate deposition control.

To further control the deposition, Ross *et al.* investigated the sticking behavior of the organic compound to the substrate in dependence of the substrate temperature.[258] The tooling of MAI changes drastically when varying the substrate temperature and the underlying transport layers. Using this enhanced deposition control, an efficiency of 20.6% was achieved for p-i-n structures with self-assembling monolayers as the hole transporter. This better understanding of sticking properties should help to further stabilize the deposition process. Furthermore, an optimal process window around room temperature was determined in this work.

This is in good agreement with the work of Lohmann *et al.*[263] and Kottokkaran *et al.*[264] Both investigated the influence of the substrate temperature on the crystal grain size over different temperature ranges. Lohmann showed that the crystallite size increases when cooling the substrate to 0 C, compared to room temperature. However, the device performance decreased with the increasing crystal grain size. Kottokkaran *et al.* observed larger crystal grains for elevated temperatures but still have the highest performing devices when depositing at room temperature. Another difference in film crystallization was found by Palazon *et al.* in 2019.[265] They reported that $MAPbI_3$ can crystallize in the thermodynamically unexpected cubic phase at room temperature although the phase transition from tetragonal to cubic phase is expected to happen at 50–60 C. By changing the deposition rate of lead iodide, they observed a change of the as deposited film to the tetragonal phase. The cubic phase has a slightly lower bandgap, which leads to an improved photovoltaic performance of 19.7%.

Although lower efficiencies are reported for small-area vacuum deposited perovskite solar cells compared to their solution processed counterparts, vacuum sublimation yields excellent performance on the module scale and shows unique properties. The increased insight into the crystallization process leads to a better understanding of the process parameters.

4. Concluding remarks

The control over the evaporation process is developing and with it the potential for more basic research, improvements, and finally industrialization. Many challenges remain and the development has been slower over the last years, but with increasing interest and research, the gap in PCE could be reduced and other important properties might prevail.

D. CVD growth of perovskites

Alex Redinger

1. Status of the area

Chemical vapor deposition (CVD) comprises a class of highly versatile deposition methods to produce epitaxial or polycrystalline films with a high degree of reproducibility, combined with excellent opto-electronic properties. An impressive recent example is the six junction solar cell grown epitaxially on GaAs via metal organic vapor phase epitaxy.[266] Unlike physical vapor deposition (PVD) or molecular beam epitaxy (MBE), which need to be carried out under high vacuum conditions, CVD is a technique that can be operated up to atmospheric pressure. This additional degree of freedom allows for a better control of the reaction and re-evaporation rates of volatile species.

A large variety of different CVD techniques have been developed over the last few years, which allow to deposit high performance solar cell absorbers, extraction layers, and electrodes (for a recent review, see Ref. 267). For the synthesis of the halide perovskite absorbers, the field is largely dominated by solution based methods, which allow for a fast combinatorial screening and rapid improvement of the opto-electronic properties and device efficiencies in the laboratory.[268,269] At first sight, it seems that most of the advantages of CVD, namely, the ability to produce semiconductors with low impurity concentrations, excellent compositional control including compositional gradients via multiple stages, and the ability to upscale combined with a highly conformal deposition, are not

© Author(s) 2021

necessary for halide perovskites. In fact, the current record efficiencies for CVD based perovskite devices are substantially lower than their chemically produced counterparts. Nevertheless, proof of concept studies have been reported for halide perovskites. Leyden *et al.* showed that efficient methylammonium (MA) and formamidinium (FA) based perovskites[270–272] can be produced via hybrid CVD, where in a first step $PbCl_2$ is deposited via PVD, followed by an exposure to a MA/FA-halide vapor. Reports on one-step CVD methods are also available but have never been pushed to a competitive device efficiency level.[273,274]

The current halide perovskite record devices are mostly based on multi-cation mixed halide absorbers.[269,275] These solar cells exhibit an improved stability and performance compared to prototypical methylammonium lead iodide[47] but impose challenges for CVD, since many precursors and deposition steps need to be developed and controlled. Consequently, reports on multi-cation/halide perovskite absorbers produced via CVD methods are scarce,[276] and a fair comparison between CVD and solution based methods in terms of device performance is not yet feasible.

The application of CVD and atomic layer deposition (ALD) techniques is more common in the perovskite community to produce high performance carrier selective layers, electrodes, and buffer- and encapsulation-layers (see Sec. IV D for a more detailed discussion on extraction layers). Most of the work on electron extraction layers has been devoted to TiO_2, ZnO, and SnO_2, whereas the most common HTL produced via CVD is NiO. Passivation layers, such as Al_2O_3, have also been developed for perovskites in order to reduce the interface recombination velocity and prevent ionic mobility induced degradation.[267]

It is generally accepted that Si-based single junction solar cells will continue to dominate the PV market. The true benefit of halide perovskites are closely linked to the ability to make high performance tandem devices with improved performance compared to single junction devices. PVD and CVD methods are ideal tools to make efficient tandem devices since large area conformal coating on any type of planar and textured substrates can be carried out. Consequently, a further thorough development of these deposition techniques is highly desirable.

2. Current and future challenges

The current challenges for CVD based high performance devices are first of all the speed and dynamics at which the field is developing. New processes, doping and passivation strategies, are being developed at high speed via solution based methods, which makes it difficult for researchers to design custom built evaporation/reaction chambers and processes that allow for highest reproducibility and device performance.

Two different strategies can be envisioned. Researchers wait until the race for the presumably best perovskite composition is over and then PVD and CVD based large area deposition processes for industrial applications can be developed. This strategy, however, assumes that the most stable high-performance halide perovskite is similar for the case of chemical deposition methods and CVD based methods. This may not be the case since impurity concentrations, interface defects, and their passivation will certainly depend on the deposition process and thereby affect the device efficiency and stability.

Therefore, the best approach is to be inspired by the current race for ultimate efficiency via solution based methods but nevertheless study as many material combinations as possible to identify the most stable and best performing CVD based halide perovskite composition. At present, not enough data are available for CVD based halide perovskites and more work is necessary. The focus should lie on developing perovskite absorbers that can be produced with a minimum number of precursors and reaction steps in order to be industrially relevant.

It needs to be emphasized that CVD is a technique that can be used very effectively to produce layers at higher processing temperatures as in PVD (60C[258] vs 140C[270]). This unique advantage, which is a direct consequence of the ability to use high partial pressures of the volatile organic component, may allow forming perovskite absorbers that are more temperature resistant since the semiconductor can be grown closer to equilibrium. CVD and PVD techniques have the advantage that very clean semiconductors can be grown with a low number of impurities that might deteriorate the PV performance. However, both techniques require very clean raw materials, which is not always the case as discussed in more detail in Sec. III C. A disadvantage of CVD compared to PVD is certainly the flexibility to grow intentional gradients in composition over the thickness of the absorber. Dedicated metal organic vapor phase epitaxy systems tuned to the properties and precursors of for halide perovskites would need to be developed, as they are currently not available.

Over the last few years, very powerful diagnostic tools have been developed that allow for early material screening, such as time resolved photoluminescence and photoluminescence quantum yield (PLQY) measurements.[277] Unfortunately, such measurements are scarce for CVD based perovskites. If perovskite layers with PLQY values and minority carrier lifetimes similar to solution based perovskites can be achieved on glass substrates, then there is no fundamental limit that impedes this material to be a suitable candidate for high efficiency devices. In large samples with intentional gradients in element concentration and temperature, combinatorial methodologies should be used to screen the whole parameter space in an efficient manner (as done, for example, for coevaporated $CsPbI_3$[278]). This is particularly simple for CVD based methods where the individual zone temperatures and flow rates can be adjusted precisely to produce compositional gradients along the sample.

In particular, the impact of the elemental composition on stability and device performance needs to be studied carefully. This, however, requires developing extraction layers that are tailored for CVD based absorbers. A simple copy of the extraction layers from solution based approaches will not lead to ultimate efficiencies. Similar combinatorial strategies combined with luminescence techniques[279] can be applied to find the best performing extraction layers that reduce interface recombination losses while providing excellent selectivity. The layers should be chosen such that they can be transferred to tandem configurations. A strong focus on low temperature CVD and ALD methods is essential, especially if these layers will be grown on top of the perovskite surface. In tandem configurations, the impact of ALD and CVD layers on the bottom cell also need to be taken into account.

Finally, CVD based perovskite absorbers should be used to design the reference material to study fundamental physical and

© Author(s) 2021

chemical properties of the semiconductors. The growth and characterization of the epitaxial material on lattice matched substrates or via van der Waals epitaxy has only been studied in some rare cases.[280] These films would be ideal to study the impact of grain boundaries on moisture induced degradation or could be used to characterize the band structure via angle resolved photoemission measurements (see Sec. IV F for details). In addition, CVD based films can be grown under very clean conditions, which would allow us to understand the impact of impurities on degradation, thereby excluding external factors, such as solvents. It is currently not clear to which extent the stability of different perovskite layers is altered by the deposition process itself. Here, PVD and CVD based methods offer an ideal playground to study the fundamental limits of the perovskite absorbers.

3. Advances in science and engineering to meet these challenges

In order to meet these challenges, the following criteria need to be considered and carefully evaluated. Studies on solution based devices have shown that the MA based perovskites are too unstable to meet the necessary stability criteria.[281] Dedicated experiments for CVD based absorbers with optimized extraction layers and diffusion barriers need to be carried out to corroborate that MA based CVD perovskites exhibit similar disadvantages as their chemically produced counterpart. Some results on evaporated[282] and CVD based MA based absorbers[270] show promising stability and this needs to be further analyzed.

In the next step, formamidinium based absorbers need to be developed to a competitive device efficiency level. Here, a combinatorial approach with FA, Cs, and Sn should be used followed by dedicated surface and interface passivation strategies and tailored extraction layers. A critical mass of studies needs to be carried out and the bottlenecks need to be evaluated via PLQY measurements after the deposition of each layer. This will finally allow to corroborate if CVD based absorbers can meet the stability and efficiency requirements for large scale manufacturing.

Strain engineering could be a valuable tool to study how the metastable photovoltaic active phase can be induced and retained in FA-based devices produced by CVD. Preliminary results of FA-based absorbers show that depending on the processing conditions, the photovoltaic active phase can be grown quite effectively.[271] Bandgap engineering via intentional compositional gradients in the perovskite absorber has already been reported to be beneficial for device performance.[276] This technique, which has been proven to be very important for other thin film solar cell technologies,[283,284] needs to be investigated and developed further.

Novel architectures via a combination of PVD/CVD based perovskites with graphene or other transition metal dichalcogenides, which may lead to van der Waals epitaxy, should be studied in order to reduce interface recombination combined with impermeable charge extraction layers. In that respect, solution based large area graphene/perovskite solar cells show very promising results, and further improvements via CVD and vapor deposition methods can be expected.[285]

Furthermore, the field of low dimensional perovskites should also be investigated further via CVD based techniques (for details, see Sec. II F). Here, the number of publications is still very low, and the true potential of CVD based low dimensional perovskites is still to be exploited. Again, a combination with other 2d materials seems to be a very attractive pathway to limit recombination and produce interfaces with low defect concentrations.

Finally, a strong focus of CVD based methods to produce high efficiency stable devices with a scalable technology is mandatory. Although the current record tandem devices are currently produced with a Si-bottom layer,[269] other high efficiency technologies, such as $Cu(In,Ga)Se_2$, offer unique properties, such as the ability to produce flexible devices[286,287] combined with a low energy payback time. CVD based extraction layers at low processing temperatures need to be developed with special emphasis on low permeation rates for water in order to improve stability. These extraction layers need to be tested on CVD based perovskite absorbers, and detailed band alignment studies via photo-electron spectroscopy methods need to be carried out.

4. Concluding remarks

CVD based methods have shown very promising results over the last few years despite the fact that the method is only used in some research groups and efficiency is driven mostly by solution based methods. However, the true potential of this technique becomes only visible when reproducibility on large scales for large volumes becomes important. It is very probable that a compromise between efficiency and processibility needs to be found. In that respect, the research should focus on developing high performance devices with the lowest possible number of elements in the solar cell in order to be as competitive as possible. The number of precursors and processing steps in CVD based perovskites needs to be reduced to a minimum. Dedicated inline process control techniques need to be developed combined with an optimization of all the layers in the device. The true potential of CVD to produce competitive high performance devices is still to be explored. Given the potential and the unique advantages of this technique, more scientific effort in that direction is likely to be very fruitful.

E. Hybrid perovskite crystals: Growth, characterization, and application

Julian Höcker, Vladmir Dyakonov

1. Status of the area

The studies of perovskite single crystals with high crystallographic quality is an important technological area of the perovskite research, which enables to estimate their full optoelectronic potential and thus to foster their future applications. It is therefore essential to grow high-quality single crystals with lowest structural as well as chemical defect densities and with a stoichiometry relevant for their thin-film counterparts. Optoelectronic devices, e.g., solar cells, are highly complex systems in which the properties of the active layer (absorber) are strongly influenced by the adjacent layers, so it is not always easy to define the targeted properties and elaborate the design rules for the active layer. Currently, metal halide perovskite single crystals with the structure ABX_3 are the most studied crystalline systems. These hybrid crystals are solids composed of an organic cation, such as methylammonium ($A = MA^+$) or formamidinium ($A = FA^+$), to form a three-dimensional periodic lattice together

© Author(s) 2021

with lead (B = Pb^{2+}) and a halogen, such as chlorine, bromine, or iodine (X = Cl^-, Br^-, or I^-). Among them are methylammonium lead tribromide ($MAPbBr_3$) and methylammonium lead triiodide ($MAPbI_3$) as well as methylammonium lead trichloride ($MAPbCl_3$).[288,289] Important representatives with the larger cation FA^+ are formamidinium lead tribromide ($FAPbBr_3$) and formamidinium lead triiodide ($FAPbI_3$).[289] Besides the exchange of cations as well as anions, it is possible to grow crystals containing two halogens to obtain mixed crystals with different proportions of chlorine to bromine and bromine to iodine, as shown in Fig. 19. By varying the mixing ratio of the halogens, it is therefore possible to vary the color and thus the absorption properties of the crystals,[290] as it can be done with thin polycrystalline perovskite films. In addition, since a few years, it is also possible to grow complex crystals that contain several cations as well as anions. These include the double cation–double halide perovskite, formamidinium lead triiodide methylammonium lead tribromide $[(FAPbI_3)_{0.9}(MAPbBr_3)_{0.1}$ (FAMA)][291] and formamidinium lead triiodide methylammonium lead tribromide cesium lead tribromide $[(FAPbI_3)_{0.9}(MAPbBr_3)_{0.05}(CsPbBr_3)_{0.05}$ (CsFAMA)],[292] which have made a significant contribution to increase the efficiency in thin-film photovoltaics. The growth of crystals to this day is performed exclusively from solution. Important preparation methods are the cooling acid-based precursor solution crystallization,[293] the inverse temperature crystallization (ITC),[294] and the antisolvent vapor-assistant crystallization (AVC).[295] In the cooling crystallization, the precursor salts AX and PbX_2 are dissolved in an aqueous halogen-containing acid at high temperatures.[296] Controlled and slow cooling finally results in a supersaturated precursor solution, which leads to spontaneous nucleation of crystal nuclei followed by subsequent crystal growth. The ITC method is based on the retrograde solubility of a dissociated perovskite in an organic solvent.[294] With the increasing temperature, the solubility of the perovskite decreases and mm-sized crystals can be grown within a few hours.[294] In the AVC method, the precursors are also dissolved in an organic solvent as well.[295] By slow evaporation of a so-called antisolvent,[296] the solubility of the perovskite in the now present solvent mixture decreases and it finally precipitates. In addition, there are many other methods with the goal of growing high quality and large crystals in a short period of time.[297]

2. Current and future challenges

The investigation of high-quality crystals not only offers the advantage of studying the pure perovskite material system but also that the crystals have fewer lattice defects in contrast to their thin film counterparts. Their excellent optoelectronic properties range from high carrier mobilities,[298] long charge carrier lifetimes,[299] and diffusion lengths[300] to high photoconductivity[301] and high sensitivity to high energy radiation.[302] For these reasons, they are already used as semiconducting components in solar cells,[296] x-ray-detectors,[302] gamma-ray-detectors,[303] and photodetectors.[304] However, there are some challenges on the way from crystal growth to the device prototypes: Many crystallization methods, such as cooling crystallization, but also the AVC method, need a much longer period of time for single crystal growth. Moreover, it is difficult to adjust the nucleation rate to grow few but large-sized crystals. The ITC method can overcome these challenges. However, the inverse solubility[294] effect can be a problem in growing defect-free crystals because the probability of lattice defects is rising with the increasing growth temperature. The use of seed crystals to obtain large crystalline solids can also be a problem, as this leads to irregularities in the crystal lattice. For future crystal growth, the

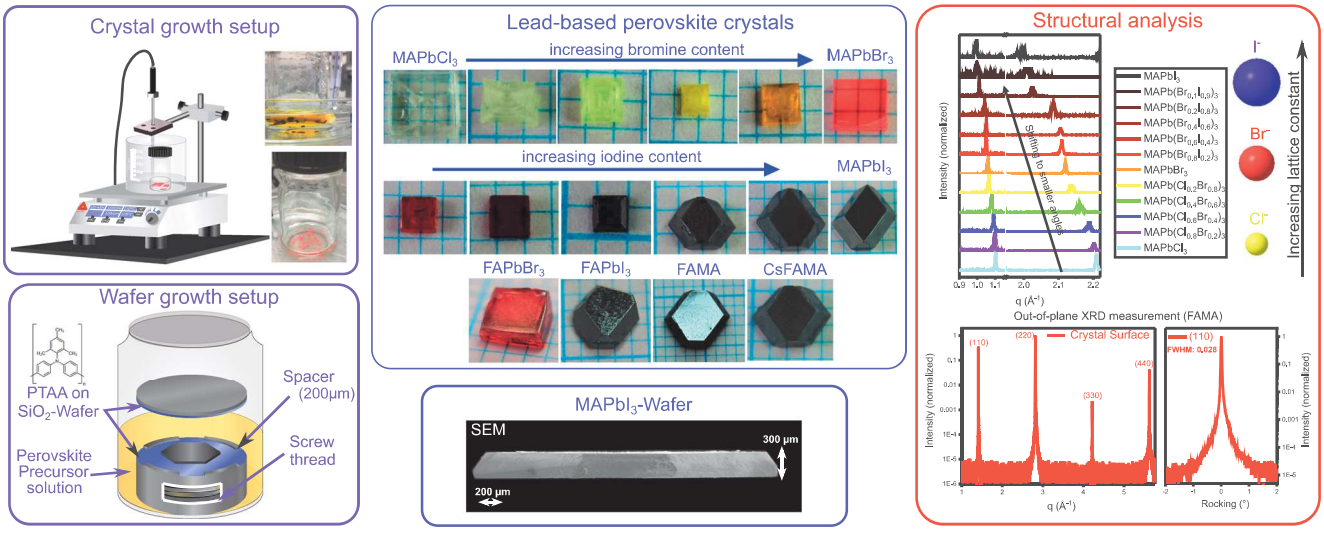


FIG. 19. (Left) Crystal and wafer growth setup to grow mm-sized perovskite single crystals from solution. (Middle) $MAPbX_3$ crystals with different chlorine/bromine ratio and bromine/iodine content. Due to the change in the stoichiometry, it is possible to change the bandgap of the crystals. $FAPbX_3$ crystals and the complex crystals FAMA and CsFAMA. Scanning electron microscope (SEM) image of a $MAPbI_3$ single crystal wafer with a maximum height of 300 μm. (Right) Powder XRD patterns of MAPbX3 crystals to examine the lattice constants. Out-of-plane XRD measurements of a FAMA single crystal surface with the corresponding rocking curve, revealing the high quality of the single crystal.

© Author(s) 2021

requirements of time, temperature, controllable nucleation rate, and the associated crystal size must play an important role. In addition, another overriding goal must be to pull large-sized single crystals from the melt rather than from solution, as is already possible with the Bridgeman method for the growth of $CsPbBr_3$,[305] in order to find large-scale applications, such as with gallium arsenide (GaAs) and silicon (Si). Besides preparative challenges, there are challenges in interpreting the experimental data obtained on perovskite crystals. In the literature, there are often strongly deviating values for the device-relevant optoelectronic parameters, for example, charge carrier mobility, which can be determined by time-of-flight (TOF), space charge limited current (SCLC), or Hall effect methods.[296] Similarly, the experimentally determined values of carrier lifetime and diffusion length can vary by up to two orders of magnitude according to the literature.[296] Finally, many optoelectronic parameters, especially for more complex crystals, such as FAMA or CsFAMA, are not yet known.

3. Advances in science and engineering to meet these challenges

The number of techniques for growing metal halide perovskite single crystals is constantly increasing. The above-mentioned crystallization techniques can be combined, and different chemical reactions are applied to grow high quality single crystals. A mechanical approach to grow complex and large-sized crystals without the use of seed crystals is realized by the re-fill crystallization method (RFCM),[306] which is based on the inverse solubility of ITC.[294] By introducing new precursor solution and simultaneously removing the depleted solution, it is possible to grow *in situ* large-sized crystals with excellent structural quality, as confirmed by the out-of-plane X-ray diffraction (XRD) measurements and the rocking curve of a FAMA single crystal in Fig. 19.[306] These quality characteristics of the crystals are not only visible from structural measurements but also show up in the physical parameter of the trap density. In contrast to perovskite thin films, the trap densities in lead-halide perovskite single crystals are usually 4–5 orders of magnitude smaller[296] due to the high quality of the crystals. With such a variety of crystallization techniques, it is now possible to grow all semiconducting perovskites known from thin-film device applications as mm-sized crystals. As mentioned above, by selectively changing the halogen ratio, it is possible to obtain crystals with a wide variety of colors and optical bandgaps, which may serve as photodetectors in the UV/VIS range.[288,296] However, the variation of the halogens not only results in a change of the optical properties but also results in an increase in the lattice constant with increasing bromine to chlorine and iodine to bromine ratios, respectively (Fig. 19). In addition, the lattice structure changes from a simple cubic lattice[288,293,294] for $MAPbCl_3$ and $MAPbBr_3$ to a body-centered tetragonal lattice for $MAPbI_3$.[293,294] An important outcome of these efforts is the successful fabrication of single crystal solar cells, which achieves over 21% power conversion efficiency, representing a new benchmark in the field of metal halide perovskite single crystal solar cells.[307–309] While mm-thick crystals were found less suitable for this purpose, μm-thick $MAPbI_3$ wafers were shown to be more promising for the production of photovoltaic devices.[310] As shown in Fig. 19, a crystal wafer can be easily grown on a poly[bis(4-phenyl)(2, 4,6-trimethylphenyl) amine] (PTAA)-coated silicon wafer, while the growth height of the crystal is limited by spacers.

4. Concluding remarks

The field of metal halide perovskite single crystals is both inspired and driven by the fact that the most efficient silicon solar cells are made with the highest quality large area crystalline absorbers. Encouragingly, the power conversion efficiency over 21% for solar cells fabricated with single-crystalline $MAPbI_3$ was reported.[308] Interestingly, other major activities in the field are focused on single-crystal-based x-ray-detectors,[311] gamma-ray-detectors,[303] and photodetectors,[304] which show promising performance in terms of sensitivity, response speed, and lowest detectable dose rate. In the future, large-area single crystalline wafers with controlled thickness and area are logically expected to come into focus. One of the possible barriers to studying optoelectronic properties even in high-quality crystals remains ion migration with the resulting complex electric field distribution, which is a similar problem to what is known for perovskite thin films and devices.[312] We would like to add that a general goal of growing large-sized crystals with a complex composition should be done together with a critical evaluation of the term "single crystal" in relation to these crystals. On the other hand, the crystallographic and stoichiometric qualities alone do not allow yet any conclusions about the "electronic quality," which should also be verified. Nevertheless, the development of large-area, highly crystalline, and low-defect density perovskites remains an important platform to design the easy-to-grow highly functional materials, on the one hand, and to understand their optoelectronic properties, on the other hand, to enable new applications, beyond what we are mainly dealing with to date. High optical bulk quality and compositional variability can make them interesting, for example, for quantum applications, spin-based ones or as coherent photon emitters, which have not yet been intensively worked on.

IV. CHARACTERIZATION AND PROPERTIES

Thomas Kirchartz, Jonathan Warby, Emilio Gutierrez-Partida, Dieter Neher, Martin Stolterfoht, Uli Würfel, Moritz Unmüssig, Jan Herterich, Clemens Baretzky, John Mohanraj, Mukundan Thelakkat, Clément Maheu, Wolfram Jaegermann, Thomas Mayer, Janek Rieger, Thomas Fauster, Daniel Niesner

A. High open circuit voltage

Thomas Kirchartz

1. Status of the area

High photovoltaic power conversion efficiencies require a combination of a high photocurrent and a high free energy per extracted electron, i.e., a high voltage at a given current. The typically used figure of merit to compare the ability of the solar cell to extract a large free energy per carrier is the voltage V_{oc} in the limit of

© Author(s) 2021

infinitely slow charge extraction, i.e., at the open circuit. This voltage can be understood as the electrostatic potential difference between the two metal electrodes of the solar cell, but qV_{oc} is furthermore also typically identical to the quasi-Fermi level splitting side of the photovoltaic absorber layer. In efficient lead-halide perovskites, this open-circuit voltage V_{oc} is remarkably high relative to its thermodynamic limit ($V_{oc,SQ}$) given by the Shockley–Queisser model.[313] The value of $V_{oc,SQ}$ is ~280 mV less than E_g/q (the bandgap divided by the elementary charge), which gives around 1.32 V for typical perovskite bandgaps of 1.6 eV. As shown in Fig. 20(a), the highest open-circuit voltages reached so far in the literature approach the thermodynamic limit by about 60 mV,[314] which is an excellent value for any solar cell technology, let alone a technology mainly based on solution-processed polycrystalline thin films. Figure 20(b) shows that the evolution of non-radiative voltage losses over the last few years has seen substantial improvements from >300 mV losses to ~60 mV.

2. Current and future challenges

The key to high open-circuit voltages relative to $V_{oc,SQ}$ is to allow a high concentration of charge carriers to build up, which leads to a high quasi-Fermi level splitting and subsequently a high voltage at the open circuit. In the absence of charge extraction, generation and recombination of electron hole pairs are the only mechanisms that control the concentrations of electrons and holes. The key is therefore to slow down recombination. Given that radiative recombination as the inverse process of photoabsorption must happen due to detailed balance,[315] the only recombination types that can be slowed down by proper device design are non-radiative recombination processes. Non-radiative recombination typically occurs via multiphonon transitions from the conduction band to a localized state in the bandgap (defects) and from there to the valence band. In the harmonic oscillator approximation, multiphonon transitions should become very unlikely if large energy steps in units of the phonon energy have to be overcome in a single transition.[316] Therefore, shallow defects are generally considered less detrimental in terms of accelerating recombination because the transition of a shallow defect to the other band edge has to bridge an energy of nearly the bandgap in a single transition. Lead-halide perovskites have antibonding valence band edges leading to a higher likelihood of shallow intrinsic defects and a lower likelihood of deep intrinsic defects. This fact is typically called "defect tolerance"[317] and could, in combination with the fairly low phonon energies of lead-halides, lead to very slow recombination as compared to other polycrystalline semiconductors. The figure of merit for slow recombination in a semiconductor is typically the charge-carrier lifetime—a quantity that will depend on charge-carrier concentration in an intrinsic or highly excited semiconductor. Therefore, the determination of charge-carrier lifetimes may not always be done at exactly the same conditions. Nevertheless, it is clear that bulk lifetimes in lead-halide perovskites can exceed several microseconds,[277,653] i.e., values that are much longer than those of other polycrystalline direct semiconductors, such as $Cu(In,Ga)Se_2$. A key requirement for such long lifetimes is a well-passivated surface of the perovskite film, which is often achieved by using passivating molecules, such as n-trioctylphosphine oxide (TOPO).[318]

By measuring the external quantum efficiency of photoluminescence (PL) of a semiconductor film, one can calculate back the quasi-Fermi level splitting ΔE_F in the film that must have led to the measured PL intensity. The same method would also work for layer stacks including interfaces to charge transport layers (CTLs). Therefore, steady-state PL is a widely used method to assess the quality and the ability of semiconductor layers or layer stacks to enable a high open-circuit voltage if used as part of a full device stack. A key finding in the literature is that TOPO passivated methylammonium lead iodide ($CH_3NH_3PbI_3$, MAPI) films achieve ΔE_F of up to 1.28 eV, i.e., 40 meV less than what would be expected from a sample without any

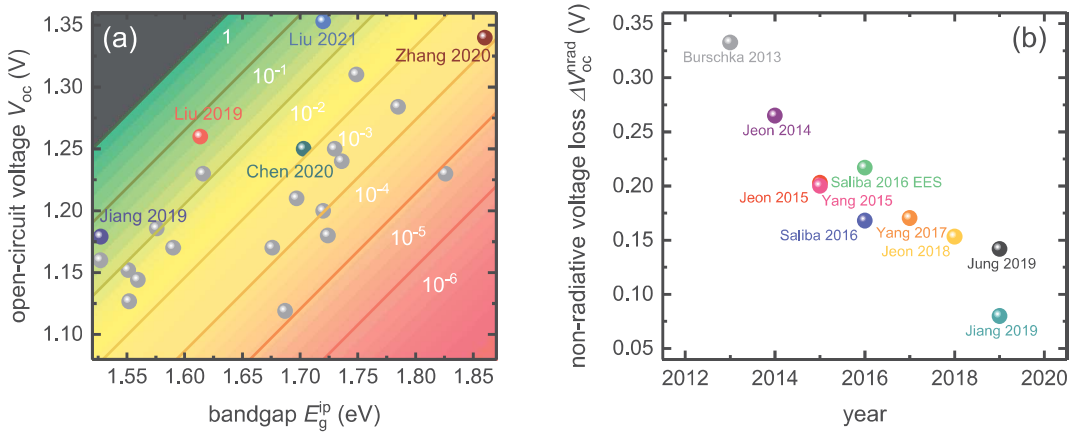


FIG. 20. (a) Open-circuit voltages as a function of the bandgap determined via the inflection point of the external quantum efficiency onset for a selection of data from the literature. In the background, the corresponding luminescence quantum efficiency is color coded with each line representing a loss of one order of magnitude in luminescence quantum efficiency and of kT/q ln(10) = 58 mV in V_{oc}. Modified from Liu *et al.*, Adv. Energy Mater. **11**, 2003386 (2021). Copyright 2021 Author(s), licensed under a Creative Commons Attribution 4.0 License. (b) Development of non-radiative voltage losses as a function of time for a selection of lead-halide perovskite solar cells [Reproduced with permission from Krückemeier *et al.*, Adv. Energy Mater. **10**, 1902573 (2019).Copyright 2019 Author(s), licensed under a Creative Commons Attribution 4.0 License].

© Author(s) 2021

non-radiative recombination.[318] Additional losses to the V_{oc} of the finished device can be extremely small in some rare cases, but for the bulk of the published data in the literature, the V_{oc} is substantially lower than what might be possible based on the quality of the bulk material. The key culprit causing these additional losses is interfaces to charge transport layers. At interfaces, the conduction and valence bands are often not perfectly aligned, thus leading to an increased product of electron and hole concentrations at a given quasi-Fermi level splitting. This is equivalent with saying that at the interface, the energy gap separating electrons and holes across the interface is lower than in the bulk. Thereby, even for reasonably low interface recombination velocities, the recombination rate at the interfaces might be substantial enough to limit the achievable quasi-Fermi level splitting and eventually V_{oc} in a finished device.

3. Advances in science

The importance of interfacial recombination for limiting V_{oc} is a result of detailed sample characterization efforts,[279] but it is also an implicit consequence of the success of surface passivation efforts to improve efficiencies and open-circuit voltages. Examples that resulted in a successful reduction in interfacial recombination are the surface treatment with salts, such as phenethylammonium iodide (PEAI),[202] n-butylammonium bromide (BABr),[319] or guanidinium bromide,[320] to name just a few. Other successful efforts to improve V_{oc} were achieved by exchanging the hole or electron transport layer (ETL) and thereby tuning of energy level alignment or introduction of interfacial dipoles.[321]

Thanks to the current level of success in implementing surface and bulk passivation strategies, the open-circuit voltages of perovskite solar cells have been approaching levels of ~10% external luminescence quantum yield and non-radiative V_{oc}-losses of around 60 mV over a range of bandgaps from around 1.5 eV to around 1.6 eV, which is better than any photovoltaic technology except for GaAs.[322] Toward higher bandgaps, however, the voltage losses usually increase, as shown in Fig. 20(a), with only rare exceptions showing lower losses.[653] Thus, one further strategy in the field should be to reduce recombination losses over a wider range of bandgap values.[323] Further reducing the voltage losses below 60 mV might require tackling not only recombination losses but also parasitic absorption losses that reduce photon recycling and thereby the charge carrier concentration and voltage at constant charge generation.[324] Reduction of parasitic absorption by, e.g., improving the optical quality of the back mirror is an important topic for achieving higher efficiencies in GaAs solar cells and might become more relevant for perovskites as well. Finally, the role of ion movement, the electric field, and the built-in voltage on charge recombination and open-circuit voltage has to be better understood. While there are some reports exploring ion movement in experiment and simulation on JV curves and photovoltage transients, the employed cells were not efficient, given today's standards.[365] In contrast, there are also publications that provide evidence that ions are hardly relevant for understanding the open-circuit voltage of efficient solar cells.[652] Furthermore, the origin of changes in V_{oc} over seconds and minutes of illumination is not fully understood. Thus, a combination of systematic experimental and modeling studies[337] on high performance cells will hopefully provide evidence on how to optimize the electrostatic potential distribution for maximum V_{oc}.

4. Concluding remarks

The open-circuit voltages of lead-halide perovskite solar cells relative to $V_{oc,SQ}$ have always been high in comparison with other photovoltaic thin-film technologies and in consideration of the maturity of the technology. Over the last few years, the gap to the thermodynamic limit has been continuously shrinking with a wide variety of passivation methods and improvements in the alignment between the absorber and charge transport layers being mainly responsible for the improvement. The underlying reasons for the remaining losses are non-radiative recombination via defects and parasitic absorption of luminescence. However, the understanding of the defect physics of perovskite solar cells is currently still at an early stage. One challenge is that the measurement of low defect densities and energetic positions of defects is difficult with most methods being prone to misinterpretation.[654] In addition, the calculation of multiphonon recombination processes between extended and localized states in highly anharmonic semiconductors, such as lead-halide perovskites, is difficult and has so far been only performed in few cases for specific defects in specific perovskite compositions.[343,655] An additional challenge for optimizing V_{oc} is the huge variety of compositions with different bandgaps and energy levels that each require slightly different contact layers as well as processing and passivation strategies.

B. Charge recombination in the bulk and at the interfaces

Jonathan Warby, Emilio Gutierrez-Partida, Dieter Neher, Martin Stolterfoht

1. Status of the area

The study of non-radiative recombination has long been at the forefront of academic research on various photovoltaic (PV) technologies. This is because non-radiative recombination is a loss mechanism in solar cells, lowering the external radiative efficiency [in the following, called the photoluminescence quantum yield (PLQY)], which, in turn, lowers the FF and V_{OC} of the cell. Non-radiative recombination in semiconductors is typically caused by defects and impurities, which leads to trap-assisted recombination through midgap states. In silicon PV, extremely high-quality wafers with low defect densities in the bulk ($\ll$1 ppb) were achieved through extended growth of single crystals at high temperatures (~1100 °C) using high purity precursors. Contrastingly, perovskites with low deep trap state densities can be fabricated from relatively impure materials and low temperature processes, which has allowed the field to rapidly progress as researchers can make efficient perovskite solar cells using simple laboratory equipment. However, in contrast to silicon where the PLQY of the "neat material" or as-cut wafers (1×10^{-8}–1×10^{-7})[326] is generally enhanced by orders of magnitude (up to >1%) upon addition of tailored passivation and charge transport layers (TLs) [Fig. 21(a)], for perovskites, this has not been achieved yet.[279] In fact, for a large number of perovskite systems, photoluminescence measurements on partial cell stacks and other transient techniques have demonstrated that the recombination losses in the complete cell remain stubbornly dominated by interfacial recombination at one or both perovskite/transport

© Author(s) 2021

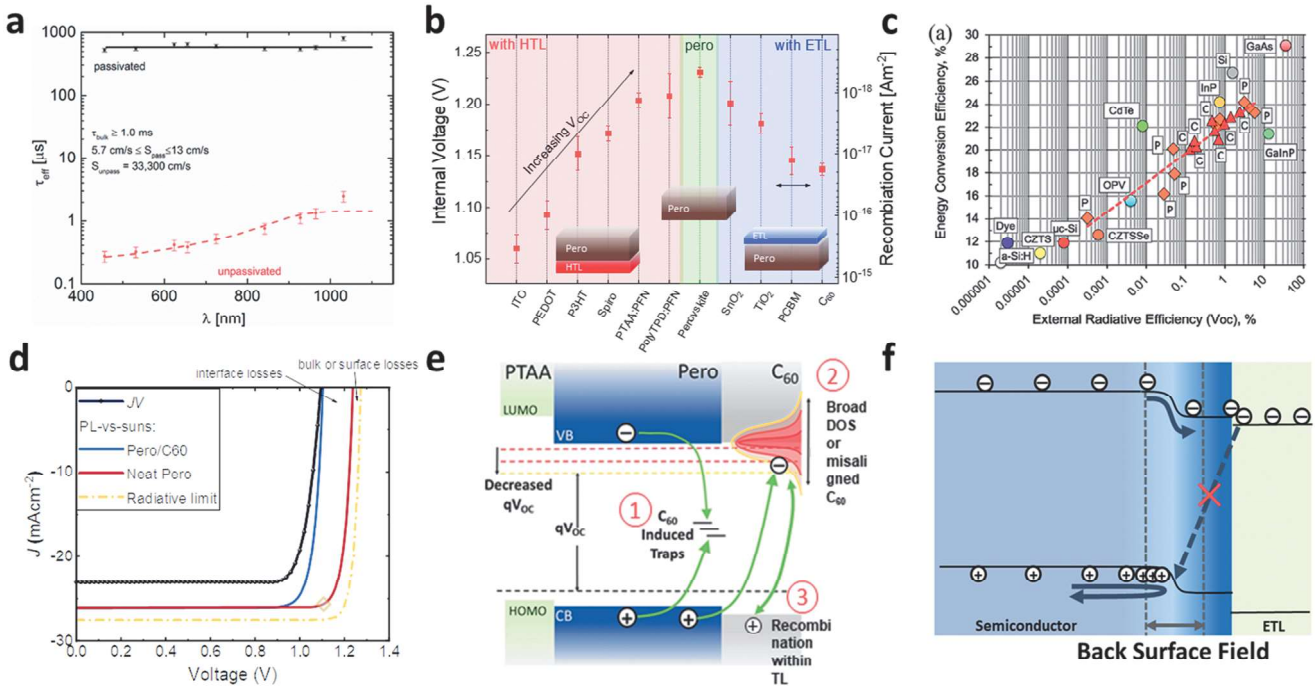


FIG. 21. (a) Measured PL lifetime vs wavelength of an unpassivated (as-cut) *n*-type HIT wafer and a passivated cell stack, which includes amorphous intrinsic silicon (~5 to 10 nm) on both sides and a doped p + a-Si layer (~5 to 10 nm) on one side and a doped n + a-Si layer (~10 to –20 nm) on the other side. Reproduced with permission from Roller *et al.*, J. Appl. Phys. **120**, 233108 (2016) with the permission of AIP Publishing.[351] The passivation and the employed charge transport layers strongly reduce the surface recombination velocity and with that the open-circuit voltage of the final cell. (b) In contrast, in perovskites, added charge transport layers typically lower the quasi-Fermi level splitting of the neat perovskite layer (data shown for triple cation perovskites). Data reproduced with permission from Stolterfoht *et al.*, Energy Environ. Sci. **12**, 2778 (2019). Copyright 2019 Royal Society of Chemistry. (c) The external radiative efficiency of various PV technologies reproduced with permission from M. A. Green and A. W. Y. Ho-Baillie, ACS Energy Lett. **4**, 1639 (2019). Copyright 2019 American Chemical Society. (d) JV-characteristics of pin-type perovskite cells using the perovskite demonstrated by Jiang *et al.*[202] as compared to pseudo-JV curves obtained on the neat perovskite and a perovskite/C_{60} stack using intensity dependent PL measurements.[352] The results demonstrate that the efficiency potential of the neat layer (28.4%) is very close to the radiative limit at the given bandgap (1.54 eV); however, non-radiative recombination at the perovskite/C_{60} heterojunction considerably limits the cell performance. (e) Possible recombination loss mechanisms at the perovskite C_{60} interface and (f) suppressing interfacial recombination through a back surface field.

layer heterojunctions [Fig. 21(b)].[279,327–330] Despite this, the study of non-radiative interfacial processes has been largely left out of the limelight in a field that has strongly focused on improving the bulk quality and the passivation of electronic defects on the surface. Clearly, to make progress further toward the thermodynamic limits, the field needs to disentangle the underlying physics that causes interfacial recombination.

Today, state-of-the-art perovskite solar cells have open-circuit voltages that are approaching the radiative limit.[202,331] Jiang *et al.*[202] showed an exceptionally high V_{OC} of 1.18 V at a bandgap of 1.54 eV, and they measured an electroluminescence quantum yield (EQE_{EL}) of ~7% at an injection current of J_{SC}, which means a non-radiative V_{OC}-loss$[kT/q\ \ln(EQE_{EL}]$ of only 69 meV. Similarly, in the paper with the highest certified efficiency of 24.4%, we can predict their EQE_{EL} of 6.8% from their V_{OC} of 1.162 V and an estimated bandgap of 1.5 eV.[331] As shown in Fig. 21(c), these values for EQE_{EL} are outperforming the best EQE_{EL} values reported for monocrystalline Si (1.6%) values and approach the highest EQE_{EL} of III-V semiconductor solar cells, e.g., GaAs (35.7%).[322] Very encouragingly, the perovskite as prepared following the work of Jiang *et al.* exhibits a PLQY of 25% with a Shockley–Read–Hall lifetime of over 18 s even without additional passivation. In such a material, the losses with respect to the radiative limits [see Fig. 21(d)] are likely related to parasitic absorption and imperfect light outcoupling management. This underlines further that perovskite solar cells can closely approach their thermodynamic limits and surpass silicon in power conversion efficiency if the losses associated with the interface recombination can be controlled.

2. Current and future challenges

The problem of interface recombination is particularly evident in (but not limited to) *pin*-type solar cells that have lower efficiencies (25.4% vs 22.3%) than *nip*-type cells. Yet, *pin*-type cells are more desirable for application in perovskite tandem solar cells, partially due to lower temperature processing (100 C). An interesting observation is that in both *nip*- and *pin*-type architectures, the transport layer deposited on top of the perovskite is often limiting the total recombination loss of the device, while near lossless transport layers, such as SnO_2,[279] different self-assembled monolayers (SAMs)[321] or PTAA/PFN-Br[332] can be employed below the perovskite [Fig. 21(b)]. This leads to the question of whether (i) there is a difference in the surface states between the front and back side of the device,

© Author(s) 2021

which causes the penalty, or (ii) if it is due to engineering considerations of what can be deposited on top without damaging the perovskite.

In *pin*-type cells, C_{60} is commonly used as the charge transport layer, which is deposited on the top surface, and it lowers the PLQY of the neat material by 1–2 orders of magnitude to 1×10^{-4}–1×10^{-3}, as shown for many different perovskites.[279,330,332–334] It is therefore of expressly high importance to address the losses at the perovskite/C_{60} interface, which currently remain poorly understood. It is likely that the loss is related to midgap states or a broad density of states in C_{60} acting as efficient non-radiative recombination centers. However, at present, an energetic misalignment at the perovskite/C_{60} interface or C_{60}-induced midgap states on the perovskite surface cannot be excluded. The potential loss mechanism is shown in [Fig. 21(e)]. In contrast, in *nip*-type cells, heavily doped spiro-OMeTAD is typically used as a hole transport layer. The strong doping and the expected increase in the built-in field[335] over the perovskite or increased back-surface field could explain why interfacial recombination can be suppressed to a minimum in record *nip*-type cells (cf. *pin*-cells). However, *n*-doping the C_{60} or PCBM has not yet been very effective at suppressing interfacial recombination, which might be due to the instability of *n*-dopants and their potential reactivity.[336] In order to clear up this confusion, the nature of the built-in potential distribution needs to be better understood, which is significantly complicated by the presence of mobile ions in the perovskite absorber layer.[337,338] Many groups have reported mobile ion densities significantly exceeding the electronic or the capacitive carrier density.[339–341] In this case, the built-in potential would drop across a relatively small portion of the absorber layer by ion accumulation at the interfaces, which impedes efficient charge extraction.[342] Therefore, the seemingly conflicting information between high performance and attenuation of the built-in field by mobile ions and their impact on the interfacial recombination remain a pressing and open topic. All this currently complicates the design rules for tailored charge transport layers that reduce surface recombination while rapidly extracting the majority carriers—again highlighting the need for deeper understanding of interfacial recombination.

3. Progress

In order to reduce the recombination rate in the bulk or at the surface of a semiconductor, there are several distinct possibilities that the experimentalist has: (i) reducing the number of defect states via chemical passivation, (ii) reducing the interfacial transfer rate through an energetic barrier for minority carriers, e.g., with wide-gap interlayers, and (iii) reducing the concentration of the minority carrier at that surface by creating a back surface field [Fig. 21(f)], e.g., through surface or TL doping or molecular dipoles. Until today, the perovskite solar cell community has predominantly focused its efforts on chemical passivation, which may be partially due to the distinct ionic nature of the perovskite that creates electronically charged defects opening a myriad of possibilities for chemical passivation (e.g., coordinate bonding, addition of Lewis bases or acids, and many more).[343,344] Moreover, the simple solution processability and defect tolerant nature of perovskites allow the addition of chemical additives to the precursor solution, which may ultimately lead to a reduced defect density in the crystallized films. However, although these methods have resulted in impressive PCE improvements, it remains unclear if additive-based passivation can push the technology to its practical PCE limit of over 30% in the next years. An alternative strategy is the use of thin insulating layers as tunnel barriers to reduce the minority carrier concentration from the critical interface (ii).[327,345,346] While early works on such wide-gap insulators have demonstrated promising performance improvements, their applicability appears to be limited to certain perovskite compositions for which the benefit of the reduced transfer of the minority carriers outweighs the negative effects associated with the increased transport resistance. Similarly, a wide-gap interlayer can also be formed through compositional engineering of the perovskite, for example, by increasing the Br content at the surface.[347] More recently, the application of wide-gap two-dimensional perovskite layers has become popular to reduced hole density at the critical perovskite/spiro-OMeTAD interface by creating 3D/2D "homojunctions" with negligible interfacial recombination and reduced surface recombination.[348] Ultimately, this approach has allowed us to improve the open-circuit voltage to over 1.3 V for 1.72 eV *nip*-type cells.[319] In contrast, the third strategy of repelling minority carriers from the interface through graded doping and the creation of a back-surface field or increased built-in voltage has proved to be challenging, although a more *n*-type surface has been found to correlate with a higher V_{OC} in *pin*-type cells.[320,349,350]

4. Concluding remarks

As perovskites have benefitted from a prolonged "honeymoon period" where improved processing of the perovskite and transport layers has allowed efficiencies to continually increase, interfacial recombination at perovskite/transport layer heterojunctions has largely been left out of the limelight. Today, as the opto-electronic quality of perovskite semiconductors is essentially at the radiative limits, the efficiency gains made by the field are beginning to plateau, necessitating the need of a clear understanding of the processes causing interfacial recombination. In particular, for *pin*-type cells, the losses at the top interface to C_{60} appear to be omnipresent and universal to various perovskite compositions. However, similar losses are also observed for various other transport layers underlining the difficulties in creating ideal perovskite/semiconductor heterojunctions. In contrast, perovskite/transport layer homojunctions (e.g., 3D/2D perovskites) may prove to be effective at suppressing the minority carrier recombination at the critical interface while allowing rapid charge extraction. Overall, understanding and solving these problems will ensure further progress toward realizing near-ideal perovskite cells at the radiative limits, possibly for different bandgaps required for multi-junction perovskite solar cells.

C. Interfaces

Uli Würfel, Moritz Unmüssig, Jan Herterich, Clemens Baretzky

1. Status of the area

Interfaces (between different materials) play a decisive role for the performance of perovskite solar cells. In contrast to conventional

© Author(s) 2021

crystalline silicon solar cells, devices based on perovskite absorbers do not make use of a pn-junction within the perovskite material. In contrast, perovskite solar cells are devices comprising a p–i–n or n–i–p heterojunction. The "i" means an intrinsic absorber sandwiched between an n-doped and a p-doped material, respectively. Note that several studies indicate that perovskite absorbers are, in fact not, very intrinsic and doping levels up to 7.6×10^{20} cm^{-3} have, e.g., been derived from Hall effect measurements.[353–358] However, note that it is not intentionally doped and that there is no pn-junction within the absorber layer itself.

The perovskite absorber is sandwiched between the electron and hole transport layers, ETL and HTL. They are used to achieve the following four conditions:

1. passivation of surface states, i.e., ensuring a low interfacial density of states with energies within the bandgap of the perovskite absorber;
2. lossless extraction of majority carriers, achieved by providing a high corresponding electric conductivity;
3. an energetic barrier for the minority carriers in order not to extract both type of charge carriers from the absorber, achieved through a large bandgap and favorable band alignment; and
4. very low absorption in the transport layers as to maximize the absorption in the perovskite absorber layer, usually achieved by application of a thin layer with a rather large bandgap.

ETL and HTL comprise in most cases a rather large bandgap and are chosen such that the conduction (valence) band of the *n*-type (*p*-type) material matches well with the conduction (valence) band of the perovskite material. Then, due to their bandgaps being larger than that of the absorber, an energetic offset results for the holes (electrons) at the absorber/*n*-type (absorber/*p*-type) interface. These energetic offsets impede the extraction of the "wrong" type of charge carrier. To ensure a good conductivity for the electrons (holes), the ETL (HTL) is usually n-doped (p-doped). Moreover, doping has also another beneficial effect, which will be discussed below.

Although an energetic offset of several hundreds of meV would suffice, it has to be considered that such materials and, especially such interfaces, are not ideal, i.e., condition (1) is not fully met. In fact, every interface constitutes an abrupt interruption of the periodicity in which atoms are arranged within the material. Consequently, there are states not only for electrons in the respective bands but also within the bandgap, the so-called interface (trap) states. For this reason, to impede significant interface recombination, the minority carriers have to be prevented from reaching that interface. In a fundamental study, it was shown that the decisive ingredient to achieve this is a very low conductivity of the holes (electrons) in the absorber close to the absorber/ETL (absorber/HTL) interface.[359] This is the second effect of the doping of the transport layers: it keeps the concentration of the minority carriers in the absorber close to the interface at a low value.

Processing techniques to apply ETL and HTL materials are either solution- or vacuum-based. Most organic materials, such as MeO-2PACz, spiro-OMeTAD, PTAA, PEDOT:PSS, and PCBM, and some inorganic materials, such as ZnO, TiO_x, ZrO_2, and graphite, as well as organic–inorganic 2D-perovskites are deposited from solution via spin-coating, blade-coating, slot-die coating, spray coating, or inkjet-printing, each requesting separate optimization.[171,321,360] Fullerenes and many inorganic materials are deposited by evaporation in ultrahigh vacuum (UHV).[361,362] Moreover, atomic layer deposition is also frequently used in the context of perovskite solar cells, e.g., for SnO_x.[363,364] Much of the impressive progress in the efficiency of perovskite solar cells in recent years is, in fact, due to improvements in the quality of the interfaces between the absorber and transport layers.

2. Current and future challenges

As mentioned in Sec. IV B, the presence of mobile ionic species (ions and ion vacancies) in the absorber makes the situation at those interfaces in perovskite solar cells even more complex.[9,339,365–368] These ionic species move within the perovskite absorber to reach electrochemical equilibrium, which includes their reaction on the electric field. Without ions, the latter originates mostly from the different work functions of the electrodes (contacts and transport layers), the so-called built-in field. There are different ionic species with (largely) differing mobilities.[33,339,368–370] Therefore, the time it takes for the ionic species to equilibrate, e.g., in the dark under thermal equilibrium, can range from ms to days.[370,371] Furthermore, if now such a device is illuminated (e.g., under open-circuit conditions), the build-up of the photovoltage changes the electric field in the absorber and so the ionic species again move to reach their new equilibrium positions. In different studies, it has been identified that the recombination occurring at the interfaces between the absorber and ETL or HTL depends sensitively on the distribution of the ionic species. This is because the recombination rate is governed by the electron and hole densities near such an interface and these densities, in turn, depend on the electric field that changes when the ion distribution changes. There are two effects that must be distinguished here: (i) the actual loss of photogenerated charge carriers due to interfacial recombination and (ii) potential voltage losses due to gradients of the quasi-Fermi levels of the majority carriers close to their respective electrode. Whereas the former loss mechanism reduces the carrier densities and hence both voltage and photoluminescence (PL), the latter almost exclusively reduces the voltage but has hardly any impact on the intensity of the PL. Hence, by measuring both V_{OC} and PL intensity, these two effects can be separated from each other. To illustrate this, Fig. 22 shows an example of both, an experiment and a simulation, where the redistribution of mobile ions in the absorber during illumination leads to a strong increase in V_{OC} over time, while the PL stays rather constant. The experiment was done with a p-i-n perovskite solar cell with a $Cs_{0.17}FA_{0.87}Pb(I_{0.73}Br_{0.27})_3$ absorber between PTAA and PCBM. The simulations are based on a model outlined in detail in our recent work.[372]

Analogously, a measurement of the current–voltage characteristics of a perovskite solar cell constitutes a dynamic change in the electric field in the absorber and causes ionic species to move. Whether they will react within the time frame of the measurement depends on their mobility. This can clearly be seen by a variation in temperature where lower temperatures lead to slower responses of the device as the ionic mobility depends strongly on temperature.[339,373,374]

© Author(s) 2021

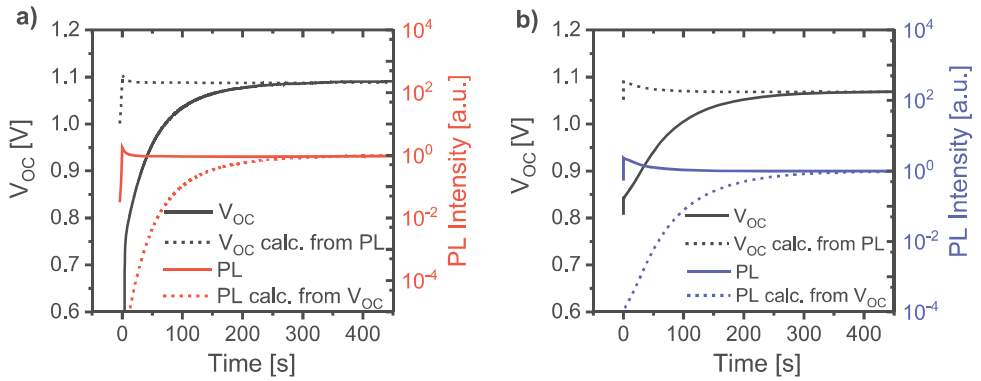


FIG. 22. Experiment (a) and simulation (b) of transient V_{OC} rise (solid black) and PL rise (solid red/blue) after switching on the illumination at t = 0 s. The simulation was performed under explicit consideration of mobile ions in the perovskite absorber layer. The dashed lines show the evolution of the PL (V_{OC}) that is expected from the actual V_{OC} (PL) data, if no gradient in the quasi-Fermi level of the majority charge carrier is considered.

3. Progress

Further improving our understanding of the interplay between mobile ions and interfacial recombination is crucial to correctly characterize the effects of interface engineering. One approach to eliminate hysteretic effects is to decrease the density of mobile ionic species, potentially also decreasing stability issues due to phase segregation.[51] On the other hand, if the selectivity of the electrodes (including, transport layers) can be increased to a high degree, the actual distribution of ionic species within the perovskite absorber will hardly have any impact and recombination occurring at those interfaces will be minimized under all operational conditions. Different materials are used to improve surface passivation, such as PEAI or polymeric interlayers, such as PMMA.[375] The latter has also shown increased resistance to moisture-based degradation.[52,376,377] While the increase in moisture resistance can be attributed to the hydrophobic nature of PMMA, there is strong evidence that it also passivates surface defects that would otherwise lead to increased recombination. However, the interlayer thickness must be carefully calibrated as not to hamper charge transfer. In this way, the long-term stability can be improved by interface engineering, either due to blocking the influx of contaminants or by passivating defects that nucleate the degradation process.

The application of 2D perovskites allows for the incorporation of larger, more hydrophobic, and stable organic molecules between multiple planes of inorganic perovskite octahedrons. As the charge transfer is usually anisotropic and specifically reduced perpendicular to the layers, the resulting lower performance must be balanced against the increased stability and selectivity. Decreased performance can be partially compensated by aligning the 2D layers more perpendicular to the perovskite surface to allow increased charge transfer along the normal direction.[378,379] This is discussed in greater detail in Sec. II F.

For the passivation of interfaces and grain boundaries, additives can be used in the perovskite precursor solution. Recent examples are ionic liquids, such as 1-butyl-3-methylimidazoliumtetrafluorborat, and surface-anchoring alkylamine ligands, phenylethylamine and butylamine.[350,380] Another approach to control surface recombination that has been successfully demonstrated is to dope the perovskite absorber in the interfacial region.[657,658]

4. Concluding remarks

Interfaces in perovskite solar cells, in particular, those between the absorber and the transport layers, are of utmost importance in order to maximize the fill factor and the open-circuit voltage of these devices. This can also be seen in the research efforts to properly characterize and control interface properties. This is very similar to all other types of heterojunction solar cells. What makes perovskite solar cells special is the fact that the absorber comprises mobile ionic species, which redistribute according to the electric field. As the latter not only depend on the device stack but also on light intensity and applied voltage, these ionic species move under solar cell operation and thereby influence the distribution of electrons and holes, especially near the interfaces to the transport layers. This can have strong effects on two types of losses correlated with interface recombination: the actual reduction of charge carrier densities due to interface recombination as well as voltage losses due to gradients of the quasi-Fermi levels of the majority charge carriers close to their respective electrode. This must be accounted for during characterization in general (see Sec. VI A) as well when engineering interfacial properties.

D. Electron and hole transport layers

John Mohanraj, Mukundan Thelakkat

1. Status of the area

In 2012, the incorporation of solid p- and n-layers in a p-i-n solar cell involving perovskite as the intrinsic semiconductor has revolutionized the field of solution processed solar cells and triggered the evolution of perovskite photovoltaics.[381,382] Charge transport layers (CTLs), in addition to extracting charges from the active

© Author(s) 2021

layer, are crucial for perovskite solar cells (PSCs) as they define the built-in field in the device along with the contacts and control the charge carrier recombination events at the active layer/CTL interfaces. Thus, a myriad of efforts has been devoted over time to develop and optimize electron transport layers (n-layer; ETL) and hole transport layers (*p*-type; HTL) for PSCs, which led to define the following criteria for suitable CTLs: (i) matching energy levels with the conduction and valence bands of perovskite; (ii) reasonable charge carrier mobility ($>10^{-4}$ cm^2 V^{-1} s^{-1}) and conductivity properties;[383,384] (iii) high transmittance in the spectral region in which perovskite absorbs, and (iv) ability to form compact and stable films. By adopting a variety of CTLs satisfying these conditions from established technologies, such as organic heterojunction photovoltaics, dye sensitized solar cells, and organic light emitting devices, perovskite photovoltaics has achieved unparalleled progress in a short time.

2. Evolution of ETL and HTL in PSCs

Historically, PSCs have derived their device geometry from dye sensitized and organic heterojunction solar cells, in which the photoactive material is deposited either on a compact TiO_2[381] or ZnO or mesoporous TiO_2 layer to facilitate electron extraction. Later, it was demonstrated that the perovskites themselves possess high electron transport properties; hence, insulating Al_2O_3 was also used as a scaffold.[382] A regular PSC contains a thin compact TiO_2 as ETL (<40 nm) with or without a mesoporous TiO_2 layer, and until now, this structure remains as a popular choice for highly efficient devices as there is a favorable conduction band energy level alignment with that of the perovskite, facilitating efficient electron transfer from the latter. Recently, SnO_2 has emerged as a promising ETL with better energy level alignment at the ETL/perovskite interface, a deeper valence band that blocks holes effectively, and offers high transparency and photostability in combination with the low temperature preparation method, which enables the device fabrication even on flexible substrates.[385] While the above device structure is considered as normal n-i-p type,[257] PSCs are further classified into inverted p-i-n[386] type based on the direction at which electrons and holes are extracted. In this device geometry, fullerene derivatives, in particular, phenyl-C_{61}-butyric acid methyl ester (PCBM) known from organic photovoltaics, are employed on top of the perovskite layer as standard ETLs.

As HTL for normal n-i-p devices, many inorganic *p*-type materials, such as CuI, NiO_x, CuSCN, and CuO_x,[387] have shown to be effective due to their high hole mobility values (0.01–0.1 cm^2 V^{-1} s^{-1}). However, the conventional triarylamine based organic small molecules and polymers, in particular, air-doped 2,2′,7,7′-tetrakis(N,N-di-*p*-methoxyphenylamino)-9,9′-spirobifluorene (spiro-OMeTAD), poly triarylamines (PTAA), and poly-3-hexyl-thiophene (P3HT), are still dominating as hole transport materials, resulting in PSCs with >20% efficiency.[320,392] As p-doping of these materials improves their bulk hole mobility as well the built-in potential of the devices and reduce the minority charge carrier concentration at the HTL/perovskite interface as discussed in Secs. IV A and IV B, many exotic p-dopants are also simultaneously developed.[388,389] In the case of p-i-n type devices, PEDOT:PSS was employed as HTL for a long time, and recently, it has been replaced by nano-crystalline NiO_x to obtain stable and efficient PSCs.[390] With a same perovskite active layer, mesoporous n-i-p type PSCs excelled with high efficiency and some p-i-n type devices displayed parasitic I–V hysteresis-free performance. Such complementary outcomes combined with the demand for stable and efficient PSCs formed the basis for further research in the field of CTLs.

3. Current and future challenges

The CTL/perovskite interfaces play a crucial role in dictating the device performance and stability. Until now, the non-radiative charge recombination events occurring at these interfaces, which are majorly controlled by the intrinsic properties of the CTLs, such as energy level alignment, carrier mobility, and trap density, are attributed to the loss in maximum achievable V_{oc} in PSCs. Optimizing such interfaces with appropriate transport materials and through passivation techniques remains as a big challenge to achieve highly efficient PSCs.

On the other hand, the bulk properties of CTLs are considered as one of the major reasons for the long standing functional photo and thermal stability issues of devices. For instance, TiO_2 and NiO_x are established photocatalysts, which could impact the stability of perovskites under UV-light irradiation.[390,391] Similar decomposition events are also observed with other metal oxides, in which the superoxide radicals formed at their intrinsic defect sites initiate the redox reactions.[390] Chemical reactions of ZnO[393] and CuSCN[394] with perovskites are also observed at elevated temperatures, causing thermal stability issues in PSCs.

With fullerene based ETLs, their affinity toward halide ions is claimed to suppress the I–V hysteresis; however, the same facilitate the halide ion migration and, consequently, perovskite degradation over time.[395] Similarly, organic HTLs permit ion/atom diffusion from perovskites[396] and electrodes[397] due to their poor mechanical properties at high temperatures (>80 C), causing stability issues. Additionally, the hygroscopic and corrosive nature of PEDOT:PSS directly influence the stability of the active layer and transparent electrodes,[398] whereas spiro-OMeTAD and PTAA play their part indirectly. These HTLs need to be p-doped due to their poor conductivity and is achieved through air-doping by adding cumbersome amounts of hygroscopic Li-TFSI and *tert*-butyl pyridine additives. The consequence of this process is many folds: (i) exposing uncompleted devices for air-doping facilitates moisture and oxygen ingression into the perovskite, initiating the device degradation process even in the dark; (ii) both additives can chemically interact with the perovskite and permanently damage the perovskite/HTL interface;[399,400] (iii) inhomogeneous films with pin-holes generation over time,[401] and (iv) as the air-doping efficiency varies with ambient conditions, the performance reproducibility of PSCs is jeopardized.[402]

Considering the commercialization prospects, the scaled up PSCs (>10 cm^2) have reached only 16% efficiency up until now, which is significantly lower than the state-of-the-art small area devices. Such a huge disparity in performance between small and large area devices is majorly attributed to the heterogeneity in perovskite and CTL films deposited on large areas.[209] At present, the scalability of PSCs without compromising their device performance remains as a pivotal challenge in the path of commercialization, which is yet to be addressed.

© Author(s) 2021

4. Advances in science and technology to meet challenges

Concerning CTLs, there is a steady progress in materials development and layer engineering with a spotlight on improving their photostability, charge carrier extraction, and transport properties and suppressing intrinsic defects density, which all have direct consequences on the performance and durability of PSCs. In this line, the concept of using ternary metal oxides, such as $ZnTiO_3$, Zn_2SnO_4, $SrTiO_3$, and $BaSnO_3$, and multilayer binary metal oxides, such as ZnO/TiO_2 and WO_x/SnO_2, as ETL is gaining interest as the resulting PSCs display over 20% efficiency and long-term stability.[384] Elemental doping of existing binary and ternary metal oxides based CTLs is also investigated to improve the performance of PSCs as this process largely suppresses the intrinsic defect density in transport layers.[404,405] Alternatively, surface passivation has also been practiced on CTLs through depositing a thin layer of organic Lewis acids or bases, which limits the defect density at the CTLs/perovskite interfaces (see Sec. IV C) This is reported to improve FF and V_{oc} of PSCs due to reduced parasitic charge recombination processes at the interfaces, and interestingly, the same has enhanced the device stability in ambient conditions as these layers form a physical barrier against moisture and oxygen ingression.[389,405] In this context, depositing a thin layer of PCBM or other fullerene derivatives on TiO_2, ZnO, and SnO_2 has become a common practice in device preparation.

In PSCs with organic CTLs, cross-linking the organic semiconducting material in both ETL and HTL has shown to improve their mechanical strength even at higher temperatures.[406,407] On the other hand, with regular organic HTLs, the key issues have been addressed in three ways: (i) small quantities of a variety of direct non-conventional dopants are tested in spiro-OMeTAD and PTAA HTLs to avoid device exposure to moisture and oxygen;[388,389,408,409] (ii) new, hydrophobic, dopant-free hole transport materials with improved intrinsic electronic properties are being developed;[410] and (iii) hybrid HTLs, such as carbon nanotubes mixed with spiro-OMeTAD or P3HT[411,412] or gradient mixture of spiro-OMeTAD and P3HT,[413] are introduced to improve stability against moisture and thermal and mechanical stresses.

Toward upscaling of PSCs, a few reported examples demonstrate high performance large area devices with CTLs, such as SnO_2, NiO_x, CuSCN, PTAA, and P3HT,[209] and indeed, further developments are foreseen in device and process engineering methods. In this context, ETL- or HTL-free PSCs technology is emerging as a viable option for mass production as they demonstrate the combined benefits of reduced CTL related issues and cost-effective production possibilities.[414,415]

5. Concluding remarks

Undoubtedly, CTL development has significantly contributed to the growth of perovskite photovoltaics in the last few years. It is also evident that some of them caused performance and stability issues in PSCs. However, recent progress in materials, device engineering, and scalable techniques are encouraging as the durability of PSCs continues to improve over thousands of hours, maintaining reasonably high efficiencies even in large area devices. On the other hand, a fundamental understanding on CTLs/perovskite interfaces to improve the performance of PSCs close to their thermodynamic limit needs further studies. Alongside, a few paradoxical observations, such as high efficiency of PSCs containing TiO_2 and air-doped spiro-OMeTAD CTLs with poorly defined electronic properties and ETL- or HTL-free PSCs superior performance, question the role played by CTLs in these devices. Gaining such basic knowledge on CTLs will certainly promote the large scale production of PSCs with improved durability and efficiency and, consequently, facilitate the commercialization of this technology.

E. Chemical composition and electronic structure of buried interfaces in perovskite solar cells using photoelectron spectroscopy

Clément Maheu, Wolfram Jaegermann, Thomas Mayer

1. Status of the area

Photoelectron Spectroscopy (PES) is a rare characterization technique that can give access to both spectroscopic (i.e., chemical) information and the electronic structure at the same time. PES has been widely used to characterize perovskite solar cells (PSCs). Béchu *et al.* recently reviewed most of the work that has been conducted in the past few years.[416] PES has been used to confirm the synthesized perovskite phases and to determine their stoichiometry.[416,417] PES was also used to determine their electronic structure and to understand the mechanism of some degradation process.

However, the strength of photoemission, namely, its surface sensitivity, prevents the investigation of buried interfaces in material stacks. The latter plays a crucial role in a device by governing its overall efficiency and its resulting I–V characteristics. The open-circuit voltage (V_{OC}) and thus the efficiency depend on the built-in potential created at these interfaces in thermodynamic equilibrium. The short-circuit current (J_{SC}) and thus the efficiency depend on the optimized charged carrier transfer from the perovskite absorber to the charge extraction layer toward the contacts. It means that recombination at the interface states should be minimized.

Therefore, to investigate buried interfaces with PES, appropriate strategies are required. They can be divided into two main families: the bottom-up approaches and the top-down approaches.

The bottom-up approach starts from a layer to progressively grown full device stacks. The so-called step-by-step interface experiments alternate step up contact layer deposition with PES analyses. The shifts of the PES spectra indicate band bending at the interfaces. This was used for several years on PSCs and decades on organic or thin-film solar cells; many of these experiments are described in Ref. 416. Recently, Hellmann *et al.* investigated the electronic structure of classical and inverted PSCs. They evidenced that the photovoltage mainly occurs at the typically *n*-type perovskite|*p*-type charge extraction layer interface. To reach such a conclusion, they compared $MAPbI_3$|spiro-OMeTAD and NiO_x|$MAPbI_3$ interface experiments in the dark and under illumination.[418]

The top-down approach starts directly with a full device stack. X-ray photoelectron spectroscopy (XPS) depth profiling alternates

© Author(s) 2021

ion gun etching cycles with XPS measurements.[419] For instance, Cacovich *et al.* addressed the effect of solar illumination on the optoelectronic properties of a state-of-the-art PSC. Hard X-ray PES (HAXPES) can also probe different depths (from 10 to 20 nm) of a given layer via photon energy tuning.[418,420] Finally, high local resolution methods probe the cross section of a full device. This is the case for Kelvin Probe Force Microscopy (KPFM) as well as Electron-Beam Induced Current (EBIC). They can inform on the electronic structure of a full device, but these methods lack the chemical information.[338,421]

2. Current and future challenges

Top-down and bottom-up approaches suffer from the challenges that are intrinsic to PES. The long time exposure of the samples to vacuum, light, and x rays may induce significant chemical modifications of the hybrid organic inorganic metal halide perovskites.[422] It can be avoided by minimizing the time of analysis and by performing careful PES measurements. For instance, Cacovich *et al.* recorded two survey spectra, one before and one after the full PES acquisitions.[419] It would reveal potential x-ray induced degradations. Another issue is the possible, unintentional, photovoltage. It can be induced by residual light in the ultrahigh vacuum (UHV) system and/or the PES source itself, leading to misinterpretation of the electronic structure. Hellmann *et al.* reported several precautions for limiting the amount of residual light and performed real "dark" measurements.[418] In addition, each of the two approaches also has limitations. The step-by-step interface experiments are limited to the study of layers that can be prepared by vacuum deposition. The PSCs with a perovskite layer prepared by vacuum deposition are often lagging behind their solution-processed counterparts. Getting information on the latter is also crucial to investigate the state-of-the-art devices. This is also the case for the extraction layers. Interface experiments with spiro-OMeTAD are numerous,[416,418] but promising alternative charge extraction materials can be found in the literature (see Sec. IV D). Some of these candidates cannot be prepared inside the UHV setup. Therefore, the bottom-up approach cannot be applied to all the buried interfaces composing PSCs.

In the top-down approach, the sample needs to be modified for revealing the buried interfaces. For KPFM or EBIC analyses, a normal cross section needs to be prepared by focused ion beam (FIB). To address the potential modification that FIB preparation may induce, Weber *et al.* evidenced that, for their system, the efficiency and the hysteretic behavior are similar before and after FIB polishing.[338] While KPFM and EBIC inform on the built-in potential along the device, PES can provide electronic information as well as chemical composition. It, however, lacks in local resolution, and it is in the range of 10 μm, while the thicknesses of the perovskite and space charge layers are in the nm range. XPS depth-profile is one alternative, but conventional argon sputtering may induce chemical and concomitant electronic variations. Damage can be minimized by sputtering with large organic molecules, such as C_{60} or coronene.

3. Advances in science

The Tapered Cross Section PES (TCS-PES) methodology is one answer for analyzing a cross section by PES without using ion etching in vacuum. This top-down approach was recently proposed to study PSCs.[423,424] Polishing a sample with a shallow angle extends the normal cross section (nm scale) to a tilted cross section (mm scale). Then, PES line scans can be taken on the resulting device. In Fig. 23, each line scan corresponds to a position of this TCS of a mixed ion lea halide PSC. Several core levels are analyzed; the detection of the elements gives an idea of the solar cell architecture (see the scheme on the left). Au mainly contributes between positions 0 and 6, the clear onset of strong Pb and I emissions at position 10 indicates the spiro-OMeTAD | perovskite interface, the $Ti2p_{3/2}$ line intensity starting at position 36 indicates the mesoporous TiO_2 and then the block the TiO_2 layer, and finally, the $Sn3d_{5/2}$ emission at position 49 corresponds to the FTO front contact.

The XPS line scans also inform on the variation of the composition and of the stoichiometry among the device. For instance, a

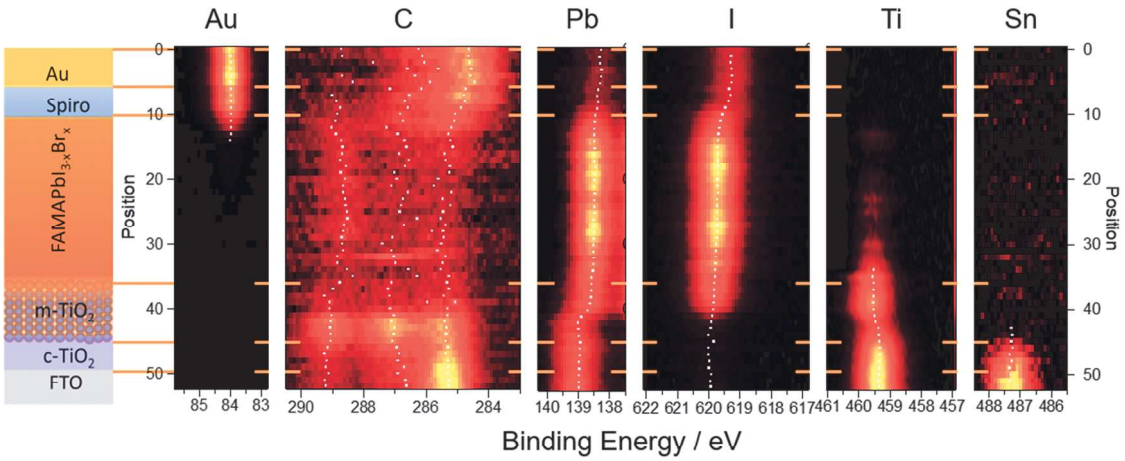


FIG. 23. Intensity contour maps of the XPS line scans performed on the TCS. The following core level spectra are depicted: $Au4f_{7/2}$, C1s, $Pb4f_{7/2}$, $I3d_{5/2}$, $Ti2p_{3/2}$, and $Sn3d_{5/2}$. On each scan, the white points correspond to local intensity maxima. The elemental distribution over this TCS leads to the expected PSC architecture sketched on the left. Adapted from Ref. 424.

© Author(s) 2021

bromine enrichment was evidenced toward the perovskite|*m*-TiO_2 interface.[423]

In addition to the chemical information, the steady variation of the binding energy of a certain core orbital indicates band bending and/or possible chemical variations. Under bias light, chemical and compositional modification will persist while band bending is flattened due to induced photovoltage.

For instance, the binding energy shift of the C1s orbital in spiro-OMeTAD (Fig. 23, positions 6–10) is due to band bending. On the contrary, the Pb4$f_{7/2}$ shift at the perovskite|*m*-TiO_2 interface (Fig. 23, positions 36–46) corresponds to variations, such as the Br/I ratio in the perovskite and to the TiO_2/perovskite ratio within the *m*-TiO_2. Thus, the band diagram across a wet chemically prepared perovskite PSC has been deduced.

In contrast to the mechanical polishing, Yang *et al.* used a chemical strategy for exposing the buried interfaces.[425] They reported a lift-off process to bring the perovskite part of the buried PTAA|perovskite interface to the top of the sample. They performed numerous characterizations, such as XPS, KPFM, or advanced microscopy, on the fresh layer and on the lifted-layer to confirm that this process has a small influence on the morphology of the layer and its chemical composition. Such work helps to conclude on the morphology of the perovskite layer at the interface. It is inhomogeneous and has sub-microscale imperfections that result in more rapid recombination.

Unfortunately, similar questions than as for the XPS depth profile or the investigation of the normal and the tapered cross section with KPFM, EBIC, or PES must be addressed. Lifting-off the perovskite layer, FIB, or the preparation of a TCS by polishing may modify the chemical composition and the electronic structure of the buried interfaces.

4. Concluding remarks

Buried interfaces played a crucial role in PSCs and in solar cells, in general. Techniques such as KPFM, EBIC, or PES can investigate such interfaces. The latter has the asset to provide both chemical and electronic information.

To access the buried interfaces of a full-stack, few methods were listed: chemical lift-off, FIB, ion gun, or mechanical polishing. The main challenge consists in accessing these buried interfaces of a device with minimized modification of the chemical composition and electronic structure.

A combination of KPFM or TCS-PES with the HAXPES for which the interfaces can remain buried would be one solution.

F. Crystalline surfaces for momentum-resolved experiments

Janek Rieger, Thomas Fauster, Daniel Niesner

1. Status of the area

Angle-resolved photoelectron spectroscopy (ARPES) gives direct access to the surface electronic band structure of a semiconductor. Hence, it is an important tool to determine essential electronic parameters of metal halide perovskites. So far, studies focused, in particular, on the occupied part of the band structure. $MAPbBr_3$, $MAPbI_3$, $MAPbCl_3$, and $CsPbBr_3$ were investigated, and they all exhibit a characteristic spectral shape of the valence bands.[426–429] The width of the dispersing valence bands, surface doping, and hole effective masses around 0.25 m_e were determined. Results are compared in a recently published review.[430] In most cases, the periodicity of the surface electronic structure reflects the pseudocubic building block of the metal halide perovskite, even if the bulk-terminated unit cell is larger due to superstructures related to the tetragonal and orthorhombic distortions. There are also some discrepancies: The bandwidths of the valence bands and the surface doping vary significantly.[430] Two studies found a Rashba effect on $MAPbBr_3$, but others did not.[427,430–432] The surface periodicity observed with low-energy electron diffraction (LEED) shows the large unit cells expected for the bulk-terminated tetragonal and orthorhombic crystal structures in contrast to the surface Brillouin zones from ARPES.

As a complementary technique, time-resolved two-photon photoemission spectroscopy (2PPE) can be used to study the unoccupied part of the band structure and relaxation dynamics. Time-resolved studies were carried out to track the charge carrier dynamics at the conduction band minima of $MAPbBr_3$, $MAPbI_3$, $CsPbBr_3$, and a quadrupole cation mixed metal halide perovskite.[49,426,433,434] Very slow cooling of hot electrons was observed and explained by the formation of large polarons.[426,434]

2. Current and future challenges

ARPES and momentum-resolved 2PPE require atomically well-ordered periodic surfaces with a defined surface orientation. Experiments must be conducted in ultra-high vacuum (UHV) because of their high surface sensitivity. Preparation of suitable surfaces under UHV conditions is the main challenge of ARPES and 2PPE. Most of the ARPES studies were done on cleaved single crystals.[430] Cleaved single crystals can deliver well-ordered surfaces but exhibit several experimental issues: Cleaving can generate varying surface terminations, which changes the surface properties.[431,435] The solution processing and subsequent cleaving of single crystals induce defects at the surface.[436] Strong doping is an indicator of high defect concentrations. All investigated $MAPbI_3$ samples were heavily *n*-doped, while the doping level of the measured $MAPbBr_3$ surfaces varied. Initial defect concentrations cause further degradation and change surface band bending during measurement.[437] Single crystals also suffer from charging, especially at low temperatures. This can pose limitations for temperature-dependent studies and methods using higher light intensities, such as synchrotron- and laser-based ARPES measurements as well as 2PPE.

An alternative surface preparation technique is needed, which reliably produces defect-free surfaces of a defined and ideally controllable surface orientation and termination. This would permit systematic investigations with multiple techniques, such as ARPES, 2PPE, scanning tunneling microscopy (STM), and LEED, at different measurement temperatures. Reproducibly prepared surfaces could also serve as a platform for investigation of adsorbates, e.g.,

© Author(s) 2021

their adsorption geometries and interface level alignment, or segregates, such as dopants.

3. Progress

A common preparation approach in surface science is the deposition of layers onto well-defined single-crystalline and atomically clean substrate surfaces under UHV conditions. Layers may be deposited using thermal sublimation (see also Sec. III C) or chemical vapor deposition (see also Sec. III D). The approach has several advantages: UHV conditions avoid external contamination. Accumulation of charge during experiments can be circumvented by a conductive substrate and a finite controllable film thickness. The stoichiometry of the surface can be controlled by the calibration of evaporation rates, allowing, for example, for bandgap engineering (see also Sec. II B). Ordering of the surface can be optimized by the substrate temperature during deposition. This approach was already applied to prepare locally ordered lead-halide perovskite surfaces for STM studies.[15,438,439] Perovskite films with a single (surface) orientation can be obtained by epitaxially matching lattice parameters of lead-halide perovskite and substrate.

4. Epitaxial growth of $CsPbBr_3$ on Au(100)

$CsPbBr_3$(001) and Au(100) have surface lattice parameters (a_S) of 5.75 Å and 2.87 Å, respectively. One unit cell of $CsPbBr_3$ fits on four unit cells of the substrate with a lattice mismatch of <1% [see Fig. 24(a)]. This epitaxial relationship supports reproducible growth of $CsPbBr_3$ with long-range order in one (surface) orientation.

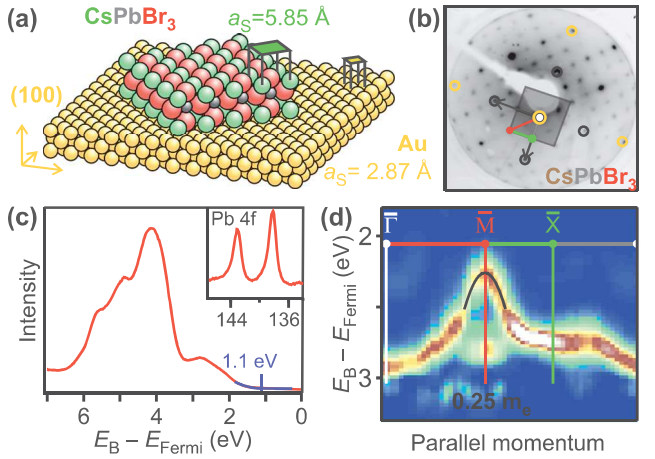


FIG. 24. Atomic and electronic structure of of 9 ML $CsPbBr_3$ on Au(100) at 90 K. (a) illustrates the concept of epitaxial growth of $CsPbBr_3$ on Au(100) surfaces. (b) shows a LEED pattern of a surface prepared this way. The diffraction spots corresponding to the Au(100) substrate are marked by golden circles. The high symmetry points $\bar{\Gamma}$, $\bar{M}$, and $\bar{X}$ associated with the pseudocubic perovskite unit cell are indicated by white, red, and green circles, respectively. An angle-integrated photoemission spectrum ($h\nu = 21.2$ eV) of the valence bands and the dispersion of the topmost valence band along $\bar{\Gamma} - \bar{M} - \bar{X} - \bar{\Gamma}$ are shown in (c) and (d), respectively. An XPS spectrum ($h\nu = 1253.6$ eV, 75° emission angle) of the Pb 4f levels is plotted in the inset of (c).

Figure 24(b) shows the LEED pattern of 9 ML (50 Å) $CsPbBr_3$ on Au(100) at 90 K. The spots corresponding to the square bulk-terminated unit cell of the Au(100) substrate are highlighted by golden circles. Additional spots can be assigned to $CsPbBr_3$. Their sharpness and the relatively low background reflect the high surface quality. The most intense diffraction spots (black circles) form a 2×2 superstructure with respect to the substrate. These spots reflect the basic pseudocubic building block of the perovskite, containing one $CsPbBr_3$ unit.

The surface shows an additional superstructure, which cannot be explained exclusively by superstructures of a bulk-terminated orthorhombic crystal but stems presumably from additional surface reconstructions.

5. Electronic structure of epitaxial $CsPbBr_3$ on Au(100)

Figure 24(c) shows an angle-integrated photoemission spectrum of 9 ML $CsPbBr_3$ on Au(100) at 90 K. The valence bands show a spectral shape similar to the one of other lead-halide perovskites.[430] Three intense peaks at binding energies between 6 and 3 eV are followed by a less intense feature close to the valence band maximum (VBM). Their sharpness indicates a high crystalline quality of our epitaxial films. The binding energy of the VBM (E_B = 1.1 ± 0.1 eV) was determined with a parabolic fit to the angle-integrated spectrum spectrum.[427] No energetic shift or change of the spectral shape could be observed after several hours under illumination. This indicates a constant Fermi level close to the middle of the bandgap and no significant doping. Surface-sensitive x-ray photoelectron spectroscopy (XPS) does not show any detectable defect density in the epitaxially grown samples. One representative spectrum of the Pb 4f levels is shown in the inset of Fig. 24(c). The peaks consist of only one component. No metallic lead can be detected.

ARPES was carried out for a further comparison of the surface electronic structure to the one of single crystals. We applied a 3D curvature method to our three-dimensional $I(E_{kin}, k_x, k_y)$ dataset to visualize the dispersion of the topmost valence band. The resulting dispersion along a high-symmetry cut in k-space [indicated in Fig. 24(b) as a guide to the eye] is shown in Fig. 24(d). The periodicity of the topmost valence band reflects a pseudocubic structure. A hole effective mass of $m^* = 0.25 \pm 0.1 m_e$ can be estimated at the VBM at $\bar{M}$, in line with $m^* = 0.26 \pm 0.2 m_e$ determined for the single crystal.[428]

6. Concluding remarks

The preparation of ultrathin epitaxial films of metal halide perovskites provides a platform to apply momentum-resolved techniques, such as LEED and ARPES. Initial experiments imply that it has the potential to be extended to a variety of metal halide perovskites, in particular, lead-free modifications. Detailed momentum-resolved measurements of the valence-band structure and conduction-band dynamics will aid in the understanding of the exceptional properties of metal halide perovskites. Using low and high photon energies, the properties of the films at their surface, bulk, and substrate interface may be investigated. Interface level alignment and dynamics could be explored by controlled exposure to adsorbates or by varying substrates.

© Author(s) 2021

V. PEROVSKITE DEVICES

Fengjiu Yang, Steve Albrecht, Thomas Riedl, Azhar Fakharuddin, Maria Vasilopoulou

A. Perovskite-based tandem solar cells

Fengjiu Yang, Steve Albrecht

1. Status of the area

Although metal halide perovskite single-junctions have achieved enormous efficiency improvements within the last few years, further improvement will become more and more challenging when approaching fundamental limits. The main losses in any single junction solar cell at given bandgap (E_g) are non-absorbed photons with energy below the absorber E_g and thermalization of high energy photons toward the band edges (see Fig. 25). A tandem architecture with complementary absorber materials is a promising solar cell concept to reduce thermalization losses while covering a wide range of sun-light absorption (see Fig. 25). In a tandem cell, perovskite based absorbers can used as the top cell, facing the sunlight. The perovskite composition can be tuned to vary the E_g around 1.6–1.8 eV (see Fig. 4). The low E_g tandem partner, i.e., the bottom cell, can be composed of crystalline silicon (1.12 eV), copper-indium-gallium-selenide (CIGS) (~1.10 eV), organic bulk heterojunctions (~1.41 eV), and tin-based perovskite itself (~1.25 eV).[321,440–442] This tandem architectures can overcome the typical Shockley–Queisser limit of single-junction solar cells being around 33% and have radiative limits of 45% for perfect E_g combination (see Fig. 25). In the case of multi-junctions with 3, 4, or an infinite number of absorber materials with perfect E_g combination, even higher radiative limits of 50.1%, 54.0%, and 65.4% efficiency could be reached at normal sun-light (1-sun) illumination.[443] Combining the high ease of production and low fabrication cost together with the high efficiency and E_g tunability, metal halide perovskites are the best partner for tandem and multi-junction applications. This fascinating material class might achieve high efficiencies at reasonable costs in future solar cell module applications.

The different tandem architectures can be divided into the simplest, mechanical stacked, individually operating four-terminal (4T) structure that needs four contacts.[444] In addition, the series-interconnected subcells in the three-terminal[445] or two-terminal (2T) and also called monolithic architecture can be utilized.[446] For common 2T structures, both subcells are connected via a recombination (tunnel) contact and connected in series. This recombination contact is needed, as electron–hole pairs from different absorption events are generated and half of these electrons and holes recombine at the recombination junction, while the other half is extracted at the outer contacts (see Fig. 25). When this selectivity in the recombination contact due to appropriate choice of energy levels is ensured, the voltage of both subcells is summed so that the tandem V_{OC} is that of the sum of the subcells (V_{top} + V_{bottom}). In addition, the overall photocurrent is limited by that of the limiting subcell, and thus, the so-called current matching between the subcells is needed for the highest J_{SC}. The tandem FF is determined by the photocurrent limiting subcell and by the amount of current mismatch.[447]

Figure 26 shows the power conversion efficiency (PCE) evaluation of perovskite-based tandem solar cells, including perovskite/silicon, perovskite/CIGS, and perovskite/perovskite. These tandem solar cells have achieved certified and reported values of 29.5%, 24.2%, and 24.2% (25.6% for 0.049 cm^2) efficiency on 2T monolithic architectures with over 1 cm^2 active area,[1,448] respectively. Additionally, the 4T perovskite/silicon, perovskite/CIGS,

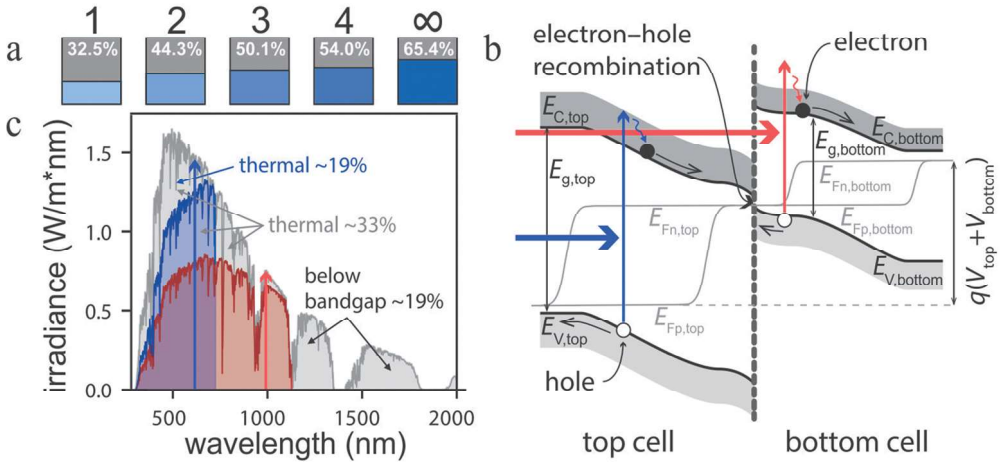


FIG. 25. (a) Detailed balance efficiency limits of single-junction (1) and multi-junction solar cells (2, 3, 4, and infinite absorbers) each with optimized bandgaps E_g under non-concentrated AM 1.5 G illumination (data from Ref. 443). (b) Energy band diagram with valence E_v and conduction band E_c of the top and bottom cell in a 2T tandem solar cell including quasi-Fermi-levels E_F for electrons and holes of each subcell. Absorption and consequent electron–hole pair generation in each subcell is also indicated. (c) Spectral irradiance and usable energy to visualize the main dominating losses for a single junction with 1.1 eV E_g, including the reduced thermalization loss when a 1.7 eV E_g top cell is added. The indicated absorption events in (b) and (c) depicted with red and blue vertical arrows refer to the same.

© Author(s) 2021

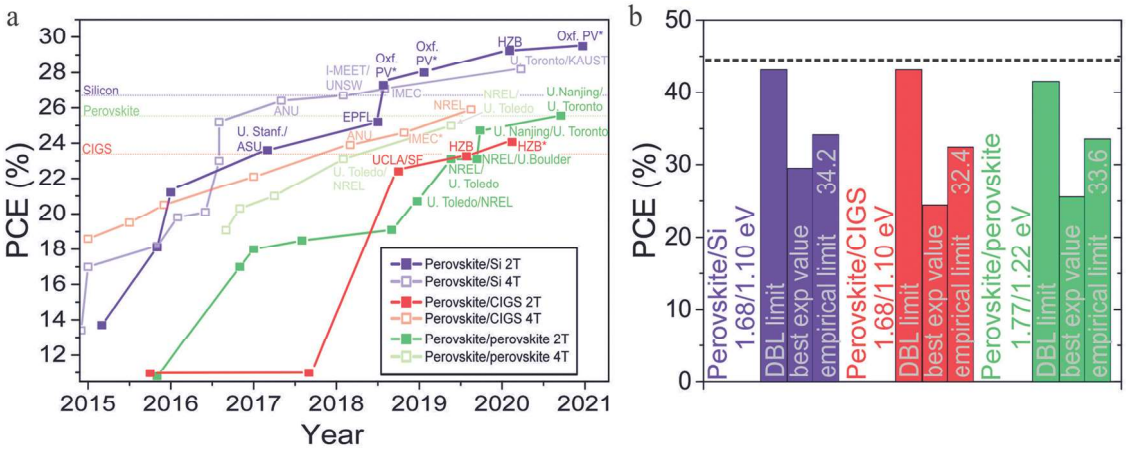


FIG. 26. (a) Efficiency evolution of perovskite-based tandem solar cells in 2T (dark) and 4T (light color) configuration, including perovskite/silicon (purple), perovskite/CIGS (red), and all-perovskite tandem (green) technologies. Dashed horizontal lines indicate the best efficiency for each single junction technology. Updated from the work of Jošt *et al.*[451] (b) Detailed balance limit (DBL) compared to the best experimental values with the corresponding E_g combination and an empirical limit for the different tandem technologies. The dashed horizontal line indicates the DBL for optimum E_g combination according to Fig. 25(a). Further details on these limits can be found in Jošt *el al.*[451]

and perovskite/perovskite tandem solar cells have reported values of 28.2%,[444] 25.9%,[449] and 25.0%[450] PCE, respectively. 2 T perovskite/silicon tandem solar cells now reach values close to 30% PCE [see Fig. 26(b)] enabled by various reports on the optimization and understanding for this tandem technology.[451] 2T perovskite/CIGS tandem solar cells with high efficiency are yet rarely reported and mostly limited by the rough CIGS bottom cell surface.[287,321,452] Here, we mainly focus on 2T perovskite/perovskite based tandem solar cells that have recently been shown to approach the efficiency of the best perovskite single junctions by using the $FAPbI_3$ based perovskite at an E_g of 1.55 eV [see Fig. 26(a)]. In order to enable higher efficiency values closer to the empirical limit well above 30% [see Fig. 26(b)], further understanding and optimization are needed.

2. Current and future challenges

For all-perovskite tandem solar cells, E_gs around 1.8 eV for the top cell and 1.2 eV for the bottom cell are recently applied. These compositions and the final tandem integration still have various individual challenges.[442,453–460] Here, we focus on four main facts: First, the wide-E_g halide-perovskite with high bromide loading undergoes phase segregation into iodide and bromide rich phases, resulting in V_{OC} limitations finally affecting the tandem performance.[461] The V_{OC} values of wide-E_g PSCs are usually less than 90% of the Shockley–Queisser limit because of strong recombination losses of the absorber and toward the charge selective interfaces.[319] Moreover, the electron and hole transport layers (ETL/HTL) {such as C_{60} or Poly[bis(4-phenyl) (2,5,6-trimethylphenyl)amine] (PTAA)} also induce significant halide segregation and nonradiative recombination losses at high bromide content with >1.7 eV E_g,[330] as seen in Fig. 27(a).

Second, the oxidation tendency of the tin–lead (Sn–Pb) low-E_g perovskite is a challenge because the divalent Sn is quite sensitive to oxygen atmosphere and oxides into quadrivalent Sn. This results in a deteriorated semiconductivity of Sn–Pb perovskite and decreases photovoltaic performance of Sn–Pb PSCs even in encapsulation condition.[462] As seen in Fig. 27(b), the color of the Sn–Pb perovskite precursor quickly changes from yellow to deep red because the divalent Sn has been oxidized in solution and generate Sn vacancies in film state with high hole carrier (p-doped) in the background. In contract, this oxidation tendency could be hindered by adding some additives, such as metallic Sn powder[457] or formamidine sulfinic acid (FSA).[442] Third, the optical management of perovskite-tandem is still far from the optimized condition with a low reflectance and parasitic absorption of incident sunlight. Additionally, several recombination layers (RLs) are stacked between wide- and low-E_g subcells for protection of one subcell from damage during the fabrication of the other. Typically, metal oxides, such as ITO or SnO_2, processed by sputtering or atomic layer deposition (ALD) are utilized as these layers to prevent dissolving of the first subcell underneath when the second subcell is processed on top. Overall, as shown in Fig. 27(c), the experimental external quantum efficiency (EQE) spectra of all-perovskite tandem solar cells are still far from the optimized estimates (dashed line), especially due to the low absorption in the infrared light region of the low-E_g subcell.[442] This optimization could be realized by thicker absorber films when high lifetimes and reduced carrier density allow effective charge extraction also for micrometer thick films.[463]

Fourth, the overall stability of all-perovskite tandem solar cells is limited by the above-mentioned factors about oxidation but also by the used perovskite composition and ETLs as well as HTLs in the tandem device stack, as presented in Fig. 27(d): organic cations such as methylammonium iodide and the poly(3,4-ethylenedioxythiophene) polystyrene sulfonate (PEDOT:PSS). The hydrophilic PEDOT:PSS is commonly used as HTL for high efficiency Sn–Pb PSCs;[442,458,464] however, the hydrophilic nature weakens the device's operational stability.

Except for these aforementioned challenges, the active area of all-perovskite tandem solar cells reported so far is only about 1 cm^2 by using non-scalable techniques, such as spin-coating.[1,442,448]

© Author(s) 2021

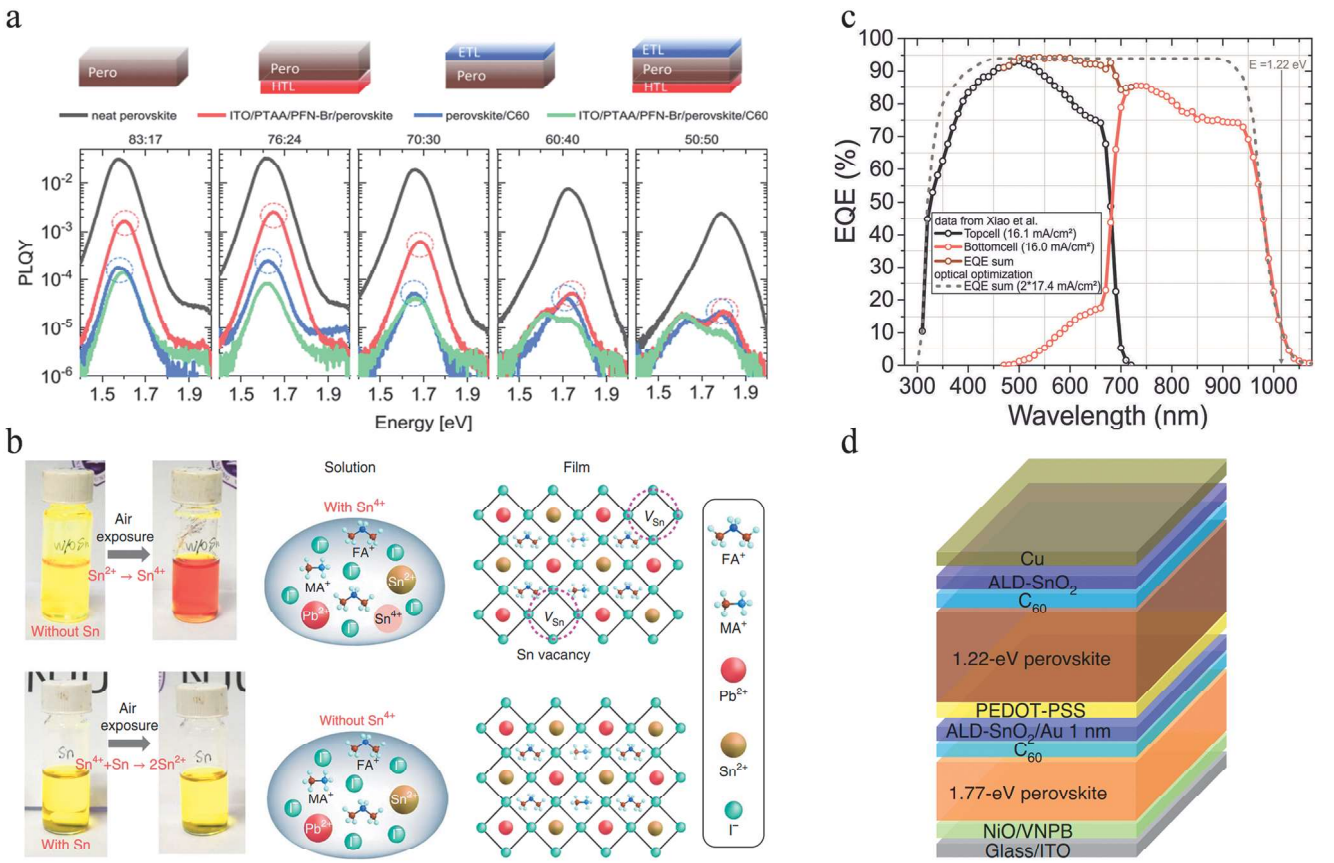


FIG. 27. (a) Photoluminescence quantum yield (PLQY) spectra of five perovskite compositions of $Cs_{0.05}(FA_xMA_y)_{0.95}Pb(I_xBr_y)_3$ as indicated by the molar FAI to MABr ratio from 83:17–50:50. Different colors indicate different layer stacks from pure perovskite films (black) to both full as indicated. Reprinted with permission from Peña-Camargo *et al.*, ACS Energy Lett. **5**, 2728 (2020). Copyright 2020 American Chemical Society. (b) Photographs exhibit the oxidation of Sn^{2+} to Sn^{4+} in ambient air and reduction of Sn^{4+} to Sn^{2+} with metallic Sn powder. Meanwhile, the illustration of the Sn vacancy formation due to the present of Sn^{4+} and the suppression of Sn vacancies with metallic Sn powder in the Sn–Pb perovskite precursor and film. Reprinted with permission from Lin *et al.*, Nat. Energy **4**, 864 (2019). Copyright 2019 Nature Publishing Group. (c) EQE spectra of the best reported all-perovskite tandem solar cell with the EQE of the individual subcells, and the sum value is extracted from Ref. 442. The dashed line refers to an empirical optimization that would allow for the matched photocurrent of 17.4 mA/cm. (d) A schematic architecture of all-perovskite tandem solar cells. Reprinted with permission from Xiao *et al.*, Nat. Energy **5**, 870 (2020). Copyright 2020 Nature Publishing Group.

Further developments need to include fully scalable methods, such as printing or thermal evaporation.

3. Advances in science

To further improve photovoltaic performance of perovskite-tandem solar cells, the halide phase segregation of wide-E_g perovskite with a high bromide content should be overcome. Mixing or replacing the organic-site cation with large organic or suitable small metal ions could promote the stability against irradiation- and moisture-erosion.[281,465–467] For example, the partial substitution of FACs composition by using the dimethylammonium cation could significantly enlarge the E_g and enhance long-term operational stability.[460,468] Additionally, the ionic solid incorporation with the perovskite precursor, a piperidinium salt, also has the potential to retard the halide composition segregation.[469] The post surface treatment with a two-dimensional (2D) perovskite would be an efficient method to prevent the halide segregation.[319] Moreover, a triple halide perovskite with chloride inclusion has been demonstrated as another approach to suppress the phase segregation of perovskite absorbers with 1.67 eV E_g and significantly improve operational stability,[470] as shown in Fig. 28(a).

Oxidation of the Sn element can be overcome by additives to prevent the oxidation, such as tin fluoride,[471] tin fluoride–pyrazine complex,[472] hydroxybenzene sulfonic acid,[473] or metallic Sn power,[457] as seen in Fig. 27(b). Furthermore, the dihydropyrazine derivative[474] and FSA[442] can reduce oxidation and thus defect density and charge carrier concentration in pure Sn and Sn–Pb perovskites. As shown in Fig. 28(b), the operational stability of all-perovskite tandem solar cells has been significantly enhanced by employing the FSA in the Sn–Pb perovskite precursor to suppress the Sn oxidation.[442] Additionally, the correct choice of solvent can ensure less oxidation.[475]

Optical management of perovskite-tandem photovoltaics should be an efficient way to improve photon utilization and reduce the light reflectance and parasitic absorption. Textured interfaces on the front side of a perovskite/silicon tandem has been demonstrated

© Author(s) 2021

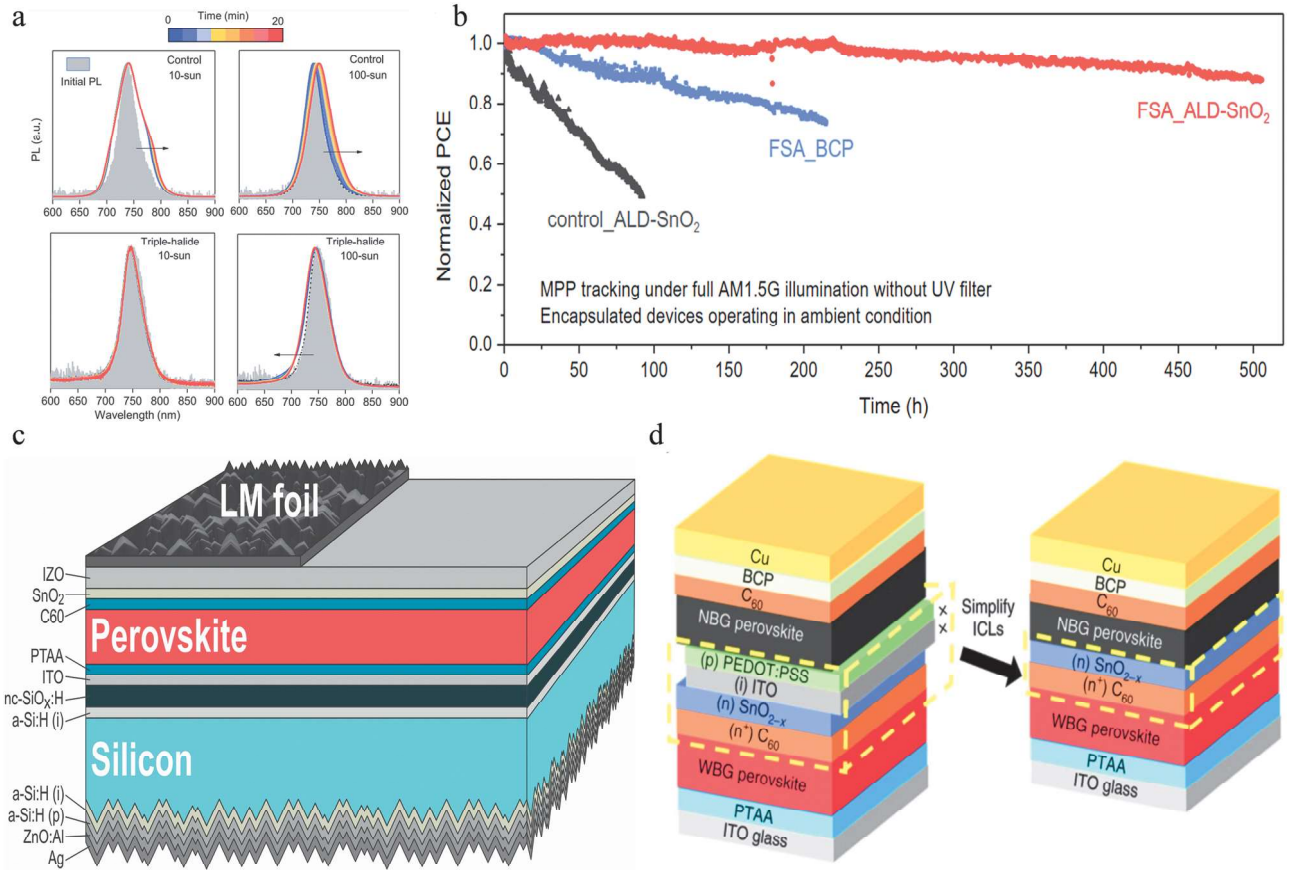


FIG. 28. (a) PL spectra of the 1.67 eV perovskite with control (25Cs20Br) and triple halide (22Cs15Br + 3Cl) compositions under 10- and 100-sun illumination for 20 min. Arrows indicate the direction of the PL shift as function of time under illumination. Reprinted with permission from Xu *et al.*, Science **367**, 1097 (2020). Copyright 2020 AAAS. (b) Maximum power point tracking (MPP) of the encapsulated all-perovskite tandem with conditions as indicated. Different devices including a control and two devices with FSA additive and BCP (Bathocuproine) as well as SnO_2 are shown. Reprinted with permission from Xiao *et al.*, Nat. Energy **5**, 870 (2020). Copyright 2020 Nature Publishing Group. (c) Schematic of perovskite-silicon tandem solar cells with textured light management (LM) foil applied to the front side. Reprinted with permission from Jošt *et al.*, Energy Environ. Sci. **11**, 3511 (2018). Copyright 2018 Royal Society of Chemistry. (d) Schematic of all-perovskite tandem solar cells with the typical interconnection layer of C_{60}/SnO_{2-x}/ITO/PEDOT:PSS and the simplified stack of C_{60}/SnO_{2-x}. Reprinted with permission from Yu *et al.*, Nat. Energy **5**, 657 (2020). Copyright 2020 Royal Society of Chemistry.

to be an efficient approach to improve light absorption and thus enhance photocurrent, especially for lower angles of incidence,[476] as seen in Fig. 28(c). In addition, a textured and transparent substrate might be an interesting approach to realize the light management (LM) of all-perovskite tandem photovoltaics. Improving light absorption in the NIR region at the band edge potentially from thicker Sn–Pb absorber films well above a micrometer thickness (without sacrificing charge extraction and thus FF) might enable photocurrent matching well above 17 mA/cm^2 [see Fig. 27(c)]. Thicker films will also enable a steeper photocurrent onset at a similar bandgap around 1.22 eV.

So far, complex interconnection layers between both subcells were used to prevent fabrication damage and enable charge selective recombination to add up the individual subcell V_{OC} values. Furthermore, simplification of the interconnection layers would be a valid approach to ensure simple processing, less parasitic absorption, and long-term operation. For example, the typical interconnection layer stack composed of C_{60}/SnO_2(BCP)/ITO/PEDOTS:PSS has been simplified into C_{60}/SnO_{2-x} with low contact resistivity between wide- and low-E_g perovskite subcells,[456] as shown in Fig. 27(d). All-perovskite tandem solar cells with this interconnection layer resulted in a 24.6% efficiency on 0.059 cm^2 active area and sustained 94% of the initial performance after 1000 h continuous simulated AM1.5G illumination at room temperature.

4. Concluding remarks

Metal halide perovskite materials are highly promising for the next generation multi-junction photovoltaics because of the tunability of the bandgap, ease of processing different compositions to tune material properties, overall low cost production, and the very high efficiency potential. In particular, all-perovskite tandem solar cells might be the flexible, light weight, and truly thin film tandem technology of the future. This fascinating tandem technology has

© Author(s) 2021

empirical efficiency limits around 34% when overcoming the aforementioned challenges of (1) halide segregation and reduced recombination at charge selective contacts for ~1.8 eV bandgaps to enable high V_{OC} and stability of the wide bandgap top cell, (2) reduced oxidation of Sn in the Sn–Pb low bandgap compositions to reduce charge carrier density and charge recombination, (3) improved optical management, with much thicker absorber films and advanced light management for highest possible photocurrent matching, and (4) optimized interconnection layers and overall tandem architecture to ensure high robustness of fabrication, low parasitic absorption, and long-term operation. Additionally, the development of large active areas with scalable methods and module integration with proper encapsulation needs to be shown and to realize practical applications of high efficiency all-perovskite tandem solar cells in the next few years.

B. Applications beyond solar cells

Thomas Riedl

1. Status of the area

With their optoelectronic properties comparable to that of the most successful semiconductors (e.g., GaAs), metal halide perovskites state an intriguing platform for applications aside from solar cells (Fig. 29). Perovskites were successfully employed in detectors for UV–NIR (i.e., 300–1000 nm)[477] or ionizing radiation (x rays and γ-rays)[478–480] and as highly efficient active materials in light emitting diodes (LEDs) or lasers.[481,482] In some of these applications, the toxicity of lead is fortunately less of an issue than it may be in solar cells (Sec. VI F).

a. Detectors. Photodetectors, i.e., photodiodes, photoconductors, or phototransistors, serve a wide range of applications. In photodiodes, the built-in electrical field is typically afforded by the interface materials sandwiching the perovskite absorber layer, while perovskite p/n-junctions, which require the controlled and stable p/n-doping similar to conventional semiconductors, are still in their infancy. The internal E-field allows for the separation of photogenerated charges without external bias, which coined the expression of "self-powered" photodetectors, which are currently prepared and studied in various material systems. On the contrary, photoconductors require external bias and exploit the increased electrical conductivity of a semiconductor due to photogenerated charges. Phototransistors come with a more complicated processing technology but provide internal amplification and a high gain in return. In phototransistors, the perovskite may either form the active channel or it may serve as photo-sensitizer that absorbs the light and transfers photogenerated charges to the adjacent channel material, such as a metal-oxide and graphene [Fig. 29(b)].[488]

For detectors, figures of merit apply that are substantially different from that of solar cells. Among them, the responsivity (R), specific detectivity (D^*), and the linear dynamic range are important characteristics. For some applications, a high response speed is also required. The specific detectivity is given by $D^* = \frac{\sqrt{A \cdot \Delta f}}{NEP}$, with A, Δf, and NEP being the area of the device, the bandwidth, and the noise equivalent power, respectively. The NEP is proportional to the inverse of the responsivity (R, given in units of A/W). R is

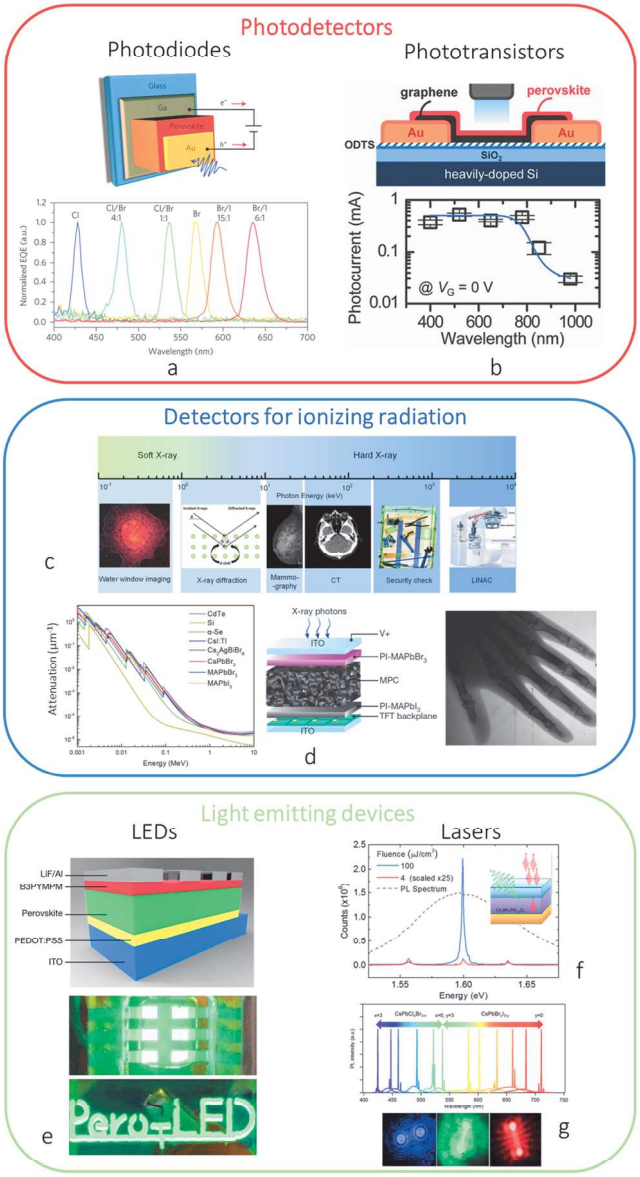


FIG. 29. (a) Device structure and normalized EQE spectra of narrow-band single-crystal photodetectors with varied halide composition. Adapted with permission from Fang *et al.*, Nat. Photonics **9**, 679 (2015). Copyright 2015 Nature Publishing Group.[483] (b) Perovskite/graphene phototransistor structure and photocurrent spectrum. Adapted with permission from Lee *et al.*, Adv. Mater. **27**, 41 (2014). Copyright 2014 John Wiley and Sons.[484] (c) X-ray energy spectrum and corresponding applications. Spectral attenuation of various representative semiconductors. Adapted with permission from Wu *et al.*, Matter **4**, 144 (2021). Copyright 2021 Elsevier.[480] (d) All-solution-processed perovskite digital x-ray detector panel (50 × 50 cm^2) used to take an x-ray image of a hand. Adapted with permission from Kim *et al.*, Nature **550**, 87 (2017). Copyright 2017 Nature Publishing Group. (e) Layer sequence of a perovskite LED and photographs of perovskite LEDs in operation. Adapted with permission from Lin *et al.*, Nature **562**, 245 (2018). Copyright 2018 Nature Publishing Group. (f) First optically pumped perovskite laser based on a vertical resonator. Adapted with permission from Deschler *et al.*, J. Phys. Chem. Lett. **5**, 1421 (2014). Copyright 2014 American Chemical Society. (g) Tunable laser emission from CsPbX3 (X = Cl, Br, and I) single-crystal nanowires. Adapted with permission from Fu *et al.*, ACS Nano **10**, 7963 (2016). Copyright 2016 American Chemical Society.[487]

© Author(s) 2021

immediately related to the external quantum efficiency (EQE). A detailed discussion on how to optimize all of these figures is out of the scope here. Some attention is given to the optimization of D^* below.

X-ray or gamma-ray detectors are very specific representatives of photodetectors that leverage the high cross section of interaction for high-energy photons with the heavy elements of the halide perovskite, e.g., Pb and I. Here, the sensitivity, given by the generated charge per area and irradiation energy dose (unit: μC Gy^{-1} cm^{-2}), is a specific figure of merit. Research is driven by the demand to lower the irradiation dose in medical applications in order to reduce possible radiation-induced health hazards. In the energy range that is relevant to medical x-ray applications (10–200 keV), $MAPbX_3$ and $Cs_2AgBiBr_6$ have been shown to perform equally or better than the best representatives in the field, e.g., a-Se or CdZnTe.[479] Aside from the direct conversion of radiation to generated charges, there is also the option to use perovskites as scintillators[489] that emit light when exposed to ionizing radiation, which can then be detected by conventional UV–NIR photodetectors.

As the interaction cross section of high energy photons with the absorber is significantly less than in the case of optical photons, the active perovskite layer needs to be very thick (0.1–1 mm) and the product of charge-carrier mobility and lifetime ($\mu\tau$-product) becomes of paramount importance, as the ultimately collected charge (Q) is given by $Q = Q_0 \cdot \frac{\mu\tau V}{d^2} \cdot \left[1 - \exp\left(-\frac{d^2}{\mu\tau V}\right)\right]$,[490] where V is the applied bias, d is the thickness, and Q_0 is the total generated charge. A high mobility and long carrier lifetime are typically provided by single crystals with a $\mu\tau = 10^{-2}\ \frac{cm^2}{V}$ and a diffusion length >100 μm due to orders of magnitude lower trap densities than in polycrystalline films.[479] Yet, for imaging applications. large area arrays (>40 × 40 cm^2) are required, where single crystals are of limited use. Kim *et al.* prepared a 50 × 50 cm^2 active matrix imaging x-ray detector with the active $MAPbI_3$ layer deposited by doctor blading from an ink based on γ-butyrolactone and α-terpineol, which afforded laterally extended perovskite crystallites with a sufficiently good $\mu\tau = 10^{-4}\ \frac{cm^2}{V}$ [Fig. 29(d)].

b. Light emitting devices. Perovskite based light emitting diodes (LEDs) have made tremendous progress as their external quantum efficiency has reached levels >20%, unlocked by a combination of surface/grain-boundary defect passivation and optimized formation of continuous pin-hole free perovskite layers by using suitable processing additives [Fig. 29(e)].[39,485] While long-term operational stability still remains one of the most critical issues for perovskite LEDs, they have the potential to become an attractive alternative to organic or quantum-dot based LEDs. Perovskite LEDs will be discussed in more detail in Sec. V C.

Beyond LEDs, lasers are a field in which perovskite semiconductors as the active medium have aroused great expectations. There is the vision that perovskites may not be subject to typical loss mechanisms that prevent electrical operation in organic gain media, such as triplet–singlet annihilation or absorption due to triplet excitons and polarons.[491,492] Thus, perovskites currently seed a new promise for the realization of electrically operated laser diodes that can be prepared from solution at low temperatures with the potential to be integrated in a number of exciting on-chip applications, such as optical sensor-arrays and integrated optoelectronics. Perovskite lasers also allow to cover the spectral region between 530–610 nm, which is difficult to achieve at room temperature with "classical" InGaN or AlGaInP semiconductors. Amplified spontaneous emission (ASE) and optically pumped lasing have been reported in a number of lead halide perovskites [Fig. 29(f)].[69,486] Single crystalline perovskite nanowires[493] and platelets,[68] which readily form resonators, have been used [Fig. 29(g)]. Vertical cavities[486] and distributed feedback (DFB) structures[494] have also been considered as resonators.

A number of resonators require some sort of patterning, which is severely complicated by the susceptibility of perovskites to a number of commonly used solvents, rendering established wet-chemical lithography techniques mostly unusable. Owing to the "soft" nature of lead-halide perovskites with relatively weak bonds, direct patterning of photonic nanostructures directly into various perovskite materials via thermal nanoimprint (NIL) has been shown [Figs. 30(a) and 30(b)].[495,496,499] The typical temperature/pressure range for imprint was around 100–150 °C and 100–150 bars, respectively. The re-crystallization during thermal imprint has been shown to concomitantly improve the crystal quality and quantum-yield, which even allowed for the first time ASE and lasing at room-temperature in thin-films of $CsPbBr_3$ that were not based on nanoparticles.[495] A variant of thermal imprint using a flat stamp (also called planar hot pressing) has shown that initially rough and polycrystalline thin films could be re-crystalized to form layers with laterally extended single crystals and a roughness below 1 nm (rms), which is essential to minimize scattering losses in a waveguide and to afford a low threshold for lasing [Fig. 30(c)]. Low lasing threshold levels are mandatory for future electrical operation of a perovskite laser diode and for continuous wave (cw) operation. The plethora of reports on perovskite lasers relies on optical pumping with a pulse duration in the range of fs–ns. Early reports have shown cw or quasi-cw operation in perovskite lasers only at cryogenic temperatures below 160 K predominantly limited by heating induced losses.[500,501] Only recently, the first convincing report of cw-lasing at room-temperature in quasi-2D perovskites has been published that highlighted the importance of triplet management in these structures to mitigate singlet–triplet annihilation, similar to organic active media [Figs. 30(d) and 30(e)].[497] More recently, perovskites have been used as an active medium in the so-called vortex lasers that can be integrated on-chip and allow for THz switching speed [Fig. 30(f)].[498,502] Their ultra-high Q-factors (10^{10}) pave a way for very low lasing thresholds, which is also beneficial for the prospects of electrical operation.

2. Current and future challenges

a. Detectors. To improve the specific detectivity (D^*) of a photodetector, it is essential to reduce the dark current and the noise. The dark current is strongly linked to the leakage current in the device under reverse bias, which is why energetically well-aligned selective interface materials (similar to the ones applied in solar cells and discussed in Sec. IV C) with a low density of interfacial defects (to avoid parasitic non-radiative recombination at the interface) are essential.[503] Mitigation of defects by processes that afford films consisting of large perovskite crystals is a further key. In this regard, the use of anti-solvents[219] or gas-quenching deposition[504] have been shown to yield high-quality

© Author(s) 2021

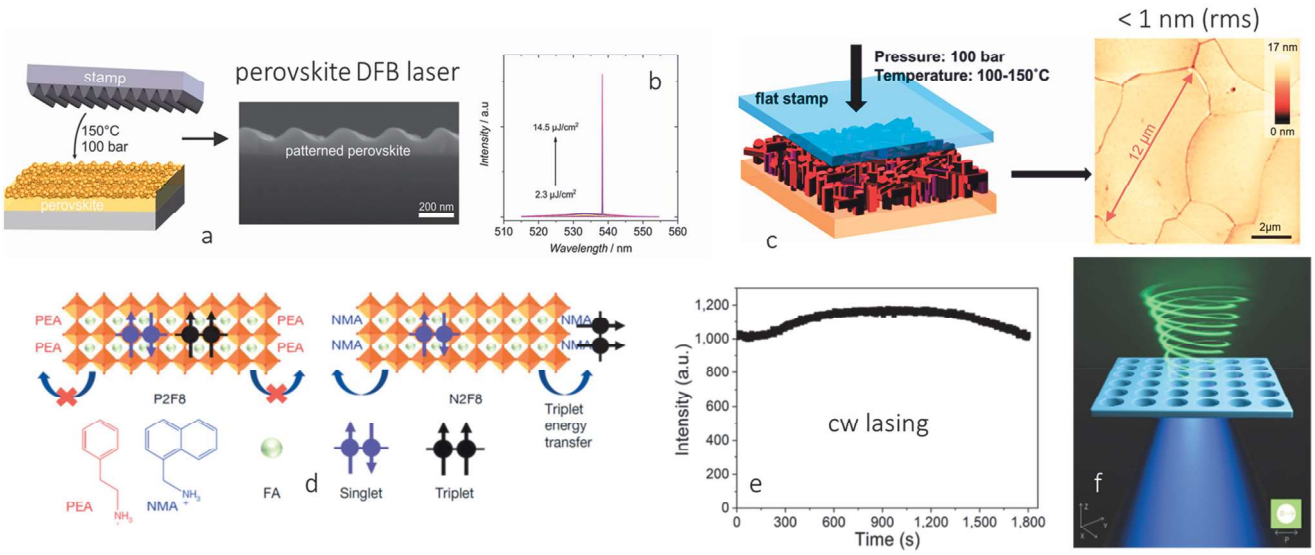


FIG. 30. (a) Direct thermal imprint of a linear distributed feedback (DFB) grating (periodicity Λ = 278 nm) into a $CsPbBr_3$ layer and SEM image of the cross section of the patterned perovskite. (b) Emission spectra of the DFB laser upon increasing the pumping energy density. Adapted with permission from Pourdavoud *et al.*, Adv. Mater. **31**, 1903717 (2019). Copyright 2019 John Wiley and Sons.[495] (c) Principle of thermal imprint using a flat stamp to re-crystallize a rough pristine $MAPbBr_3$ layer resulting in a flat film with large crystals. Adapted with permission from Pourdavoud *et al.*, Adv. Mater. Technol. **3**, 1700253 (2018). Copyright 2018 John Wiley and Sons.[496] (d) Chemical structure of two quasi-2D perovskites and their cations. Triplet energy can be transferred from N2F8 to NMA. (e) Stable emission under optical cw excitation. Adapted with permission from Qin *et al.*, Nature **585**, 53 (2020). Copyright 2020 Nature Publishing Group. (f) Schematic of a $MAPbBr_3$ metasurface pumped by a blue laser emitting a green vortex beam in the vertical direction. Adapted with permission from Huang *et al.*, Science **367**, 1018 (2020). Copyright 2020 American Association for the Advancement of Science.

perovskite films. Moreover, the passivation of defects at the surface and grain-boundaries of the perovskite has turned out to be very effective,[505,506] for example, small molecule Lewis bases/acids,[507] addition of excess lead,[508] or the modification of the perovskite surface by bulky molecules, such as the organic halide salt phenethylammonium iodide (PEAI).[202] The latter were shown to promote the formation of a 2D cap that additionally may introduce a means of engineering the interface energetics.

A further challenge for detectors will be to extend the sensitive spectral region beyond 1000 nm and to address the bands relevant for optical communication, such as 1300 or 1550 nm. The most common Sn-based perovskites are limited to an energy gap of around 1.2 eV.[79] At the same time, the response speed of perovskite photodetectors needs to be improved by facilitating fast charge extraction and by designing device architectures with low parasitic RC elements.

For x-ray detectors, there is a need to further improve on sensitivity by reducing the dark current and noise level. To this end, the (still too high) background carrier densities even in perovskite single crystals need to be lowered further. To determine the energy of the ionizing radiation (mostly in γ-ray detection), the energy resolution of perovskite detectors is still inferior to that of the established CdZnTe analog, calling for larger perovskite single crystals with concomitantly high collection efficiency (i.e., ultra-high purity and low defect densities).[509] Large bias voltages may be required to efficiently extract charges, while the elevated internal field may give rise to detrimental ionic motion, which needs to be mitigated for further progress.

b. Lasers. Demonstration of the first perovskite laser diode remains the holy grail in the field of perovskite photonics.[510] While the work toward the perovskite laser diode can draw from the progress in efficiency and stability of perovskite LEDs, there are some critical differences. LEDs are typically operated at current densities <100 mA/cm^2. The exciton density estimated to reach the threshold for lasing in a perovskite laser is on the order of 10^{18} cm^{-3} projecting threshold current densities in excess of 100 A/cm^2.[511] For perovskite LEDs, the so-called "efficiency roll-off" at elevated current densities (already way below 100 A/cm^2) is a typical phenomenon that has been attributed to charge injection imbalance, Auger recombination, which scales with the third power of the carrier density, and/or Joule heating.[511,512] Charge carrier balance can be improved by a proper selection of charge transport/injection/blocking layers. In a direct comparison, 3D perovskites have shown a smaller Auger coefficient than their lower dimensional analogues.[512] Therefore, 3D perovskites may be the better choice for electrically driven lasers despite the enormous success of nanoparticles in LEDs and optically pumped lasers. Mitigation of trapped charges has been found to be likewise important to reduce Auger recombination.[513] Joule heating remains a critical issue that is linked to the generally low thermal conductivity of halide perovskites.[514] Substrates with a high thermal conductivity, such as sapphire, can be a part of the thermal management. Most likely, the first perovskite laser diode will require pulsed electrical operation and active cooling. At a later stage, operational stability of perovskite laser diodes can be expected to be an enormous challenge, as degradation effects occur at excitation densities relevant for solar cells or

© Author(s) 2021

LEDs will likely be amplified under high excitation densities in a laser.

3. Concluding remarks

In the long history of semiconductors, the recent re-discovery of halide perovskite semiconductors has almost created the impression that perovskites are able to serve every application—better than existing materials. This impression has been fueled by their tremendous initial progress in photovoltaics and the concomitant euphoria in the scientific community. Like in all hype-cycle scenarios, some of the enormous expectations will certainly meet disappointment. It remains to be hoped that the more detailed and maybe less glamorous work that remains to be done will generate insights to mitigate some of the specific remaining challenges discussed above or that it may at least help to unravel the fundamental limitations associated with this class of materials and to come up with more realistic expectations in the wide range of applications beyond solar cells.

C. Perovskite materials for light emission

Azhar Fakharuddin, Maria Vasilopoulou

1. Status of the area

The unique optoelectronic properties of hybrid perovskite materials are also beneficial for applications beyond solar cells, e.g., for LEDs. For instance, the high mobility of perovskite materials contributes to the high electrical efficiency of perovskite LEDs (PeLEDs). Similarly, the low defect density and high defect tolerance lead to high photoluminescence quantum yield (Φ_{PL}) of the perovskite emitter layer (EML). Φ_{PL} determines the competition between radiative to total (radiative + nonradiative) recombination events within the EML.[515,516] In addition, perovskite materials show a narrow emission linewidth (FWHM of electroluminescence emission 18–35 nm)[517,518] that promises a high color purity for display devices. Perovskite nanocrystals show PL emission FWHM in the range of 12–40 nm, thus promising a color gamut for display applications that covers up to 140% of National Television System Committee standards.[519] The tuneable bandgap of the perovskite EML is further advantageous as it determines the emission color of PeLEDs from ultraviolet (UV) to near infrared (NIR) part of the electromagnetic spectrum and thus their application. For instance, UV PeLEDs can be used in bio-medical applications, disinfection and sterilization, security, sensing, lithography, and so on, whereas visible PeLEDs are a strong candidate for display, general purpose illumination, aesthetic, consumer electronic, optical storage, etc. NIR PeLEDs can find their application in surveillance/night vision, communication, data storage, optogenetics, medical sensors, and so on. PeLEDs offer some advantages that the existing LED technologies may not. For example, the narrow FWHM of perovskite emitters makes them preferred over their organic semiconductor counterparts used in OLEDs. For integrated photonic applications, solution processing of PeLEDs is advantageous than III–V thin film-based LEDs. The latter requires a high-temperature epitaxial growth of III–V semiconductors to minimize the defect density in the EML. Compared with colloidal quantum dots-based LEDs (QDLEDs), PeLEDs offer higher stability and have shown to withstand a higher current density, corresponding to much higher luminance. QDLEDs, however, are still a choice at low brightness levels, e.g., for common display devices, such as smart phones or TV screens.

A typical LED consists of an EML sandwiched between charge (electron/hole) injection layers (EIL/HIL) [Fig. 31(a)]. A range of organic and inorganic electron and hole injection layers are employed in PeLEDs, such as those based on metal oxides, small molecules, and polymers [see Figs. 31(c) and 31(e)]. At forward bias, charge pairs that are injected via respective injection layers reach the EML and recombine radiatively resulting in light emission. The performance of LEDs is determined by their electrical (wallplug) efficiency, which is the ratio between input electrical power to output optical power (both in watts). External quantum efficiency (EQE) is another important figure of merit when characterizing LEDs, which is the ratio between the flux of photons emitted to the number of electrons injected per unit time. The EQE is determined by (i) internal QE (IQE), i.e., the ratio between photon generated within the EML to electrons injected per unit time, and (ii) light outcoupling efficiency that describes the percentage of photons escaping the LED. IQE depends on the Φ_{PL} and charge balance in the device. A charge carrier leaving the device without contributing to radiative recombination lowers the IQE.

The first report on PeLEDs surfaced in 2014, where a 20 nm thick $MAPbI_{3-x}Cl_x$ EML was sandwiched between electron and hole injection layers.[518] This device demonstrated an EQE of 0.76% at a peak emission wavelength of 754 nm (IQE ~4% only). Appropriate selection of perovskite EML and its subsequent defect passivation played a key role in improving the EQE of PeLEDs. Figure 31(b) shows three most common perovskite EML structures, namely, 3D perovskites, mixed phase 2D/3D perovskites, and perovskite NCs. Optimizing the EML properties to enhance radiative recombination as well as device heterojunctions to attain a balanced charge injection enabled PeLEDs to demonstrate EQE between 20% and 22% [Fig. 31(b)]. For example, radiative efficiency of the EML can be enhanced by geometrically confining the charge-pairs, e.g., in the form of nanocrystals (NCs) that provide nearly unity Φ_{PL} or by spatially confining charges in mixed phase 2D/3D perovskite EMLs.[520,521] The latter EML demonstrates a cascaded bandgap where charges are confined into to the smallest bandgap domain, thus enhancing radiative efficiency. Passivation of the nonradiative defects has also been a key strategy to improve the optical quality of the EML leading to Φ_{PL} in the range of 80%–100% and EQE approaching 20%.[522] Research also focused on improving light outcoupling efficiency via engineering the EML morphology and via tuning the refractive index of the various layers in the device.[523]

Typical LEDs are fabricated in a planar device architecture that involves rigid (glass) or flexible (conducting plastic) substrates. These can limit commercial prospects for future applications that require omni-directional flexibility, super light weight, and extreme bendability. This brings into account fiber- or wire-shaped devices, which not only can overcome the limitation of conventional planar electrodes but can also be integrated into complex systems, such as wearable electronic devices. Recently, a bi-functional fiber-based perovskite light emitting/detecting device based on perovskite NCs is demonstrated with a FWHM of 19 nm.[664] The PeLEDs coupled with a perovskite based photodetecting device

© Author(s) 2021

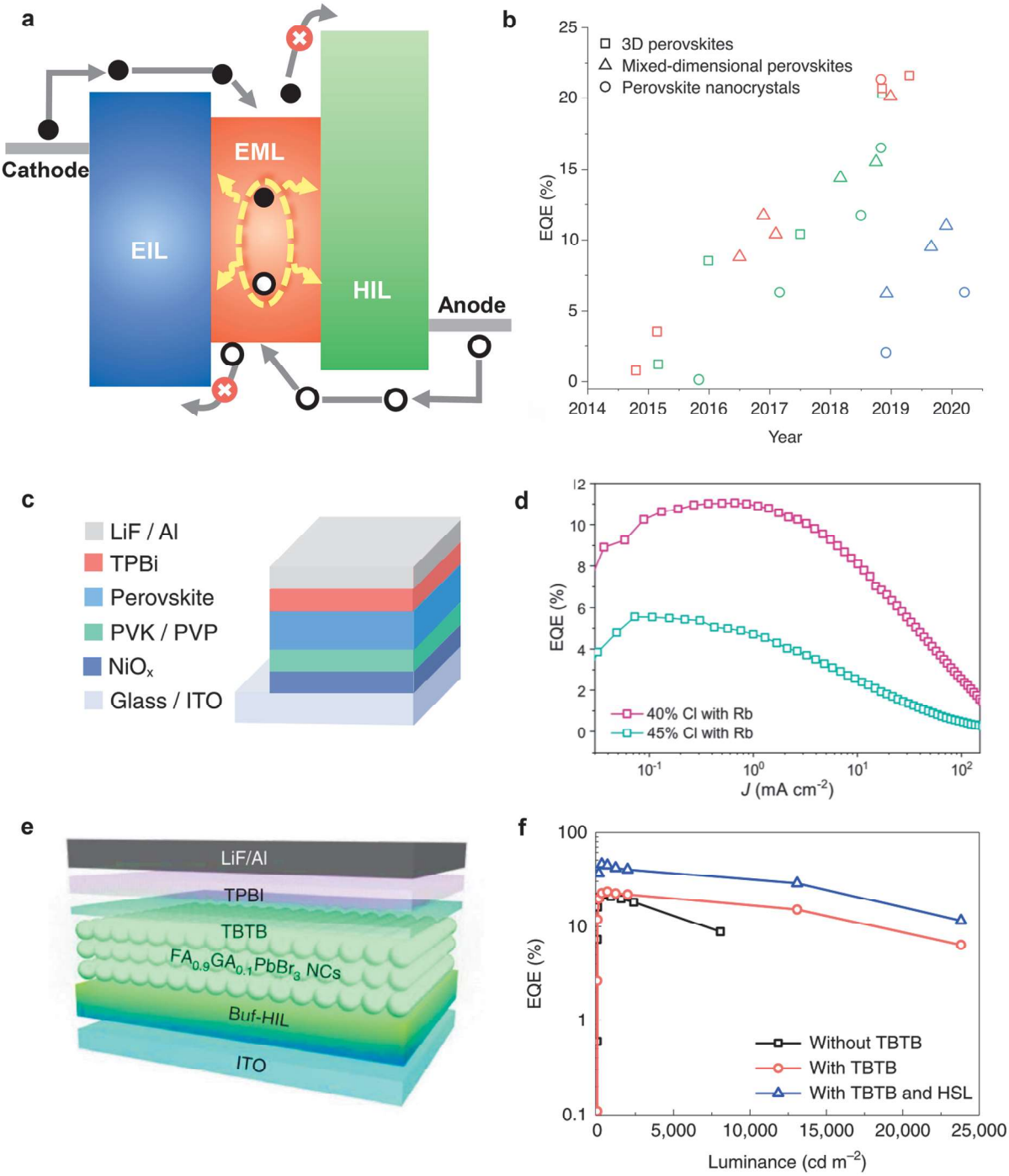


FIG. 31. (a) A schematic showing simplified PeLED architecture. EIL and HIL represent electron and hole injection layers, respectively. Electrons and holes are injected from their respective electrodes into the EML where they recombine and emit light (shown in yellow arrows). The figure is drawn free of scale for illustration. (b) EQE trends of the state-of-the-art PeLEDs. The color of each symbol represents emission color (blue, green, and red/NIR) of the PeLED. Adapted with permission from Liu *et al.*, Nat. Mater. **20**, 10 (2020). Copyright 2020 Nature Publishing Group. (c) and (d) Device architecture and EQE curves of one of the best performing blue PeLEDs employing a mixed 2D/3D perovskite EML. Adapted with permission from Karlsson *et al.*, Nat. Commun. **12**, 361 (2021). Copyright 2021 Author(s), licensed under a Creative Commons Attribution 4.0 License.[656] (e) and (f) Device architecture and EQE plots of state-of-the-art green PeLEDs (EQE of 23.4%) employing a perovskite nanocrystal EML. The high EQE is achieved owing to a comprehensive defect passivation of the EML, which yielded Φ_{PL} of 92.45% in films and defect density of 3.10 10^{12} cm^3. Adapted with permission from Liu *et al.*, Nat. Mater. **20**(1), 10–21 (2021). Copyright 2021 Nature.[515]

© Author(s) 2021

successfully demonstrated simultaneous transmitting and receiving of information and can be a potential candidate light fidelity (LiFi) communication.

2. Current and future challenges

PeLEDs encounter various challenges in terms of efficiency, light output, and stability that are related to the EML as well as the charge injection layers. For instance, the most successful EMLs are Pb-based, which raise **toxicity** concerns. Pb-free EMLs, for example, those based on tin (Sn), suffer from processing related issues that limits Φ_{PL} due to a high concentration of nonradiative defects density and an inferior ambient stability. The EQE in the Pb-free PeLEDs is limited to below 4% only,[524] primarily due to their lower Φ_{PL} than their Pb-based counterparts. Future research needs to focus on effective defect passivation of Pb-free EMLs and their phase stabilization. It is important to note that Sn-based perovskite EMLs can emit deeper into the NIR (beyond 900 nm) and are of particular interest for applications, such as *in vivo* biomedical imaging.

The efficiency of **blue PeLEDs** is much lower than the red and green counterparts due to the high defect density in perovskite EMLs and limitations imposed by the device architecture[525] [see Figs. 31(c) and 31(d)]. Recently, an effective surface passivation of $CsPbBr_3$ NCs using a bipolar shell (inner anion and outer cation shell) featuring high carrier mobility and a reduced trap density resulted in Φ_{PL} > 90% and EQE of 12.3%.[526] The device, however, suffered from a poor stability of only a few minutes (a half lifetime, T_{50} of 20 min at a brightness level of 90 cd m^{-2}). Surface passivation strategies and compositional engineering can offer routes toward efficient and stable blue PeLEDs. For example, A-site doping with a Rb–Cs alloy into 2D/3D perovskite Φ_{PL} ~80% (emission peak at 476 nm) and the device showed a stable emission spectrum even upon thermal annealing.[517] Another key issues in the PeLEDs is the **ionic nature** of perovskite EMLs. Under the influence of an electric field, mobile ions redistribute themselves within the EML and lead to the so-called hysteresis in the current–voltage–luminance curves,[527] spectral instability due to phase-segregation,[367] and change (rise/drop) in the EQE that may take hours to stabilize[528] (due to the slow time constant of mobile ions). These mobile ions can also contribute to device efficiency positively, e.g., via filling vacancies and interstitial related defects, which is evident from a continuous increase in the EL intensity of PeLEDs.[527] Notably, over time, the mobile ions at device interfaces can also alter the barrier for charge injection, thus distorting the charge balance in the device. The role of these mobile ions under the influence of electric field is not yet fully understood and requirse in-depth research to be carried out.

An important application for LEDs is in **high-brightness** (HB) applications, such as in projection displays and automobiles. HBLEDs typically require a high operating current density (J). PeLEDs, like other solution processed LEDs (organic and quantum dots based), show a drop in the EQE at elevated J, also called EQE roll-off. The EQE roll-off leads to a drop in electrical efficiency of LEDs because not all the current passing through the device contributes to photon emission. Plausible explanations to the EQE roll-off in PeLEDs include charge carrier unbalance,[528] especially at elevated current densities and Joule heating.[511] Perovskite materials with balanced and high mobility to ensure a spread of charge carrier concentration within the EML and selection of injection layers featuring balanced charge transport/injection can help in overcoming the EQE roll-off. Electrical properties of injection layers are also important for barrier-free charge transport/injection to reduce Joule heating.

Finally, the PeLEDs currently suffer from a **low operating lifetime** in the range of 10–100 h. Commercial LEDs, however, require a lifetime of several thousand hours at a moderate brightness equivalent to 100–1000 cd/m^2 (for visible emitting LEDs). Typically, a higher lifetime is demonstrated at low J and low brightness levels. It is important to note that the representation of lifetime as a function of injection current density—as often demonstrated in the literature—is not a valid practice.[529] This is because not all the injected charge carriers reach the EML and contribute to the photon emission. A more meaningful representation of lifetime should include reporting operational stability at different brightness levels. Currently, it seems that the 3D hybrid perovskite EMLs, especially those employing MA cations, are less stable than their inorganic and 2D (or 2D/3D) counterparts.[530] From a device engineering point of view, charge injection balancing has also shown to systematically improve the lifetime from a few minutes to a few tens of hours.[528] Future research toward stable PeLED operation should focus on developing non-volatile phase stable EMLs, on interface engineering to avoid reactivity at the device heterojunctions, and on balancing charge injection/transport within the device.

3. Concluding remarks

In summary, perovskite LEDs are promising for future display applications and beyond. Immense research in improving the optical quality of perovskite emitter layers led to near unity photoluminescence quantum yield. This together with efficient device architectures demonstrated external quantum efficiency in PeLEDs at par with organic and quantum dot LEDs. However, PeLEDs still faces challenges pertaining to their inferior lifetime, particularly at high-brightness conditions, stable emission color, and toxicity. Research is also needed to develop novel emitter layers for UV (deep UV) and NIR emission to extend the potential of PeLEDs beyond display devices.

VI. CURRENT CHALLENGES

Lukas Schmidt-Mende, Yana Vaynzof, Davide Moia, Joachim Maier, Marius Franckevicius, Vidmantas Gulbinas, Ross A. Kerner, Lianfeng Zhao, Barry P. Rand, Nadja Glück, Thomas Bein, Fabio Matteocci, Luigi Angelo Castriotta, Aldo Di Carlo, Claudia Draxl, Matthias Scheffler

A. Measurement protocol

Lukas Schmidt-Mende

1. Status of the area

Only reliable measurements of all type of solar cells allow a comparison and clear definition of improvements. A reliably mea-

© Author(s) 2021

sured device efficiency is a prerequisite to define a scientifically meaningful improvement across different research groups. Wrongly reported values for the power conversion efficiency or device lifetime can mislead the community and trigger research in the wrong direction. Therefore, it is extremely important to ensure reliable values under transparent measurement conditions. In particular, record efficiencies need to be reproducible to have any real scientific value as they attract the attention of many researchers in the field.

This topic has been addressed already several times, and reliable measurement procedures and conditions have been defined.[531–536] As the market is dominated by Si solar cells, current industrial protocols and standards are mainly based on inorganic solar cells. Established protocols given by the International Electrochemical Commission (IEC), e.g., IEC 60891,[537] and others. However, also for organic solar cells protocols exist, such as the International Summit on Organic Photovoltaic Stability (ISOS) protocols.[537] Based on this, including additional procedures for perovskites solar cells have been suggested in a consensus statement of stability assessment and reporting for perovskite solar cells.[536]

The most important parameter of a solar cell is the power conversion efficiency (PCE or often h), which is defined as

$$PCE = \frac{P_{out}}{P_{in}} = \frac{V_{MPP} \cdot J_{MPP}}{P_{in}} = \frac{FF \cdot V_{OC} \cdot J_{SC}}{P_{in}}.$$

The incoming power is defined by the light source, where the air mass 1.5 global (AM1.5g) spectra is selected as the standard condition with a power intensity of 100 mW/cm^2. The PCE is measured at a temperature of 25 °C as solar cells efficiencies can vary with temperature. The PCE is measured by performing a J–V scan to extract the data for the open circuit voltage (V_{OC}), the short circuit current density (J_{SC}), and the maximum power point (MPP), which is defined as the largest square under the J–V curve giving the largest product of ($J_{MPP} \cdot V_{MPP}$). The fill factor (FF) is another important parameter defining the squareness of the diode characteristic, which is defined as the quotient of the largest square possible under the J–V curve ($J_{MPP} \cdot V_{MPP}$) and the maximum possible square given by a rectangular diode characteristic ($J_{SC} \cdot V_{OC}$) (for illustration, see Fig. 32).

For organic, dye sensitized, and certainly even more pronounced perovskite solar cells, additional attention has to be taken to allow reliable measurements as to conventional solar cells, as they do behave differently in some aspects from inorganic solar cells. One important issue especially in perovskite solar cells is its sometimes observed hysteretic behavior, meaning that the J–V characteristic can significantly differ depending on the scan rate and scan direction while taking the J–V characteristic. In Fig. 32, this is illustrated by the different curves for scanning in forward and reverse bias directions (indicated by the arrows). As can be seen, this leads to two possible values for the PCE, which can differ quite significantly. As the PCE should give us a reliable idea about the possible power output by a solar cell over time, only stabilized values are of real interest. Therefore, for perovskite solar cells with such hysteretic behavior, maximum power point tracking needs to be performed to enable to report stabilized values.

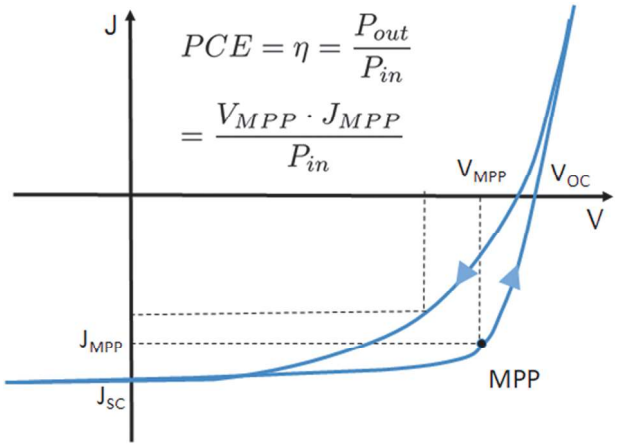


FIG. 32. Possible J–V characteristic (with characteristic values indicated) by perovskite solar cells demonstrating hysteretic behavior as forward and reverse scan directions (indicated by the arrows) leading to different values for the MPP.

2. Current and future challenges

Over the last decade, interface engineering and perovskite optimization has not only led to a drastically improved solar cell performance but also to a significant increase in device stability and reliability (see Sec. VI B). In the course of this, also many high performing perovskite solar cells now show no or negligible hysteretic behavior. However, a reliable measurement protocol should always give correct efficiency values independent of the specific solar cell under consideration. There is clear evidence that the hysteretic behavior is strongly connected to ion migration, which leads to build-up of space charges (on different time scales depending on the specific device under consideration) and results in a scan rate dependence.[538] The large differences on devices depend strongly on the chosen interface layers and indicate a strong influence of the interfacial process often triggered by the ion migration. Trapping and de-trapping in different time scales depending on the perovskite film and its interfaces can explain the observed large differences in the settle time, and even the inversion of the hysteretic effect to the so-called "anomalous hysteresis" of a perovskite solar cell has been observed.[532,539–541]

The hysteretic behavior has been only one obstacle to make measurements of different work-groups comparable. Next to a high efficiency, also the stability of solar cells is an important parameter when it comes to its application as renewable power sources. Stable perovskite photovoltaics are now an important research issue with many researchers trying to understand and overcome different degradation mechanisms. The lifetime of each solar cell depends on different stress factors, which can induce degradation. Five stress categories with different stress levels have been defined as follows: shelf-lifetime (in dark, not connected); outdoor testing; light soaking testing; thermal cycling testing; and finally light, humidity, and thermal cycling testing.[536] While most perovskite solar cells have a long lifetime concerning the shelf-lifetime, they often quickly degrade under thermal cycling testing under illumination in humid air. In

© Author(s) 2021

many laboratories, cells are just measured after fabrication, but no encapsulation is employed. Certainly, this leads to shorter lifetimes, compared to encapsulated devices. While both measurements can give valuable information on stability issues, the non-encapsulated device performance gives indications on the intrinsic stability, while the lifetime of the encapsulated device also strongly depends on the quality of encapsulation. Therefore, it is extremely important to select the specific device adapted protocol and report transparently about the specific parameters chosen for the experiment.

3. Proposed measurement procedures

To be able to report reliable measurement values for the efficiency of a perovskite solar cell, most laboratories now report stabilized values by tracking the maximum power point (MPP) of a solar cell until it has stabilized. MPP tracking over time allows visualizing the change in efficiency over time. For a fast degrading device, the MPP curve will continue to lower with time. However, cells with strong hysteresis often show a fast decay of the MPP in the beginning and then a slower decay for longer times. The observed time scales largely differ and depend on the specific device architecture and processing parameters. Such a MPP tracking curve over time allows an excellent judgment over the realistic efficiency and in addition gives already some hints on the device stability. In most cases, the MPP tracking allows an easy adaptation of existing ISOS protocols to be also valid for perovskite measurements. Therefore, it should be performed and reported for all perovskite solar cells. In most setups for measurements of J–V curves, it has already been or easily can be implemented (e.g., the matlab code for implementation on a Keithly 2400 is published at the GitHub repository of Eugen Zimmermann.[534,542])

As long lifetimes of the solar cells are a prerequisite for a successful market implementation, it is important to have also here reliable protocols. Accelerated aging is used to predict the lifetime of solar cells. This accelerated aging is induced by external stress factors. Here, it is extremely important to know the major degradation mechanism to ensure that the stress factors are adjusted to these mechanisms. However, in many cases, these are not well known, which makes it more difficult to know the stress factors, which need to be induced for the accelerated aging and which would allow an extrapolation to estimate the real lifetime of a solar cell. For example, if the combination of UV-light and humidity is inducing degradation, the aging can be adapted to use a light source with increased UV-emission. If, however, for the measurement, an illumination source with low or no UV-portion is used, the measurement will give a wrong picture of the stability. Another consequence could be to protect the solar cell by an encapsulation equipped with a UV filter to avoid this type of degradation.

Therefore, one of the most important conditions is to report the exact measurement parameters, concerning light source and intensity, humidity, measurement environment, temperature and cycling times, device protection, etc. Understanding the degradation parameter then enables to specifically address the dominant degradation mechanisms and also allows finding adequate protection mechanisms for the photovoltaic devices to avoid this type of degradation.

The above-mentioned five different stress categories of lifetimes can give already good indications about the overall stability of the cell. If solar cells survive for a reasonable time in the most harshest condition, thermal cycling under light at elevated humidity, this will allow the most reliable prediction for the lifetime also under realistic conditions as the dominant degradation mechanisms are most certainly addressed under these stress conditions. However, in some cases, the real lifetime on realistic conditions might be even much longer than these predictions might allow to estimate.

4. Concluding remarks

For all solar cells, a reliable measurement is necessary to enable researchers to compare their results. For perovskite measurements, the common protocols (such as ISOS) have to be extend, as perovskite photovoltaics often show a hysteretic behavior in J–V scans, leading to different power conversion efficiency values depending on scan direct and speed. To ensure reliable values for the PCE, researchers should consider next to the common protocols additional conditions as summarized in Table II. For every perovskite solar cell, a power point tracking needs to be done to ensure a stabilized power output. Such power point tracking can also give some information on the stability of the specific device. For real lifetime measurements, different stress categories should be applied and the precise measurement conditions clearly stated when such measurements are reported. Only with the information of all measurement conditions, a clear judgment on the real lifetime of a cell will be possible. The selected measurement conditions should reflect the dominating degradation mechanisms of the specific device under investigation. Such measurements will allow us to systematically improve efficiency and lifetime of perovskite devices.

B. Reproducibility

Yana Vaynzof

1. Status of the area

Perovskite photovoltaics is a thriving field of research resulting in many thousands of publications reporting advances in the

TABLE II. Next, to the standard measurement protocols for solar cells, we proposed additional measurement conditions for perovskite solar cell efficiency and their stability.

Measurement type	Parameters and conditions
Standard measurement condition	Spectrum: AM 1.5 g Light intensity: 100 mW cm^{-2} Temperature: 25 °C
Perovskite solar cells	MPP tracking and stabilization
Stability and accelerated aging	Increased light intensity Increased temperature (65 and 85 °C) Increased humidity (e.g., 50% and 85%) Increased number of cycling times Device encapsulation Combination of the above stress conditions

© Author(s) 2021

understanding of material and device physics, engineering and optimizing of high performance devices, and many other aspects of perovskite materials. However, examining the body of literature on perovskite solar cells reveals significant variations in many of the reported material properties and photovoltaic performance parameters—often for the same perovskite composition and device architecture. Even the most basic properties, such as the optical bandgap of the material, its ionization potential, dielectric constant, and others, seem to vary drastically between different reports. The observed distribution in the photovoltaic parameters has led to a change in the method of reporting photovoltaic performance: early reports often displayed a single current density–voltage curve showing the maximum performance, while in recent years, it became ubiquitous to report histograms of photovoltaic performance obtained on dozens or even hundreds of devices. There can be many reasons for the different material properties reported for the same perovskite compositions and the relatively poor reproducibility of perovskite photovoltaic devices. In some cases, the choice of the measurement technique and the method of data analysis can lead to differences in the obtained values of a certain property. For example, Kahn and co-workers showed that analyzing the same ultraviolet photoemission spectrum measured on a perovskite sample may lead to different values of ionization potential, depending on whether the spectrum was presented in a linear or a logarithmic scale.[543] The exact method of fitting the valence band edge (e.g., linear tangential fit vs a fitting of the density of states) can also influence the extracted value of the ionization potential.[544] Moreover, surface photovoltage effects may further complicate the determination of the band position.[180] Similar difficulties arise also with other measurements techniques. Another possible reason for the large variation in the reported properties of perovskite materials is the presence of 'hidden' factors that influence these properties and thus also the measurements of different groups in different ways. For example, Goetz *et al.* compared the photoluminescence quantum efficiency (PLQE) of methylammonium lead triiodide ($MAPbI_3$) perovskites and revealed that the results can vary over several orders of magnitude, even for the same excitation power (Fig. 33).[545] This discrepancy highlights that other factors influence the results of the measurement and need to be accounted for in order to allow for a meaningful comparison of results.

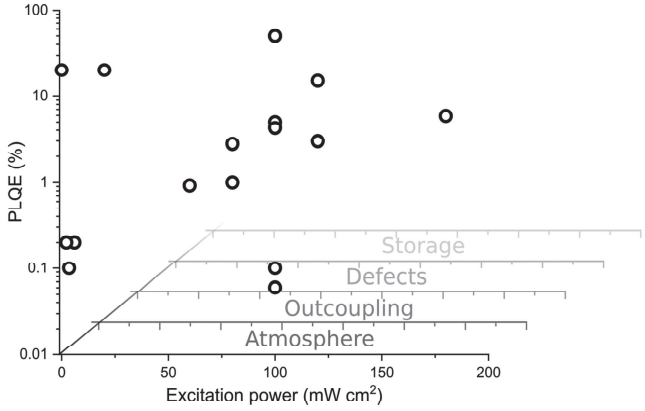


FIG. 33. Selection of PLQE values reported in the literature as a function of excitation power for $MAPbI_3$ without modifications. Adapted with permission from Goetz *et al.*, Adv. Funct. Mater. **30**, 1910004 (2020). Copyright 2020 John Wiley and Sons.[545]

2. Current and future challenges

Currently, many steps in perovskite solar cell fabrication include factors that are hard to control but that may influence the final performance of the device. For example, the use of different precursors—either from different suppliers or even different batches from the same supplier—may lead to different performance of otherwise identical devices. The environment in which the perovskite layer is deposited is also important. The levels of humidity or the presence of other solvent vapors influences the formation of the perovskite layer but cannot always be controlled even in laboratory settings since multiple users will lead to varying environment. Another factor that influences the reproducibility of perovskite devices is the fact that they are fabricated by hand, which introduces human factors into the equation. Indeed, it is common that even in the same research group, devices made by different people may vary in their performance, despite having the same architecture and perovskite composition. While studies aiming to isolate the causes of irreproducibility in perovskite materials are notoriously difficult since they require a single parameter to be varied in a consistent and systematic fashion, without introducing other factors that may influence the results, some examples of such investigations exist. For instance it has been recently identified that fractional, unintentional, variations in the stoichiometry of the perovskite solution have a significant impact on the properties, performance, and stability of perovskite solar cells (Fig. 34).[546,552] A change as small as 0.1% in the precursor stoichiometry can change the properties of the resultant perovskite layer, such as its surface composition, ionization potential, and photoluminescence properties,[547] leading to significant changes in the built-in potential and open-circuit voltage of the photovoltaic devices. Recently, it was also shown that any excess of deficiency of precursor components introduced via even the slightest deviation from the correct stoichiometry lead to a significant variation in the density of ionic defects in the perovskite layers and, consequently the properties of the layers and photovoltaic devices.[548] A more recent study identified another source of irreproducibility in perovskite solar cells fabricated by the antisolvent quenching method.[549] It was shown that the rate of antisolvent application—which naturally varies between different researchers—strongly influences the properties of the perovskite layer and consequently the photovoltaic performance. In fact, controlling the rate of antisolvent application made possible the fabrication of highly efficient solar cells from any antisolvent and from a broad range of precursor stoichiometries.

Another challenge is related to the fact that even individual samples of perovskite materials exhibit inhomogeneities on various length scales.[550,551] The presence of such heterogeneities means that not only their properties, but also their photovoltaic performance varies across the layer. While this situation clearly complicates progress in research of perovskite materials, with different researchers obtaining different results based on the area of the sample which is probed, it is even more unacceptable when it comes to the commercialization of perovskite solar cells. These issues of reproducibility, reliability, and uniformity must be addressed before perovskite solar cells can enter the market.

© Author(s) 2021

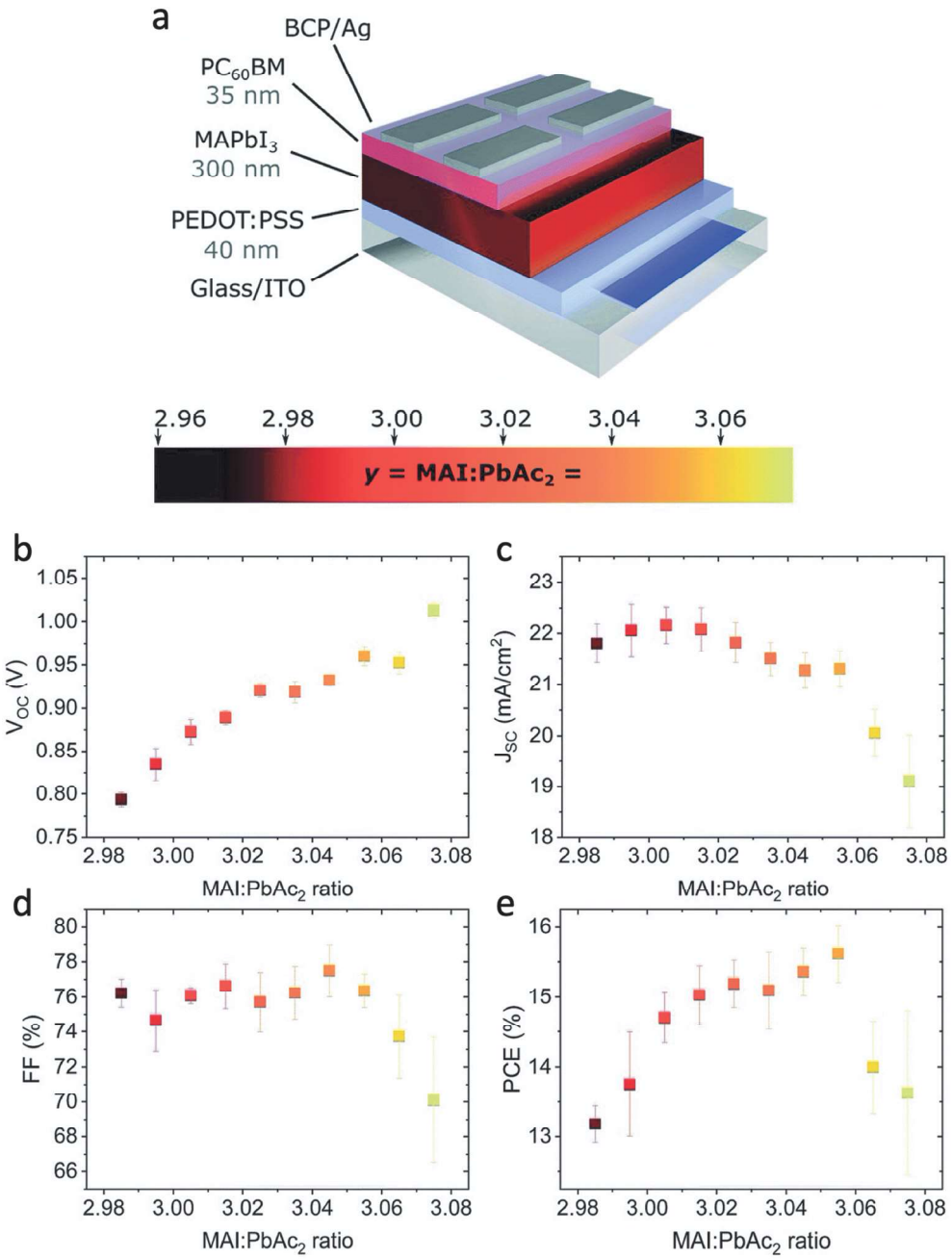


FIG. 34. (a) Schematic of the photovoltaic device architecture: ITO/PEDOT:PSS/$MAPbI_3$/$PC_{60}BM$/BCP/Ag and the fitting color scale used throughout the manuscript for illustrating stoichiometric changes of the precursor solution, with the stoichiometry y representing the molar ratio of MAI to $PbAc_2$. (b)–(e) Variation of the photovoltaic parameters (V_{OC}, J_{SC}, FF, and PCE) of solar cells with changing stoichiometry ($2.985 < y < 3.075$). Adapted with permission from Fassl *et al.*, Energy Environ. Sci. **11**, 3380 (2018). Copyright 2018 The Royal Society of Chemistry.

3. Advances in science and engineering to meet these challenges

The many factors that influence the reproducibility of perovskite materials are hard to identify and control without understanding the fundamental mechanisms of film formation of perovskite materials. While the focus of the research community has naturally fallen on improving the efficiency, and more recently the stability, of perovskite solar cells, much attention has to be devoted to understanding the processing of these materials. For example, the fundamental understanding of the processes of crystallization, microstructure formation, and defect creation in perovskite

© Author(s) 2021

materials is at least partly lacking. To investigate these processes—and the influence of various factors on these processes—a standardization and a certain degree of automation would have to be introduced into laboratory-scale fabrication of perovskite thin films and solar cells. This would be especially powerful in eliminating the human-introduced variation in the fabrication procedures that are otherwise very difficult to control. In solution-processed spin-coated perovskite devices, for example, such automation can be achieved by constructing a robotic-like system that dispenses the perovskite precursor solution and, consequently, the antisolvent, thus allowing a complete control over all the deposition parameters. It is noteworthy, however, that other perovskite deposition techniques, such as thermal evaporation, also suffer from reproducibility issues,[197] and a similar automation of the evaporation system may assist in identifying the roles of the individual parameters on the properties of the evaporated perovskite layer.

In addition to standardizing deposition techniques, *in situ* characterization of the perovskite film during its fabrication can aid at identifying the processes and elements that influence its properties. For example, a recent study by Lee *et al.* investigated the formation of $MAPbI_3$ thin films by implementing *in situ* grazing incidence wide-angle x-ray scattering experiments.[552] The authors identified that the use of additives influences the solvate phase, thus in certain cases allowing to control the film's properties in a highly reproducible way. While such spectroscopic and microscopic characterization experiments remain rare and are very difficult to implement for a variety of reasons, future advances in engineering may make it possible to monitor the process of perovskite film formation in great detail.

4. Concluding remarks

Reproducibility issues plague the field of perovskite photovoltaics and significantly more research efforts are required to address them before this technology matures to a level of mass-scale commercialization. In particular, subtle changes in the fabrication conditions of perovskite materials, which can lead to significant changes in their properties, need to be identified and investigated in detail. Furthermore, more effort needs to be devoted to increasing the homogeneity of samples, especially in the case of large area fabrication. Finally, characterization procedures need to be carefully evaluated and standardized so that results from different researchers can be compared in a meaningful way—as addressed in Sec. VI A.

C. Ion migration

Davide Moia, Joachim Maier

1. Status of the area

Since the early observations of current–voltage hysteresis,[531] switchable photovoltaic effects,[34] and huge capacitive and inductive features,[553] ion migration in hybrid perovskite based devices has been invoked to interpret device behavior and is a defining feature of this material class. Conduction of ionic defects in methylammonium lead iodide ($MAPbI_3$) has been extensively investigated both experimentally[554] and computationally.[33,555] Characterization through electrical, chemical, and spectroscopic techniques highlighted the role of iodide vacancies in the ion conduction properties of $MAPbI_3$, with a less pronounced migration expected for methylammonium ions and for other defects.[556,557]

Schottky disorder is most likely controlling the majority ionic defects' concentrations in hybrid perovskites in the intrinsic regime [Fig. 35(a)],[341] while the role of extrinsic (including impurity) doping may also play a role as a background charged defect population. Reversible variation of the iodine content in these materials is possible at room temperature with sensitive consequences on the transport properties [Fig. 35(b)] according to the following reaction:

$$\frac{1}{2}I_2 + V_I^{\cdot} \leftrightarrow I_I^X + h^{\cdot}.$$

Investigation on the electrical response of hybrid perovskite devices, where partial or full substitution of methylammonium with different A-cations, or of iodide with bromide takes place, showed results consistent with the predicted dominant contribution of halide defects to the measured conductivity.[558–560] It also emphasized the complex relation between activation energy for ion migration and the structural and chemical parameters of the lattice,

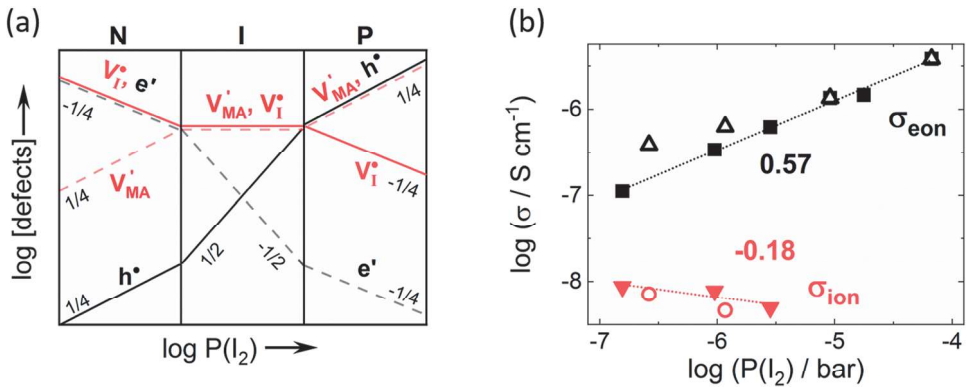


FIG. 35. (a) Kröger–Vink defect concentration diagram as a function of iodine partial pressure [$P(I_2)$]. (b) Experimental data on electronic (σ_{eon}) and ionic (σ_{ion}) conductivities as a function of $P(I_2)$ for a $MAPbI_3$ pellet measured at 373 K in the dark. The observed trend is consistent with and being dominated by the contributions of holes ($h^{\cdot}$) and iodide vacancies ($V_I^{\cdot}$), respectively. Adapted from Ref. 555, further permissions related to the material excerpted should be directed to the ACS. (b) Reprinted with permission from Senocrate *et al.*, Solid State Ionics **321**, 69 (2018). Copyright 2018 Elsevier.

© Author(s) 2021

such as the size of the mobile ion, unit cell size, and lattice distortions. The A-cation mobility is distinctly lower than the anion mobility but may well play an important role in kinetic effects in thin films.[561]

Large concentrations of mobile ionic charge carriers have been predicted and indirectly measured experimentally, suggesting that ionic defects are majority carriers in the active layer of hybrid perovskites in the dark and also in many relevant out of equilibrium conditions.[341,562,563] One important implication that is widely accepted is that mobile ions in hybrid perovskites respond to applied bias and contribute to varying the electrostatic potential profile in devices.[338] The effect of ion conduction on the electrical response of devices has been explored through several types of optoelectronic measurements[564] and reproduced by simulations that included mobile ionic defects in the drift diffusion equations.[8,9,365,565] The description of devices' optoelectronic behavior through a variety of equivalent circuit models has also stressed the importance of ion migration as a core feature determining the response of hybrid perovskite solar cells.[554,566,567]

2. Current and future challenges

Despite the recent progress in the characterization of ion migration in hybrid perovskites and despite the analogy with oxide perovskites, the development of models, including a complete analytical description of their bulk and interfacial defect chemistry, remains a major challenge. In the dark, the behavior of mobile ionic defects in the bulk of $MAPbI_3$ is relatively well understood, while the behavior of hybrid perovskite interfaces with contacts and at grain boundaries is still under debate.[568] It was recently shown that ionic interactions can induce redistribution of defects at interfaces in the dark and can be a decisive factor on the determination of the space charge equilibrium between hybrid perovskites and contact materials. This shows that even the basic understanding of equilibrium at photovoltaic interfaces has to be revisited in the presence of mobile ionic defects.[562]

The situation is even more complex for devices out of equilibrium. Recent work on $MAPbI_3$ thin films exposed to light has indicated intriguing interactions between electronic and ionic defects and revealed that higher order defect formation modes and trapping mechanisms are likely to occur in the soft environment of iodide perovskites.[569,570] The role of these effects on the overall recombination kinetics is currently unknown and deserves future investigation. Furthermore, differences in the nature and extent of this electronic–ionic interaction for the iodide based compared to the bromide-based perovskites can provide a driving force for another process relevant to ion migration in these compounds, commonly referred to as "photo-demixing."[560,571,572] More generally, this phenomenon highlights that because of the pronounced ion transport in halide perovskites even at room temperature, it is challenging to kinetically stabilize unstable phases for this class of materials.

Ion migration introduces several challenges as far as the operation of solar cells is concerned. Ionic conduction and modulation of electronic currents due to ionic redistribution underlie much of the low frequency behavior of solar cell devices, including current voltage hysteresis, huge values of capacitance, and inductive behavior.[566,573,574] The presence of mobile defects also has implications for the minimum applied voltages at which decomposition of the active layer occurs.[555] For these reasons, it is widely accepted that suppressing ion migration is key to improve the reliability and long-term stability of hybrid perovskite solar cells. The apparent absence of compositions showing negligible ion migration implies that further progress is needed in this direction, also indicating that different approaches to these questions have to be considered.

3. Advances in science

The challenges outlined above indicate that ion migration should be an integral part of the device parameter space for the optimization of hybrid perovskite solar cells. One first important question concerns methods to quantify the influence of mobile ionic defects in experimental observations. Ion migration in solar cells is often evaluated on the basis of the degree of hysteresis in current–voltage curves. Based on the discussion above, it is evident that this does not yield accurate comparisons.[365] Electrochemical techniques combined with other characterization methods benefit the exploration of ion transport and the influence of halide and other mobile defects on electronic charge carrier dynamics.[558,575,576] Enriching this description will also address the role of both the point defect chemistry (e.g., trapping related to migrating ions and[577,578] high order ionic defect formation modes[579]) and of extended defects (within the grains[580] and at grain boundaries[581]) in the determination of non-radiative recombination processes limiting solar cell performance.

Ion migration in hybrid perovskite solar cells is most often considered a problem and only occasionally viewed as an opportunity. The observation of pronounced changes in the low frequency behavior of devices upon changes in material composition and stoichiometry emphasizes the potential of applying established Solid State Ionics strategies to these systems. Furthermore, the influence of ion migration on electronic recombination currents at interfaces is expected to vary with different contact materials due to differences in parameters such as nature of traps, interfacial capacitance, and space charge potential profile.[566] This indicates the relevance of other "non-classical" solid state ionics strategies (Fig. 36) that can aid device design.

Therefore, diversifying research approaches to ion migration in hybrid perovskite solar cells is key to improve both their reliability and stability as well as their performance. Further material optimization might lead to guidelines for hybrid perovskite compositions for which ion migration is suppressed over the target lifetime for solar cell modules. Until then, research into mitigating the effects of ion migration should be a priority in the field, mostly through contact and encapsulation design. Further understanding of the ionics of bulk, grain boundaries, and interfaces with contacts as well as of the role of ionic conduction on material decomposition may point to solutions for reliable and inherently stable (mixed conducting) solar cells. Integrating mobile ionic defects as an additional tool for solar cell optimization may prove to be a useful silver lining. This is relevant to interfacial properties,[562] trap management,[582] and self-healing effects.[583]

Finally, discovering ways for controlling and even enhancing ionic conduction in hybrid perovskites will inspire new directions toward optoelectronic and optoionic devices for and beyond photovoltaics.[579]

4. Concluding remarks

Including ion migration in the description of the photovoltaic operation of hybrid perovskites has had a key role in explaining

© Author(s) 2021

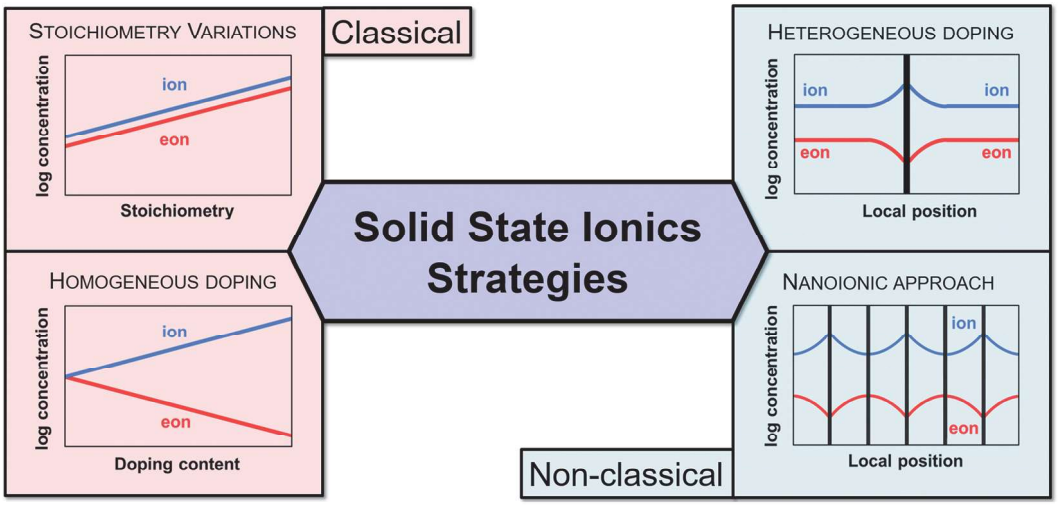


FIG. 36. Strategies in the field of Solid State Ionics that can be applied to hybrid perovskites include approaches addressing stoichiometry and doping of ionic and mixed conducting materials as well as routes to leverage interfacial effects to control defect transport properties. The labels "ion" and "eon" refer to ionic and electronic charge carrier concentrations, respectively.

the many anomalies observed in perovskite devices (e.g., current voltage hysteresis and photo-demixing) as well as degradation phenomena. Progress in the ionics of hybrid perovskites is a necessity to design mitigation strategies for these anomalies and to address device degradation routes. Additionally, controlling the ionic interactions between active layer and contact materials in solar cells may represent an additional tool for performance optimization and for added functionality. While the ionics of $MAPbI_3$ has been extensively investigated for the dark situation at equilibrium, important steps forward include extending the defect chemical picture to out of equilibrium situations relevant to solar cells operation. Finally, integrating the investigation of ionic properties in the exploration of new hybrid perovskite compositions and solar cells' architectures will accelerate the search for high performance and high stability materials.

D. Stability

Marius Franckevicius, Vidmantas Gulbinas

1. Status of the area

Despite the spectacular progress made in recent years in increasing the conversion efficiency of hybrid PSCs, their long-term operational stability is rather poor and remains a critical issue hindering their commercialization prospects. PSCs typically show a decrease in device performance in real operating conditions, which is due to the degradation of the perovskite and charge transporting materials, as well as their interfaces. Low stability of MHPs used in solar cells is, unfortunately, their intrinsic property caused by the low formation energy of the three-dimensional perovskite lattice, which is prone to deformation and vulnerable. The possible causes responsible for the degradation of the perovskite material can be broadly divided into external and intrinsic factors. The external factors include UV light, moisture, oxygen, and temperature, which can be considered as climatic effects. Meanwhile, intrinsic instability is mainly due to electric field-induced ion and other charged defect migration and interfacial reactions.[35,397,659] All these factors cause a broad variety of the degradation processes and are closely interrelated with each other [Fig. 37(a)]. Figure 37(b) show typical stability tests of PSCs performed under different aging conditions. Perovskite degradation in humid and oxygen-saturated atmosphere is much faster than in dry and oxygen-free conditions. In the case of oxygen, highly reactive superoxide species formed upon photoexcitation can initiate an acid–base reaction with organic cations, thus destroying the perovskite structure [Fig. 37(c)],[660] while in humid atmosphere, water molecules can easily penetrate and diffuse through the perovskite structure also promoting its degradation.[390] High temperature is another important factor causing not only decomposition of the perovskite material by sublimation of organic components (CH_3NH_2, HI)[661] but can also initiate interfacial reactions[397] and degradation of other materials contained throughout the device.[662] The bonds holding perovskite crystals, particularly hydrogen and electrostatic interactions between organic cations and inorganic negatively charged cavity, are weak and thus can easily be broken even under mild conditions. A substantial change in the perovskite crystal can occur during the light illumination initiating ion migration, halide segregation, photodecomposition, etc. The electric field is an additional source of perovskite degradation in operating PSCs.[663] As in the case of light, an electric field can initiate ion migration[339] and their accumulation at interfaces,[664] where the interaction of ions with selective contacts or electrodes can induce interface degradation.[665,666] Corrosion of contacts, as a special case of degradation processes, will be discussed in more detail in Sec. VI E. The electric field can also modify the electronic band structure of perovskite crystals, affecting charge carrier transport and in some cases hindering charge separation.[667] The local electric fields induced by trapped charges can deprotonate organic cations, ultimately decomposing PSCs.[668]

© Author(s) 2021

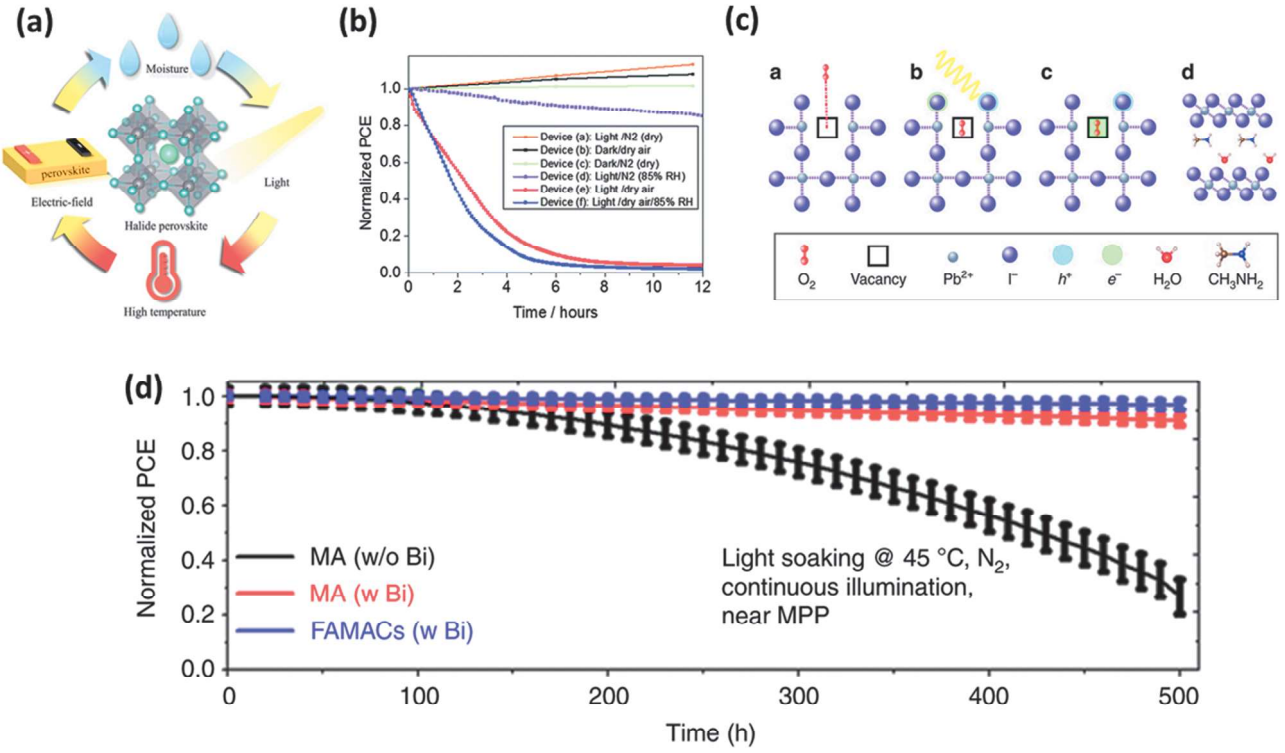


FIG. 37. (a) Typical causes of degradation of PSCs. Adapted from Ref. 667. (b) Normalized power conversion efficiencies of methylammonium lead iodide PSCs measured under different environmental conditions. Adapted from Ref. 688. (c) Schematics of the oxygen induced photodegradation of $CH_3NH_3PbI_3$ perovskite: (a) molecular oxygen diffuses within the perovskite crystal and incorporates into the lattice, (b) light-induced generation of charge carriers, (c) electrons react with molecular oxygen to form superoxide, and (d) perovskite decomposition into PbI_2, H_2O, I_2, and CH_3NH_2. Adapted from Ref. 660. (d) Improved stability of PSCs employing compositional and interfacial engineering. Reproduced with permission from Wu *et al.*, Nat. Commun. **10**, 1161 (2019). Copyright 2019 Nature Publishing Group.[689]

2. Current and future challenges in this area

Although the first PSCs degraded within minutes,[669] several groups have recently demonstrated improvement of PSCs lifetimes to few hundreds and even thousands of hours.[22,670,671] This was achieved mainly, thanks to considerable progress in recent years, in identifying possible degradation mechanisms and development of new methods to stabilize perovskite material and device interfaces. Notable strategies for improving the stability of PSCs include compositional engineering to stabilize heterostructures of soft halide perovskites, doping of photoactive perovskite material and charge transport layers, interface engineering, and development of encapsulation techniques. The former two will be discussed in more detail, which are the most effective approaches for making efficient and stabile PSCs [Fig. 37(d)].

a. Compositional engineering. Compositional engineering is realized when the organic or inorganic cations constituting perovskite materials are substituted with one or more new cations of similar characteristics. It is an attractive approach because it allows controlling the material structure and, therefore, has the advantage of directly influencing the intrinsic material properties and its stability. In particular, mixed cation halide perovskites led to greatly improved thermal stability of PSCs.[46,256] The introduction of the triple cation perovskite $[FA_{0.95-x}MA_xCs_{0.05}Pb(I_{1-y}Br_y)_3]$ composition by Saliba *et al.* has caused significant breakthrough in the area.[46] It has been reported that small amount of cesium was able to stabilize black phase of FA-based perovskites, which allowed for an increase in thermal stability of PSCs extending their operation time to more than 250 h [Fig. 37(b)]. Inspired by this achievement, the effect of cesium has been also widely explored by many groups for the stabilization of other mixed cation perovskite systems, such as CsFAMA and $CsFAPbI_3$.[672] In addition, other small inorganic cations, such as rubidium, potassium, or their mixtures, were also used as alternatives to the Cs cation in FAMA and $FAPbI_3$ perovskites.[48,673] However, a more detailed information about their effect on the device stability is still lacking. To tackle this, several large organic cations, such as ethylammonium[674] or guanidinium,[675] were also proposed to incorporate into the perovskite lattice. A small amount of large guanidinium cation was successfully incorporated into the $MAPbI_3$ perovskite, which resulted in improved thermal and environmental stability due to the highly stable perovskite structure, resulted from the increased number of hydrogen bonds.[675] Although there have been many more studies on different perovskite compositions, this approach alone still cannot ensure operational stability of the devices necessary for practical applications. Nevertheless, screening for new small inorganic cations, as well as organic amine cations and cations possessing heteroatoms other than nitrogen, remains an important task promising further stability improvements.

© Author(s) 2021

b. Interface engineering. The surface of solution deposited polycrystalline perovskite films is the region where the highest density of various types of defects, such as dangling bonds, vacancies, and charge point defects, is present. Moreover, the degradation of the perovskite usually starts at the surface at these defect sites as they are least resistant to moisture and oxygen. Therefore, protection of the perovskite surface from degradation is an important step toward the long-term stability of PSCs.

Passivation of the negatively and positively charged defects on the hybrid perovskite surface by Lewis acids/bases is a widely used interface engineering strategy introduced by Noel *et al.*[676] Thus, Lewis base molecules (such as derivatives of pyridine, thiophene, and some amines) containing electron-donating oxygen, nitrogen, or sulfur atoms can effectively passivate positively charged defects, such as undercoordinated Pb_2^+, iodine, or Pb clusters. Lewis acid compounds (such as metal cations and fullerene derivatives) are electron acceptors and thus passivate MA^+ vacancies and uncoordinated I^- and antisite PbI_3^- defects. Significant results have been obtained in stabilizing the efficiency of PSCs by using both Lewis bases and Lewis acid compounds. Recently, Zhang *et al.* demonstrated unprecedented two-month moisture stability for unencapsulated $MAPbI_3$ PSCs passivated with a bidentate 2-mercaptopyridine molecule.[677] Wang *et al.* presented PSCs stabilized with 1,3,7-trimethylxanthine (caffeine), which exhibited excellent thermal stability and retained 86% of their original efficiency after 1300 h at 85 °C in a nitrogen atmosphere.[678] Triple-cation PSCs passivated with potassium retained about 80% of their original performance after 300 h of continuous operation.[467] In a very recent example, Li *et al.* demonstrated MA-free $(Cs_{0.17}FA_{0.83})Pb(I_{0.8}Br_{0.2})_3$ PSCs modified with bis-fulleropyrrolidium iodide (bFPI), which showed more than 500 h of stabilized power output with less than 5% power loss.[679]

Obviously, Levis base/acid-based perovskite passivation is a powerful strategy to improve device stability, but most passivation materials generally contain a limited number of functional groups to passivate different defects simultaneously. Moreover, the commonly used passivation layers are composed of insulating materials with wide bandgap, which hinder the charge transfer from the perovskite to transport materials. Therefore, the future challenge in this field is to create new multifunctional materials that might be able to simultaneously passivate different types of defects and provide efficient charge carrier transfer across the interfaces.

Passivation of perovskite grain boundaries, surface, and bulk defects using two-dimensional (2D) perovskites is another effective strategy that has great potential for achieving high-efficiency PSCs. Due to the high formation energy of 2D perovskites and less volatile long-chain organic cations used for two-dimensional perovskite formation, they are thermodynamically more stable than their 3D counterparts and exhibit high resistance to water and moisture. When mixed directly into the bulk or coated onto the 3D perovskite surface, they can significantly improve the stability of 3D films and devices. Impressive results were obtained by Grancini *et al.* when they used aminovaleric acid to prepare a mixed 2D/3D perovskite composite that allowed stable PSCs modules with an efficiency of 11.2% retaining for one year in ambient atmosphere at a temperature of 55 °C.[22] Although 2D/3D perovskites are extremely stable, solar cell efficiencies were limited mainly because of unfavorable growth of 2D layers resulting in poor transport of charge carriers and formation of not completely pure-phase thus thermodynamically less stable 2D perovskites. Recently, Jang *et al.* demonstrated the solvent-free solid-phase in-plane growth method to deposit 2D perovskites on a 3D film, resulting in an intact 2D/3D heterojunction. The PSCs fabricated using this method yielded a certified efficiency of 24.35% and stability of more than 1000 hours at 85 °C and relative humidity of 85%.[680] Despite the high efficiencies and operational stabilities achieved for 2D/3D PSCs, there is still a need to better understand how orientation of 2D perovskites with respect to 3D affects charge carrier transport and to develop new strategies to achieve highly oriented and phase-pure 2D perovskites to ensure their high thermodynamic stability.[681]

As was already mentioned, the degradation of the perovskite solar cell is not only related to the poor stability of the perovskite itself. Stability of other layers constituting the solar cell is also of great importance. The HTL is an important component of the PSCs. Thus, when designing HTLs, one should not only focus on how to achieve the highest PSCs efficiency but must also meet the stringent stability requirements. To date, the most regular architecture of perovskite solar cells uses spiro-OMeTAD or PTAA as hole transport materials, which are usually doped with Li-TFSI and tBP to improve hole mobility and increase conductivity. Ultimately, both additives deteriorate the long-term stability of the perovskite material due to the hygroscopic nature of Li-TFSI and the corrosive effect of tBP.[682] Moreover, the glass transition temperature of doped spiro-OMeTAD is below 100 C, indicating poor stability at high temperatures. All these shortcomings point to the need to implement new dopant-free hole transport layers with high transition temperature, which should also satisfy a number of other requirements.[683] A particularly interesting example is the multifunctional dopant-free hole transport material reported by Zhao *et al.*,[684] which simultaneously acts as an efficient surface defect passivation layer and efficient HTL, possessing high carrier mobilities similar to those of doped spiro-OMeTAD. The dopant-free HTL-based devices produced a PCE of 22.4% with significantly improved operational stability under continuous illumination compared to doped spiro-OMeTAD. In another interesting research by Arora *et al.*,[670] significant improvement in device stability was achieved by using inorganic copper thiocyanate (CuSCN) as HTL. The CuSCN-based solar cells retained more than 95% of the initial efficiency for 1000 h when aged at 60 °C under solar irradiation. This is the highest reported stability obtained with inorganics hole transporting materials. Other promising categories among these examples are dopant-free hole-transporting self-assembled monolayers and polymeric HTLs. A novel approach was demonstrated by Magomedov *et al.* who formed a self-assembling molecular monolayer on the surface ITO that served as a HTL in their p-i-n PSCs and achieved an efficiency of 17.8% together with improved stability.[685] Jung *et al.* proposed a novel device architecture that enabled a high efficiency of 22.7% to be achieved for PSCs with an undopped P3HT polymer as the HTL.[45]

Although hundreds of different hole transport materials have been reported so far, there are only a few examples that have successfully contributed to the long-term stabilization of perovskite solar cells. Therefore, further development of the technology requires optimization of HTL to obtain reproducible, high-purity, low-cost, and stable materials.

© Author(s) 2021

As described above, many different materials and device architectures have been proposed to improve the efficiency and increase the stability of PSCs. However, in order to commercialize PCS technology, such as Si, CIGS, and GaAs, it must provide long-term (20–25 years) stable performance toward repeated illumination cycles and outdoor temperature fluctuations. Although the reproducibility of PCSs fabricated in different laboratories has improved, thanks to the available transparent protocols (see Sec. VI A),[686] the repeatability in stability tests is still poor.[536] This is because the durability of PSCs is mainly determined by the purity of the starting materials, the fabrication conditions, and the properties of the bulk and interfaces.[659] Moreover, stability tests in different laboratories are often performed under different control conditions rather than following a uniform procedure, which makes it difficult to repeat the experiments and compare the results. Therefore, for a reliable stability evaluation of PSCs, one should use the recently proposed ISOS protocols[536] originally offered for organic photovoltaic devices,[687] as well as some extended ISOS protocols proposed considering the unusual PSC stability properties as explained in more detail in Sec. VI A.

3. Concluding remarks

We have briefly touched upon the main processes causing the rapid degradation of PSCs and some achievements toward their stabilization. As mentioned above, there are a variety of problematic aspects in the material structure and design architectures that cause the degradation of PSCs under severe real operating conditions. All these issues should be solved in order to meet the stringent stability requirements for PSCs. It can hardly be expected that there is a magic stabilization method that can solve all these problems at once, so a wide range of different measures should be developed and combined to address different types of instabilities.

E. Corrosion of contacts

Ross A. Kerner, Lianfeng Zhao, Barry P. Rand

1. Status of the area

Metals are integral components of photovoltaic devices and modules, serving as low resistance conductors to ensure that the converted solar power is harvested with minimal Ohmic losses. Unfortunately, organic–inorganic halide perovskites are intrinsically corrosive toward metals as they contain Pb^{II}, mobile protons, and halides. Corrosion, here, specifically refers to any undesirable reduction/oxidation (redox) reactions that oxidize a neutral metal to the respective metal cations. Reduction and oxidation can occur in the same location (simple redox), or reduction and oxidation can occur at spatially separated sites if electrically and electrolytically connected (electrochemical corrosion). Electrical connection over entire cell areas is guaranteed by the conductive substrate and top current collectors, increasing the risk and severity of electrochemical corrosion. Several mechanisms of metal corrosion in various situations are discussed below, illustrating the complexity of the phenomenon and challenge.

2. Current and future challenges

Hybrid organic–inorganic halide perovskites, which can to some extent be classified as solid-state proton and halide electrolytes, are known to be corrosive toward many metals,[396] yet perovskite/metal interfaces are common for fundamental characterization studies and may also result from P2 and P3 scribes during module fabrication. Many reductive metals (e.g., Al, Yb, or Cr) and even some noble metals (e.g., Ag) spontaneously corrode in direct contact with lead halide perovskites.[584] Identical corrosion behavior at metal/PbI_2 (lacking MA and, therefore, HI) interfaces reveals the reduction potential of $Pb^{II} + 2e \rightarrow Pb^0$ as the main driving force [Fig. 38(a)].[584] The abundance of mobile halide anions determine the Nerstian potentials and facilitate the Pb^{II} redox driven corrosion. Oxidation of other more stable noble metals (e.g., Au) contacted to perovskites is not thermodynamically favorable (i.e., spontaneous); however, application of a small voltage (0.8 V) is sufficient to anodically oxidize Au in solid-state perovskite devices.[585] This result establishes anodic voltage limits for Au as well as elucidates a subtle general design rule for perovskites: metals should be more stable as cathodes instead of anodes motivating a need to increase p-i-n efficiencies to those of n-i-p. Spontaneity of and low electrochemical thresholds to reactions at perovskite/metal interfaces require the perovskite always be buffered from a metal electrode by an inorganic or organic material and careful examination of corrosion mechanisms at such buffered interfaces.

The main effect of buffering this interface [shown in Fig. 38(b)] is to impede iodide conduction causing an "open" in the electrochemical circuit while maintaining electronic conduction. Indeed, the spontaneous reaction between Al and $MAPbI_3$ is strongly suppressed by organic buffer layers that poorly conduct ions[584] but does not completely eliminate corrosion under all conditions. As depicted in Fig. 38(b), interface reactivity with the ETL or HTL can degrade MHPs, releasing neutral HI and/or I_2 to overcome low ion conductance.[396] Metal corrosion at ETL or HTL buffered interfaces typically originates from slight degradation of the perovskite active layer generating mobile corrosive species; however, perovskite degradation itself is extremely undesireable and potentially detrimental to device performance. It is therefore critical to understand and prevent interface reactivity between MHPs and metal oxide or organic transport layers. Furthermore, environmental conditions, such as humidity and temperature, may also play a role on the metal corrosion by enhancing ion diffusion and migration.[584] Minimizing detrimental reactions at all interfaces within an MHP device should simultaneously limit the rate of metal corrosion in most high performance device architectures.

Coinciding mobile ions and electrical connections enable electrochemical corrosion mechanisms, where reduction and oxidation can occur very far apart spatially. Electrochemical circuits can be formed within or across perovskite devices, as shown in Fig. 39(a), allowing corrosion to proceed uninhibited. This manifests when the mobility of iodide is increased by exposure to H_2O or alcohol vapor (ion conductance increases by many orders of magnitude for even small levels of H_2O).[586] Corrosion in this geometry is again observed when $MAPbI_3$ is replaced by PbI_2, precluding an HI intermediate. Importantly, Fig. 39(a) differs from Fig. 38(b) in that *neither I_2 nor HI intermediates are needed.* Thus, understanding

© Author(s) 2021

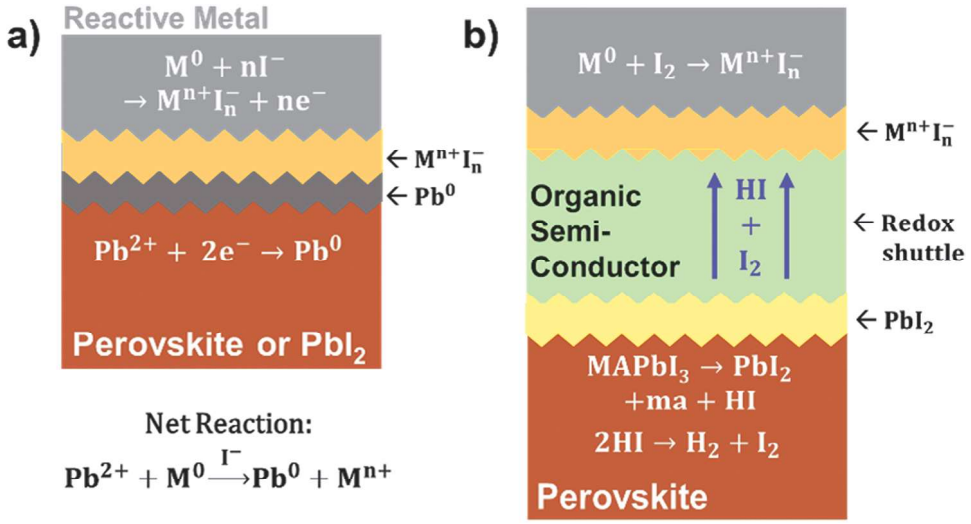


FIG. 38. Reduction/oxidation (redox) mechanisms for metal electrode (M) corrosion in (a) direct contact with a perovskite, such as $MAPbI_3$, and (b) buffered by an organic semiconductor, where ma is methylamine (CH_3NH_2) and MA is methylammonium ($CH_3NH_3^+$). In the latter, oxidation of M is enabled by acid–base or redox reactions releasing I_2, forming a type of redox shuttle.

iodine/triiodide/iodide speciation and mass transport within various layers of a device, beyond currently available "ion migration" models, is critical to identify correct corrosion mechanisms, but a knowledge gap limits the development of efficient mitigation strategies.

Electrochemical corrosion over macroscopic distances can be observed in typical perovskite devices, as shown in Fig. 39(b) for a device degraded in atmosphere in the dark with 30%–50% relative humidity. Moisture increases the ion mobility, allowing Pb^{II} to react even when it is far from the Al^0 electrode but *only where perovskite is connected to Al by ITO*. Electronically isolated regions of perovskite on glass, despite the same distance to the Al, do not react. This observation exemplifies a consequence of spatially separated electrochemical corrosion facilitated by electrical connection over the device area. Similar parasitic electrochemical "circuits" may unintentionally be built into perovskite modules that contain many

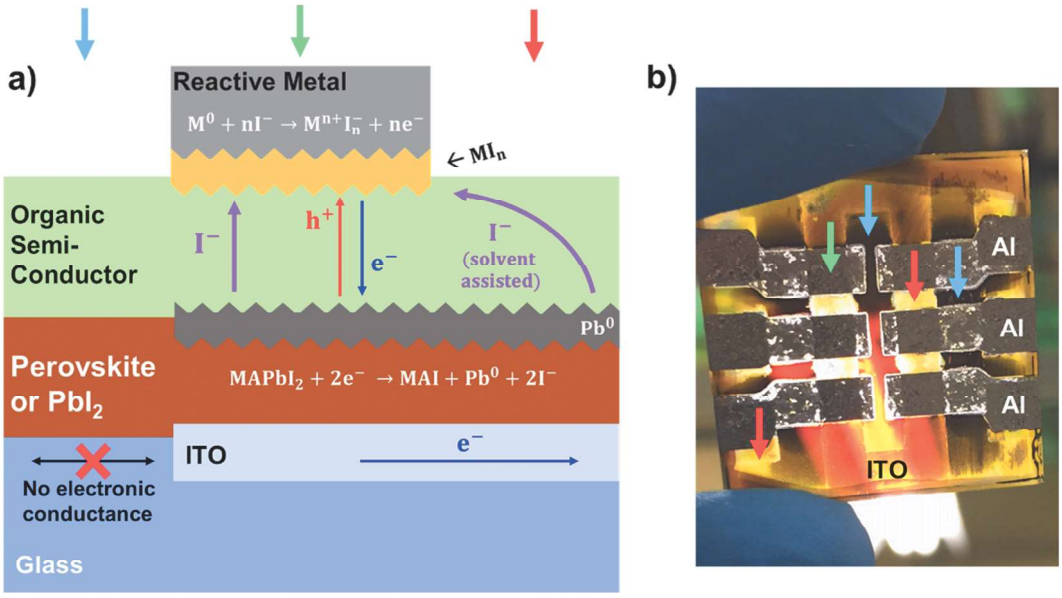


FIG. 39. (a) Mechanism of electrochemical corrosion showing how electrical conduction can facilitate redox over very long distances. (b) Photograph of a device with Al contacts degraded in the dark in atmosphere. The substrate dimensions are 1 × 1 $in.^2$, and pixel areas are ~0.12 cm^2. The colored arrows point to the indicated regions in (a), highlighting perovskite reacting with the ITO (red arrow) despite being macroscopic distances from the Al, as well as the opposite behavior for glass regions that are electronically isolated from the Al.

© Author(s) 2021

and varied interconnects. In addition, such interconnects in modules tend to be over short distances to minimize "dead" regions of the module area, meaning ions need not travel very long distances to close these "circuits."

3. Advances in science and engineering to meet these challenges

The above discussions summarize the state-of-the-art understanding of the why and how of corrosion mechanisms in halide perovskite devices, which provide insight into how to inform mitigation strategies. One approach to slow corrosion is to cut off halide or halogen conductance through at least one layer in the device. This requisite eliminates many semiconducting organic molecules and polymers, since these materials are relatively easily doped by counter ions creating an electrolyte *in situ*.[587] Metal oxides and 2D materials (e.g., graphene) are denser and less permeable to ions than organic materials and significantly slow metal electrode corrosion.[588,589]

Metal oxides have been widely employed in perovskite solar cells. Unfortunately, perovskites are reactive toward metal oxides when in direct contact (typically via the methylammonium or formamidinium protons).[588] Although these reactions are, in general, not as rapid as those with metal contacts (e.g., rapid Al contact corrosion[584]), they may trigger fabrication or long-term instability issues, and as noted above, products released from interfacial reactions enable metal corrosion to compound degradation effects. Reactions at MHP/oxide interfaces can be suppressed by surface treatments,[588] omitting the more acidic MA cation[590] or buffering the interface with an organic layer.[591] Optimizing MHP/organic/oxide/metal stacks is complicated by extra material interactions, making it difficult to provide general design rules. For example, MoO_x/Al improves device stability relative to MoO_x/Au by blocking mobile halides,[591] but the spiro-OMeTAD/MoO_x bilayers are morphologically unstable under operating conditions leading to catastrophic failure. The MoO_x instability was overcome by employing a different organic and replacing MoO_x with VO_x.[592] Developing and characterizing ion blocking composite electrodes that are stable under stressful operating conditions represents a major challenge to the perovskite technology. Direct deposition of oxides on the MHP omitting the organic buffer without damaging the interface properties is challenging yet would enable new and more stable device architectures. It is worth mentioning that an ion impermeable oxide may require an amorphous morphology; grain and domain boundaries in dense polycrystalline films enable ion pipe diffusion.[593] The ability to coat perovskites with an amorphous conformal metal oxide would open many new processing techniques, providing researchers with new architectures to potentially eliminate this degradation pathway altogether.

Unlike metals and metal oxides, carbon-based materials, such as graphene, are more chemically inert and have been shown to be efficient in iodine/iodide blocking.[589] This strategy represents a potential path to mitigate metal contact corrosion and warrants more attention. In fact, developing carbon-based electrodes to substitute metals may eventually resolve corrosion concerns, provided reactivity at other interfaces is managed, allowing for stable MHP LEDs, solar cells, and modules.

In addition to new architectures, technological progress would be accelerated by high throughput, quantitative, and predictive characterization techniques for device components. Deducing exact degradation mechanisms, such as that of spiro-OMeTAD/MoO_x, from post-mortem characterization of aged perovskite devices requires an immense amount of time and effort. Several hundreds of hours are needed simply to age the devices, the amount of reaction products is typically below detection limits of widely available techniques, and kinetic parameters are rarely quantifiable. Fortunately, mechanistic insight permits studies on model devices and simplified testing platforms of individual device components that address a particular degradation pathway. This type of methodology is exemplified by an Ag:I_2 corrosion test, an adaptation of the Ca:H_2O test that allows quantification of permeation rates of iodine species through common organic buffer layers, organic/oxide composites, and many other barrier layers that can be incorporated into models to predict improvements to device stability.[587] The Ca:H_2O test contributes substantially to Si technology development by testing water transmission rates without needing to fabricate and test full modules. More and similar quantitative techniques should be developed for perovskites to divide and share the workload and expedite stability improvements.

4. Concluding remarks

In summary, the reactivity of halide perovskites directly contributes to corrosion of metals used in devices and modules; the latter has numerous interfaces and interconnects to consider. Many mechanisms can work in concert to drive corrosion, and several of them are discussed here to provide guidance toward mitigation approaches. Perovskite technology would greatly benefit from new architectures afforded by the ability to process iodide/I_2 blocking, chemically inert, and conformal layers, such as amorphous metal oxides and carbon-based materials, that effectively protect metals from corrosion, yet it will not solve every nuance. In parallel, developing specialized measurement techniques that quantify parameters, such as ion permeability, and models incorporating these parameters to predict device and module stability will better align halide perovskites with the status of mature technologies such as Si as well as establish new testing and quality control protocols that are required for scale-up and commercialization.

F. Replacement of toxic lead

Nadja Glück, Thomas Bein

1. Status of the area

The stability concerns regarding lead-based perovskites not only pose challenges for the production of efficient and stable solar cells but also raise concerns about the heavy metal lead in the system. Thus, the toxicity of lead is a significant roadblock for the commercialization of the somewhat soluble perovskite materials in solar cells. The lead salts are harmful to humans if swallowed or inhaled. In particular, the lead-based hazards are attributed to the binding affinity of lead to thiol and cellular phosphate groups of numerous enzymes, proteins, and cell membranes. Therefore, the exposure to lead presents health risks for blood, kidneys, liver, testes, brain, and nervous system. These toxicity concerns have strongly motivated research into strategies for the replacement of lead by other central metals.[594]

© Author(s) 2021

Besides the low toxicity, the perovskite absorber replacement requires comparable physical properties achieved with lead. Hence, the following properties are mainly pursued: high defect tolerance, low exciton binding energy, long diffusion length, relatively week charge-carrier-phonon coupling, high conductivity, and high charge-carrier mobility.[595]

2. Current and future challenges

In the quest to replace lead, the main goal is to find a material with similar physical properties (mentioned above) as the lead-based perovskites and eliminate their drawbacks. Hence, three main challenges arise, i.e., retaining the superior absorber properties and solution processability while achieving environmental stability.

Achieving absorber-layer characteristics similar to those of lead-based perovskite materials without the central metal lead is probably the most challenging goal. The most prominent approach so far has been to replace lead with a metal cation crystallizing in a comparable perovskite crystal structure. The high symmetry and the high electronic dimensionality in the lead-based perovskite structure have, among others, a significant impact on the physical properties of the lead-based absorber layers. Thus, investigations focus on finding lead-free combinations with crystal structures related to the perovskite structure, resulting in various combinations of central metal ions all over the Periodic Table. To date, research on replacing lead has focused on the metal ions tin, germanium, copper, bismuth, antimony, gold, titanium, and palladium. All of these central metal cations can feature (near) octahedral coordination with halides or chalcogenides and a crystal structure built of corner-sharing octahedral building blocks as in the lead-based perovskites. In Fig. 40, the crystal structures of the most prominent lead-free systems are schematically illustrated. So far, only tin- and germanium-based compounds strongly resemble the 3D network of lead-halide perovskites, which also correlates with their comparable physical properties. However, they tend to be much less stable. Higher environmental stability but less preferable physical properties are achieved with the 3D "double perovskites" built by alternating monovalent and trivalent metal halide octahedral networks. Many other cation–halide combinations crystallize in perovskite-like systems with reduced dimensionality limiting their physical properties, e.g., Ruddlesden–Popper phases and "defect-ordered" or "vacancy-ordered" structures. On the other hand, many of these latter compounds are fairly stable at ambient conditions.[595,596]

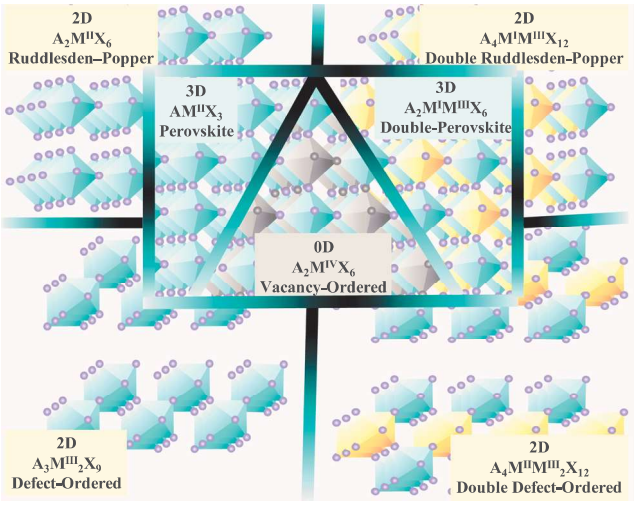


FIG. 40. Schematic illustration of the lead-free structure types related to the perovskite motif. Blue octahedra represent the $M(II)X_6$ or $M(IV)X_6$ metal halide-networks in systems with one central metal cation. In the double perovskite structures, the blue octahedra represent $M(III)X_6$ and the octahedra built from lower oxidation state metal cations are shown in yellow. The voids in the vacancy-ordered structure are indicated in gray.

Even though the solution processibility of the lead-based perovskites is one of the reasons for their instability issues, it is also viewed as one of the main advantages for their application in various optoelectronics. Moreover, in addition to the facile fabrication of lead-based perovskites from solution, the emerging narrow bandgap polycrystalline thin films show superior defect chemistry, resulting mostly in the formation of shallow traps. In the investigation of lead-free replacements, solution processibility is, therefore, an essential requirement. As a result, the focus has been mainly on compounds with more ionic bonding nature, such as halides, instead of the more covalent bonding observed with chalcogenides. However, the defect chemistry of the resulting polycrystalline thin-films is still challenging for most of these compounds.

It is still an open—and exciting—question if perovskite-like compounds can be found featuring optoelectronic characteristics as superior as those of the lead halide perovskites. The third essential requirement for lead-free absorbers is to be more stable than the hybrid perovskites, including the stability against illumination, moisture, air, or elevated temperatures. With the lead-free compounds, the stability depends to a largely on the nature and oxidation state of the central metal cations.[596]

3. Advances in science and engineering to meet these challenges

Replacing lead with elements of the same group in the Periodic Table like tin or germanium results in compounds similar to the 3D perovskite structures with direct and narrow bandgaps, strong absorption, low exciton binding energies, inefficient electron–phonon coupling, high conductivity, and high charge carrier mobility. However, both central divalent metal ions are prone to oxidation, limiting the efficiency of tin-based devices to presently 14% and mostly preventing the application of germanium in devices. Therefore, tin- and germanium-based absorbers suffer severely from degradation and the impact of defects, but recently their stabilization via surface passivation using various organic additives has been demonstrated.[597]

The divalent metal cations, tin, germanium, and copper, can also form Ruddlesden–Popper phases, which are more environmentally stable than the 3D tin- and germanium-based compounds due to the large organic cations separating the octahedral sheets. With the decreased dimensionality in the tin- and germanium-based materials, the bandgap broadens and the charge carrier transport is compromised. Copper-based 2D compounds similarly suffer from low conductivity and feature weaker optical absorption.

Another approach aimed at more stable compounds is to combine a trivalent and a monovalent instead of two divalent metal cations, resulting in double perovskite structures. The most investigated compound is $Cs_2AgBiBr_6$, showing high stability

© Author(s) 2021

toward moisture, air, high temperatures, and illumination. Here, the materials' limitation lies in the indirect nature of the bandgap of around 2 eV, large trap-density, high excitonic binding energy, and strong electron–phonon coupling, limiting the photovoltaic efficiency so far to below 3%. However, a wide variety of double perovskite combinations remains unexplored, such as pure gold-based double perovskites. The gold-based compounds feature favorable light-absorbing properties with bandgaps below 2 eV, but challenges regarding thin film synthesis so far have hindered device fabrication.[598,599]

Employing only trivalent metal ions, such as bismuth or antimony, can result in compounds with direct bandgaps of around 2 eV and strong optical absorption. Their higher ionic charge compared to the divalent lead ions leads to vacancy formation in the perovskite-like structures with resulting "2D" defect-ordered building blocks. Most narrow bandgap materials containing iodide as the anion and methylammonium or cesium as the second cation thermodynamically prefer to form "0D" polymorphs with isolated metal halide moieties in the lattice. Thus, to create the corresponding 2D compounds, the synthesis procedure needs to be adapted to trap the desired phases. Once the 2D polymorph is formed, the resulting absorber, inorganic or hybrid, is stable in air at relatively high temperatures and resistant toward moisture. Photovoltaic devices using these absorber layers already show efficiencies exceeding 3%. The limited performance stems from high excitonic binding energies, strong electron–phonon coupling, and significant structural disorder leading to deep traps. However, an increase in dimensionality with the addition of a divalent metal cation like copper can modify the physical properties by forming a double defect-ordered structure such that the direct bandgap reduces to 1 eV.[596,600] With tetravalent metal cations, such as tin, titanium, or palladium, perovskite-like vacancy-ordered 0D structures form with metal halide octahedra isolated by octahedral voids in each neighboring position. All of these perovskite defect structures, regardless of the nature of the central metal cation, feature certain defect tolerance and show good stability toward illumination, humidity, and heat. The inorganic Cs_2SnI_6 also resembles the divalent tin compound in its physical properties with a highly symmetric cubic structure, strong absorption, and high carrier mobility. The direct bandgaps of tin-based compounds and the indirect bandgaps of titanium- or palladium-based compounds are narrow with values typically below 1.7 eV, and titanium-based devices with photovoltaic efficiencies of over 3% have been reported. So far, the main limitations for these compounds are the poor film quality and severe charge recombination.[596,601]

4. Concluding remarks

The possibilities to replace lead in related halide perovskite-like structures are numerous. However, with the lead-free compounds investigated to date, the fabrication of high-quality thin films appears to be more challenging, and therefore, the full potential of the absorbers in optoelectronic devices remains an open question. So far, research on lead-free materials is still at the stage of fundamental studies and early development and requires significant optimization of the materials' quality and enhanced mechanistic understanding of charge carrier dynamics and of film deposition methods. However, the prospect of replacing toxic lead and the already established high stability of many lead-free halide perovskite-like materials present a strong motivation for future research in this exciting field.

G. Perovskite solar modules: Progress, challenges, and future applications

Fabio Matteocci, Luigi Angelo Castriotta, Aldo Di Carlo

1. State of the art

Among the third-generation photovoltaic technology, the perovskite solar cell demonstrates an impressive growth in the last few years as emergent thin film photovoltaic technology reaching outstanding results in terms of power conversion efficiency (PCE). The scaling up became rapidly a hot topic in the PSC field with the aim to demonstrate the feasibility of the manufacturing process and its further exploitation at the industrial scale.

The first evaluation of the scaling up processing in PSC have been demonstrated in 2014 showing the first perovskite solar module (PSM) made by the monolithic interconnection of individual cells in series configuration.[602] From the beginning, two main topics appeared crucial for the demonstration of an efficient scaling up: the scalability of the deposition of the constituent layers forming the device stack[603–605] [Fig. 41(a)] and the design of the monolithic interconnections[606–608] [Fig. 41(b)].

Important efforts have been made on the evaluation of scalable deposition techniques able to guarantee excellent uniformity of the perovskite layer.[609] In particular, solution processing techniques attracted huge interest, thanks to the high throughput and cost-effective manufacturing steps.[610,611] Nowadays, blade coating,[603,612] spray coating,[613,614] and inkjet and slot die coating[615,616] emerged as suitable techniques for the PSM manufacturing replacing the spin coating generally used for laboratory cells. Very recently, together with a perovskite leader company in the sector (Saule Technologies), Castriotta *et al.* were able to fabricate modules on the flexible substrate, which is one of the advantages of this technology as a thin film material that can be fabricated over any rigid or flexible conductive film, using methylammonium-free perovskite and N_2-assisted blade coating, reaching efficiency over 10.5% over 16 cm^2.[617] Furthermore, huge efforts have been made on the development of flexible PSM fabricated via roll-to-roll processing at low temperature.[618] Crucial needs are represented from the development of customized perovskite inks with the aim to deposit a uniform and pin-hole free perovskite layer with excellent optoelectronic properties.[619,620] A further crucial topic in PSM is the interconnection design where a laser assisted ablation process called P1–P2–P3 is performed during the manufacturing flow. The P1 and P3 ablations guarantee the electrical insulation of the constituent cells forming the PSM, and the P2 ablation is optimized to remove the device stack at the interconnections to minimize the contact resistance between cells. The optimization of the laser parameters (laser fluence, processing speed, and pulse duration) plays a crucial role in P1–P2–P3 process. In the literature, important achievements have been demonstrated regarding the reduction of the area destined to the PSM interconnections reaching an aspect ratio (also called geometrical fill factor) up to 95%.[608] Up until now, the improving research efforts

© Author(s) 2021

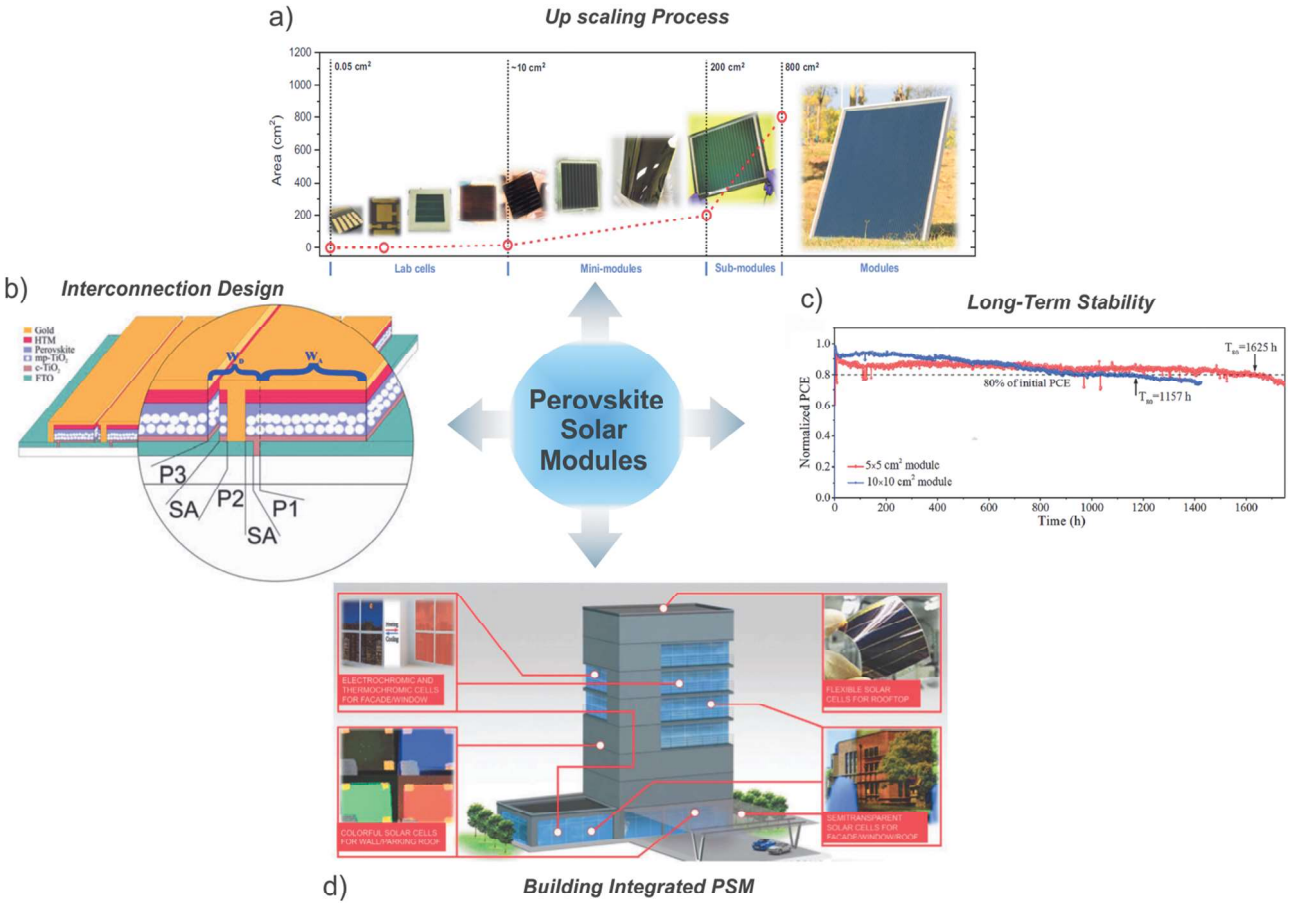


FIG. 41. Current and future challenges in perovskite solar modules (PSMs): (a) Up-scaling progress of PSM. Reproduced with permission from Hu *et al.*, Joule **3**, 2076 (2019). Copyright 2019 Elsevier. (b) Interconnection design. Reproduced with permission from Palma *et al.*, IEEE J. Photovoltaics **7**, 1674 (2017). Copyright 2017 IEEE.[608] (c) Long-Term stability of PSM, reproduced with permission Tong *et al.*, Adv. Energy Mater. **11**, 2003712 (2021). Copyright 2021 John Wiley and Sons.[629] (d) Building integrated PSM, reproduced with permission from Batmunkh *et al.*, Adv. Mater. **32**, 2000631 (2020). Copyright 2020 John Wiley and Sons.

from Academics and Research Institutes carried out outstanding results reaching PCE close to 19% for PSM with active areas in the range of 10–100 cm^2.[621] 19 Further efforts have been demonstrated from industrial players (Toshiba, Microquanta, UtmoLight, Panasonic) pushing up the record PCE to 17.9% on 800 cm^2-sized PSM (Panasonic).[622]

2. Current and future challenges

Nowadays, the current challenges in PSM manufacturing are mainly related to the deposition of the perovskite layer concerning its deposition technique and the ink formulation. Furthermore, the design of the interconnections and the long-term stability are extremely needed to bring PSM in the market.[623] The choice of ABX_3 perovskite composition and the deposition of a defect-free thin film are crucial optimization steps for PSM in order to prevent phase segregation and current mismatch between the series connected cells.[624]

Although the use of the solvent quenching method by spin coating limits the formation of δ-phases during perovskite growth, it is not a suitable method for the up-scaling process in PSM. To address this issue, the scientific community is moving to alternative approaches to get stable α-phases.[259,625] Regarding the perovskite composition, the methylammonium-free perovskite seems to be a robust perovskite layer and more intrinsically stable than any other counterpart containing methylammonium (MA). MA has been shown to be a volatile organic compound, easily to degas when treated under thermal stress for prolonged time.[626] A further interesting topic is the fabrication of the entire device stack in the controlled air environment (temperature and moisture level) without working in the N_2/Ar filled glovebox that increase manufacturing and maintenance costs. It is important to choose also stable transport layers, avoiding using the doped layer that over time might diffuse into perovskite and accelerate degradation.[627] Long-term stability in PSM is a challenging topic not so investigated from the scientific community. In fact, only few reports demonstrated the development of efficient and stable PSM measured under working conditions[628–630] [Fig. 41(c)]. Further degradation paths are present in PSM due to the presence of monolithic interconnections.[631] Important topic referred to the PSM stability is also the impact of reverse bias due to the partial shading of the constituent cells in PSM. In

© Author(s) 2021

particular, the use of by-pass diodes can inhibit Joule heating and irreversible chemical reaction activated from the reverse bias condition.[632] Challenging issues come from the requirement of certified measurements and characterization techniques in order to further exploit the potential of PSM. In particular, non-disruptive characterization techniques, like dark-lock-in thermography (DLIT), PL/EL mapping, and light beam induced current (LBIC), are useful to detect defects in the aperture area of the PSM and correlate them to the degradation factors. The goal is the achievement of intrinsic and extrinsic long-term stabilities opening the way to the exploitation of PSM at high Technology Readiness Levels (TRLs) in industrial relevant environments. Future challenges are the evaluation of strategies for lead trapping where cation-exchange resins (CERs) have been used to prevent the lead leakage induced from the damaged PSM. The CERs can effectively work as the lead absorbing layer when deposited on the surface of the metal electrode.[633] In parallel, the development of lead-free perovskite composition can relax the constraints referred to the use of lead in PSM. Further investigations on life cycle assessment (LCA), end-life recycling, and re-use can assist the industrialization process toward more environmentally and economically competitive PSMs.[634] From the application point of view, PSM technology could be applied in the field of Building Integrated Photovoltaics for the development of PV façades and/or building elements for Nearly-zero Energy Building [Fig. 41(d)]. In this field, the development of visible semi-transparent PSM can match the requirement in terms of conversion efficiency and average visible transmittance needed for the integration in building facades.[635,636] Several actions are required to guarantee the high PCE and average visible transmittance (AVT) value obtained from the device stack, such as the development of visible transparent electrodes, the reduction of the parasitic absorbance introduced by the constituent layers, and the optimization of the composition of wider bandgap perovskites.

3. Concluding remarks

The future of perovskite solar technology is moving to the industrialization with many companies interested to its application in the stock market (Hunt Technologies, Perovskia, Evolar, Oxford PV, Toshiba, Panasonic, Saule Technologies, etc.) Perovskite thin film PV technology has huge opportunities to be exploited as third generation PV technology due to the tunable bandgap, the growth on rigid and flexible substrate, and the low manufacturing cost. These peculiar features allow the application on building integrated photovoltaics field and the production of tandem architectures together with well-established technologies, such as Silicon and CIGS. Although the up-scaling process is deeply investigated for the development of highly efficient PSM, some concerns are referred to the lack of long-term stability results under outdoor working conditions. Further achievements are expected on the research of encapsulation procedures of the PSM in order to discard the role of extrinsic degradation factors affecting the stability of the device stack and the interconnection. Results on LCA investigation and end-life recycling tests have to be carefully considered for the evaluation of the environmental impact of the PSM production and application. The application of PSMs in Building Integrated Photovoltaics and/or Agrivoltaics appears very interesting for future developments moving toward the reduction of the land use from terrestrial PV application.

H. Data-driven prediction of novel hybrid perovskites

Claudia Draxl and Matthias Scheffler

1. Status of the area

Traditionally, finding and testing materials with desired properties is often guided by experience, intuition, and possibly prejudice, involving a significant amount of trial and error. This approach cannot meet the increasing demand of our society for advanced materials. As a consequence, high-throughput screening (HTS) studies (see https://mgi.gov/) have become a popular way of enhancing materials research, also boosted by the Materials Genome Initiative of the White House.[638] The resulting HTS computations and experiments create huge data collections in the USA and all over the world.

Although HTS provides much information, it will never cover the vast chemical and structural space of possible materials. Let us recall that their number is practically infinite, and even among the known materials, the knowledge about their properties is very shallow. Thus, it is likely that the best candidate for a given application has neither been synthesized to date nor will it be identified by HTS. Artificial Intelligence (AI) is expected to enhance our (future) research to go beyond current capabilities. Indeed, Big-Data and AI revolutionize many areas of our life already, establishing the fourth paradigm of research.[639] This naturally also applies to materials science, with the ambitious aims of predicting trends and outliers in the wide materials space, based on advanced machine-learning (ML) and AI tools.

Data-driven materials discovery involves several key aspects. They concern (i) data acquisition by HTS experiments and computations, (ii) the establishment of a proper FAIR data infrastructure (FAIR stands for Findable, Accessible, Interoperable, Reusable[640]), and (iii) the development of powerful data-driven algorithms and tools. To be successful, this requires a most synergistic interplay between experiment, theory and computation, data-analytics, and computer science.

Obviously, data-driven approaches hold also great promise for the field of metal halide perovskites. Several experimental (e.g., 2D,[641] CBiM[63,195]) and theoretical (e.g., HybriD3)[642–644] HT initiatives aim at establishing large data collections. Several others are still being in their development phase or not open to the public. Based on the respective data, various ML approaches have been used to predict bandgaps and[645] perovskite phases[56,64,143] or to determine descriptors for their stability[5,56] and for bandgaps.[646] In view of the metal halide perovskite complexity, a true breakthrough in predicting a yet unknown candidate material with the desired properties nevertheless remains a huge challenge.

2. Current and future challenges

What are the bottlenecks in predicting novel materials? What makes the description and prediction of metal halide perovskites specifically demanding?

Starting with data acquisition, significant HT synthesis efforts for this class of materials aim at obtaining stable compounds by compositional engineering. The complexity of the materials, however, may hamper fast progress as screening of all suitable chemical compositions may appear hopeless, and even if big data are created, success by machine learning is not guaranteed. Note that the

© Author(s) 2021

concept of ML is to fit data, also employing a regularization. The line between achieving a good fit and a generalizable model is very narrow. Thus, one largely remains at the level of interpolation. Materials with exceptional performance may be missed if they are not represented well in the employed data already. Thus, more efficient strategies need to be found, involving advanced AI techniques. Until now, a significant amount of consistent materials data is needed for reliable predictions. Ideally, the data collection should cover the breadth of the chemical space to an as large as possible extent to capture the intricacies of this materials class. In any case, data-quality assurance is key not only for our understanding but also for the consistency of data in view of any machine-learning application. This, in turn, requires control over all parameters that impact the materials properties. For the challenges related to this, we refer to Secs. II and VI B.

From the theory point of view, the accurate description of metal halide perovskites is highly demanding. Pronounced many-body effects, significant spin–orbit coupling, and strong interaction of charge carriers with lattice vibrations[128,136] require the methodology beyond standard density-functional theory (DFT), even for structural properties.[136] As an example, a critical review of literature results and in-depth analysis of the bandgaps of metal halide perovskites and their inorganic precursors (see Ref. 647 and references therein) reveal that a fully quantitative description of metal halide perovskites from first principles is not yet in place. As such, large-scale data acquisition from high-level first-principles methods will remain an open issue.

The uncertainties related to data quality, for both experimental and theoretical results, provoke the questions how *FAIR* metal halide perovskites data are. Even if open databases enable the F, A, and R, the issue of interoperability is critical. It concerns, in particular, the challenge of fully annotating the research data, be it from synthesis, experimental characterization, or computational results.[648] Interoperability will finally be decisive for the success of AI when bringing together data from different sources. For the ultimate success of AI,[649] however, not only data quality is crucial. A critical role will be on identifying the relevant set of descriptive parameters that characterize the material and the key physical processes,[650] be it for addressing stability or structural properties but even more so for the various key characteristics of high-performance solar cells.

3. Progress

Indeed, the challenges are enormous. However, one may ask what level of accuracy and detail is needed for what kind of prediction? Is it trends or precise numbers? Indeed, errors of low-cost methods may be sufficiently systematic to allow for identifying trends and narrowing down the search space for deeper analysis. Most important are consistent datasets, even, e.g., if not highest-level methodology is used or if simplifying assumptions must be made or certain parameters are not addressed directly when devising a model. An example for the former concerns bandgaps that are heavily underestimated by most DFT functionals. However, for a given functional, the errors can be considered systematic when staying within a class of materials like the metal halide perovskites. For the latter, simplifications concern, for instance, the neglect of vibrational effects on the structure and physical properties[645] or the existence of local minima[646] in the energy landscape despite the sensitivity of structure and properties to the starting configuration. Obviously, such "low-level trends" will fail, when the mechanism that is ignored in the modeling changes significantly across the data space. This may be often unlikely but it cannot be ruled out.

A particular focus of recent ML efforts is placed on structure prediction. With the aim of covering the full range of inorganic perovskites, Filip and Giustino[143] predicted the existence of 90 000 unknown perovskites by revisiting the model proposed by Goldschmidt.[2] For this huge set of candidate materials, verification by DFT calculations and characterization in terms of their properties is still lacking. Bartel and co-workers[5] introduced an improved tolerance factor (enhancing the reliability from about 75% to 92%) for predicting the stability of perovskite oxides and halides and identified 23 new double perovskites.

Concerning physical properties, most machine-learning efforts for so far have addressed bandgaps, e.g., of inorganic double perovskites[651] or, more recently, of metal halide perovskites.[54] Hardly anything is available, however, on most application-relevant quantities, be it light–matter coupling, charge-carrier mobilities, open-circuit voltage, or other device characteristics. One limiting factor here is that computations are restricted to relatively small structures that may be far from realistic systems. In addition, typical studies do not capture real conditions, such as temperature and environment. This appears critical as the temperature significantly impacts bandgaps, effective masses, and Rashba coupling,[645] and structural fluctuations and thermal disorder play a crucial role.[136] In addition, although metal halide perovskites represent a very active field in first-principles research, in particular, studies of their optical excitations are still largely geared toward understanding their properties by single investigations.

4. Concluding remarks

Presently, researchers are performing not-fully controlled approximate computations, i.e., neglecting certain effects. These quantitatively not very accurate results may well reproduce important trends as demonstrated by existing studies. Identifying such trends may be enhanced by ML methods. More systematic high-level calculations would help to remedy the risks of failure. It may, however, well be that the complexity and intricacy are so high that modeling metal halide perovskite properties and performance from first principles is not a realistic goal. Here, AI may provide the necessary bridge to connect theoretical data of free atoms as well as structure and elastic properties of metal halide perovskites with high-quality experimental data of the properties and functions of interest. This bridge could be a viable model that may be generalizable to not yet studied metal halide perovskites.

What about the predictive power of AI approaches that is needed to think out of the box? At the present stage, prediction of "THE" metal halide perovskite without the scientists' intuition is pretty unlikely due to a lack of data. Changing our scientific culture and publishing *all* data related to the investigated materials is just getting started. The metal halide perovskites appear to be on a good track in this respect.

ACKNOWLEDGMENTS

We thank the German Research Foundation for funding SPP2196 "Perovskite Semiconductors," a priority program in which many authors of this Roadmap participate.

© Author(s) 2021

L.H. acknowledges the Institute for Advanced Studies of the TU Munich (Grant No. TUM-IAS) for a Hans Fischer Senior Fellowship.

J.M. and M.T. acknowledge financial support from the DFG (Grant Nos. SFB 840 and Th 807/8-1) and the Bavarian Ministry of State for Science and Arts (Soltech).

J.R., D.N., and T.F. acknowledge funding from the Deutsche Forschungsgemeinschaft (DFG, German Research Foundation) (Project No. 395604916).

C.D. and M.S. acknowledge support for the NOMAD CoE from the European Union's Horizon 2020 research and innovation program under Grant Agreement No. 951786.

A.R. acknowledges financial support from the Luxembourg Fonds National de la Recherche, "SUNSPOT," No. Nr.11244141.

D.A.E. acknowledges financial support from the Alexander von Humboldt Foundation within the framework of the Sofja Kovalevskaja Award, endowed by the German Federal Ministry of Education and Research, and the Technical University of Munich—Institute for Advanced Study, funded by the German Excellence Initiative and the European Union Seventh Framework Programme under Grant Agreement No. 291763. D.M. is grateful to the Alexander von Humboldt Foundation for funding.

A.C. acknowledges financial support by the Deutsche Forschungsgemeinschaft within the framework of the Emmy Noether Program (Grant No. CH 1672/1).

DATA AVAILABILITY

Data sharing is not applicable to this article as no new data were created or analyzed in this study.

REFERENCES

[1]See https://www.nrel.gov/pv/cell-efficiency.html fot Best Research-Cell Efficiency Chart (NREL).
[2]V. M. Goldschmidt, Naturwissenschaften **14**, 477 (1926).
[3]M. Johnsson and P. Lemmens, J. Phys.: Condens. Matter **20**, 264001 (2008).
[4]W. Li, A. Stroppa, Z. Wang, and S. Gao, *Hybrid Organic–Inorganic Perovskites* (Wiley, 2020).
[5]C. J. Bartel, C. Sutton, B. R. Goldsmith, R. Ouyang, C. B. Musgrave, L. M. Ghiringhelli, and M. Scheffler, Sci. Adv. **5**, eaav0693 (2019).
[6]J. Zhang, X. Yang, H. Deng, K. Qiao, U. Farooq, M. Ishaq, F. Yi, H. Liu, J. Tang, and H. Song, Nano-Micro Lett. **9**, 36 (2017).
[7]E. Mosconi and F. De Angelis, ACS Energy Lett. **1**, 182 (2016).
[8]S. van Reenen, M. Kemerink, and H. J. Snaith, J. Phys. Chem. Lett. **6**, 3808 (2015).
[9]G. Richardson, S. E. J. O'Kane, R. G. Niemann, T. A. Peltola, J. M. Foster, P. J. Cameron, and A. B. Walker, Energy Environ. Sci. **9**, 1476 (2016).
[10]B. Saparov and D. B. Mitzi, Chem. Rev. **116**, 4558 (2016).
[11]W. Li, Z. Wang, F. Deschler, S. Gao, R. H. Friend, and A. K. Cheetham, Nat. Rev. Mater. **2**, 16099 (2017).
[12]B. Luo, F. Li, K. Xu, Y. Guo, Y. Liu, Z. Xia, and J. Z. Zhang, J. Mater. Chem. C **7**, 2781 (2019).
[13]G. E. Eperon and D. S. Ginger, ACS Energy Lett. **2**, 1190 (2017).
[14]N. Rybin, D. Ghosh, J. Tisdale, S. Shrestha, M. Yoho, D. Vo, J. Even, C. Katan, W. Nie, A. J. Neukirch, and S. Tretiak, Chem. Mater. **32**, 1854 (2020).
[15]J. Hieulle, X. Wang, C. Stecker, D.-Y. Son, L. Qiu, R. Ohmann, L. K. Ono, A. Mugarza, Y. Yan, and Y. Qi, J. Am. Chem. Soc. **141**, 3515 (2019).
[16]J. H. Noh, S. H. Im, J. H. Heo, T. N. Mandal, and S. I. Seok, Nano Lett. **13**, 1764 (2013).
[17]S. T. Williams, F. Zuo, C.-C. Chueh, C.-Y. Liao, P.-W. Liang, and A. K.-Y. Jen, ACS Nano **8**, 10640 (2014).
[18]S. D. Stranks, G. E. Eperon, G. Grancini, C. Menelaou, M. J. P. Alcocer, T. Leijtens, L. M. Herz, A. Petrozza, and H. J. Snaith, Science **342**, 341 (2013).
[19]F. Ünlü, E. Jung, J. Haddad, A. Kulkarni, S. Öz, H. Choi, T. Fischer, S. Chakraborty, T. Kirchartz, and S. Mathur, APL Mater. **8**, 070901 (2020).
[20]M. I. Saidaminov, O. F. Mohammed, and O. M. Bakr, ACS Energy Lett. **2**, 889 (2017).
[21]D. B. Mitzi, *Progress in Inorganic Chemistry* (John Wiley & Sons, Inc., 2007), pp. 1–121.
[22]G. Grancini, C. Roldán-Carmona, I. Zimmermann, E. Mosconi, X. Lee, D. Martineau, S. Narbey, F. Oswald, F. D. Angelis, M. Graetzel, and M. K. Nazeeruddin, Nat. Commun. **8**, 15684 (2017).
[23]M. Yuan, L. N. Quan, R. Comin, G. Walters, R. Sabatini, O. Voznyy, S. Hoogland, Y. Zhao, E. M. Beauregard, P. Kanjanaboos, Z. Lu, D. H. Kim, and E. H. Sargent, Nat. Nanotechnol. **11**, 872 (2016).
[24]Y. Ogomi, A. Morita, S. Tsukamoto, T. Saitho, N. Fujikawa, Q. Shen, T. Toyoda, K. Yoshino, S. S. Pandey, T. Ma, and S. Hayase, J. Phys. Chem. Lett. **5**, 1004 (2014).
[25]G. M. Kim, A. Ishii, S. Öz, and T. Miyasaka, Adv. Energy Mater. **10**, 1903299 (2020).
[26]K. Nishimura, M. A. Kamarudin, D. Hirotani, K. Hamada, Q. Shen, S. Iikubo, T. Minemoto, K. Yoshino, and S. Hayase, Nano Energy **74**, 104858 (2020).
[27]J. Navas, A. Sánchez-Coronilla, J. J. Gallardo, N. C. Hernández, J. C. Piñero, R. Alcántara, C. Fernández-Lorenzo, D. M. De los Santos, T. Aguilar, and J. Martín-Calleja, Nanoscale **7**, 6216 (2015).
[28]D. Pérez-del-Rey, D. Forgács, E. M. Hutter, T. J. Savenije, D. Nordlund, P. Schulz, J. J. Berry, M. Sessolo, and H. J. Bolink, Adv. Mater. **28**, 9839 (2016).
[29]Y. Hu, F. Bai, X. Liu, Q. Ji, X. Miao, T. Qiu, and S. Zhang, ACS Energy Lett. **2**, 2219 (2017).
[30]X. Ma, L. Yang, K. Lei, S. Zheng, C. Chen, and H. Song, Nano Energy **78**, 105354 (2020).
[31]Y. Zhou, J. Chen, O. M. Bakr, and H.-T. Sun, Chem. Mater. **30**, 6589 (2018).
[32]J. Mizusaki, K. Arai, and K. Fueki, Solid State Ionics **11**, 203 (1983).
[33]C. Eames, J. M. Frost, P. R. F. Barnes, B. C. O'Regan, A. Walsh, and M. S. Islam, Nat. Commun. **6**, 7497 (2015).
[34]Z. Xiao, Y. Yuan, Y. Shao, Q. Wang, Q. Dong, C. Bi, P. Sharma, A. Gruverman, and J. Huang, Nat. Mater. **14**, 193 (2014).
[35]D. Di Girolamo, N. Phung, F. U. Kosasih, F. Di Giacomo, F. Matteocci, J. A. Smith, M. A. Flatken, H. Köbler, S. H. T. Cruz, A. Mattoni, L. Cinà, B. Rech, A. Latini, G. Divitini, C. Ducati, A. Di Carlo, D. Dini, and A. Abate, Adv. Energy Mater. **10**, 2000310 (2020).
[36]J. Cho and P. V. Kamat, Chem. Mater. **32**, 6206 (2020).
[37]Y. Rong, Y. Hu, A. Mei, H. Tan, M. I. Saidaminov, S. I. Seok, M. D. McGehee, E. H. Sargent, and H. Han, Science **361**, eaat8235 (2018).
[38]T. Niu, J. Lu, R. Munir, J. Li, D. Barrit, X. Zhang, H. Hu, Z. Yang, A. Amassian, K. Zhao, and S. (Frank) Liu, Adv. Mater. **30**, 1706576 (2018).
[39]W. Xu, Q. Hu, S. Bai, C. Bao, Y. Miao, Z. Yuan, T. Borzda, A. J. Barker, E. Tyukalova, Z. Hu, M. Kawecki, H. Wang, Z. Yan, X. Liu, X. Shi, K. Uvdal, M. Fahlman, W. Zhang, M. Duchamp, J.-M. Liu, A. Petrozza, J. Wang, L.-M. Liu, W. Huang, and F. Gao, Nat. Photonics **13**, 418 (2019).
[40]R. Wang, J. Xue, K.-L. Wang, Z.-K. Wang, Y. Luo, D. Fenning, G. Xu, S. Nuryyeva, T. Huang, Y. Zhao, J. L. Yang, J. Zhu, M. Wang, S. Tan, I. Yavuz, K. N. Houk, and Y. Yang, Science **366**, 1509 (2019).
[41]A. Kogo, Y. Sanehira, Y. Numata, M. Ikegami, and T. Miyasaka, ACS Appl. Mater. Interfaces **10**(3), 2224–2229 (2018).
[42]Y. Zhang, S. Seo, S. Y. Lim, Y. Kim, S.-G. Kim, D.-K. Lee, S.-H. Lee, H. Shin, H. Cheong, and N.-G. Park, ACS Energy Lett. **5**(2), 360–366 (2020).
[43]Y. Zhang, G. Grancini, Y. Feng, A. M. Asiri, and M. K. Nazeeruddin, ACS Energy Lett. **2**(4), 802–806 (2017).
[44]J. J. Yoo, S. Wieghold, M. C. Sponseller, M. R. Chua, S. N. Bertram, N. T. P. Hartono, J. S. Tresback, E. C. Hansen, J.-P. Correa-Baena, V. Bulović, T. Buonassisi, S. S. Shin, and M. G. Bawendi, Energy Environ. Sci. **12**(7), 2192–2199 (2019).
[45]E. H. Jung, N. J. Jeon, E. Y. Park, C. S. Moon, T. J. Shin, T.-Y. Yang, J. H. Noh, and J. Seo, Nature **567**(7749), 511–515 (2019).

© Author(s) 2021

[46]M. Saliba, T. Matsui, J.-Y. Seo, K. Domanski, J.-P. Correa-Baena, M. K. Nazeeruddin, S. M. Zakeeruddin, W. Tress, A. Abate, A. Hagfeldt, and M. Grätzel, Energy Environ. Sci. **9**, 1989 (2016).
[47]M. Saliba, T. Matsui, K. Domanski, J.-Y. Seo, A. Ummadisingu, S. M. Zakeeruddin, J.-P. Correa-Baena, W. R. Tress, A. Abate, A. Hagfeldt, and M. Gratzel, Science **354**, 206 (2016).
[48]T. Bu, X. Liu, Y. Zhou, J. Yi, X. Huang, L. Luo, J. Xiao, Z. Ku, Y. Peng, F. Huang, Y.-B. Cheng, and J. Zhong, Energy Environ. Sci. **10**(12), 2509–2515 (2017).
[49]E. Jung, K. Budzinauskas, S. Öz, F. Ünlü, H. Kuhn, J. Wagner, D. Grabowski, B. Klingebiel, M. Cherasse, J. Dong, P. Aversa, P. Vivo, T. Kirchartz, T. Miyasaka, P. H. M. van Loosdrecht, L. Perfetti, and S. Mathur, ACS Energy Lett. **5**, 785 (2020).
[50]Y. Lin, Y. Bai, Y. Fang, Q. Wang, Y. Deng, and J. Huang, ACS Energy Lett. **2**, 1571 (2017).
[51]A. J. Knight and L. M. Herz, Energy Environ. Sci. **13**, 2024 (2020).
[52]D. Bi, C. Yi, J. Luo, J.-D. Décoppet, F. Zhang, S. M. Zakeeruddin, X. Li, A. Hagfeldt, and M. Grätzel, Nat. Energy **1**, 16142 (2016).
[53]L. Zuo, H. Guo, D. W. deQuilettes, S. Jariwala, N. D. Marco, S. Dong, R. DeBlock, D. S. Ginger, B. Dunn, M. Wang, and Y. Yang, Sci. Adv. **3**, e1700106 (2017).
[54]W. A. Saidi, W. Shadid, and I. E. Castelli, npj Comput. Mater. **6**, 36 (2020).
[55]J. Li, B. Pradhan, S. Gaur, and J. Thomas, Adv. Energy Mater. **9**, 1901891 (2019).
[56]Z. Li, Q. Xu, Q. Sun, Z. Hou, and W.-J. Yin, Adv. Funct. Mater. **29**, 1807280 (2019).
[57]I. E. Castelli, D. D. Landis, K. S. Thygesen, S. Dahl, I. Chorkendorff, T. F. Jaramillo, and K. W. Jacobsen, Energy Environ. Sci. **5**, 9034 (2012).
[58]I. E. Castelli, T. Olsen, S. Datta, D. D. Landis, S. Dahl, K. S. Thygesen, and K. W. Jacobsen, Energy Environ. Sci. **5**, 5814 (2012).
[59]W. Li, R. Jacobs, and D. Morgan, Comput. Mater. Sci. **150**, 454 (2018).
[60]Q. Tao, P. Xu, M. Li, and W. Lu, npj Comput. Mater. **7**, 23 (2021).
[61]K. Takahashi, L. Takahashi, I. Miyazato, and Y. Tanaka, ACS Photonics **5**, 771 (2018).
[62]X. Li, Y. Dan, R. Dong, Z. Cao, C. Niu, Y. Song, S. Li, and J. Hu, Appl. Sci. **9**, 5510 (2019).
[63]J. Kirman, A. Johnston, D. A. Kuntz, M. Askerka, Y. Gao, P. Todorović, D. Ma, G. G. Privé, and E. H. Sargent, Matter **2**, 938 (2020).
[64]N. T. P. Hartono, J. Thapa, A. Tiihonen, F. Oviedo, C. Batali, J. J. Yoo, Z. Liu, R. Li, D. F. Marrón, M. G. Bawendi, T. Buonassisi, and S. Sun, Nat. Commun. **11**, 5675 (2020).
[65]A. Extance, Nature **570**, 429 (2019).
[66]F. Corsini and G. Griffini, J. Phys.: Energy **2**, 031002 (2020).
[67]Z. Li, Y. Zhao, X. Wang, Y. Sun, Z. Zhao, Y. Li, H. Zhou, and Q. Chen, Joule **2**, 1559 (2018).
[68]Q. Zhang, S. T. Ha, X. Liu, T. C. Sum, and Q. Xiong, Nano Lett. **14**, 5995 (2014).
[69]G. Xing, N. Mathews, S. S. Lim, N. Yantara, X. Liu, D. Sabba, M. Grätzel, S. Mhaisalkar, and T. C. Sum, Nat. Mater. **13**, 476 (2014).
[70]S. P. Senanayak, M. Abdi-Jalebi, V. S. Kamboj, R. Carey, R. Shivanna, T. Tian, G. Schweicher, J. Wang, N. Giesbrecht, D. D. Nuzzo, H. E. Beere, P. Docampo, D. A. Ritchie, D. Fairen-Jimenez, R. H. Friend, and H. Sirringhaus, Sci. Adv. **6**, eaaz4948 (2020).
[71]J. Miao and F. Zhang, J. Mater. Chem. C **7**, 1741 (2019).
[72]C. Bao, J. Yang, W. Zhu, X. Zhou, H. Gao, F. Li, G. Fu, T. Yu, and Z. Zou, Chem. Commun. **51**, 15426 (2015).
[73]A. Nuraini and I. Oh, RSC Adv. **10**, 12982 (2020).
[74]X. Fu, S. Jiao, N. Dong, G. Lian, T. Zhao, S. Lv, Q. Wang, and D. Cui, RSC Adv. **8**, 390 (2018).
[75]S. Tao, I. Schmidt, G. Brocks, J. Jiang, I. Tranca, K. Meerholz, and S. Olthof, Nat. Commun. **10**, 2560 (2019).
[76]T. Umebayashi, K. Asai, T. Kondo, and A. Nakao, Phys. Rev. B **67**, 155405 (2003).
[77]J. Barrett, S. R. A. Bird, J. D. Donaldson, and J. Silver, J. Chem. Soc. A **1971**, 3105.
[78]D. Weber, Z. Naturforsch. B **33**, 1443 (1978).
[79]R. Prasanna, A. Gold-Parker, T. Leijtens, B. Conings, A. Babayigit, H.-G. Boyen, M. F. Toney, and M. D. McGehee, J. Am. Chem. Soc. **139**, 11117 (2017).
[80]A. Sadhanala, F. Deschler, T. H. Thomas, S. E. Dutton, K. C. Goedel, F. C. Hanusch, M. L. Lai, U. Steiner, T. Bein, P. Docampo, D. Cahen, and R. H. Friend, J. Phys. Chem. Lett. **5**, 2501 (2014).
[81]A. L. Abdelhady, M. I. Saidaminov, B. Murali, V. Adinolfi, O. Voznyy, K. Katsiev, E. Alarousu, R. Comin, I. Dursun, L. Sinatra, E. H. Sargent, O. F. Mohammed, and O. M. Bakr, J. Phys. Chem. Lett. **7**, 295 (2016).
[82]P. K. Nayak, M. Sendner, B. Wenger, Z. Wang, K. Sharma, A. J. Ramadan, R. Lovrinčić, A. Pucci, P. K. Madhu, and H. J. Snaith, J. Am. Chem. Soc. **140**, 574 (2018).
[83]M. A. Green, Y. Jiang, A. M. Soufiani, and A. Ho-Baillie, J. Phys. Chem. Lett. **6**, 4774 (2015).
[84]R. J. Elliott, Phys. Rev. **108**, 1384 (1957).
[85]M. Baranowski and P. Plochocka, Adv. Energy Mater. **10**, 1903659 (2020).
[86]L. K. Ono, E. J. Juarez-Perez, and Y. Qi, ACS Appl. Mater. Interfaces **9**, 30197 (2017).
[87]J. Borchert, I. Levchuk, L. C. Snoek, M. U. Rothmann, R. Haver, H. J. Snaith, C. J. Brabec, L. M. Herz, and M. B. Johnston, ACS Appl. Mater. Interfaces **11**, 28851 (2019).
[88]E. S. Parrott, T. Green, R. L. Milot, M. B. Johnston, H. J. Snaith, and L. M. Herz, Adv. Funct. Mater. **28**, 1802803 (2018).
[89]A. Rajagopal, R. J. Stoddard, H. W. Hillhouse, and A. K.-Y. Jen, J. Mater. Chem. A **7**, 16285 (2019).
[90]N. K. Kumawat, A. Dey, A. Kumar, S. P. Gopinathan, K. L. Narasimhan, and D. Kabra, ACS Appl. Mater. Interfaces **7**, 13119 (2015).
[91]R. E. Beal, D. J. Slotcavage, T. Leijtens, A. R. Bowring, R. A. Belisle, W. H. Nguyen, G. F. Burkhard, E. T. Hoke, and M. D. McGehee, J. Phys. Chem. Lett. **7**, 746 (2016).
[92]G. E. Eperon, S. D. Stranks, C. Menelaou, M. B. Johnston, L. M. Herz, and H. J. Snaith, Energy Environ. Sci. **7**, 982 (2014).
[93]D. P. McMeekin, G. Sadoughi, W. Rehman, G. E. Eperon, M. Saliba, M. T. Horantner, A. Haghighirad, N. Sakai, L. Korte, B. Rech, M. B. Johnston, L. M. Herz, and H. J. Snaith, Science **351**, 151 (2016).
[94]T. Jesper Jacobsson, J.-P. Correa-Baena, M. Pazoki, M. Saliba, K. Schenk, M. Grätzel, and A. Hagfeldt, Energy Environ. Sci. **9**, 1706 (2016).
[95]K. A. Bush, K. Frohna, R. Prasanna, R. E. Beal, T. Leijtens, S. A. Swifter, and M. D. McGehee, ACS Energy Lett. **3**, 428 (2018).
[96]F. Hao, C. C. Stoumpos, D. H. Cao, R. P. H. Chang, and M. G. Kanatzidis, Nat. Photonics **8**, 489 (2014).
[97]M. L. Lai, T. Y. S. Tay, A. Sadhanala, S. E. Dutton, G. Li, R. H. Friend, and Z.-K. Tan, J. Phys. Chem. Lett. **7**, 2653 (2016).
[98]L. Peedikakkandy and P. Bhargava, RSC Adv. **6**, 19857 (2016).
[99]C. C. Stoumpos, C. D. Malliakas, and M. G. Kanatzidis, Inorg. Chem. **52**, 9019 (2013).
[100]F. Hao, C. C. Stoumpos, R. P. H. Chang, and M. G. Kanatzidis, J. Am. Chem. Soc. **136**, 8094 (2014).
[101]A. Pisanu, A. Mahata, E. Mosconi, M. Patrini, P. Quadrelli, C. Milanese, F. De Angelis, and L. Malavasi, ACS Energy Lett. **3**, 1353 (2018).
[102]H. A. Schwartz, H. Laurenzen, A. Marzouk, M. Runkel, K. O. Brinkmann, D. Rogalla, T. Riedl, S. Ashhab, and S. Olthof, ACS Appl. Mater. Interfaces **13**, 4203 (2021).
[103]N. Pellet, P. Gao, G. Gregori, T.-Y. Yang, M. K. Nazeeruddin, J. Maier, and M. Grätzel, Angew. Chem., Int. Ed. **53**, 3151 (2014).
[104]A. Pisanu, C. Ferrara, P. Quadrelli, G. Guizzetti, M. Patrini, C. Milanese, C. Tealdi, and L. Malavasi, J. Phys. Chem. C **121**, 8746 (2017).
[105]C. Ferrara, M. Patrini, A. Pisanu, P. Quadrelli, C. Milanese, C. Tealdi, and L. Malavasi, J. Mater. Chem. A **5**, 9391 (2017).
[106]L. L. Hench and J. K. West, *Principles of Electronic Ceramics* (Wiley, New York, 1990).
[107]M. E. Lines and A. M. Glass, *Principles and Applications of Ferroelectrics and Related Materials* (Clarendon Press, Oxford, 1977).

© Author(s) 2021

[108]Y. Ishibashi, "Polarization reversal kinetics in ferroelectric liquid crystals," Jpn. J. Appl. Phys., Part 1 **24**, 126–129 (1985).
[109]J. Even, L. Pedesseau, and C. Katan, J. Phys. Chem. C **118**, 11566 (2014).
[110]I. Anusca, S. Balčiūnas, P. Gemeiner, Š. Svirskas, M. Sanlialp, G. Lackner, C. Fettkenhauer, J. Belovickis, V. Samulionis, M. Ivanov, B. Dkhil, J. Banys, V. V. Shvartsman, and D. C. Lupascu, Adv. Energy Mater. **7**, 1700600 (2017).
[111]K. Miyata, R. Nagaoka, M. Hada, T. Tanaka, R. Mishima, T. Kuroda, S. Sueta, T. Iida, Y. Yamashita, T. Nishikawa, K. Tsuruta, Y. Hayashi, K. Onda, T. Kiwa, and T. Teranishi, J. Chem. Phys. **152**, 084704 (2020).
[112]Y. Chen, H. T. Yi, X. Wu, R. Haroldson, Y. N. Gartstein, Y. I. Rodionov, K. S. Tikhonov, A. Zakhidov, X.-Y. Zhu, and V. Podzorov, Nat. Commun. **7**, 12253 (2016).
[113]J. M. Frost, K. T. Butler, F. Brivio, C. H. Hendon, M. van Schilfgaarde, and A. Walsh, Nano Lett. **14**, 2584 (2014).
[114]A. Gómez, Q. Wang, A. R. Goñi, M. Campoy-Quiles, and A. Abate, Energy Environ. Sci. **12**, 2537 (2019).
[115]J. Liang, P. Zhao, C. Wang, Y. Wang, Y. Hu, G. Zhu, L. Ma, J. Liu, and Z. Jin, J. Am. Chem. Soc. **139**, 14009 (2017).
[116]Š. Svirskas, S. Balčiūnas, M. Šimėnas, G. Usevičius, M. Kinka, M. Velička, D. Kubicki, M. E. Castillo, A. Karabanov, V. V. Shvartsman, M. de Rosário Soares, V. Šablinskas, A. N. Salak, D. C. Lupascu, and J. Banys, J. Mater. Chem. A **8**, 14015 (2020).
[117]D. H. Fabini, R. Seshadri, and M. G. Kanatzidis, MRS Bull. **45**, 467 (2020).
[118]M. J. Hong, L. Zhu, C. Chen, L. Tang, Y.-H. Lin, W. Li, R. Johnson, S. Chattopadhyay, H. J. Snaith, C. Fang, and J. G. Labram, J. Am. Chem. Soc. **142**, 19799 (2020).
[119]X.-G. Chen, X.-J. Song, Z.-X. Zhang, H.-Y. Zhang, Q. Pan, J. Yao, Y.-M. You, and R.-G. Xiong, J. Am. Chem. Soc. **142**, 10212–10218 (2020).
[120]H.-Y. Zhang, Z.-X. Zhang, X.-J. Song, X.-G. Chen, and R.-G. Xiong, J. Am. Chem. Soc. **142**(47), 20208–20215 (2020).
[121]H.-Y. Liu, H.-Y. Zhang, X.-G. Chen, and R.-G. Xiong, J. Am. Chem. Soc. **142**(36), 15205–15218 (2020).
[122]C. K. Yang, W. N. Chen, Y. T. Ding, J. Wang, Y. Rao, W. Q. Liao, Y. Y. Tang, P. F. Li, Z. X. Wang, and R. G. Xiong, Adv. Mater. **31**, 1808088 (2019).
[123]L. Li, Z. Sun, P. Wang, W. Hu, S. Wang, C. Ji, M. Hong, and J. Luo, Angew. Chem., Int. Ed. **56**, 12150 (2017).
[124]Y. Hou, C. Wu, D. Yang, T. Ye, V. G. Honavar, A. C. T. van Duin, K. Wang, and S. Priya, J. Appl. Phys. **128**, 060906 (2020).
[125]Y. Hu, F. Florio, Z. Chen, W. A. Phelan, M. A. Siegler, Z. Zhou, Y. Guo, R. Hawks, J. Jiang, J. Feng, L. Zhang, B. Wang, Y. Wang, D. Gall, E. F. Palermo, Z. Lu, X. Sun, T.-M. Lu, H. Zhou, Y. Ren, E. Wertz, R. Sundararaman, and J. Shi, Sci. Adv. **6**, eaay4213 (2020).
[126]L. M. Herz, ACS Energy Lett. **2**, 1539 (2017).
[127]L. M. Herz, J. Phys. Chem. Lett. **9**, 6853 (2018).
[128]A. D. Wright, C. Verdi, R. L. Milot, G. E. Eperon, M. A. Pérez-Osorio, H. J. Snaith, F. Giustino, M. B. Johnston, and L. M. Herz, Nat. Commun. **7**, 11755 (2016).
[129]M. Sendner, P. K. Nayak, D. A. Egger, S. Beck, C. Müller, B. Epding, W. Kowalsky, L. Kronik, H. J. Snaith, A. Pucci, and R. Lovrinčić, Mater. Horiz. **3**, 613 (2016).
[130]S. Poncé, M. Schlipf, and F. Giustino, ACS Energy Lett. **4**, 456 (2019).
[131]H. Fröhlich, Adv. Phys. **3**, 325 (1954).
[132]W. Rehman, D. P. McMeekin, J. B. Patel, R. L. Milot, M. B. Johnston, H. J. Snaith, and L. M. Herz, Energy Environ. Sci. **10**, 361 (2017).
[133]M. T. Klug, R. L. Milot, J. B. Patel, T. Green, H. C. Sansom, M. D. Farrar, A. J. Ramadan, S. Martani, Z. Wang, B. Wenger, J. M. Ball, L. Langshaw, A. Petrozza, M. B. Johnston, L. M. Herz, and H. J. Snaith, Energy Environ. Sci. **13**, 1776 (2020).
[134]R. L. Milot, M. T. Klug, C. L. Davies, Z. Wang, H. Kraus, H. J. Snaith, M. B. Johnston, and L. M. Herz, Adv. Mater. **30**, 1804506 (2018).
[135]K. J. Savill, A. M. Ulatowski, M. D. Farrar, M. B. Johnston, H. J. Snaith, and L. M. Herz, Adv. Funct. Mater. **30**, 2005594 (2020).
[136]O. Yaffe, Y. Guo, L. Z. Tan, D. A. Egger, T. Hull, C. C. Stoumpos, F. Zheng, T. F. Heinz, L. Kronik, M. G. Kanatzidis, J. S. Owen, A. M. Rappe, M. A. Pimenta, and L. E. Brus, Phys. Rev. Lett. **118**, 136001 (2017).
[137]M. Z. Mayers, L. Z. Tan, D. A. Egger, A. M. Rappe, and D. R. Reichman, Nano Lett. **18**, 8041 (2018).
[138]H. Oga, A. Saeki, Y. Ogomi, S. Hayase, and S. Seki, J. Am. Chem. Soc. **136**, 13818 (2014).
[139]R. L. Milot, G. E. Eperon, H. J. Snaith, M. B. Johnston, and L. M. Herz, Adv. Funct. Mater. **25**, 6218 (2015).
[140]J. M. Frost, Phys. Rev. B **96**, 195202 (2017).
[141]K. Alberi, M. B. Nardelli, A. Zakutayev, L. Mitas, S. Curtarolo, A. Jain, M. Fornari, N. Marzari, I. Takeuchi, M. L. Green, M. Kanatzidis, M. F. Toney, S. Butenko, B. Meredig, S. Lany, U. Kattner, A. Davydov, E. S. Toberer, V. Stevanovic, A. Walsh, N.-G. Park, A. Aspuru-Guzik, D. P. Tabor, J. Nelson, J. Murphy, A. Setlur, J. Gregoire, H. Li, R. Xiao, A. Ludwig, L. W. Martin, A. M. Rappe, S.-H. Wei, and J. Perkins, J. Phys. D: Appl. Phys. **52**, 013001 (2018).
[142]L. R. V. Buizza and L. M. Herz, Adv. Mater. **33**, 2007057 (2021).
[143]M. R. Filip and F. Giustino, Proc. Natl. Acad. Sci. U. S. A. **115**, 5397 (2018).
[144]J.-P. Correa-Baena, A. Abate, M. Saliba, W. Tress, T. Jesper Jacobsson, M. Grätzel, and A. Hagfeldt, Energy Environ. Sci. **10**, 710 (2017).
[145]T. Baikie, N. S. Barrow, Y. Fang, P. J. Keenan, P. R. Slater, R. O. Piltz, M. Gutmann, S. G. Mhaisalkar, and T. J. White, J. Mater. Chem. A **3**, 9298 (2015).
[146]J. Li, M. Bouchard, P. Reiss, D. Aldakov, S. Pouget, R. Demadrille, C. Aumaitre, B. Frick, D. Djurado, M. Rossi, and P. Rinke, J. Phys. Chem. Lett. **9**, 3969 (2018).
[147]J. Schlipf and P. Müller-Buschbaum, Adv. Energy Mater. **7**, 1700131 (2017).
[148]Y. Liu, S. Akin, A. Hinderhofer, F. T. Eickemeyer, H. Zhu, J. Y. Seo, J. Zhang, F. Schreiber, H. Zhang, S. M. Zakeeruddin, A. Hagfeldt, M. I. Dar, and M. Grätzel, Angew. Chem., Int. Ed. Engl. **59**, 15688 (2020).
[149]T. Baumeler, N. Arora, A. Hinderhofer, S. Akin, A. Greco, M. Abdi-Jalebi, R. Shivanna, R. Uchida, Y. Liu, F. Schreiber, S. M. Zakeeruddin, R. H. Friend, M. Graetzel, and M. I. Dar, J. Phys. Chem. Lett. **11**, 10188 (2020).
[150]Y. Liu, S. Akin, L. Pan, R. Uchida, N. Arora, J. V. Milić, A. Hinderhofer, F. Schreiber, A. R. Uhl, S. M. Zakeeruddin, A. Hagfeldt, M. I. Dar, and M. Grätzel, Sci. Adv. **5**, eaaw2543 (2019).
[151]A. Greco, A. Hinderhofer, M. I. Dar, N. Arora, J. Hagenlocher, A. Chumakov, M. Grätzel, and F. Schreiber, J. Phys. Chem. Lett. **9**, 6750 (2018).
[152]K. Lin, N. Wang, L. You, Q. Li, K. Kato, J. Chen, J. Deng, and X. Xing, Dalton Trans. **46**, 733 (2017).
[153]D. B. Mitzi, Chem. Mater. **8**, 791 (1996).
[154]C. C. Stoumpos, D. H. Cao, D. J. Clark, J. Young, J. M. Rondinelli, J. I. Jang, J. T. Hupp, and M. G. Kanatzidis, Chem. Mater. **28**, 2852 (2016).
[155]T. Ishihara, J. Lumin. **60–61**, 269 (1994).
[156]M. Menahem, Z. Dai, S. Aharon, R. Sharma, M. Asher, Y. Diskin-Posner, R. Korobko, A. M. Rappe, and O. Yaffe, ACS Nano **15**, 10153 (2021).
[157]H. Tsai, W. Nie, J.-C. Blancon, C. C. Stoumpos, R. Asadpour, B. Harutyunyan, A. J. Neukirch, R. Verduzco, J. J. Crochet, S. Tretiak, L. Pedesseau, J. Even, M. A. Alam, G. Gupta, J. Lou, P. M. Ajayan, M. J. Bedzyk, M. G. Kanatzidis, and A. D. Mohite, Nature **536**, 312 (2016).
[158]O. Yaffe, A. Chernikov, Z. M. Norman, Y. Zhong, A. Velauthapillai, A. van der Zande, J. S. Owen, and T. F. Heinz, Phys. Rev. B **92**, 045414 (2015).
[159]M. Dyksik, H. Duim, X. Zhu, Z. Yang, M. Gen, Y. Kohama, S. Adjokatse, D. K. Maude, M. A. Loi, D. A. Egger, M. Baranowski, and P. Plochocka, ACS Energy Lett. **5**, 3609 (2020).
[160]Y. Hu, T. Qiu, F. Bai, W. Ruan, and S. Zhang, Adv. Energy Mater. **8**(19), 1703620 (2018).
[161]A. A. Sutanto, R. Szostak, N. Drigo, V. I. E. Queloz, P. E. Marchezi, J. C. Germino, H. C. N. Tolentino, M. K. Nazeeruddin, A. F. Nogueira, and G. Grancini, Nano Lett. **20**(5), 3992–3998 (2020).
[162]S. Deng, E. Shi, L. Yuan, L. Jin, L. Dou, and L. Huang, Nat. Commun. **11**, 664 (2020).
[163]M. Seitz, A. J. Magdaleno, N. Alcázar-Cano, M. Meléndez, T. J. Lubbers, S. W. Walraven, S. Pakdel, E. Prada, R. Delgado-Buscalioni, and F. Prins, Nat. Commun. **11**, 2035 (2020).

© Author(s) 2021

[164]J. D. Ziegler, J. Zipfel, B. Meisinger, M. Menahem, X. Zhu, T. Taniguchi, K. Watanabe, O. Yaffe, D. A. Egger, and A. Chernikov, Nano Lett. **20**, 6674 (2020).
[165]X. Xiao, M. Wu, Z. Ni, S. Xu, S. Chen, J. Hu, P. N. Rudd, W. You, and J. Huang, Adv. Mater. **32**, 2004080 (2020).
[166]M. J. Schilcher, P. J. Robinson, D. J. Abramovitch, L. Z. Tan, A. M. Rappe, D. R. Reichman, and D. A. Egger, ACS Energy Lett. **6**, 2162–2173 (2021).
[167]K. X. Steirer, P. Schulz, G. Teeter, V. Stevanovic, M. Yang, K. Zhu, and J. J. Berry, ACS Energy Lett. **1**, 360 (2016).
[168]B. Conings, A. Babayigit, M. Klug, S. Bai, N. Gauquelin, N. Sakai, J. T.-W. Wang, J. Verbeeck, H.-G. Boyen, and H. Snaith, in *2018 IEEE 7th World Conference on Photovoltaic Energy Conversion (WCPEC) (A Joint Conference of 45th IEEE PVSC 28th PVSEC and 34th EU PVSEC)* (IEEE, 2018).
[169]J. Yi, J. Zhuang, Z. Ma, Z. Guo, W. Zhou, S. Zhao, H. Zhang, X. Luo, and H. Li, Org. Electron. **69**, 69 (2019).
[170]L. Zeng, S. Chen, K. Forberich, C. J. Brabec, Y. Mai, and F. Guo, Energy Environ. Sci. **13**, 4666 (2020).
[171]R. Swartwout, M. T. Hoerantner, and V. Bulović, Energy Environ. Mater. **2**, 119 (2019).
[172]K. G. Stamplecoskie, J. S. Manser, and P. V. Kamat, Energy Environ. Sci. **8**, 208 (2015).
[173]J. Stevenson, B. Sorenson, V. H. Subramaniam, J. Raiford, P. P. Khlyabich, Y.-L. Loo, and P. Clancy, Chem. Mater. **29**, 2435 (2017).
[174]J. C. Hamill, J. Schwartz, and Y.-L. Loo, ACS Energy Lett. **3**, 92 (2017).
[175]O. Shargaieva, H. Näsström, J. A. Smith, D. Többens, R. Munir, and E. Unger, Mater. Adv. **1**, 3314 (2020).
[176]L. Ma, Z. Yan, X. Zhou, Y. Pi, Y. Du, J. Huang, K. Wang, K. Wu, C. Zhuang, and X. Han, Nat. Commun. **12**, 2023 (2021).
[177]J. Song, Q. Hu, Q. Zhang, S. Xiong, Z. Zhao, J. Ali, Y. Zou, W. Feng, Z. Yang, Q. Bao, Y. Zhang, T. P. Russell, and F. Liu, Adv. Funct. Mater. **31**(14), 2009103 (2021).
[178]A. J. Huckaba, Y. Lee, R. Xia, S. Paek, V. C. Bassetto, E. Oveisi, A. Lesch, S. Kinge, P. J. Dyson, H. Girault, and M. K. Nazeeruddin, Energy Technol. **7**, 317 (2018).
[179]A. Giuri, E. Saleh, A. Listorti, S. Colella, A. Rizzo, C. Tuck, and C. Esposito Corcione, Nanomaterials **9**, 582 (2019).
[180]C.-Y. Chang, C.-Y. Chu, Y.-C. Huang, C.-W. Huang, S.-Y. Chang, C.-A. Chen, C.-Y. Chao, and W.-F. Su, ACS Appl. Mater. Interfaces **7**(8), 4955–4961 (2015).
[181]Y. Deng, C. H. V. Brackle, X. Dai, J. Zhao, B. Chen, and J. Huang, Sci. Adv. **5**, eaax7537 (2019).
[182]N. K. Noel, S. N. Habisreutinger, B. Wenger, M. T. Klug, M. T. Hörantner, M. B. Johnston, R. J. Nicholas, D. T. Moore, and H. J. Snaith, Energy Environ. Sci. **10**, 145 (2017).
[183]G. Wang, L. Liao, L. Chen, C. Xu, Y. Yao, D. Liu, P. Li, J. Deng, and Q. Song, Org. Electron. **86**, 105918 (2020).
[184]J. Li, J. Dagar, O. Shargaieva, M. A. Flatken, H. Köbler, M. Fenske, C. Schultz, B. Stegemann, J. Just, D. M. Többens, A. Abate, R. Munir, and E. Unger, Adv. Energy Mater. **11**, 2003460 (2021).
[185]S. Rahimnejad, A. Kovalenko, S. M. Forés, C. Aranda, and A. Guerrero, ChemPhysChem **17**, 2795 (2016).
[186]J. Tomasi, B. Mennucci, and R. Cammi, Chem. Rev. **105**, 2999 (2005).
[187]S. P. Huber, S. Zoupanos, M. Uhrin, L. Talirz, L. Kahle, R. Häuselmann, D. Gresch, T. Müller, A. V. Yakutovich, C. W. Andersen, F. F. Ramirez, C. S. Adorf, F. Gargiulo, S. Kumbhar, E. Passaro, C. Johnston, A. Merkys, A. Cepellotti, N. Mounet, N. Marzari, B. Kozinsky, and G. Pizzi, Sci. Data **7**, 300 (2020).
[188]K. L. Gardner, J. G. Tait, T. Merckx, W. Qiu, U. W. Paetzold, L. Kootstra, M. Jaysankar, R. Gehlhaar, D. Cheyns, P. Heremans, and J. Poortmans, Adv. Energy Mater. **6**, 1600386 (2016).
[189]F. P. Byrne, S. Jin, G. Paggiola, T. H. M. Petchey, J. H. Clark, T. J. Farmer, A. J. Hunt, C. R. McElroy, and J. Sherwood, Sustainable Chem. Processes **4**, 7 (2016).
[190]K. Suchan, J. Just, P. Becker, E. L. Unger, and T. Unold, J. Mater. Chem. A **8**, 10439 (2020).
[191]K. H. Stone, A. Gold-Parker, V. L. Pool, E. L. Unger, A. R. Bowring, M. D. McGehee, M. F. Toney, and C. J. Tassone, Nat. Commun. **9**, 3458 (2018).
[192]M. Jung, S.-G. Ji, G. Kim, and S. I. Seok, Chem. Soc. Rev. **48**, 2011 (2019).
[193]S. Ternes, T. Börnhorst, J. A. Schwenzer, I. M. Hossain, T. Abzieher, W. Mehlmann, U. Lemmer, P. Scharfer, W. Schabel, B. S. Richards, and U. W. Paetzold, Adv. Energy Mater. **9**, 1901581 (2019).
[194]A. M. Valencia, O. Shargaieva, R. Schier, E. Unger, and C. Cocchi, J. Phys. Chem. Lett. **12**, 2299 (2021).
[195]E. Gu, X. Tang, S. Langner, P. Duchstein, Y. Zhao, I. Levchuk, V. Kalancha, T. Stubhan, J. Hauch, H. J. Egelhaaf, D. Zahn, A. Osvet, and C. J. Brabec, Joule **4**, 1806 (2020).
[196]C. Liu, Y.-B. Cheng, and Z. Ge, Chem. Soc. Rev. **49**, 1653 (2020).
[197]Y. Vaynzof, Adv. Energy Mater. **10**(48), 2003073 (2020).
[198]J. Burschka, N. Pellet, S.-J. Moon, R. Humphry-Baker, P. Gao, M. K. Nazeeruddin, and M. Grätzel, Nature **499**(7458), 316–319 (2013).
[199]J.-H. Im, I.-H. Jang, N. Pellet, M. Grätzel, and N.-G. Park, Nat. Nanotechnol. **9**(11), 927–932 (2014).
[200]J. Jeong, M. Kim, J. Seo, H. Lu, P. Ahlawat, A. Mishra, Y. Yang, M. A. Hope, F. T. Eickemeyer, M. Kim, Y. J. Yoon, I. W. Choi, B. P. Darwich, S. J. Choi, Y. Jo, J. H. Lee, B. Walker, S. M. Zakeeruddin, L. Emsley, U. Rothlisberger, A. Hagfeldt, D. S. Kim, M. Grätzel, and J. Y. Kim, Nature **592**(7854), 381–385 (2021).
[201]J. J. Yoo, G. Seo, M. R. Chua, T. G. Park, Y. Lu, F. Rotermund, Y.-K. Kim, C. S. Moon, N. J. Jeon, J.-P. Correa-Baena, V. Bulović, S. S. Shin, M. G. Bawendi, and J. Seo, Nature **590**(7847), 587–593 (2021).
[202]Q. Jiang, Y. Zhao, X. Zhang, X. Yang, Y. Chen, Z. Chu, Q. Ye, X. Li, Z. Yin, and J. You, Nat. Photonics **13**, 460 (2019).
[203]Y. Chen, S. Tan, N. Li, B. Huang, X. Niu, L. Li, M. Sun, Y. Zhang, X. Zhang, C. Zhu, N. Yang, H. Zai, Y. Wu, S. Ma, Y. Bai, Q. Chen, F. Xiao, K. Sun, and H. Zhou, Joule **4**(9), 1961–1976 (2020).
[204]N. J. Jeon, J. H. Noh, Y. C. Kim, W. S. Yang, S. Ryu, and S. Il Seok, Nat. Mater. **13**, 897 (2014).
[205]G. Grancini and M. K. Nazeeruddin, Nat. Rev. Mater. **4**, 4 (2018).
[206]W. Chen, X. Li, Y. Li, and Y. Li, Energy Environ. Sci. **13**, 1971 (2020).
[207]N. Ahn, D.-Y. Son, I.-H. Jang, S. M. Kang, M. Choi, and N.-G. Park, J. Am. Chem. Soc. **137**, 8696 (2015).
[208]J.-W. Lee, Z. Dai, C. Lee, H. M. Lee, T.-H. Han, N. De Marco, O. Lin, C. S. Choi, B. Dunn, J. Koh, D. Di Carlo, J. H. Ko, H. D. Maynard, and Y. Yang, J. Am. Chem. Soc. **140**, 6317 (2018).
[209]Z. Li, T. R. Klein, D. H. Kim, M. Yang, J. J. Berry, M. F. A. M. van Hest, and K. Zhu, Nat. Rev. Mater. **3**, 18017 (2018).
[210]X. Gu, Y. Zhou, K. Gu, T. Kurosawa, Y. Guo, Y. Li, H. Lin, B. C. Schroeder, H. Yan, F. Molina-Lopez, C. J. Tassone, C. Wang, S. C. B. Mannsfeld, H. Yan, D. Zhao, M. F. Toney, and Z. Bao, Adv. Energy Mater. **7**, 1602742 (2017).
[211]B. Dou, J. B. Whitaker, K. Bruening, D. T. Moore, L. M. Wheeler, J. Ryter, N. J. Breslin, J. J. Berry, S. M. Garner, F. S. Barnes, S. E. Shaheen, C. J. Tassone, K. Zhu, and M. F. A. M. Van Hest, ACS Energy Lett. **3**, 2558 (2018).
[212]D. Burkitt, R. Swartwout, J. McGettrick, P. Greenwood, D. Beynon, R. Brenes, V. Bulović, and T. Watson, RSC Adv. **9**, 37415 (2019).
[213]F. Ye, H. Chen, F. Xie, W. Tang, M. Yin, J. He, E. Bi, Y. Wang, X. Yang, and L. Han, Energy Environ. Sci. **9**, 2295 (2016).
[214]L. Zhang, S. Chen, X. Wang, D. Wang, Y. Li, Q. Ai, X. Sun, J. Chen, Y. Li, X. Jiang, S. Yang, and B. Xu, Sol. RRL **5**(5), 2100106 (2021).
[215]L. Gao, I. Spanopoulos, W. Ke, S. Huang, I. Hadar, L. Chen, X. Li, G. Yang, and M. G. Kanatzidis, ACS Energy Lett. **4**, 1763 (2019).
[216]M. Hashemi, S. M. B. Ghorashi, F. Tajabadi, and N. Taghavinia, J. Mater. Sci.: Mater. Electron. **8**, 1 (2020).
[217]J. Griffin, A. J. Pearson, N. W. Scarratt, T. Wang, D. G. Lidzey, and A. R. Buckley, Org. Electron. **15**, 692 (2014).
[218]J. E. Bishop, T. J. Routledge, and D. G. Lidzey, J. Phys. Chem. Lett. **9**, 1977 (2018).
[219]M. Xiao, F. Huang, W. Huang, Y. Dkhissi, Y. Zhu, J. Etheridge, A. Gray-Weale, U. Bach, Y.-B. Cheng, and L. Spiccia, Angew. Chem., Int. Ed. **53**, 9898 (2014).

© Author(s) 2021

[220]M. M. Byranvand, S. Song, L. Pyeon, G. Kang, G.-Y. Lee, and T. Park, Nano Energy **34**, 181 (2017).
[221]M. Yin, F. Xie, H. Chen, X. Yang, F. Ye, E. Bi, Y. Wu, M. Cai, and L. Han, J. Mater. Chem. A **4**, 8548 (2016).
[222]M. Yavari, M. Mazloum-Ardakani, S. Gholipour, M. M. Tavakoli, S.-H. Turren-Cruz, N. Taghavinia, M. Grätzel, A. Hagfeldt, and M. Saliba, Adv. Energy Mater. **8**, 1800177 (2018).
[223]M. Ramesh, K. M. Boopathi, T.-Y. Huang, Y.-C. Huang, C.-S. Tsao, and C.-W. Chu, ACS Appl. Mater. Interfaces **7**, 2359 (2015).
[224]S. S. Kim, J. H. Heo, and S. H. Im, RSC Adv. **10**, 33651 (2020).
[225]J. Li, R. Munir, Y. Fan, T. Niu, Y. Liu, Y. Zhong, Z. Yang, Y. Tian, B. Liu, J. Sun, D.-M. Smilgies, S. Thoroddsen, A. Amassian, K. Zhao, and S. (Frank) Liu, Joule **2**, 1313 (2018).
[226]M.-C. Tang, Y. Fan, D. Barrit, X. Chang, H. X. Dang, R. Li, K. Wang, D.-M. Smilgies, S. (Frank) Liu, S. De Wolf, T. D. Anthopoulos, K. Zhao, and A. Amassian, J. Mater. Chem. A **8**, 1095 (2020).
[227]X. Jiang, J. Zhang, S. Ahmad, D. Tu, X. Liu, G. Jia, X. Guo, and C. Li, Nano Energy **75**, 104892 (2020).
[228]J. Zhang, T. Bu, J. Li, H. Li, Y. Mo, Z. Wu, Y. Liu, X.-L. Zhang, Y.-B. Cheng, and F. Huang, J. Mater. Chem. A **8**, 8447 (2020).
[229]P. W.-K. Fong, H. Hu, Z. Ren, K. Liu, L. Cui, T. Bi, Q. Liang, Z. Wu, J. Hao, and G. Li, Adv. Sci. **8**, 2003359 (2021).
[230]J. Küffner, T. Wahl, M. Schultes, J. Hanisch, J. Zillner, E. Ahlswede, and M. Powalla, ACS Appl. Mater. Interfaces **12**, 52678 (2020).
[231]B. Conings, A. Babayigit, M. T. Klug, S. Bai, N. Gauquelin, N. Sakai, J. T.-W. Wang, J. Verbeeck, H.-G. Boyen, and H. J. Snaith, Adv. Mater. **28**, 10701 (2016).
[232]J. Hu, C. Wang, S. Qiu, Y. Zhao, E. Gu, L. Zeng, Y. Yang, C. Li, X. Liu, K. Forberich, C. J. Brabec, M. K. Nazeeruddin, Y. Mai, and F. Guo, Adv. Energy Mater. **10**, 2000173 (2020).
[233]T. Zhang, C. Hu, and S. Yang, Small Methods **4**, 1900552 (2020).
[234]X. Li, D. Bi, C. Yi, J.-D. Décoppet, J. Luo, S. M. Zakeeruddin, A. Hagfeldt, and M. Grätzel, Science **353**(6294), 58–62 (2016).
[235]H. Hu, K. K. Wong, T. Kollek, F. Hanusch, S. Polarz, P. Docampo, and L. Schmidt-Mende, Molecules **21**(4), 542 (2016).
[236]F. Guo, W. He, S. Qiu, C. Wang, X. Liu, K. Forberich, C. J. Brabec, and Y. Mai, Adv. Funct. Mater. **29**, 1900964 (2019).
[237]Z. Xiao, Q. Dong, C. Bi, Y. Shao, Y. Yuan, and J. Huang, Adv. Mater. **26**(37), 6503–6509 (2014).
[238]K. Bruening, B. Dou, J. Simonaitis, Y.-Y. Lin, M. F. A. M. Van Hest, and C. J. Tassone, Joule **2**, 2464 (2018).
[239]Z. Ouyang, M. Yang, J. B. Whitaker, D. Li, and M. F. A. M. Van Hest, ACS Appl. Energy Mater. **3**, 3714–3720 (2020).
[240]S. H. Huang, C. K. Guan, P. H. Lee, H. C. Huang, C. F. Li, Y. C. Huang, and W. F. Su, Adv. Energy Mater. **10**, 2001567 (2020).
[241]J. Troughton, C. Charbonneau, M. J. Carnie, M. L. Davies, D. A. Worsley, and T. M. Watson, J. Mater. Chem. A **3**, 9123 (2015).
[242]P. Sha, V. Ling, A. Hagfeldt, and S. Sanchez, J. Vis. Exp. **168**, e61730 (2021).
[243]S. Sanchez, U. Steiner, and X. Hua, Chem. Mater. **31**, 3498 (2019).
[244]K. Ankireddy, B. W. Lavery, and T. Druffel, J. Electron. Mater. **47**, 1285 (2018).
[245]P. Li, H. Dong, J. Xu, J. Chen, B. Jiao, X. Hou, J. Li, and Z. Wu, ACS Energy Lett. **5**, 2327 (2020).
[246]B. Dou, V. L. Pool, M. F. Toney, and M. F. A. M. Van Hest, Chem. Mater. **29**, 5931 (2017).
[247]V. L. Pool, B. Dou, D. G. Van Campen, T. R. Klein-stockert, F. S. Barnes, S. E. Shaheen, M. I. Ahmad, M. F. A. M. Van Hest, and M. F. Toney, Nat. Commun. **8**, 14075 (2017).
[248]I. Konidakis, T. Maksudov, E. Serpetzoglou, G. Kakavelakis, E. Kymakis, and E. Stratakis, ACS Appl. Energy Mater. **1**, 5101–5111 (2018).
[249]P. You, G. Li, G. Tang, J. Cao, and F. Yan, Energy Environ. Sci. **13**, 1187 (2020).
[250]J. Xu, Z. Hu, X. Jia, L. Huang, X. Huang, L. Wang, P. Wang, H. Zhang, J. Zhang, J. Zhang, and Y. Zhu, Org. Electron. **34**, 84 (2016).
[251]Z. Ouyang, H. Abrams, R. Bergstone, Q. Li, F. Zhu, and D. Li, Adv. Energy Mater. **10**, 1902898 (2019).
[252]T. Su, X. Li, Y. Zhang, F. Zhang, and Z. Sheng, Phys. Chem. Chem. Phys. **19**, 13147 (2017).
[253]W. Peng, B. Anand, L. Liu, S. Sampat, B. E. Bearden, A. V. Malko, and Y. J. Chabal, Nanoscale **8**, 1627 (2016).
[254]A. Dualeh, N. Tétreault, T. Moehl, P. Gao, M. K. Nazeeruddin, and M. Grätzel, Adv. Funct. Mater. **24**, 3250 (2014).
[255]J. Wang, F. Di Giacomo, J. Brüls, H. Gorter, I. Katsouras, P. Groen, R. A. J. Janssen, R. Andriessen, and Y. Galagan, Sol. RRL **1**, 1700091 (2017).
[256]S. Sánchez, M. Vallés-Pelarda, J.-A. Alberola-Borràs, R. Vidal, J. J. Jerónimo-Rendón, M. Saliba, P. P. Boix, and I. Mora-Seró, Mater. Today **31**, 39 (2019).
[257]M. Liu, M. B. Johnston, and H. J. Snaith, Nature **501**, 395 (2013).
[258]M. Ross, L. Gil-Escrig, A. Al-Ashouri, P. Tockhorn, M. Jošt, B. Rech, and S. Albrecht, ACS Appl. Mater. Interfaces **12**, 39261 (2020).
[259]J. Li, H. Wang, X. Y. Chin, H. A. Dewi, K. Vergeer, T. W. Goh, J. W. M. Lim, J. H. Lew, K. P. Loh, C. Soci, T. C. Sum, H. J. Bolink, N. Mathews, S. Mhaisalkar, and A. Bruno, Joule **4**, 1035 (2020).
[260]L. Gil-Escrig, C. Momblona, M.-G. La-Placa, P. P. Boix, M. Sessolo, and H. J. Bolink, Adv. Energy Mater. **8**, 1703506 (2018).
[261]R. Ji, Z. Zhang, C. Cho, Q. An, F. Paulus, M. Kroll, M. Löffler, F. Nehm, B. Rellinghaus, K. Leo, and Y. Vaynzof, J. Mater. Chem. C **8**, 7725 (2020).
[262]A. M. Igual-Muñoz, A. Castillo, C. Dreessen, P. P. Boix, and H. J. Bolink, ACS Appl. Energy Mater. **3**, 2755 (2020).
[263]K. B. Lohmann, J. B. Patel, M. U. Rothmann, C. Q. Xia, R. D. J. Oliver, L. M. Herz, H. J. Snaith, and M. B. Johnston, ACS Energy Lett. **5**, 710 (2020).
[264]R. Kottokkaran, H. A. Gaonkar, H. A. Abbas, M. Noack, and V. Dalal, J. Mater. Sci.: Mater. Electron. **30**, 5487 (2019).
[265]F. Palazon, D. Pérez-del-Rey, B. Dänekamp, C. Dreessen, M. Sessolo, P. P. Boix, and H. J. Bolink, Adv. Mater. **31**, 1902692 (2019).
[266]J. F. Geisz, R. M. France, K. L. Schulte, M. A. Steiner, A. G. Norman, H. L. Guthrey, M. R. Young, T. Song, and T. Moriarty, Nat. Energy **5**, 326 (2020).
[267]J. A. Raiford, S. T. Oyakhire, and S. F. Bent, Energy Environ. Sci. **13**, 1997 (2020).
[268]A. K. Jena, A. Kulkarni, and T. Miyasaka, Chem. Rev. **119**, 3036 (2019).
[269]M. A. Green, E. D. Dunlop, J. Hohl-Ebinger, M. Yoshita, N. Kopidakis, and A. W. Y. Ho-Baillie, Prog. Photovoltaics: Res. Appl. **28**, 3 (2019).
[270]M. R. Leyden, L. K. Ono, S. R. Raga, Y. Kato, S. Wang, and Y. Qi, J. Mater. Chem. A **2**, 18742 (2014).
[271]M. R. Leyden, M. V. Lee, S. R. Raga, and Y. Qi, J. Mater. Chem. A **3**, 16097 (2015).
[272]M. R. Leyden, Y. Jiang, and Y. Qi, J. Mater. Chem. A **4**, 13125 (2016).
[273]M. M. Tavakoli, L. Gu, Y. Gao, C. Reckmeier, J. He, A. L. Rogach, Y. Yao, and Z. Fan, Sci. Rep. **5**, 14083 (2015).
[274]D. S. Bhachu, D. O. Scanlon, E. J. Saban, H. Bronstein, I. P. Parkin, C. J. Carmalt, and R. G. Palgrave, J. Mater. Chem. A **3**, 9071 (2015).
[275]J. Y. Kim, J.-W. Lee, H. S. Jung, H. Shin, and N.-G. Park, Chem. Rev. **120**, 7867 (2020).
[276]Y. Jiang, M. R. Leyden, L. Qiu, S. Wang, L. K. Ono, Z. Wu, E. J. Juarez-Perez, and Y. Qi, Adv. Funct. Mater. **28**, 1703835 (2017).
[277]T. Kirchartz, J. A. Márquez, M. Stolterfoht, and T. Unold, Adv. Energy Mater. **10**, 1904134 (2020).
[278]P. Becker, J. A. Márquez, J. Just, A. Al-Ashouri, C. Hages, H. Hempel, M. Jošt, S. Albrecht, R. Frahm, and T. Unold, Adv. Energy Mater. **9**, 1900555 (2019).
[279]M. Stolterfoht, P. Caprioglio, C. M. Wolff, J. A. Márquez, J. Nordmann, S. Zhang, D. Rothhardt, U. Hörmann, Y. Amir, A. Redinger, L. Kegelmann, F. Zu, S. Albrecht, N. Koch, T. Kirchartz, M. Saliba, T. Unold, and D. Neher, Energy Environ. Sci. **12**, 2778 (2019).
[280]L. Wang, I. King, P. Chen, M. Bates, and R. R. Lunt, APL Mater. **8**, 100904 (2020).
[281]S.-H. Turren-Cruz, A. Hagfeldt, and M. Saliba, Science **362**, 449 (2018).
[282]T. Abzieher, J. A. Schwenzer, S. Moghadamzadeh, F. Sutterluti, I. M. Hossain, M. Pfau, E. Lotter, M. Hetterich, B. S. Richards, U. Lemmer, M. Powalla, and U. W. Paetzold, IEEE J. Photovoltaics **9**, 1249 (2019).

© Author(s) 2021

[283]W. Witte, D. Abou-Ras, K. Albe, G. H. Bauer, F. Bertram, C. Boit, R. Brüggemann, J. Christen, J. Dietrich, A. Eicke, D. Hariskos, M. Maiberg, R. Mainz, M. Meessen, M. Müller, O. Neumann, T. Orgis, S. Paetel, J. Pohl, H. Rodriguez-Alvarez, R. Scheer, H.-W. Schock, T. Unold, A. Weber, and M. Powalla, Prog. Photovoltaics: Res. Appl. **23**, 717 (2014).
[284]T. A. M. Fiducia, B. G. Mendis, K. Li, C. R. M. Grovenor, A. H. Munshi, K. Barth, W. S. Sampath, L. D. Wright, A. Abbas, J. W. Bowers, and J. M. Walls, Nat. Energy **4**, 504 (2019).
[285]A. Agresti, S. Pescetelli, A. L. Palma, B. Martín-García, L. Najafi, S. Bellani, I. Moreels, M. Prato, F. Bonaccorso, and A. Di Carlo, ACS Energy Lett. **4**, 1862 (2019).
[286]F. Fu, T. Feurer, T. P. Weiss, S. Pisoni, E. Avancini, C. Andres, S. Buecheler, and A. N. Tiwari, Nat. Energy **2**, 14083 (2016).
[287]M. Jošt, T. Bertram, D. Koushik, J. A. Marquez, M. A. Verheijen, M. D. Heinemann, E. Köhnen, A. Al-Ashouri, S. Braunger, F. Lang, B. Rech, T. Unold, M. Creatore, I. Lauermann, C. A. Kaufmann, R. Schlatmann, and S. Albrecht, ACS Energy Lett. **4**, 583 (2019).
[288]G. Maculan, A. D. Sheikh, A. L. Abdelhady, M. I. Saidaminov, M. A. Haque, B. Murali, E. Alarousu, O. F. Mohammed, T. Wu, and O. M. Bakr, J. Phys. Chem. Lett. **6**, 3781 (2015).
[289]M. I. Saidaminov, A. L. Abdelhady, G. Maculan, and O. M. Bakr, Chem. Commun. **51**, 17658 (2015).
[290]W. Wang, J. Su, L. Zhang, Y. Lei, D. Wang, D. Lu, and Y. Bai, CrystEngComm **20**, 1635 (2018).
[291]L.-Q. Xie, L. Chen, Z.-A. Nan, H.-X. Lin, T. Wang, D.-P. Zhan, J.-W. Yan, B.-W. Mao, and Z.-Q. Tian, J. Am. Chem. Soc. **139**, 3320 (2017).
[292]L. Chen, Y.-Y. Tan, Z.-X. Chen, T. Wang, S. Hu, Z.-A. Nan, L.-Q. Xie, Y. Hui, J.-X. Huang, C. Zhan, S.-H. Wang, J.-Z. Zhou, J.-W. Yan, B.-W. Mao, and Z.-Q. Tian, J. Am. Chem. Soc. **141**, 1665 (2019).
[293]A. Poglitsch and D. Weber, J. Chem. Phys. **87**, 6373 (1987).
[294]M. I. Saidaminov, A. L. Abdelhady, B. Murali, E. Alarousu, V. M. Burlakov, W. Peng, I. Dursun, L. Wang, Y. He, G. Maculan, A. Goriely, T. Wu, O. F. Mohammed, and O. M. Bakr, Nat. Commun. **6**, 7586 (2015).
[295]D. Shi, V. Adinolfi, R. Comin, M. Yuan, E. Alarousu, A. Buin, Y. Chen, S. Hoogland, A. Rothenberger, K. Katsiev, Y. Losovyj, X. Zhang, P. A. Dowben, O. F. Mohammed, E. H. Sargent, and O. M. Bakr, Science **347**, 519 (2015).
[296]Y. Liu, Z. Yang, and S. F. Liu, Adv. Sci. **5**, 1700471 (2017).
[297]J. Höcker, F. Brust, M. Armer, and V. Dyakonov, CrystEngComm **23**(11), 2202–2207 (2021).
[298]S. Shrestha, G. J. Matt, A. Osvet, D. Niesner, R. Hock, and C. J. Brabec, J. Phys. Chem. C **122**, 5935 (2018).
[299]Q. Dong, Y. Fang, Y. Shao, P. Mulligan, J. Qiu, L. Cao, and J. Huang, Science **347**, 967 (2015).
[300]A. A. Zhumekenov, M. I. Saidaminov, M. A. Haque, E. Alarousu, S. P. Sarmah, B. Murali, I. Dursun, X.-H. Miao, A. L. Abdelhady, T. Wu, O. F. Mohammed, and O. M. Bakr, ACS Energy Lett. **1**, 32 (2016).
[301]Q. Han, S. H. Bae, P. Sun, Y. T. Hsieh, Y. (Michael) Yang, Y. S. Rim, H. Zhao, Q. Chen, W. Shi, G. Li, and Y. Yang, Adv. Mater. **28**, 2253 (2016).
[302]F. Yao, J. Peng, R. Li, W. Li, P. Gui, B. Li, C. Liu, C. Tao, Q. Lin, and G. Fang, Nat. Commun. **11**, 1194 (2020).
[303]H. Wei, D. DeSantis, W. Wei, Y. Deng, D. Guo, T. J. Savenije, L. Cao, and J. Huang, Nat. Mater. **16**, 826 (2017).
[304]Y. Liu, Y. Zhang, Z. Yang, J. Feng, Z. Xu, Q. Li, M. Hu, H. Ye, X. Zhang, M. Liu, K. Zhao, and S. (Frank) Liu, Mater. Today **22**, 67 (2019).
[305]J. Song, Q. Cui, J. Li, J. Xu, Y. Wang, L. Xu, J. Xue, Y. Dong, T. Tian, H. Sun, and H. Zeng, Adv. Opt. Mater. **5**, 1700157 (2017).
[306]J. Höcker, M. Ozcan, S. Hammer, M. Fischer, B. Bichler, M. Armer, P. Rieder, V. Drach, J. Pflaum, B. Nickel, and V. Dyakonov, J. Mater. Chem. C **8**, 8275 (2020).
[307]Z. Chen, Q. Dong, Y. Liu, C. Bao, Y. Fang, Y. Lin, S. Tang, Q. Wang, X. Xiao, Y. Bai, Y. Deng, and J. Huang, Nat. Commun. **8**, 1890 (2017).
[308]Z. Chen, B. Turedi, A. Y. Alsalloum, C. Yang, X. Zheng, I. Gereige, A. AlSaggaf, O. F. Mohammed, and O. M. Bakr, ACS Energy Lett. **4**, 1258 (2019).
[309]A. Y. Alsalloum, B. Turedi, X. Zheng, S. Mitra, A. A. Zhumekenov, K. J. Lee, P. Maity, I. Gereige, A. AlSaggaf, I. S. Roqan, O. F. Mohammed, and O. M. Bakr, ACS Energy Lett. **5**, 657 (2020).
[310]Y. Liu, Y. Zhang, Z. Yang, D. Yang, X. Ren, L. Pang, and S. F. Liu, Adv. Mater. **28**, 9204 (2016).
[311]W. Wei, Y. Zhang, Q. Xu, H. Wei, Y. Fang, Q. Wang, Y. Deng, T. Li, A. Gruverman, L. Cao, and J. Huang, Nat. Photonics **11**, 315 (2017).
[312]E. A. Duijnstee, J. M. Ball, V. M. Le Corre, L. J. A. Koster, H. J. Snaith, and J. Lim, ACS Energy Lett. **5**, 376 (2020).
[313]W. Shockley and H. J. Queisser, J. Appl. Phys. **32**, 510 (1961).
[314]L. Krückemeier, U. Rau, M. Stolterfoht, and T. Kirchartz, Adv. Energy Mater. **10**, 1902573 (2019).
[315]W. van Roosbroeck and W. Shockley, Phys. Rev. **94**, 1558 (1954).
[316]B. Das, I. Aguilera, U. Rau, and T. Kirchartz, Phys. Rev. Mater. **4**, 024602 (2020).
[317]R. E. Brandt, J. R. Poindexter, P. Gorai, R. C. Kurchin, R. L. Z. Hoye, L. Nienhaus, M. W. B. Wilson, J. A. Polizzotti, R. Sereika, R. Žaltauskas, L. C. Lee, J. L. MacManus-Driscoll, M. Bawendi, V. Stevanović, and T. Buonassisi, Chem. Mater. **29**, 4667 (2017).
[318]I. L. Braly, D. W. deQuilettes, L. M. Pazos-Outón, S. Burke, M. E. Ziffer, D. S. Ginger, and H. W. Hillhouse, Nat. Photonics **12**, 355 (2018).
[319]S. Gharibzadeh, B. A. Nejand, M. Jakoby, T. Abzieher, D. Hauschild, S. Moghadamzadeh, J. A. Schwenzer, P. Brenner, R. Schmager, A. A. Haghighirad, L. Weinhardt, U. Lemmer, B. S. Richards, I. A. Howard, and U. W. Paetzold, Adv. Energy Mater. **9**, 1803699 (2019).
[320]D. Luo, W. Yang, Z. Wang, A. Sadhanala, Q. Hu, R. Su, R. Shivanna, G. F. Trindade, J. F. Watts, Z. Xu, T. Liu, K. Chen, F. Ye, P. Wu, L. Zhao, J. Wu, Y. Tu, Y. Zhang, X. Yang, W. Zhang, R. H. Friend, Q. Gong, H. J. Snaith, and R. Zhu, Science **360**, 1442 (2018).
[321]A. Al-Ashouri, A. Magomedov, M. Roß, M. Jošt, M. Talaikis, G. Chistiakova, T. Bertram, J. A. Márquez, E. Köhnen, E. Kasparavičius, S. Levcenco, L. Gil-Escrig, C. J. Hages, R. Schlatmann, B. Rech, T. Malinauskas, T. Unold, C. A. Kaufmann, L. Korte, G. Niaura, V. Getautis, and S. Albrecht, Energy Environ. Sci. **12**, 3356 (2019).
[322]M. A. Green and A. W. Y. Ho-Baillie, ACS Energy Lett. **4**, 1639 (2019).
[323]J. Zhang, Z. Wang, A. Mishra, M. Yu, M. Shasti, W. Tress, D. J. Kubicki, C. E. Avalos, H. Lu, Y. Liu, B. I. Carlsen, A. Agarwalla, Z. Wang, W. Xiang, L. Emsley, Z. Zhang, M. Grätzel, W. Guo, and A. Hagfeldt, Joule **4**, 222 (2020).
[324]M. G. Abebe, A. Abass, G. Gomard, L. Zschiedrich, U. Lemmer, B. S. Richards, C. Rockstuhl, and U. W. Paetzold, Phys. Rev. B **98**, 075141 (2018).
[325]X. Zhang, M. E. Turiansky, J.-X. Shen, and C. G. V. de Walle, Phys. Rev. B **101**, 140101 (2020).
[326]T. Trupke, B. Mitchell, J. W. Weber, W. McMillan, R. A. Bardos, and R. Kroeze, Energy Procedia **15**, 135 (2012).
[327]C. M. Wolff, F. Zu, A. Paulke, L. P. Toro, N. Koch, and D. Neher, Adv. Mater. **29**, 1700159 (2017).
[328]V. Sarritzu, N. Sestu, D. Marongiu, X. Chang, S. Masi, A. Rizzo, S. Colella, F. Quochi, M. Saba, A. Mura, and G. Bongiovanni, Sci. Rep. **7**, 44629 (2017).
[329]J. Wang, W. Fu, S. Jariwala, I. Sinha, A. K.-Y. Jen, and D. S. Ginger, ACS Energy Lett. **4**, 222 (2018).
[330]F. Peña-Camargo, P. Caprioglio, F. Zu, E. Gutierrez-Partida, C. M. Wolff, K. Brinkmann, S. Albrecht, T. Riedl, N. Koch, D. Neher, and M. Stolterfoht, ACS Energy Lett. **5**, 2728 (2020).
[331]H. Min, M. Kim, S.-U. Lee, H. Kim, G. Kim, K. Choi, J. H. Lee, and S. I. Seok, Science **366**, 749 (2019).
[332]M. Stolterfoht, C. M. Wolff, J. A. Márquez, S. Zhang, C. J. Hages, D. Rothhardt, S. Albrecht, P. L. Burn, P. Meredith, T. Unold, and D. Neher, Nat. Energy **3**, 847 (2018).
[333]S. Zhang, S. M. Hosseini, R. Gunder, A. Petsiuk, P. Caprioglio, C. M. Wolff, S. Shoaee, P. Meredith, S. Schorr, T. Unold, P. L. Burn, D. Neher, and M. Stolterfoht, Adv. Mater. **31**, 1901090 (2019).
[334]C. M. Wolff, L. Canil, C. Rehermann, N. N. Linh, F. Zu, M. Ralaiarisoa, P. Caprioglio, L. Fiedler, M. Stolterfoht, S. Kogikoski, I. Bald, N. Koch, E. L. Unger, T. Dittrich, A. Abate, and D. Neher, ACS Nano **14**, 1445 (2020).

© Author(s) 2021

[335]J. Diekmann, P. Caprioglio, M. H. Futscher, V. M. Le Corre, S. Reichert, F. Jaiser, M. Arvind, L. P. Toro, E. Gutierrez-Partida, F. Peña-Camargo, C. Deibel, B. Ehrler, T. Unold, T. Kirchartz, D. Neher, and M. Stolterfoht, Sol. RRL **5**, 2100219 (2021).
[336]C. Momblona, L. Gil-Escrig, E. Bandiello, E. M. Hutter, M. Sessolo, K. Lederer, J. Blochwitz-Nimoth, and H. J. Bolink, Energy Environ. Sci. **9**, 3456 (2016).
[337]N. E. Courtier, J. M. Cave, J. M. Foster, A. B. Walker, and G. Richardson, Energy Environ. Sci. **12**, 396 (2019).
[338]S. A. L. Weber, I. M. Hermes, S.-H. Turren-Cruz, C. Gort, V. W. Bergmann, L. Gilson, A. Hagfeldt, M. Graetzel, W. Tress, and R. Berger, Energy Environ. Sci. **11**, 2404 (2018).
[339]M. H. Futscher, J. M. Lee, L. McGovern, L. A. Muscarella, T. Wang, M. I. Haider, A. Fakharuddin, L. Schmidt-Mende, and B. Ehrler, Mater. Horiz. **6**, 1497 (2019).
[340]L. Bertoluzzi, C. C. Boyd, N. Rolston, J. Xu, R. Prasanna, B. C. O'Regan, and M. D. McGehee, Joule **4**, 109 (2020).
[341]A. Walsh, D. O. Scanlon, S. Chen, X. G. Gong, and S. H. Wei, Angew. Chem., Int. Ed. **54**, 1791 (2014).
[342]O. J. Sandberg, J. Kurpiers, M. Stolterfoht, D. Neher, P. Meredith, S. Shoaee, and A. Armin, Adv. Mater. Interfaces **7**, 2000041 (2020).
[343]H. Jin, E. Debroye, M. Keshavarz, I. G. Scheblykin, M. B. J. Roeffaers, J. Hofkens, and J. A. Steele, Mater. Horiz. **7**, 397 (2020).
[344]B. Chen, P. N. Rudd, S. Yang, Y. Yuan, and J. Huang, Chem. Soc. Rev. **48**, 3842 (2019).
[345]Q. Wang, Q. Dong, T. Li, A. Gruverman, and J. Huang, Adv. Mater. **28**, 6734 (2016).
[346]J. Peng, J. I. Khan, W. Liu, E. Ugur, T. Duong, Y. Wu, H. Shen, K. Wang, H. Dang, E. Aydin, X. Yang, Y. Wan, K. J. Weber, K. R. Catchpole, F. Laquai, S. De Wolf, and T. P. White, Adv. Energy Mater. **8**, 1801208 (2018).
[347]K. T. Cho, S. Paek, G. Grancini, C. Roldán-Carmona, P. Gao, Y. Lee, and M. K. Nazeeruddin, Energy Environ. Sci. **10**, 621 (2017).
[348]K. T. Cho, Y. Zhang, S. Orlandi, M. Cavazzini, I. Zimmermann, A. Lesch, N. Tabet, G. Pozzi, G. Grancini, and M. K. Nazeeruddin, Nano Lett. **18**, 5467 (2018).
[349]P. Caprioglio, F. Zu, C. M. Wolff, J. A. M. Prieto, M. Stolterfoht, P. Becker, N. Koch, T. Unold, B. Rech, S. Albrecht, and D. Neher, Sustainable Energy Fuels **3**, 550 (2019).
[350]X. Zheng, Y. Hou, C. Bao, J. Yin, F. Yuan, Z. Huang, K. Song, J. Liu, J. Troughton, N. Gasparini, C. Zhou, Y. Lin, D.-J. Xue, B. Chen, A. K. Johnston, N. Wei, M. N. Hedhili, M. Wei, A. Y. Alsalloum, P. Maity, B. Turedi, C. Yang, D. Baran, T. D. Anthopoulos, Y. Han, Z.-H. Lu, O. F. Mohammed, F. Gao, E. H. Sargent, and O. M. Bakr, Nat. Energy **5**, 131 (2020).
[351]J. F. Roller, Y.-T. Li, M. Dagenais, and B. H. Hamadani, J. Appl. Phys. **120**, 233108 (2016).
[352]M. Stolterfoht, M. Grischek, P. Caprioglio, C. M. Wolff, E. Gutierrez-Partida, F. Peña-Camargo, D. Rothhardt, S. Zhang, M. Raoufi, J. Wolansky, M. Abdi-Jalebi, S. D. Stranks, S. Albrecht, T. Kirchartz, and D. Neher, Adv. Mater. **32**, 2000080 (2020).
[353]L. A. Frolova, N. N. Dremova, and P. A. Troshin, Chem. Commun. **51**, 14917 (2015).
[354]Q. Wang, Y. Shao, H. Xie, L. Lyu, X. Liu, Y. Gao, and J. Huang, Appl. Phys. Lett. **105**, 163508 (2014).
[355]J. M. Ball and A. Petrozza, Nat. Energy **1**, 16149 (2016).
[356]W.-J. Yin, T. Shi, and Y. Yan, Appl. Phys. Lett. **104**, 063903 (2014).
[357]L. Huang, S. Bu, D. Zhang, R. Peng, Q. Wei, Z. Ge, and J. Zhang, Sol. RRL **3**, 1800274 (2018).
[358]D. Song, P. Cui, T. Wang, D. Wei, M. Li, F. Cao, X. Yue, P. Fu, Y. Li, Y. He, B. Jiang, and M. Trevor, J. Phys. Chem. C **119**, 22812 (2015).
[359]U. Wurfel, A. Cuevas, and P. Wurfel, IEEE J. Photovoltaics **5**, 461 (2015).
[360]S. Pitchaiya, M. Natarajan, A. Santhanam, V. Asokan, A. Yuvapragasam, V. M. Ramakrishnan, S. E. Palanisamy, S. Sundaram, and D. Velauthapillai, Arabian J. Chem. **13**, 2526 (2020).
[361]H.-S. Lin, I. Jeon, R. Xiang, S. Seo, J.-W. Lee, C. Li, A. Pal, S. Manzhos, M. S. Goorsky, Y. Yang, S. Maruyama, and Y. Matsuo, ACS Appl. Mater. Interfaces **10**, 39590 (2018).
[362]C. Xu, Z. Liu, and E.-C. Lee, J. Mater. Chem. C **7**, 6956 (2019).
[363]A. Hultqvist, T. J. Jacobsson, S. Svanström, M. Edoff, U. B. Cappel, H. Rensmo, E. M. J. Johansson, G. Boschloo, and T. Törndahl, ACS Appl. Energy Mater. **4**, 510 (2021).
[364]S. Jeong, S. Seo, H. Park, and H. Shin, Chem. Commun. **55**, 2433 (2019).
[365]P. Calado, A. M. Telford, D. Bryant, X. Li, J. Nelson, B. C. O'Regan, and P. R. F. Barnes, Nat. Commun. **7**, 13831 (2016).
[366]L. Bertoluzzi, R. A. Belisle, K. A. Bush, R. Cheacharoen, M. D. McGehee, and B. C. O'Regan, J. Am. Chem. Soc. **140**, 12775 (2018).
[367]H. Zhang, X. Fu, Y. Tang, H. Wang, C. Zhang, W. W. Yu, X. Wang, Y. Zhang, and M. Xiao, Nat. Commun. **10**, 1088 (2019).
[368]L. McGovern, M. H. Futscher, L. A. Muscarella, and B. Ehrler, J. Phys. Chem. Lett. **11**, 7127 (2020).
[369]D. Walter, A. Fell, Y. Wu, T. Duong, C. Barugkin, N. Wu, T. White, and K. Weber, J. Phys. Chem. C **122**, 11270 (2018).
[370]K. Domanski, B. Roose, T. Matsui, M. Saliba, S.-H. Turren-Cruz, J.-P. Correa-Baena, C. R. Carmona, G. Richardson, J. M. Foster, F. De Angelis, J. M. Ball, A. Petrozza, N. Mine, M. K. Nazeeruddin, W. Tress, M. Grätzel, U. Steiner, A. Hagfeldt, and A. Abate, Energy Environ. Sci. **10**, 604 (2017).
[371]M. T. Neukom, A. Schiller, S. Züfle, E. Knapp, J. Ávila, D. Pérez-del-Rey, C. Dreessen, K. P. S. Zanoni, M. Sessolo, H. J. Bolink, and B. Ruhstaller, ACS Appl. Mater. Interfaces **11**, 23320 (2019).
[372]J. Herterich, M. Unmüssig, G. Loukeris, M. Kohlstädt, and U. Würfel, Energy Technol. **9**, 2001104 (2021).
[373]M. H. Futscher, M. K. Gangishetty, D. N. Congreve, and B. Ehrler, J. Chem. Phys. **152**, 044202 (2020).
[374]T. Elmelund, R. A. Scheidt, B. Seger, and P. V. Kamat, ACS Energy Lett. **4**, 1961 (2019).
[375]T. Zhu, D. Zheng, J. Liu, L. Coolen, and T. Pauporté, ACS Appl. Mater. Interfaces **12**, 37197 (2020).
[376]F. Wang, A. Shimazaki, F. Yang, K. Kanahashi, K. Matsuki, Y. Miyauchi, T. Takenobu, A. Wakamiya, Y. Murata, and K. Matsuda, J. Phys. Chem. C **121**, 1562 (2017).
[377]J. Peng, Y. Wu, W. Ye, D. A. Jacobs, H. Shen, X. Fu, Y. Wan, T. Duong, N. Wu, C. Barugkin, H. T. Nguyen, D. Zhong, J. Li, T. Lu, Y. Liu, M. N. Lockrey, K. J. Weber, K. R. Catchpole, and T. P. White, Energy Environ. Sci. **10**, 1792 (2017).
[378]M. E. F. Bouduban, V. I. E. Queloz, V. M. Caselli, K. T. Cho, A. R. Kirmani, S. Paek, C. Roldan-Carmona, L. J. Richter, J. E. Moser, T. J. Savenije, M. K. Nazeeruddin, and G. Grancini, J. Phys. Chem. Lett. **10**, 5713 (2019).
[379]S. Paek, C. Roldán-Carmona, K. T. Cho, M. Franckevičius, H. Kim, H. Kanda, N. Drigo, K. H. Lin, M. Pei, R. Gegevičius, H. J. Yun, H. Yang, P. A. Schouwink, C. Corminboeuf, A. M. Asiri, and M. K. Nazeeruddin, Adv. Sci. **7**, 2001014 (2020).
[380]S. Bai, P. Da, C. Li, Z. Wang, Z. Yuan, F. Fu, M. Kawecki, X. Liu, N. Sakai, J. T.-W. Wang, S. Huettner, S. Buecheler, M. Fahlman, F. Gao, and H. J. Snaith, Nature **571**, 245 (2019).
[381]H.-S. Kim, C.-R. Lee, J.-H. Im, K.-B. Lee, T. Moehl, A. Marchioro, S.-J. Moon, R. Humphry-Baker, J.-H. Yum, J. E. Moser, M. Grätzel, and N.-G. Park, Sci. Rep. **2**, 591 (2012).
[382]M. M. Lee, J. Teuscher, T. Miyasaka, T. N. Murakami, and H. J. Snaith, Science **338**, 643 (2012).
[383]G. W. Kim, H. Choi, M. Kim, J. Lee, S. Y. Son, and T. Park, Adv. Energy Mater. **10**, 1903403 (2020).
[384]Z. Cao, C. Li, X. Deng, S. Wang, Y. Yuan, Y. Chen, Z. Wang, Y. Liu, L. Ding, and F. Hao, J. Mater. Chem. A **8**, 19768 (2020).
[385]Q. Jiang, X. Zhang, and J. You, Small **14**, 1801154 (2018).
[386]S. Sun, T. Salim, N. Mathews, M. Duchamp, C. Boothroyd, G. Xing, T. C. Sum, and Y. M. Lam, Energy Environ. Sci. **7**, 399 (2014).
[387]Z. Yu and L. Sun, Small Methods **2**, 1700280 (2017).
[388]J. Mohanraj, M. Stihl, E. Simon, O. von Sicard, G. Schmidt, M. Fleischer, C. Neuber, and M. Thelakkat, ACS Appl. Energy Mater. **2**, 3469 (2019).
[389]B. Tan, S. R. Raga, A. S. R. Chesman, S. O. Fürer, F. Zheng, D. P. McMeekin, L. Jiang, W. Mao, X. Lin, X. Wen, J. Lu, Y. B. Cheng, and U. Bach, Adv. Energy Mater. **9**, 1901519 (2019).

© Author(s) 2021

[390]C. C. Boyd, R. Cheacharoen, T. Leijtens, and M. D. McGehee, Chem. Rev. **119**, 3418 (2018).
[391]S. Ito, S. Tanaka, K. Manabe, and H. Nishino, J. Phys. Chem. C **118**, 16995 (2014).
[392]W. Li, H. Dong, G. Dong, and L. Wang, Org. Electron. **26**, 208 (2015).
[393]J. Yang, B. D. Siempelkamp, E. Mosconi, F. De Angelis, and T. L. Kelly, Chem. Mater. **27**, 4229 (2015).
[394]J. Liu, S. K. Pathak, N. Sakai, R. Sheng, S. Bai, Z. Wang, and H. J. Snaith, Adv. Mater. Interfaces **3**, 1600571 (2016).
[395]X. Sun, L. Y. Ji, W. W. Chen, X. Guo, H. H. Wang, M. Lei, Q. Wang, and Y. F. Li, J. Mater. Chem. A **5**, 20720 (2017).
[396]Y. Kato, L. K. Ono, M. V. Lee, S. Wang, S. R. Raga, and Y. Qi, Adv. Mater. Interfaces **2**, 1500195 (2015).
[397]K. Domanski, J.-P. Correa-Baena, N. Mine, M. K. Nazeeruddin, A. Abate, M. Saliba, W. Tress, A. Hagfeldt, and M. Grätzel, ACS Nano **10**, 6306 (2016).
[398]H. Choi, C.-K. Mai, H.-B. Kim, J. Jeong, S. Song, G. C. Bazan, J. Y. Kim, and A. J. Heeger, Nat. Commun. **6**, 7348 (2015).
[399]S. N. Habisreutinger, N. K. Noel, H. J. Snaith, and R. J. Nicholas, Adv. Energy Mater. **7**, 1601079 (2016).
[400]J. A. Dawson, A. J. Naylor, C. Eames, M. Roberts, W. Zhang, H. J. Snaith, P. G. Bruce, and M. S. Islam, ACS Energy Lett. **2**, 1818 (2017).
[401]L. K. Ono, S. R. Raga, M. Remeika, A. J. Winchester, A. Gabe, and Y. Qi, J. Mater. Chem. A **3**, 15451 (2015).
[402]Z. Hawash, L. K. Ono, and Y. Qi, Adv. Mater. Interfaces **5**, 1700623 (2017).
[403]N.-G. Park and H. Segawa, ACS Photonics **5**, 2970 (2018).
[404]B. Roose, Q. Wang, and A. Abate, Adv. Energy Mater. **9**, 1803140 (2018).
[405]A. Rajagopal, K. Yao, and A. K. Y. Jen, Adv. Mater. **30**, 1800455 (2018).
[406]Y. Bai, Q. Dong, Y. Shao, Y. Deng, Q. Wang, L. Shen, D. Wang, W. Wei, and J. Huang, Nat. Commun. **7**, 12806 (2016).
[407]Z. Zhu, D. Zhao, C.-C. Chueh, X. Shi, Z. Li, and A. K.-Y. Jen, Joule **2**, 168 (2018).
[408]A. Pellaroque, N. K. Noel, S. N. Habisreutinger, Y. Zhang, S. Barlow, S. R. Marder, and H. J. Snaith, ACS Energy Lett. **2**, 2044 (2017).
[409]J. Liu, W. Liu, E. Aydin, G. T. Harrison, F. H. Isikgor, X. Yang, A. S. Subbiah, and S. De Wolf, ACS Appl. Mater. Interfaces **12**, 23874 (2020).
[410]H. D. Pham, T. C. J. Yang, S. M. Jain, G. J. Wilson, and P. Sonar, Adv. Energy Mater. **10**, 1903326 (2020).
[411]K. Aitola, K. Domanski, J.-P. Correa-Baena, K. Sveinbjörnsson, M. Saliba, A. Abate, M. Grätzel, E. Kauppinen, E. M. J. Johansson, W. Tress, A. Hagfeldt, and G. Boschloo, Adv. Mater. **29**, 1606398 (2017).
[412]S. N. Habisreutinger, T. Leijtens, G. E. Eperon, S. D. Stranks, R. J. Nicholas, and H. J. Snaith, Nano Lett. **14**, 5561 (2014).
[413]G.-W. Kim, G. Kang, M. M. Byranvand, G.-Y. Lee, and T. Park, ACS Appl. Mater. Interfaces **9**, 27720 (2017).
[414]J.-F. Liao, W.-Q. Wu, Y. Jiang, J.-X. Zhong, L. Wang, and D.-B. Kuang, Chem. Soc. Rev. **49**, 354 (2020).
[415]A. Mei, X. Li, L. Liu, Z. Ku, T. Liu, Y. Rong, M. Xu, M. Hu, J. Chen, Y. Yang, M. Gratzel, and H. Han, Science **345**, 295 (2014).
[416]S. Béchu, M. Ralaiarisoa, A. Etcheberry, and P. Schulz, Adv. Energy Mater. **10**, 1904007 (2020).
[417]P. Fassl, V. Lami, A. Bausch, Z. Wang, M. T. Klug, H. J. Snaith, and Y. Vaynzof, Energy Environ. Sci. **11**, 3380 (2018).
[418]T. Hellmann, C. Das, T. Abzieher, J. A. Schwenzer, M. Wussler, R. Dachauer, U. W. Paetzold, W. Jaegermann, and T. Mayer, Adv. Energy Mater. **10**, 2002129 (2020).
[419]S. Cacovich, D. Messou, A. Bercegol, S. Béchu, A. Yaiche, H. Shafique, J. Rousset, P. Schulz, M. Bouttemy, and L. Lombez, ACS Appl. Mater. Interfaces **12**, 34784 (2020).
[420]B. Philippe, M. Saliba, J.-P. Correa-Baena, U. B. Cappel, S.-H. Turren-Cruz, M. Grätzel, A. Hagfeldt, and H. Rensmo, Chem. Mater. **29**, 3589 (2017).
[421]J. Byeon, J. Kim, J.-Y. Kim, G. Lee, K. Bang, N. Ahn, and M. Choi, ACS Energy Lett. **5**, 2580 (2020).
[422]C. Das, M. Wussler, T. Hellmann, T. Mayer, and W. Jaegermann, Phys. Chem. Chem. Phys. **20**, 17180 (2018).
[423]C. Das, M. Wussler, T. Hellmann, T. Mayer, I. Zimmermann, C. Maheu, M. K. Nazeeruddin, and W. Jaegermann, ACS Appl. Mater. Interfaces **12**, 40949 (2020).
[424]M. Wussler, T. Mayer, C. Das, E. Mankel, T. Hellmann, C. Prabowo, I. Zimmermann, M. K. Nazeeruddin, and W. Jaegermann, Adv. Funct. Mater. **30**, 1910679 (2020).
[425]X. Yang, D. Luo, Y. Xiang, L. Zhao, M. Anaya, Y. Shen, J. Wu, W. Yang, Y. H. Chiang, Y. Tu, R. Su, Q. Hu, H. Yu, G. Shao, W. Huang, T. P. Russell, Q. Gong, S. D. Stranks, W. Zhang, and R. Zhu, Adv. Mater. **33**, 2006435 (2021).
[426]D. Niesner, H. Zhu, K. Miyata, P. P. Joshi, T. J. S. Evans, B. J. Kudisch, M. T. Trinh, M. Marks, and X.-Y. Zhu, J. Am. Chem. Soc. **138**, 15717 (2016).
[427]D. Niesner, M. Wilhelm, I. Levchuk, A. Osvet, S. Shrestha, M. Batentschuk, C. Brabec, and T. Fauster, Phys. Rev. Lett. **117**, 126401 (2016).
[428]M. Puppin, S. Polishchuk, N. Colonna, A. Crepaldi, D. N. Dirin, O. Nazarenko, R. D. Gennaro, G. Gatti, S. Roth, T. Barillot, L. Poletto, R. P. Xian, L. Rettig, M. Wolf, R. Ernstorfer, M. V. Kovalenko, N. Marzari, M. Grioni, and M. Chergui, Phys. Rev. Lett. **124**, 206402 (2020).
[429]P. Nandi, S. K. Pandey, C. Giri, V. Singh, L. Petaccia, U. Manju, S. D. Mahanti, and D. Topwal, J. Phys. Chem. Lett. **11**, 5719 (2020).
[430]D. Niesner, APL Mater. **8**, 090704 (2020).
[431]J. Yang, M. Meissner, T. Yamaguchi, B. Xi, K. Takahashi, S. A. A. Rahman, X. Liu, H. Yoshida, M. Fahlman, and S. Kera, Phys. Rev. B **102**, 245101 (2020).
[432]M. Sajedi, M. Krivenkov, D. Marchenko, A. Varykhalov, J. Sánchez-Barriga, E. D. L. Rienks, and O. Rader, Phys. Rev. B **102**, 081116 (2020).
[433]Z. Chen, M.-i. Lee, Z. Zhang, H. Diab, D. Garrot, F. Lédée, P. Fertey, E. Papalazarou, M. Marsi, C. Ponseca, E. Deleporte, A. Tejeda, and L. Perfetti, Phys. Rev. Mater. **1**, 045402 (2017).
[434]T. J. S. Evans, K. Miyata, P. P. Joshi, S. Maehrlein, F. Liu, and X.-Y. Zhu, J. Phys. Chem. C **122**, 13724 (2018).
[435]H.-C. Hsu, B.-C. Huang, S.-C. Chin, C.-R. Hsing, D.-L. Nguyen, M. Schnedler, R. Sankar, R. E. Dunin-Borkowski, C.-M. Wei, C.-W. Chen, P. Ebert, and Y.-P. Chiu, ACS Nano **13**, 4402 (2019).
[436]R. Ohmann, L. K. Ono, H.-S. Kim, H. Lin, M. V. Lee, Y. Li, N.-G. Park, and Y. Qi, J. Am. Chem. Soc. **137**, 16049 (2015).
[437]F.-S. Zu, P. Amsalem, I. Salzmann, R.-B. Wang, M. Ralaiarisoa, S. Kowarik, S. Duhm, and N. Koch, Adv. Opt. Mater. **5**, 1700139 (2017).
[438]L. She, M. Liu, X. Li, Z. Cai, and D. Zhong, Surf. Sci. **656**, 17 (2017).
[439]J. Hieulle, C. Stecker, R. Ohmann, L. K. Ono, and Y. Qi, Small Methods **2**, 1700295 (2017).
[440]A. Al-Ashouri, E. Köhnen, B. Li, A. Magomedov, H. Hempel, P. Caprioglio, J. A. Márquez, A. B. M. Vilches, E. Kasparavicius, J. A. Smith, N. Phung, D. Menzel, M. Grischek, L. Kegelmann, D. Skroblin, C. Gollwitzer, T. Malinauskas, M. Jošt, G. Matič, B. Rech, R. Schlatmann, M. Topič, L. Korte, A. Abate, B. Stannowski, D. Neher, M. Stolterfoht, T. Unold, V. Getautis, and S. Albrecht, Science **370**, 1300 (2020).
[441]X. Chen, Z. Jia, Z. Chen, T. Jiang, L. Bai, F. Tao, J. Chen, X. Chen, T. Liu, X. Xu, C. Yang, W. Shen, W. E. I. Sha, H. Zhu, and Y. (Michael) Yang, Joule **4**, 1594 (2020).
[442]K. Xiao, R. Lin, Q. Han, Y. Hou, Z. Qin, H. T. Nguyen, J. Wen, M. Wei, V. Yeddu, M. I. Saidaminov, Y. Gao, X. Luo, Y. Wang, H. Gao, C. Zhang, J. Xu, J. Zhu, E. H. Sargent, and H. Tan, Nat. Energy **5**, 870 (2020).
[443]A. Martí and G. L. Araújo, Sol. Energy Mater. Sol. Cells **43**, 203 (1996).
[444]B. Chen, S.-W. Baek, Y. Hou, E. Aydin, M. D. Bastiani, B. Scheffel, A. Proppe, Z. Huang, M. Wei, Y.-K. Wang, E.-H. Jung, T. G. Allen, E. V. Kerschaver, F. P. G. de Arquer, M. I. Saidaminov, S. Hoogland, S. D. Wolf, and E. H. Sargent, Nat. Commun. **11**, 1257 (2020).
[445]P. Tockhorn, P. Wagner, L. Kegelmann, J.-C. Stang, M. Mews, S. Albrecht, and L. Korte, ACS Appl. Energy Mater. **3**, 1381 (2020).
[446]J. Werner, B. Niesen, and C. Ballif, Adv. Mater. Interfaces **5**, 1700731 (2017).
[447]M. Boccard and C. Ballif, ACS Energy Lett. **5**, 1077 (2020).
[448]M. A. Green, E. D. Dunlop, J. Hohl-Ebinger, M. Yoshita, N. Kopidakis, and X. Hao, Prog. Photovoltaics: Res. Appl. **28**, 629 (2020).

© Author(s) 2021

[449]D. H. Kim, C. P. Muzzillo, J. Tong, A. F. Palmstrom, B. W. Larson, C. Choi, S. P. Harvey, S. Glynn, J. B. Whitaker, F. Zhang, Z. Li, H. Lu, M. F. A. M. van Hest, J. J. Berry, L. M. Mansfield, Y. Huang, Y. Yan, and K. Zhu, Joule **3**, 1734 (2019).
[450]J. Tong, Z. Song, D. H. Kim, X. Chen, C. Chen, A. F. Palmstrom, P. F. Ndione, M. O. Reese, S. P. Dunfield, O. G. Reid, J. Liu, F. Zhang, S. P. Harvey, Z. Li, S. T. Christensen, G. Teeter, D. Zhao, M. M. Al-Jassim, M. F. A. M. van Hest, M. C. Beard, S. E. Shaheen, J. J. Berry, Y. Yan, and K. Zhu, Science **364**, 475 (2019).
[451]M. Jošt, L. Kegelmann, L. Korte, and S. Albrecht, Adv. Energy Mater. **10**, 1904102 (2020).
[452]Q. Han, Y.-T. Hsieh, L. Meng, J.-L. Wu, P. Sun, E.-P. Yao, S.-Y. Chang, S.-H. Bae, T. Kato, V. Bermudez, and Y. Yang, Science **361**, 904 (2018).
[453]G. E. Eperon, T. Leijtens, K. A. Bush, R. Prasanna, T. Green, J. T.-W. Wang, D. P. McMeekin, G. Volonakis, R. L. Milot, R. May, A. Palmstrom, D. J. Slotcavage, R. A. Belisle, J. B. Patel, E. S. Parrott, R. J. Sutton, W. Ma, F. Moghadam, B. Conings, A. Babayigit, H.-G. Boyen, S. Bent, F. Giustino, L. M. Herz, M. B. Johnston, M. D. McGehee, and H. J. Snaith, Science **354**, 861 (2016).
[454]D. Zhao, C. Chen, C. Wang, M. M. Junda, Z. Song, C. R. Grice, Y. Yu, C. Li, B. Subedi, N. J. Podraza, X. Zhao, G. Fang, R.-G. Xiong, K. Zhu, and Y. Yan, Nat. Energy **3**, 1093 (2018).
[455]Z. Yang, Z. Yu, H. Wei, X. Xiao, Z. Ni, B. Chen, Y. Deng, S. N. Habisreutinger, X. Chen, K. Wang, J. Zhao, P. N. Rudd, J. J. Berry, M. C. Beard, and J. Huang, Nat. Commun. **10**, 4498 (2019).
[456]Z. Yu, Z. Yang, Z. Ni, Y. Shao, B. Chen, Y. Lin, H. Wei, Z. J. Yu, Z. Holman, and J. Huang, Nat. Energy **5**, 657 (2020).
[457]R. Lin, K. Xiao, Z. Qin, Q. Han, C. Zhang, M. Wei, M. I. Saidaminov, Y. Gao, J. Xu, M. Xiao, A. Li, J. Zhu, E. H. Sargent, and H. Tan, Nat. Energy **4**, 864 (2019).
[458]C. Li, Z. Song, C. Chen, C. Xiao, B. Subedi, S. P. Harvey, N. Shrestha, K. K. Subedi, L. Chen, D. Liu, Y. Li, Y.-W. Kim, C.-s. Jiang, M. J. Heben, D. Zhao, R. J. Ellingson, N. J. Podraza, M. Al-Jassim, and Y. Yan, Nat. Energy **5**, 768 (2020).
[459]M. Wei, K. Xiao, G. Walters, R. Lin, Y. Zhao, M. I. Saidaminov, P. Todorović, A. Johnston, Z. Huang, H. Chen, A. Li, J. Zhu, Z. Yang, Y. K. Wang, A. H. Proppe, S. O. Kelley, Y. Hou, O. Voznyy, H. Tan, and E. H. Sargent, Adv. Mater. **32**, 1907058 (2020).
[460]A. F. Palmstrom, G. E. Eperon, T. Leijtens, R. Prasanna, S. N. Habisreutinger, W. Nemeth, E. A. Gaulding, S. P. Dunfield, M. Reese, S. Nanayakkara, T. Moot, J. Werner, J. Liu, B. To, S. T. Christensen, M. D. McGehee, M. F. A. M. van Hest, J. M. Luther, J. J. Berry, and D. T. Moore, Joule **3**, 2193 (2019).
[461]Y. Zhou, F. Wang, Y. Cao, J.-P. Wang, H.-H. Fang, M. A. Loi, N. Zhao, and C.-P. Wong, Adv. Energy Mater. **7**, 1701048 (2017).
[462]D. Zhao, Y. Yu, C. Wang, W. Liao, N. Shrestha, C. R. Grice, A. J. Cimaroli, L. Guan, R. J. Ellingson, K. Zhu, X. Zhao, R.-G. Xiong, and Y. Yan, Nat. Energy **2**, 17018 (2017).
[463]T. Leijtens, K. A. Bush, R. Prasanna, and M. D. McGehee, Nat. Energy **3**, 828 (2018).
[464]X. Yi, Z. Zhang, A. Chang, Y. Mao, Y. Luan, T. Lin, Y. Wei, Y. Zhang, F. Wang, S. Cao, C. Li, and J. Wang, Adv. Energy Mater. **9**, 1901726 (2019).
[465]Z. Wang, Q. Lin, F. P. Chmiel, N. Sakai, L. M. Herz, and H. J. Snaith, Nat. Energy **2**, 17135 (2017).
[466]B. Saparov, F. Hong, J.-P. Sun, H.-S. Duan, W. Meng, S. Cameron, I. G. Hill, Y. Yan, and D. B. Mitzi, Chem. Mater. **27**, 5622 (2015).
[467]M. Abdi-Jalebi, Z. Andaji-Garmaroudi, S. Cacovich, C. Stavrakas, B. Philippe, J. M. Richter, M. Alsari, E. P. Booker, E. M. Hutter, A. J. Pearson, S. Lilliu, T. J. Savenije, H. Rensmo, G. Divitini, C. Ducati, R. H. Friend, and S. D. Stranks, Nature **555**, 497 (2018).
[468]G. E. Eperon, K. H. Stone, L. E. Mundt, T. H. Schloemer, S. N. Habisreutinger, S. P. Dunfield, L. T. Schelhas, J. J. Berry, and D. T. Moore, ACS Energy Lett. **5**, 1856 (2020).
[469]Y.-H. Lin, N. Sakai, P. Da, J. Wu, H. C. Sansom, A. J. Ramadan, S. Mahesh, J. Liu, R. D. J. Oliver, J. Lim, L. Aspitarte, K. Sharma, P. K. Madhu, A. B. Morales-Vilches, P. K. Nayak, S. Bai, F. Gao, C. R. M. Grovenor, M. B. Johnston, J. G. Labram, J. R. Durrant, J. M. Ball, B. Wenger, B. Stannowski, and H. J. Snaith, Science **369**, 96 (2020).
[470]J. Xu, C. C. Boyd, Z. J. Yu, A. F. Palmstrom, D. J. Witter, B. W. Larson, R. M. France, J. Werner, S. P. Harvey, E. J. Wolf, W. Weigand, S. Manzoor, M. F. A. M. van Hest, J. J. Berry, J. M. Luther, Z. C. Holman, and M. D. McGehee, Science **367**, 1097 (2020).
[471]L. Ma, F. Hao, C. C. Stoumpos, B. T. Phelan, M. R. Wasielewski, and M. G. Kanatzidis, J. Am. Chem. Soc. **138**, 14750 (2016).
[472]S. J. Lee, S. S. Shin, Y. C. Kim, D. Kim, T. K. Ahn, J. H. Noh, J. Seo, and S. I. Seok, J. Am. Chem. Soc. **138**, 3974 (2016).
[473]Q. Tai, X. Guo, G. Tang, P. You, T.-W. Ng, D. Shen, J. Cao, C.-K. Liu, N. Wang, Y. Zhu, C.-S. Lee, and F. Yan, Angew. Chem., Int. Ed. **58**, 806 (2018).
[474]T. Nakamura, S. Yakumaru, M. A. Truong, K. Kim, J. Liu, S. Hu, K. Otsuka, R. Hashimoto, R. Murdey, T. Sasamori, H. D. Kim, H. Ohkita, T. Handa, Y. Kanemitsu, and A. Wakamiya, Nat. Commun. **11**, 3008 (2020).
[475]J. Pascual, G. Nasti, M. H. Aldamasy, J. A. Smith, M. Flatken, N. Phung, D. Di Girolamo, S.-H. Turren-Cruz, M. Li, A. Dallmann, R. Avolio, and A. Abate, Mater. Adv. **1**, 1066 (2020).
[476]M. Jošt, E. Köhnen, A. B. Morales-Vilches, B. Lipovšek, K. Jäger, B. Macco, A. Al-Ashouri, J. Krč, L. Korte, B. Rech, R. Schlatmann, M. Topič, B. Stannowski, and S. Albrecht, Energy Environ. Sci. **11**, 3511 (2018).
[477]C. Li, Y. Ma, Y. Xiao, L. Shen, and L. Ding, InfoMat **2**, 1247 (2020).
[478]Y. C. Kim, K. H. Kim, D.-Y. Son, D.-N. Jeong, J.-Y. Seo, Y. S. Choi, I. T. Han, S. Y. Lee, and N.-G. Park, Nature **550**, 87 (2017).
[479]H. Wei and J. Huang, Nat. Commun. **10**, 1066 (2019).
[480]H. Wu, Y. Ge, G. Niu, and J. Tang, Matter **4**, 144 (2021).
[481]S. Adjokatse, H.-H. Fang, and M. A. Loi, Mater. Today **20**, 413 (2017).
[482]B. R. Sutherland and E. H. Sargent, Nat. Photonics **10**, 295 (2016).
[483]Y. Fang, Q. Dong, Y. Shao, Y. Yuan, and J. Huang, Nat. Photonics **9**, 679 (2015).
[484]Y. Lee, J. Kwon, E. Hwang, C.-H. Ra, W. J. Yoo, J.-H. Ahn, J. H. Park, and J. H. Cho, Adv. Mater. **27**, 41 (2014).
[485]K. Lin, J. Xing, L. N. Quan, F. P. G. de Arquer, X. Gong, J. Lu, L. Xie, W. Zhao, D. Zhang, C. Yan, W. Li, X. Liu, Y. Lu, J. Kirman, E. H. Sargent, Q. Xiong, and Z. Wei, Nature **562**, 245 (2018).
[486]F. Deschler, M. Price, S. Pathak, L. E. Klintberg, D.-D. Jarausch, R. Higler, S. Hüttner, T. Leijtens, S. D. Stranks, H. J. Snaith, M. Atatüre, R. T. Phillips, and R. H. Friend, J. Phys. Chem. Lett. **5**, 1421 (2014).
[487]Y. Fu, H. Zhu, C. C. Stoumpos, Q. Ding, J. Wang, M. G. Kanatzidis, X. Zhu, and S. Jin, ACS Nano **10**, 7963 (2016).
[488]C. Xie, C. K. Liu, H. L. Loi, and F. Yan, Adv. Funct. Mater. **30**, 1903907 (2019).
[489]Q. Chen, J. Wu, X. Ou, B. Huang, J. Almutlaq, A. A. Zhumekenov, X. Guan, S. Han, L. Liang, Z. Yi, J. Li, X. Xie, Y. Wang, Y. Li, D. Fan, D. B. L. Teh, A. H. All, O. F. Mohammed, O. M. Bakr, T. Wu, M. Bettinelli, H. Yang, W. Huang, and X. Liu, Nature **561**, 88 (2018).
[490]K. Hecht, Z. Phys. **77**, 235 (1932).
[491]M. Lehnhardt, T. Riedl, T. Weimann, and W. Kowalsky, Phys. Rev. B **81**, 165206 (2010).
[492]T. Rabe, P. Görrn, M. Lehnhardt, M. Tilgner, T. Riedl, and W. Kowalsky, Phys. Rev. Lett. **102**, 137401 (2009).
[493]Y. Fu, H. Zhu, A. W. Schrader, D. Liang, Q. Ding, P. Joshi, L. Hwang, X.-Y. Zhu, and S. Jin, Nano Lett. **16**, 1000 (2016).
[494]Y. Jia, R. A. Kerner, A. J. Grede, A. N. Brigeman, B. P. Rand, and N. C. Giebink, Nano Lett. **16**, 4624 (2016).
[495]N. Pourdavoud, T. Haeger, A. Mayer, P. J. Cegielski, A. L. Giesecke, R. Heiderhoff, S. Olthof, S. Zaefferer, I. Shutsko, A. Henkel, D. Becker-Koch, M. Stein, M. Cehovski, O. Charfi, H. H. Johannes, D. Rogalla, M. C. Lemme, M. Koch, Y. Vaynzof, K. Meerholz, W. Kowalsky, H. C. Scheer, P. Görrn, and T. Riedl, Adv. Mater. **31**, 1903717 (2019).
[496]N. Pourdavoud, A. Mayer, M. Buchmüller, K. Brinkmann, T. Häger, T. Hu, R. Heiderhoff, I. Shutsko, P. Görrn, Y. Chen, H.-C. Scheer, and T. Riedl, Adv. Mater. Technol. **3**, 1700253 (2018).
[497]C. Qin, A. S. D. Sandanayaka, C. Zhao, T. Matsushima, D. Zhang, T. Fujihara, and C. Adachi, Nature **585**, 53 (2020).
[498]C. Huang, C. Zhang, S. Xiao, Y. Wang, Y. Fan, Y. Liu, N. Zhang, G. Qu, H. Ji, J. Han, L. Ge, Y. Kivshar, and Q. Song, Science **367**, 1018 (2020).

© Author(s) 2021

[499]N. Pourdavoud, S. Wang, A. Mayer, T. Hu, Y. Chen, A. Marianovich, W. Kowalsky, R. Heiderhoff, H.-C. Scheer, and T. Riedl, Adv. Mater. **29**, 1605003 (2017).
[500]Y. Jia, R. A. Kerner, A. J. Grede, B. P. Rand, and N. C. Giebink, Nat. Photonics **11**, 784 (2017).
[501]P. Brenner, O. Bar-On, M. Jakoby, I. Allegro, B. S. Richards, U. W. Paetzold, I. A. Howard, J. Scheuer, and U. Lemmer, Nat. Commun. **10**, 988 (2019).
[502]W. Sun, Y. Liu, G. Qu, Y. Fan, W. Dai, Y. Wang, Q. Song, J. Han, and S. Xiao, Nat. Commun. **11**, 4862 (2020).
[503]P. Schulz, D. Cahen, and A. Kahn, Chem. Rev. **119**, 3349 (2019).
[504]K. O. Brinkmann, J. He, F. Schubert, J. Malerczyk, C. Kreusel, F. van gen Hassend, S. Weber, J. Song, J. Qu, and T. Riedl, ACS Appl. Mater. Interfaces **11**, 40172 (2019).
[505]F. Wang, S. Bai, W. Tress, A. Hagfeldt, and F. Gao, npj Flexible Electron. **2**, 22 (2018).
[506]L. Fu, H. Li, L. Wang, R. Yin, B. Li, and L. Yin, Energy Environ. Sci. **13**, 4017 (2020).
[507]D. W. deQuilettes, S. Koch, S. Burke, R. K. Paranji, A. J. Shropshire, M. E. Ziffer, and D. S. Ginger, ACS Energy Lett. **1**, 438 (2016).
[508]B.-W. Park, N. Kedem, M. Kulbak, D. Y. Lee, W. S. Yang, N. J. Jeon, J. Seo, G. Kim, K. J. Kim, T. J. Shin, G. Hodes, D. Cahen, and S. I. Seok, Nat. Commun. **9**, 3301 (2018).
[509]Y. He, M. Petryk, Z. Liu, D. G. Chica, I. Hadar, C. Leak, W. Ke, I. Spanopoulos, W. Lin, D. Y. Chung, B. W. Wessels, Z. He, and M. G. Kanatzidis, Nat. Photonics **15**, 36 (2020).
[510]W. B. Gunnarsson and B. P. Rand, APL Mater. **8**, 030902 (2020).
[511]H. Kim, L. Zhao, J. S. Price, A. J. Grede, K. Roh, A. N. Brigeman, M. Lopez, B. P. Rand, and N. C. Giebink, Nat. Commun. **9**, 4893 (2018).
[512]C. Zou, Y. Liu, D. S. Ginger, and L. Y. Lin, ACS Nano **14**, 6076 (2020).
[513]S. Watanabe, G. Tumen-Ulzii, T. Cheng, T. Matsushima, and C. Adachi, J. Phys. Chem. C **124**, 27422 (2020).
[514]R. Heiderhoff, T. Haeger, N. Pourdavoud, T. Hu, M. Al-Khafaji, A. Mayer, Y. Chen, H.-C. Scheer, and T. Riedl, J. Phys. Chem. C **121**, 28306 (2017).
[515]X.-K. Liu, W. Xu, S. Bai, Y. Jin, J. Wang, R. H. Friend, and F. Gao, Nat. Mater. **20**, 10 (2020).
[516]A. Fakharuddin, U. Shabbir, W. Qiu, T. Iqbal, M. Sultan, P. Heremans, and L. Schmidt-Mende, Adv. Mater. **31**, 1807095 (2019).
[517]Y. Jiang, C. Qin, M. Cui, T. He, K. Liu, Y. Huang, M. Luo, L. Zhang, H. Xu, S. Li, J. Wei, Z. Liu, H. Wang, G.-H. Kim, M. Yuan, and J. Chen, Nat. Commun. **10**, 1868 (2019).
[518]Z.-K. Tan, R. S. Moghaddam, M. L. Lai, P. Docampo, R. Higler, F. Deschler, M. Price, A. Sadhanala, L. M. Pazos, D. Credgington, F. Hanusch, T. Bein, H. J. Snaith, and R. H. Friend, Nat. Nanotechnol. **9**, 687 (2014).
[519]L. Protesescu, S. Yakunin, M. I. Bodnarchuk, F. Krieg, R. Caputo, C. H. Hendon, R. X. Yang, A. Walsh, and M. V. Kovalenko, Nano Lett. **15**, 3692 (2015).
[520]N. Wang, L. Cheng, R. Ge, S. Zhang, Y. Miao, W. Zou, C. Yi, Y. Sun, Y. Cao, R. Yang, Y. Wei, Q. Guo, Y. Ke, M. Yu, Y. Jin, Y. Liu, Q. Ding, D. Di, L. Yang, G. Xing, H. Tian, C. Jin, F. Gao, R. H. Friend, J. Wang, and W. Huang, Nat. Photonics **10**, 699 (2016).
[521]B. A. Koscher, J. K. Swabeck, N. D. Bronstein, and A. P. Alivisatos, J. Am. Chem. Soc. **139**, 6566 (2017).
[522]H. Wang, F. U. Kosasih, H. Yu, G. Zheng, J. Zhang, G. Pozina, Y. Liu, C. Bao, Z. Hu, X. Liu, L. Kobera, S. Abbrent, J. Brus, Y. Jin, M. Fahlman, R. H. Friend, C. Ducati, X.-K. Liu, and F. Gao, Nat. Commun. **11**, 891 (2020).
[523]Y. Cao, N. Wang, H. Tian, J. Guo, Y. Wei, H. Chen, Y. Miao, W. Zou, K. Pan, Y. He, H. Cao, Y. Ke, M. Xu, Y. Wang, M. Yang, K. Du, Z. Fu, D. Kong, D. Dai, Y. Jin, G. Li, H. Li, Q. Peng, J. Wang, and W. Huang, Nature **562**, 249 (2018).
[524]W.-L. Hong, Y.-C. Huang, C.-Y. Chang, Z.-C. Zhang, H.-R. Tsai, N.-Y. Chang, and Y.-C. Chao, Adv. Mater. **28**, 8029 (2016).
[525]M. K. Gangishetty, S. Hou, Q. Quan, and D. N. Congreve, Adv. Mater. **30**, 1706226 (2018).
[526]Y. Dong, Y.-K. Wang, F. Yuan, A. Johnston, Y. Liu, D. Ma, M.-J. Choi, B. Chen, M. Chekini, S.-W. Baek, L. K. Sagar, J. Fan, Y. Hou, M. Wu, S. Lee, B. Sun, S. Hoogland, R. Quintero-Bermudez, H. Ebe, P. Todorovic, F. Dinic, P. Li, H. T. Kung, M. I. Saidaminov, E. Kumacheva, E. Spiecker, L.-S. Liao, O. Voznyy, Z.-H. Lu, and E. H. Sargent, Nat. Nanotechnol. **15**, 668 (2020).
[527]L. Zhao, J. Gao, Y. L. Lin, Y. W. Yeh, K. M. Lee, N. Yao, Y. L. Loo, and B. P. Rand, Adv. Mater. **29**, 1605317 (2017).
[528]A. Fakharuddin, W. Qiu, G. Croes, A. Devižis, R. Gegevičius, A. Vakhnin, C. Rolin, J. Genoe, R. Gehlhaar, A. Kadashchuk, V. Gulbinas, and P. Heremans, Adv. Funct. Mater. **29**, 1904101 (2019).
[529]M. Anaya, B. P. Rand, R. J. Holmes, D. Credgington, H. J. Bolink, R. H. Friend, J. Wang, N. C. Greenham, and S. D. Stranks, Nat. Photonics **13**, 818 (2019).
[530]H. Cho, Y.-H. Kim, C. Wolf, H.-D. Lee, and T.-W. Lee, Adv. Mater. **30**, 1704587 (2018).
[531]H. J. Snaith, A. Abate, J. M. Ball, G. E. Eperon, T. Leijtens, N. K. Noel, S. D. Stranks, J. T.-W. Wang, K. Wojciechowski, and W. Zhang, J. Phys. Chem. Lett. **5**, 1511 (2014).
[532]E. L. Unger, E. T. Hoke, C. D. Bailie, W. H. Nguyen, A. R. Bowring, T. Heumüller, M. G. Christoforo, and M. D. McGehee, Energy Environ. Sci. **7**, 3690 (2014).
[533]J. A. Christians, J. S. Manser, and P. V. Kamat, J. Phys. Chem. Lett. **6**, 852 (2015).
[534]E. Zimmermann, K. K. Wong, M. Müller, H. Hu, P. Ehrenreich, M. Kohlstädt, U. Würfel, S. Mastroianni, G. Mathiazhagan, A. Hinsch, T. P. Gujar, M. Thelakkat, T. Pfadler, and L. Schmidt-Mende, APL Mater. **4**, 091901 (2016).
[535]Y. Wang, X. Liu, Z. Zhou, P. Ru, H. Chen, X. Yang, and L. Han, Adv. Mater. **31**, 1803231 (2019).
[536]M. V. Khenkin, E. A. Katz, A. Abate, G. Bardizza, J. J. Berry, C. Brabec, F. Brunetti, V. Bulović, Q. Burlingame, A. Di Carlo, R. Cheacharoen, Y.-B. Cheng, A. Colsmann, S. Cros, K. Domanski, M. Dusza, C. J. Fell, S. R. Forrest, Y. Galagan, D. Di Girolamo, M. Grätzel, A. Hagfeldt, E. von Hauff, H. Hoppe, J. Kettle, H. Köbler, M. S. Leite, S. Liu, Y.-L. Loo, J. M. Luther, C.-Q. Ma, M. Madsen, M. Manceau, M. Matheron, M. McGehee, R. Meitzner, M. K. Nazeeruddin, A. F. Nogueira, Ç. Odabaşı, A. Osherov, N.-G. Park, M. O. Reese, F. De Rossi, M. Saliba, U. S. Schubert, H. J. Snaith, S. D. Stranks, W. Tress, P. A. Troshin, V. Turkovic, S. Veenstra, I. Visoly-Fisher, A. Walsh, T. Watson, H. Xie, R. Yıldırım, S. M. Zakeeruddin, K. Zhu, and M. Lira-Cantu, Nat. Energy **5**, 35 (2020).
[537]D. Polverini, G. Tzamalis, and H. Müllejans, Prog. Photovoltaics: Res. Appl. **20**, 650 (2011).
[538]W. Tress, N. Marinova, T. Moehl, S. M. Zakeeruddin, M. K. Nazeeruddin, and M. Grätzel, Energy Environ. Sci. **8**, 995 (2015).
[539]H.-S. Kim and N.-G. Park, J. Phys. Chem. Lett. **5**, 2927 (2014).
[540]Y. Zhang, M. Liu, G. E. Eperon, T. C. Leijtens, D. McMeekin, M. Saliba, W. Zhang, M. de Bastiani, A. Petrozza, L. M. Herz, M. B. Johnston, H. Lin, and H. J. Snaith, Mater. Horiz. **2**, 315 (2015).
[541]G. A. Nemnes, C. Besleaga, V. Stancu, D. E. Dogaru, L. N. Leonat, L. Pintilie, K. Torfason, M. Ilkov, A. Manolescu, and I. Pintilie, J. Phys. Chem. C **121**, 11207 (2017).
[542]See https://github.com/EugenZimmermann/matlab-keithley-jv for Github repository EugenZimmermann/matlab-keithley-jv.
[543]J. Endres, D. A. Egger, M. Kulbak, R. A. Kerner, L. Zhao, S. H. Silver, G. Hodes, B. P. Rand, D. Cahen, L. Kronik, and A. Kahn, J. Phys. Chem. Lett. **7**(14), 2722 (2016).
[544]F. Zhang, S. H. Silver, N. K. Noel, F. Ullrich, B. P. Rand, and A. Kahn, Adv. Energy Mater. **10**(26), 1903252 (2020).
[545]K. P. Goetz, A. D. Taylor, F. Paulus, and Y. Vaynzof, Adv. Funct. Mater. **30**(23), 1910004 (2020).
[546]L. M. Falk, K. P. Goetz, V. Lami, Q. An, P. Fassl, J. Herkel, F. Thome, A. D. Taylor, F. Paulus, and Y. Vaynzof, Energy Technol. **8**(4), 1900737 (2020).
[547]P. Fassl, Y. Zakharko, L. M. Falk, K. P. Goetz, F. Paulus, A. D. Taylor, J. Zaumseil, and Y. Vaynzof, J. Mater. Chem. C **7**, 5285–5292 (2019).
[548]S. Reichert, Q. An, Y.-W. Woo, A. Walsh, Y. Vaynzof, and C. Deibel, Nat. Commun. **11**, 6098 (2020).
[549]A. D. Taylor, Q. Sun, K. P. Goetz, Q. An, T. Schramm, Y. Hofstetter, M. Litterst, F. Paulus, and Y. Vaynzof, Nat. Commun. **12**, 1878 (2021).
[550]E. M. Tennyson, T. A. S. Doherty, and S. D. Stranks, Nat. Rev. Mater. **4**, 573–587 (2019).

© Author(s) 2021

[551]Q. Sun, P. Fassl, and Y. Vaynzof, ACS Appl. Energy Mater. **1**(6), 2410–2416 (2018).
[552]S. Lee, M.-C. Tang, R. Munir, D. Barrit, Y.-J. Kim, R. Kang, J.-M. Yun, D.-M. Smilgies, A. Amassian, and D.-Y. Kim, J. Mater. Chem. A **8**, 7695–7703 (2020).
[553]E. Ghahremanirad, A. Bou, S. Olyaee, and J. Bisquert, J. Phys. Chem. Lett. **8**, 1402 (2017).
[554]T.-Y. Yang, G. Gregori, N. Pellet, M. Grätzel, and J. Maier, Angew. Chem., Int. Ed. **54**, 7905 (2015).
[555]A. Senocrate and J. Maier, J. Am. Chem. Soc. **141**, 8382 (2019).
[556]A. Senocrate, I. Moudrakovski, G. Y. Kim, T.-Y. Yang, G. Gregori, M. Grätzel, and J. Maier, Angew. Chem., Int. Ed. **56**, 7755 (2017).
[557]A. Senocrate, T.-Y. Yang, G. Gregori, G. Y. Kim, M. Grätzel, and J. Maier, Solid State Ionics **321**, 69 (2018).
[558]D. W. Ferdani, S. R. Pering, D. Ghosh, P. Kubiak, A. B. Walker, S. E. Lewis, A. L. Johnson, P. J. Baker, M. S. Islam, and P. J. Cameron, Energy Environ. Sci. **12**, 2264 (2019).
[559]R. García-Rodríguez, D. Ferdani, S. Pering, P. J. Baker, and P. J. Cameron, J. Mater. Chem. A **7**, 22604 (2019).
[560]G. Y. Kim, A. Senocrate, Y. R. Wang, D. Moia, and J. Maier, Angew. Chem., Int. Ed. **60**, 820 (2020).
[561]Y. Yuan and J. Huang, Acc. Chem. Res. **49**, 286 (2016).
[562]G. Y. Kim, A. Senocrate, D. Moia, and J. Maier, Adv. Funct. Mater. **30**, 2002426 (2020).
[563]A. Senocrate, T. Acartürk, G. Y. Kim, R. Merkle, U. Starke, M. Grätzel, and J. Maier, J. Mater. Chem. A **6**, 10847 (2018).
[564]R. A. Belisle, W. H. Nguyen, A. R. Bowring, P. Calado, X. Li, S. J. C. Irvine, M. D. McGehee, P. R. F. Barnes, and B. C. O'Regan, Energy Environ. Sci. **10**, 192 (2017).
[565]D. A. Jacobs, Y. Wu, H. Shen, C. Barugkin, F. J. Beck, T. P. White, K. Weber, and K. R. Catchpole, Phys. Chem. Chem. Phys. **19**, 3094 (2017).
[566]D. Moia, I. Gelmetti, P. Calado, W. Fisher, M. Stringer, O. Game, Y. Hu, P. Docampo, D. Lidzey, E. Palomares, J. Nelson, and P. R. F. Barnes, Energy Environ. Sci. **12**, 1296 (2019).
[567]H. Wang, A. Guerrero, A. Bou, A. M. Al-Mayouf, and J. Bisquert, Energy Environ. Sci. **12**, 2054 (2019).
[568]J.-S. Park and A. Walsh, Annu. Rev. Condens. Matter Phys. **12**, 95 (2020).
[569]G. Y. Kim, A. Senocrate, T.-Y. Yang, G. Gregori, M. Grätzel, and J. Maier, Nat. Mater. **17**, 445 (2018).
[570]L. D. Whalley, R. Crespo-Otero, and A. Walsh, ACS Energy Lett. **2**, 2713 (2017).
[571]M. C. Brennan, S. Draguta, P. V. Kamat, and M. Kuno, ACS Energy Lett. **3**, 204 (2017).
[572]E. T. Hoke, D. J. Slotcavage, E. R. Dohner, A. R. Bowring, H. I. Karunadasa, and M. D. McGehee, Chem. Sci. **6**, 613 (2015).
[573]A. Pockett, G. E. Eperon, N. Sakai, H. J. Snaith, L. M. Peter, and P. J. Cameron, Phys. Chem. Chem. Phys. **19**, 5959 (2017).
[574]D. A. Jacobs, H. Shen, F. Pfeffer, J. Peng, T. P. White, F. J. Beck, and K. R. Catchpole, J. Appl. Phys. **124**, 225702 (2018).
[575]S. T. Birkhold, J. T. Precht, H. Liu, R. Giridharagopal, G. E. Eperon, L. Schmidt-Mende, X. Li, and D. S. Ginger, ACS Energy Lett. **3**, 1279 (2018).
[576]C. Li, A. Guerrero, S. Huettner, and J. Bisquert, Nat. Commun. **9**, 5113 (2018).
[577]C.-J. Tong, L. Li, L.-M. Liu, and O. V. Prezhdo, J. Am. Chem. Soc. **142**, 3060 (2020).
[578]Y. Rakita, I. Lubomirsky, and D. Cahen, Mater. Horiz. **6**, 1297 (2019).
[579]A. Senocrate, E. Kotomin, and J. Maier, Helv. Chim. Acta **103**, e2000073 (2020).
[580]S. Jariwala, H. Sun, G. W. P. Adhyaksa, A. Lof, L. A. Muscarella, B. Ehrler, E. C. Garnett, and D. S. Ginger, Joule **3**, 3048 (2019).
[581]J.-S. Park, J. Calbo, Y.-K. Jung, L. D. Whalley, and A. Walsh, ACS Energy Lett. **4**, 1321 (2019).
[582]T. A. S. Doherty, A. J. Winchester, S. Macpherson, D. N. Johnstone, V. Pareek, E. M. Tennyson, S. Kosar, F. U. Kosasih, M. Anaya, M. Abdi-Jalebi, Z. Andaji-Garmaroudi, E. L. Wong, J. Madéo, Y.-H. Chiang, J.-S. Park, Y.-K. Jung, C. E. Petoukhoff, G. Divitini, M. K. L. Man, C. Ducati, A. Walsh, P. A. Midgley, K. M. Dani, and S. D. Stranks, Nature **580**, 360 (2020).
[583]D. R. Ceratti, A. V. Cohen, R. Tenne, Y. Rakita, L. Snarski, L. Cremonesi, I. Goldian, I. Kaplan-Ashiri, T. Bendikov, V. Kalchenko, M. Elbaum, M. A. C. Potenza, L. Kronik, G. Hodes, D. Cahen, arXiv:2009.14617 (2020).
[584]L. Zhao, R. A. Kerner, Z. Xiao, Y. L. Lin, K. M. Lee, J. Schwartz, and B. P. Rand, ACS Energy Lett. **1**, 595 (2016).
[585]R. A. Kerner, L. Zhao, S. P. Harvey, J. J. Berry, J. Schwartz, and B. P. Rand, ACS Energy Lett. **5**, 3352 (2020).
[586]D. R. Ceratti, A. Zohar, R. Kozlov, H. Dong, G. Uraltsev, O. Girshevitz, I. Pinkas, L. Avram, G. Hodes, and D. Cahen, Adv. Mater. **32**, 2002467 (2020).
[587]R. A. Kerner, S. Heo, K. Roh, K. MacMillan, B. W. Larson, and B. P. Rand, ACS Energy Lett. **6**, 501 (2021).
[588]C. C. Boyd, R. C. Shallcross, T. Moot, R. Kerner, L. Bertoluzzi, A. Onno, S. Kavadiya, C. Chosy, E. J. Wolf, J. Werner, J. A. Raiford, C. de Paula, A. F. Palmstrom, Z. J. Yu, J. J. Berry, S. F. Bent, Z. C. Holman, J. M. Luther, E. L. Ratcliff, N. R. Armstrong, and M. D. McGehee, Joule **4**, 1759 (2020).
[589]L. Zhao, H. Tian, S. H. Silver, A. Kahn, T.-L. Ren, and B. P. Rand, Joule **2**, 2133 (2018).
[590]K. Schutt, P. K. Nayak, A. J. Ramadan, B. Wenger, Y. H. Lin, and H. J. Snaith, Adv. Funct. Mater. **29**, 1900466 (2019).
[591]E. M. Sanehira, B. J. T. de Villers, P. Schulz, M. O. Reese, S. Ferrere, K. Zhu, L. Y. Lin, J. J. Berry, and J. M. Luther, ACS Energy Lett. **1**, 38 (2016).
[592]T. H. Schloemer, J. A. Raiford, T. S. Gehan, T. Moot, S. Nanayakkara, S. P. Harvey, R. C. Bramante, S. Dunfield, A. E. Louks, A. E. Maughan, L. Bliss, M. D. McGehee, M. F. A. M. van Hest, M. O. Reese, S. F. Bent, J. J. Berry, J. M. Luther, and A. Sellinger, ACS Energy Lett. **5**, 2349 (2020).
[593]C. C. Boyd, R. Cheacharoen, K. A. Bush, R. Prasanna, T. Leijtens, and M. D. McGehee, ACS Energy Lett. **3**, 1772 (2018).
[594]G. Flora, D. Gupta, and A. Tiwari, Interdiscip. Toxicol. **5**(2), 47–58 (2012).
[595]Z. Xiao, Z. Song, and Y. Yan, Adv. Mater. **31**(47), 1803792 (2019).
[596]N. Glück and T. Bein, Energy Environ. Sci. **13**(12), 4691–4716 (2020).
[597]G. Nasti and A. Abate, Adv. Energy Mater. **10**(13), 1902467 (2020).
[598]P.-K. Kung, M.-H. Li, P.-Y. Lin, J.-Y. Jhang, M. Pantaler, D. C. Lupascu, G. Grancini, and P. Chen, Sol. RRL **4**(2), 1900306 (2020).
[599]J. A. Steele, P. Puech, M. Keshavarz, R. Yang, S. Banerjee, E. Debroye, C. W. Kim, H. Yuan, N. H. Heo, J. Vanacken, A. Walsh, J. Hofkens, and M. B. J. Roeffaers, ACS Nano **12**(8), 8081–8090 (2018).
[600]K. M. McCall, C. C. Stoumpos, S. S. Kostina, M. G. Kanatzidis, and B. W. Wessels, Chem. Mater. **29**(9), 4129–4145 (2017).
[601]S. Ullah, J. Wang, P. Yang, L. Liu, J. Khan, S.-E. Yang, T. Xia, H. Guo, and Y. Chen, Sol. RRL **5**(5), 2000830 (2021).
[602]F. Matteocci, S. Razza, F. Di Giacomo, S. Casaluci, G. Mincuzzi, T. M. Brown, A. D'Epifanio, S. Licoccia, and A. Di Carlo, Phys. Chem. Chem. Phys. **16**(9), 3918 (2014).
[603]S. Razza, F. Di Giacomo, F. Matteocci, L. Cinà, A. L. Palma, S. Casaluci, P. Cameron, A. D'Epifanio, S. Licoccia, A. Reale, T. M. Brown, and A. Di Carlo, J. Power Sources **277**, 286 (2015).
[604]H. Chen, F. Ye, W. Tang, J. He, M. Yin, Y. Wang, F. Xie, E. Bi, X. Yang, M. Grätzel, and L. Han, Nature **550**, 92 (2017).
[605]W. Qiu, T. Merckx, M. Jaysankar, C. Masse De La Huerta, L. Rakocevic, W. Zhang, U. W. Paetzold, R. Gehlhaar, L. Froyen, J. Poortmans, D. Cheyns, H. J. Snaith, and P. Heremans, Energy Environ. Sci. **9**, 484 (2016).
[606]S.-J. Moon, J.-H. Yum, L. Lofgren, A. Walter, L. Sansonnens, M. Benkhaira, S. Nicolay, J. Bailat, and C. Ballif, IEEE J. Photovoltaics **5**, 1087 (2015).
[607]J. A. Christians, F. Zhang, R. C. Bramante, M. O. Reese, T. H. Schloemer, A. Sellinger, M. F. A. M. Van Hest, K. Zhu, J. J. Berry, and J. M. Luther, ACS Energy Lett. **3**, 2502 (2018).
[608]A. L. Palma, F. Matteocci, A. Agresti, S. Pescetelli, E. Calabrò, L. Vesce, S. Christiansen, M. Schmidt, and A. Di Carlo, IEEE J. Photovoltaics **7**, 1674 (2017).
[609]N.-G. Park and K. Zhu, Nat. Rev. Mater. **5**, 333 (2020).

© Author(s) 2021

[610]Z. Song, C. L. McElvany, A. B. Phillips, I. Celik, P. W. Krantz, S. C. Watthage, G. K. Liyanage, D. Apul, and M. J. Heben, Energy Environ. Sci. **10**, 1297 (2017).
[611]J.-A. Alberola-Borràs, J. A. Baker, F. De Rossi, R. Vidal, D. Beynon, K. E. A. Hooper, T. M. Watson, and I. Mora-Seró, iScience **9**, 542 (2018).
[612]F. Matteocci, L. Vesce, F. U. Kosasih, L. A. Castriotta, S. Cacovich, A. L. Palma, G. Divitini, C. Ducati, and A. Di Carlo, ACS Appl. Mater. Interfaces **11**, 25195 (2019).
[613]Y. Jiang, M. Remeika, Z. Hu, E. J. Juarez-Perez, L. Qiu, Z. Liu, T. Kim, L. K. Ono, D. Y. Son, Z. Hawash, M. R. Leyden, Z. Wu, L. Meng, J. Hu, and Y. Qi, Adv. Energy Mater. **9**(13), 1803047 (2019).
[614]N. Rolston, W. J. Scheideler, A. C. Flick, J. P. Chen, H. Elmaraghi, A. Sleugh, O. Zhao, M. Woodhouse, and R. H. Dauskardt, Joule **4**, 2675 (2020).
[615]F. Di Giacomo, S. Shanmugam, H. Fledderus, B. J. Bruijnaers, W. J. H. Verhees, M. S. Dorenkamper, S. C. Veenstra, W. Qiu, R. Gehlhaar, T. Merckx, T. Aernouts, R. Andriessen, and Y. Galagan, Sol. Energy Mater. Sol. Cells **181**, 53 (2018).
[616]T. Bu, J. Li, F. Zheng, W. Chen, X. Wen, Z. Ku, Y. Peng, J. Zhong, Y. B. Cheng, and F. Huang, Nat. Commun. **9**(1), 4609 (2018).
[617]L. A. Castriotta, R. F. Pineda, V. Babu, P. Spinelli, B. Taheri, F. Matteocci, F. Brunetti, K. Wojciechowski, and A. Di Carlo, ACS Appl. Mater. Interfaces **13**, 29576 (2021).
[618]F. D. Giacomo, H. Fledderus, H. Gorter, G. Kirchner, I. d. Vries, I. Dogan, W. Verhees, V. Zardetto, M. Najafi, D. Zhang, H. Lifka, Y. Galagan, T. Aernouts, S. Veenstra, P. Groen, and R. Andriesse, presented at the 2018 IEEE 7th World Conference on Photovoltaic Energy Conversion (WCPEC) (A Joint Conference of 45th IEEE PVSC, 28th PVSEC and 34th EU PVSEC), 2018.
[619]M. Yang, Z. Li, M. O. Reese, O. G. Reid, D. H. Kim, S. Siol, T. R. Klein, Y. Yan, J. J. Berry, M. F. A. M. van Hest, and K. Zhu, Nat. Energy **2**, 17038 (2017).
[620]H. Li, T. Bu, J. Li, Z. Lin, J. Pan, Q. Li, X.-L. Zhang, Z. Ku, Y.-B. Cheng, and F. Huang, ACS Appl. Mater. Interfaces **13**, 18724 (2021).
[621]Y. Deng, Z. Ni, A. F. Palmstrom, J. Zhao, S. Xu, C. H. Van Brackle, X. Xiao, K. Zhu, and J. Huang, Joule **4**, 1949 (2020).
[622]Y. Hu, Y. Chu, Q. Wang, Z. Zhang, Y. Ming, A. Mei, Y. Rong, and H. Han, Joule **3**, 2076 (2019).
[623]D. H. Kim, J. B. Whitaker, Z. Li, M. F. A. M. van Hest, and K. Zhu, Joule **2**, 1437 (2018).
[624]S. P. Dunfield, L. Bliss, F. Zhang, J. M. Luther, K. Zhu, M. F. A. M. van Hest, M. O. Reese, and J. J. Berry, Adv. Energy Mater. **10**, 1904054 (2020).
[625]L. A. Castriotta, F. Matteocci, L. Vesce, L. Cinà, A. Agresti, S. Pescetelli, A. Ronconi, M. Löffler, M. M. Stylianakis, F. Di Giacomo, P. Mariani, M. Stefanelli, E. M. Speller, A. Alfano, B. Paci, A. Generosi, F. Di Fonzo, A. Petrozza, B. Rellinghaus, E. Kymakis, and A. Di Carlo, ACS Appl. Mater. Interfaces **13**, 11741 (2021).
[626]B. Conings, J. Drijkoningen, N. Gauquelin, A. Babayigit, J. D'Haen, L. D'Olieslaeger, A. Ethirajan, J. Verbeeck, J. Manca, E. Mosconi, F. De Angelis, and H.-G. Boyen, Adv. Energy Mater. **5**, 1500477 (2015).
[627]Y. Sha, E. Bi, Y. Zhang, P. Ru, W. Kong, P. Zhang, X. Yang, H. Chen, and L. Han, Adv. Energy Mater. **11**(5), 2003301 (2021).
[628]E. Bi, W. Tang, H. Chen, Y. Wang, J. Barbaud, T. Wu, W. Kong, P. Tu, H. Zhu, X. Zeng, J. He, S. I. Kan, X. Yang, M. Grätzel, and L. Han, Joule **3**, 2748 (2019).
[629]G. Tong, D. Y. Son, L. K. Ono, Y. Liu, Y. Hu, H. Zhang, A. Jamshaid, L. Qiu, Z. Liu, and Y. Qi, Adv. Energy Mater. **11**(10), 2003712 (2021).
[630]Z. Liu, L. Qiu, L. K. Ono, S. He, Z. Hu, M. Jiang, G. Tong, Z. Wu, Y. Jiang, D. Y. Son, Y. Dang, S. Kazaoui, and Y. Qi, Nat. Energy **5**, 596 (2020).
[631]F. U. Kosasih, L. Rakocevic, T. Aernouts, J. Poortmans, and C. Ducati, ACS Appl. Mater. Interfaces **11**, 45646 (2019).
[632]E. J. Wolf, I. E. Gould, L. B. Bliss, J. J. Berry, and M. D. McGehee, "Designing modules to prevent reverse bias degradation in perovskite solar cells when partial shading occurs," Sol. RRL (published online).
[633]S. Chen, Y. Deng, H. Gu, S. Xu, S. Wang, Z. Yu, V. Blum, and J. Huang, Nat. Energy **5**, 1003 (2020).
[634]J. M. Kadro and A. Hagfeldt, Joule **1**, 29 (2017).
[635]C. Traverse, R. Pandey, M. Barr, and R. Lunt, Nat. Energy **2**, 849 (2017).
[636]M. Batmunkh, Y. L. Zhong, and H. Zhao, Adv. Mater. **32**, 2000631 (2020).
[637]A. Mittasch, *Geschichte Der Ammoniaksynthese* (Weinheim Verlag Chemie, 1951).
[638]See https://obamawhitehouse.archives.gov/node/164866 for about the Materials Genome Initiative.
[639]T. Hey, S. Tansley, and K. Tolle, *The Fourth Paradigm: Data-Intensive Scientific Discovery—Microsoft Research* (Microsoft Research, 2009).
[640]M. D. Wilkinson, M. Dumontier, I. J. J. Aalbersberg, G. Appleton, M. Axton, A. Baak, N. Blomberg, J.-W. Boiten, L. B. da Silva Santos, P. E. Bourne, J. Bouwman, A. J. Brookes, T. Clark, M. Crosas, I. Dillo, O. Dumon, S. Edmunds, C. T. Evelo, R. Finkers, A. Gonzalez-Beltran, A. J. G. Gray, P. Groth, C. Goble, J. S. Grethe, J. Heringa, P. A. C. 't Hoen, R. Hooft, T. Kuhn, R. Kok, J. Kok, S. J. Lusher, M. E. Martone, A. Mons, A. L. Packer, B. Persson, P. Rocca-Serra, M. Roos, R. van Schaik, S.-A. Sansone, E. Schultes, T. Sengstag, T. Slater, G. Strawn, M. A. Swertz, M. Thompson, J. van der Lei, E. van Mulligen, J. Velterop, A. Waagmeester, P. Wittenburg, K. Wolstencroft, J. Zhao, and B. Mons, Sci. Data **3**, 160018 (2016).
[641]See http://pdb.nmse-lab.ru for 2D Perovskites Database—The Laboratory of New Materials for Solar Energetics.
[642]See https://materials.hybrid3.duke.edu/ for Materials database.
[643]I. E. Castelli, J. M. García-Lastra, K. S. Thygesen, and K. W. Jacobsen, APL Mater. **2**, 081514 (2014).
[644]C. Kim, T. D. Huan, S. Krishnan, and R. Ramprasad, Sci. Data **4**, 170057 (2017).
[645]W. A. Saidi and A. Kachmar, J. Phys. Chem. Lett. **9**, 7090 (2018).
[646]M. R. Filip, G. E. Eperon, H. J. Snaith, and F. Giustino, Nat. Commun. **5**, 5757 (2014).
[647]C. Vona, D. Nabok, and C. Draxl "Electronic structure of (organic-)inorganic metal halide perovskites: The dilemma of choosing the right functional" (unpublished).
[648]M. Scheffler, M. Aeschlimann, M. Albrecht, T. Bereau, H.-J. Bungartz, C. Felser, M. Greiner, A. Groß, C. T. Koch, K. Kremer, W. E. Nagel, M. Scheidgen, C. Wöll, and C. Draxl, "FAIR data—New horizons for materials research" Nature (submitted) (2021).
[649]C. Draxl and M. Scheffler, in *Handbook of Materials Modeling Perspective in Handbook of Materials Modeling*, edited by W. Andreoni and S. Yip (Springer, Cham, 2019), pp. 49–73.
[650]L. M. Ghiringhelli, J. Vybiral, S. V. Levchenko, C. Draxl, and M. Scheffler, Phys. Rev. Lett. **114**, 105503 (2015).
[651]G. Pilania, A. Mannodi-Kanakkithodi, B. P. Uberuaga, R. Ramprasad, J. E. Gubernatis, and T. Lookman, Sci. Rep. **6**, 19375 (2016).
[652]N. Tessler and Y. Vaynzof, ACS Energy Lett. **5**, 1260 (2020).
[653]Z. Liu, J. Siekmann, B. Klingebiel, U. Rau, and T. Kirchartz, Adv. Energy Mater. **11**, 2003386 (2021).
[654]L. Krückemeier, B. Krogmeier, Z. Liu, U. Rau, and T. Kirchartz, Adv. Energy Mater. **11**, 2003489 (2021).
[655]X. Zhang, J. X. Shen, M. E. Turiansky, and C. G. van de Walle, Nat. Mater. **20**, 971 (2021).
[656]M. Karlsson, Z. Yi, S. Reichert, X. Luo, W. Lin, Z. Zhang, C. Bao, R. Zhang, S. Bai, G. Zheng, P. Teng, L. Duan, Y. Lu, K. Zheng, T. Pullerits, C. Deibel, W. Xu, R. Friend, and F. Gao, Nat. Commun. **12**(1), 361 (2021).
[657]Q. Jiang, Z. Ni, G. Xu, Y. Lin, P. N. Rudd, R. Xue, Y. Li, Y. Li, Y. Gao, and J. Huang, Adv. Mater. **32**, 2001581 (2020).
[658]N. K. Noel, S. N. Habisreutinger, A. Pellaroque, F. Pulvirenti, B. Wenger, F. Zhang, Y.-H. Lin, O. G. Reid, J. Leisen, Y. Zhang, S. Barlow, S. R. Marder, A. Kahn, H. J. Snaith, C. B. Arnold, and B. P. Rand, Energy Environ. Sci. **12**, 3063–3073 (2019).
[659]A. Fakharuddin, L. Schmidt-Mende, G. Garcia-Belmonte, R. Jose, and I. Mora-Sero, Adv. Energy Mater. **7**, 1700623 (2017).
[660]N. Aristidou, C. Eames, I. Sanchez-Molina, X. Bu, J. Kosco, M. S. Islam, and S. A. Haque, Nat. Commun. **8**, 15218 (2017).
[661]T. T. Ava, A. Al Mamun, S. Marsillac, and G. Namkoong, Appl. Sci. **9**, 188 (2019).

© Author(s) 2021

[662]T. Malinauskas, D. Tomkute-Luksiene, R. Sens, M. Daskeviciene, R. Send, H. Wonneberger, V. Jankauskas, I. Bruder, and V. Getautis, ACS Appl. Mater. Interfaces **7**, 11107 (2015).
[663]K. Domanski, E. A. Alharbi, A. Hagfeldt, M. Grätzel, and W. Tress, Nat. Energy **3**, 61 (2018).
[664]R. Gegevičius, M. Franckevičius, J. Chmeliov, W. Tress, and V. Gulbinas, J. Phys. Chem. Lett. **10**, 1779 (2019).
[665]T. Sekimoto, T. Matsui, T. Nishihara, R. Uchida, T. Sekiguchi, and T. Negami, ACS Appl. Energy Mater. **2**, 5039 (2019).
[666]J. M. Azpiroz, E. Mosconi, J. Bisquert, and F. De Angelis, Energy Environ. Sci. **8**, 2118 (2015).
[667]C.-X. Zhang, T. Shen, D. Guo, L.-M. Tang, K. Yang, and H.-X. Deng, InfoMat **2**, 1034 (2020).
[668]N. Ahn, K. Kwak, M. S. Jang, H. Yoon, B. Y. Lee, J.-K. Lee, P. V. Pikhitsa, J. Byun, and M. Choi, Nat. Commun. **7**, 13422 (2016).
[669]J.-H. Im, C.-R. Lee, J.-W. Lee, S.-W. Park, and N.-G. Park, Nanoscale **3**, 4088 (2011).
[670]N. Arora, M. I. Dar, A. Hinderhofer, N. Pellet, F. Schreiber, S. M. Zakeeruddin, and M. Grätzel, Science **358**, 768 (2017).
[671]F. Giordano, A. Abate, J. P. Correa Baena, M. Saliba, T. Matsui, S. H. Im, S. M. Zakeeruddin, M. K. Nazeeruddin, A. Hagfeldt, and M. Graetzel, Nat. Commun. **7**, 10379 (2016).
[672]J.-W. Lee, D.-H. Kim, H.-S. Kim, S.-W. Seo, S. M. Cho, and N.-G. Park, Adv. Energy Mater. **5**, 1501310 (2015).
[673]M. Zhang, J. S. Yun, Q. Ma, J. Zheng, C. F. J. Lau, X. Deng, J. Kim, D. Kim, J. Seidel, M. A. Green, S. Huang, and A. W. Y. Ho-Baillie, ACS Energy Lett. **2**, 438 (2017).
[674]H.-L. Hsu, C.-C. Chang, C.-P. Chen, B.-H. Jiang, R.-J. Jeng, and C.-H. Cheng, J. Mater. Chem. A **3**, 9271 (2015).
[675]A. D. Jodlowski, C. Roldán-Carmona, G. Grancini, M. Salado, M. Ralaiarisoa, S. Ahmad, N. Koch, L. Camacho, G. De Miguel, and M. K. Nazeeruddin, Nat. Energy **2**, 972 (2017).
[676]N. K. Noel, A. Abate, S. D. Stranks, E. S. Parrott, V. M. Burlakov, A. Goriely, and H. J. Snaith, ACS Nano **8**, 9815 (2014).
[677]H. Zhang, Y. Wu, C. Shen, E. Li, C. Yan, W. Zhang, H. Tian, L. Han, and W.-H. Zhu, Adv. Energy Mater. **9**, 1803573 (2019).
[678]R. Wang, J. Xue, L. Meng, J.-W. Lee, Z. Zhao, P. Sun, L. Cai, T. Huang, Z. Wang, Z.-K. Wang, Y. Duan, J. L. Yang, S. Tan, Y. Yuan, Y. Huang, and Y. Yang, Joule **3**, 1464 (2019).
[679]S. Li, K. Fan, Y. Cui, S. Leng, Y. Ying, W. Zou, Z. Liu, C.-Z. Li, K. Yao, and H. Huang, ACS Energy Lett. **5**, 2015 (2020).
[680]Y.-W. Jang, S. Lee, K. M. Yeom, K. Jeong, K. Choi, M. Choi, and J. H. Noh, Nat. Energy **6**, 63 (2021).
[681]M.-Y. Kuo, N. Spitha, M. P. Hautzinger, P.-L. Hsieh, J. Li, D. Pan, Y. Zhao, L.-J. Chen, M. H. Huang, S. Jin, Y.-J. Hsu, and J. C. Wright, J. Am. Chem. Soc. **143**, 4969 (2021).
[682]A. Magomedov, E. Kasparavičius, K. Rakstys, S. Paek, N. Gasilova, K. Genevičius, G. Juška, T. Malinauskas, M. K. Nazeeruddin, and V. Getautis, J. Mater. Chem. C **6**, 8874 (2018).
[683]X. Yin, Z. Song, Z. Li, and W. Tang, Energy Environ. Sci. **13**, 4057 (2020).
[684]B. X. Zhao, C. Yao, K. Gu, T. Liu, Y. Xia, and Y.-L. Loo, Energy Environ. Sci. **13**, 4334 (2020).
[685]A. Magomedov, A. Al-Ashouri, E. Kasparavičius, S. Strazdaite, G. Niaura, M. Jošt, T. Malinauskas, S. Albrecht, and V. Getautis, Adv. Energy Mater. **8**, 1801892 (2018).
[686]M. Saliba, J.-P. Correa-Baena, C. M. Wolff, M. Stolterfoht, N. Phung, S. Albrecht, D. Neher, and A. Abate, Chem. Mater. **30**, 4193 (2018).
[687]M. O. Reese, S. A. Gevorgyan, M. Jørgensen, E. Bundgaard, S. R. Kurtz, D. S. Ginley, D. C. Olson, M. T. Lloyd, P. Morvillo, E. A. Katz, A. Elschner, O. Haillant, T. R. Currier, V. Shrotriya, M. Hermenau, M. Riede, K. R. Kirov, G. Trimmel, T. Rath, O. Inganäs, F. Zhang, M. Andersson, K. Tvingstedt, M. Lira-Cantu, D. Laird, C. McGuiness, S. (Jimmy) Gowrisanker, M. Pannone, M. Xiao, J. Hauch, R. Steim, D. M. DeLongchamp, R. Rösch, H. Hoppe, N. Espinosa, A. Urbina, G. Yaman-Uzunoglu, J.-B. Bonekamp, A. J. J. M. van Breemen, C. Girotto, E. Voroshazi, and F. C. Krebs, Sol. Energy Mater. Sol. Cells **95**, 1253 (2011).
[688]D. Bryant, N. Aristidou, S. Pont, I. Sanchez-Molina, T. Chotchunangatchaval, S. Wheeler, J. R. Durrant, and S. A. Haque, Energy Environ. Sci. **9**, 1655 (2016).
[689]S. Wu, R. Chen, S. Zhang, B. H. Babu, Y. Yue, H. Zhu, Z. Yang, C. Chen, W. Chen, Y. Huang, S. Fang, T. Liu, L. Han, and W. Chen, Nat. Commun. **10**, 1161 (2019).
[690]Z. Zhang, R. Ji, M. Kroll, Y. J. Hofstetter, X. Jia, D. Becker-Koch, F. Paulus, M. Löffler, F. Nehm, K. Leo, and Y. Vaynzof, Adv. Energy Mater. **11**(29), 2100299 (2021).

AFFILIATIONS

[1]Department of Physics, University of Konstanz, Universitaetsstr. 10, 78457 Konstanz, Germany
[2]Experimental Physics VI, University of Würzburg, Am Hubland, 97074 Würzburg, Germany
[3]Department of Chemistry, University of Cologne, Greinstraße 4-6, 50939 Cologne, Germany
[4]Institute for Materials Science and Center for Nanointegration Duisburg-Essen (CENIDE), University of Duisburg-Essen, 45141 Essen, Germany
[5]Clarendon Laboratory, Department of Physics, University of Oxford, Parks Road, Oxford OX1 3PU, United Kingdom
[6]TUM Institute for Advanced Study, 85748 Garching bei München, Germany
[7]Institute of Applied Physics, University of Tübingen, Auf der Morgenstelle 10, 72076 Tübingen, Germany
[8]Department of Physics, University of Regensburg, 93053 Regensburg, Germany
[9]Dresden Integrated Center for Applied Physics and Photonic Materials (IAPP) and Würzburg-Dresden Cluster of Excellence ct.qmat, Technische Universität Dresden, 01062 Dresden, Germany
[10]Department of Physics, Technical University of Munich, 85748 Garching, Germany
[11]Helmholtz-Zentrum Berlin für Materialien und Energie GmbH, Young Investigator Group 'Hybrid Materials Formation and Scaling,' Kekulestr. 5, 12489 Berlin, Germany
[12]Carl von Ossietzky Universität Oldenburg, Institute of Physics, Carl-von-Ossietzky-Straße 9, 26129 Oldenburg, Germany
[13]Institute for Photovoltaics (ipv), University of Stuttgart, Pfaffenwaldring 47, 70569 Stuttgart, Germany and Helmholtz Young Investigator Group, IEK5-Photovoltaik, Forschungszentrum Jülich, 52425 Jülich, Germany
[14]Dresden Integrated Center for Applied Physics and Photonic Materials (IAPP), Technische Universität Dresden, 01062 Dresden, Germany
[15]Department of Physics and Materials Science, University of Luxembourg, Luxembourg, Luxembourg
[16]IEK5-Photovoltaik, Forschungszentrum Jülich, 52425 Jülich, Germany and Faculty of Engineering and CENIDE, University of Duisburg-Essen, Carl-Benz-Str. 199, 47057 Duisburg, Germany
[17]Institute of Physics and Astronomy, University of Potsdam, Karl-Liebknecht-Str. 24-25, D-14476 Potsdam-Golm, Germany

© Author(s) 2021

[18] Freiburg Materials Research Center (FMF), University of Freiburg, Stefan-Meier-Str. 21, 79104 Freiburg, Germany
[19] Department of Organic and Perovskite Photovoltaics, Fraunhofer Institute for Solar Energy Systems (ISE), Heidenhofstraße 2, 79110 Freiburg, Germany
[20] Applied Functional Polymers, Macromolecular Chemistry I, University of Bayreuth, 95440 Bayreuth, Germany
[21] Bavarian Polymer Institute, University of Bayreuth, 95440 Bayreuth, Germany
[22] Surface Science Laboratory, Department of Materials and Earth Sciences, Technical University of Darmstadt, Otto-Berndt-Strasse 3, 64287 Darmstadt, Germany
[23] Lehrstuhl für Festkörperphysik, Friedrich-Alexander-Universität Erlangen-Nürnberg (FAU), Staudtstr. 7, 91058 Erlangen, Germany
[24] Helmholtz-Zentrum Berlin für Materialien und Energie GmbH, Young Investigator Group Perovskite Tandem Solar Cells, 12489 Berlin, Germany
[25] Technical University Berlin, Faculty IV, Electrical Engineering and Computer Science, 10587 Berlin, Germany
[26] Institute of Electronic Devices, University of Wuppertal, 42119 Wuppertal, Germany
[27] Wuppertal Center for Smart Materials and Systems, University of Wuppertal, 42119 Wuppertal, Germany
[28] Institute of Nanoscience and Nanotechnology, National Center for Scientific Research Demokritos, 15341 Agia Paraskevi, Attica, Greece
[29] Integrated Center for Applied Physics and Photonic Materials (IAPP) and Center for Advancing Electronics Dresden (cfaed), Technische Universität Dresden, Nöthnitzer Straße 61, 01187 Dresden, Germany
[30] Max Planck Institute for Solid State Research, Heisenbergstrasse 1, 70569 Stuttgart, Germany
[31] Department of Molecular Compound Physics, Center for Physical Sciences and Technology (FTMC), Saulėtekio Avenue 3, Vilnius LT-10257, Lithuania
[32] Department of Electrical Engineering, Princeton University, Princeton, New Jersey 08544, USA
[33] Andlinger Center for Energy and the Environment, Princeton University, Princeton, New Jersey 08544, USA
[34] Department of Chemistry, Ludwig-Maximilians-University Munich, Butenandtstr. 5-13, 81377 Munich, Germany
[35] CHOSE—Centre for Hybrid and Organic Solar Energy, Department of Electronic Engineering, University of Rome Tor Vergata, Roma 00133, Italy
[36] LASE—Laboratory for Advanced Solar Energy, National University of Science and Technology MISiS, 119049 Moscow, Russia
[37] Physics Department and IRIS Adlershof, Humboldt-Universität zu Berlin, Zum Großen Windkanal 2, 12489 Berlin, Germany
[38] Fritz-Haber-Institut der Max-Planck-Gesellschaft, Faradayweg 4-6, 14195 Berlin, Germany
[a] **Author to whom correspondence should be addressed:** lukas.schmidt-mende@uni-konstanz.de

© Author(s) 2021